Synthesis, Characterization and Application of Phosphazenyl Phosphines

Sebastian Wagner

Marburg 2023

Synthesis, Characterization and Application of Phosphazenyl Phosphines

Dissertation

Zur Erlangung des Doktorgrades der Naturwissenschaften
(Dr. rer. nat.)

dem Fachbereich Chemie
der Philipps-Universität Marburg
(Hochschulkennziffer 1180)

vorgelegt von

Sebastian Wagner
(M.Sc.)

aus Tegernsee

Marburg/Lahn 2023

Die vorliegende Arbeit wurde in der Zeit von Januar 2019 bis März 2023 unter der Leitung von Herrn Prof. Dr. Jörg Sundermeyer am Fachbereich Chemie der Philipps-Universität Marburg angefertigt.

Vom Fachbereich Chemie der Philipps-Universität Marburg (Hochschulkennziffer: 1180) als Dissertation angenommen am: 24.03.23

Erstgutachter: Prof. Dr. Jörg Sundermeyer
Zweitgutachter: Prof. Dr. Eric Meggers

Tag der mündlichen Prüfung: 25.05.2023

Erklärung

Ich erkläre, dass eine Promotion noch an keiner anderen Hochschule als der Philipps-Universität Marburg, Fachbereich Chemie versucht wurde.

Hiermit versichere ich, dass ich die vorliegende Dissertation:

"Synthesis, Characterization and Application of Phosphazenyl Phosphines"

ohne unerlaubte Hilfe Dritter angefertigt und andere als die in der Dissertation angegebenen Hilfsmittel nicht benutzt habe. Alle Stellen, die wörtlich oder sinngemäß aus veröffentlichten oder unveröffentlichten Schriften entnommen sind, habe ich als solche kenntlich gemacht. Dritte waren an der inhaltlich-materiellen Erstellung der Dissertation nicht beteiligt; insbesondere habe ich hierfür nicht die Hilfe eines Promotionsberaters in Anspruch genommen. Kein Teil dieser Arbeit ist in einem anderen Promotions- oder Habilitationsverfahren der Antragstellerin oder des Antragsstellers verwendet worden. Mit dem Einsatz von Software zur Erkennung von Plagiaten bin ich einverstanden.

Marburg, den 24.03.23

Because the universe was full of ignorance all around and the scientist panned through it like a prospector crouched over a mountain stream, looking for the gold of knowledge among the gravel of unreason, the sand of uncertainty and the little whiskery eight-legged swimming things of superstition.

Terry Pratchett, Witches Abroad

Danksagung

Als erstes Danke ich Prof. Dr. Jörg Sundermeyer, der es mir ermöglichte diese Arbeit in seinem Arbeitskreis anzufertigen und mir bei Fragen und Problemen immer zur Seite stand.

Ich möchte auch Prof. Dr. Eric Meggers für die Übernahme des Zweitgutachtens danken sowie Prof. Dr. Andreas Seubert für die Teilnahme an der Prüfungskommission.

Großer Dank geht auch an die Serviceabteilungen der Universität Marburg für die Durchführung von unzähligen Messungen. Besonderer Dank geht an Frau Xie für die Durchführung und Unterstützung der zahlreichen NMR Experimente.

Ein besonderer Dank gilt der Arbeitsgruppe Sundermeyer, besonders meinem Boxenpartner Eugen, der auch die Strukturlösungen meiner Kristalle übernommen hat. Danke an die Besucher des Chez Ambros: Igor, Morten, Olaf, Eugen und Kevin für die vielen Spieleabende. Auch dem restlichen und ehemaligen Arbeitskreismitgliedern: Marwa, Alex, Simon, Tobi, Marius K., Lisa, Subhankar und Ahmed sowie den zahlreichen Vertiefern will ich danken für den angenehmen und immer witzigen Laboralltag.

Schließlich möchte ich meiner Familie, insbesondere meinen Eltern, meinen herzlichen Dank für ihre unerschütterliche Unterstützung und Ermutigung aussprechen. Ihre ständige Motivation und ihr Glaube an mich waren eine treibende Kraft, und ich bin für ihre Präsenz in meinem Leben für immer dankbar.

Danke, dass ihr alle Teil dieser Reise mit mir wart!

Abbreviations

*t*Bu-ind	1-*tert*-butyl-indenyl
ad	Adamantyl
BIG	*N*-*N*'-bis(imidazolyl)guanidine
CAAC	Cyclic alkylaminocarbene
CDP	Carbodiphosphorane
COD	Cyclooctadien
CPCM	Conductor-like polarizable continuum model
cy	Cyclohexyl
DABCO	1,4-Diazabicyclo(2.2.2)octane
DACN	1,8-Bis(bis(diisopropylamino)cyclopropeniminyl)naphthalene
DBU	1,8-Diazabicyclo(5.4.0)undec-7-ene
DCM	Dichloromethane
DFT	Density functional theory
DIPEA	Diisopropylethylamine
Dipp	Di*iso*propylphenyl
DMA	Dimethylamine
DMAN	1,8-Bis(dimethylamino)naphthalene
DMAP	4-Dimethylaminopyridine
DME	Dimethoxyethane
DMF	Dimethylformamide
DMSO	Dimethylsulfoxide
eq	Equivalent
ESI	Electron spray ionisation
FT-ICR	Fourier-transform ion cyclotron resonance
GB	Gas phase basicity
HMPA	Hexamethylphosphorus acid trisamide
HOMO	Highest occupied molecular orbital

HPMS	High pressure mass spectrometry
HSAB	Hard and soft (Lewis) acids and bases
IAP	Pyridinylidenaminophosphines
IHB	Intramolecular hydrogen bonding
IMes	1,3-Dimesitylimidazol-2-ylidene
in vacuo	Under reduced pressure
IR	Infrared
IUPAC	International Union of Pure and Applied Chemistry
JohnPhos	(2-Biphenyl)di-*tert*-butylphosphine
KHMDS	Potassium hexamethyldisilazane
LDA	Lithium diisopropylamide
LIFDI	Liquid injection field desorption ionisation
LUMO	Lowest unoccupied molecular orbital
MeCN	Acetonitrile
MHPN	1,8-Bis(methanyliden(hexamethyltriamino)- phosphoranyl)naphthaline
MLEP	Metal ligand electronic parameter
MO	Molecular orbital
MS	Mass spectrometry
MTBD	7-Methyl-1,5,7-triazabicyclo(4.4.0)dec-5-ene
n/a	Not available
NAC	Nitrogen acyclic carbene
NHC	N-heterocyclic carbene
NHI	N-heterocyclic imine
NMR	Nuclear magnetic resonance
OLED	Organic light-emitting diode
PAP	Phosphazenylphosphines
PBE	Perdew–Burke-Ernzerhof
PEPPSI	Pyridine-enhanced precatalyst preparation stabilization
PMG	*N*,*N*,*N*',*N*',*N*"-Pentamethylguanidine
ppm	parts per million
pyrr	Pyrrolidine
SPhos	Dicyclohexyl(2',6'-dimethoxy[1,1'-biphenyl]-2-yl)phosphine
TBAF	Tetrabutylammoniumfluoride

TBD	1,5,7-Triazabicyclo(4.4.0)dec-5-en
TEP	Tolman electronic parameter
THF	Tetrahydrofuran
TMGN	1,8-Bis(tetramethylguanidino)naphthalene
TMS	Trimethylsilyl
tzvp	Triple-zeta valence polarization
UV-Vis	Ultraviolet–visible
VE	Valence electron
XRD	X-ray diffraction
YPhos	Ylide functionalized phosphines

List of compounds

Phosphazenes and precursors

$R^1 = NMe_2$	**1a**
R^1 = pyrr	**1b**
R^1 = cy	**1c**
R^1 = *t*Bu	**1d**

$R^1 = NMe_2$	**2a**
R^1 = pyrr	**2b**
R^1 = cy	**2c**
R^1 = *t*Bu	**2d**

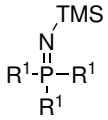

$R^1 = NMe_2$	**3a**
R^1 = pyrr	**3b**
R^1 = cy	**3c**
R^1 = *t*Bu	**3d**

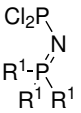

$R^1 = NMe_2$	**4a**
R^1 = pyrr	**4b**
R^1 = cy	**4c**
R^1 = *t*Bu	**4d**

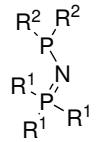

$R^1 = NMe_2$, R^2 = *t*Bu	**5a**
R^1 = pyrr, R^2 = *t*Bu	**5b**
R^1 = cy, R^2 = *t*Bu	**5c**
$R^1 = R^2$ = *t*Bu	**5d**
$R^1 = R^2 = NMe_2$	**5e**
$R^1 = R^2$ = Pyrr	**5f**

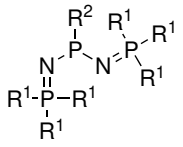

$R^1 = NMe_2$, R^2 = *t*Bu	**6a**
R^1 = pyrr, R^2 = *t*Bu	**6b**

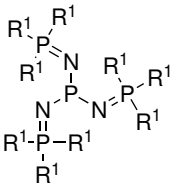

$R^1 = NMe_2$	**7a**
R^1 = pyrr	**7b**

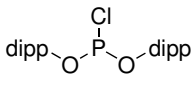

8

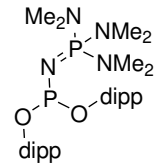

9

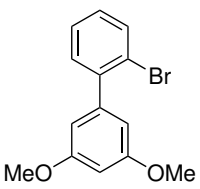

10

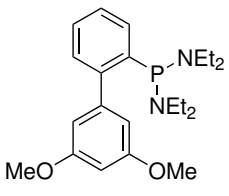

11

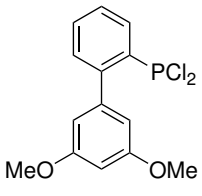

12

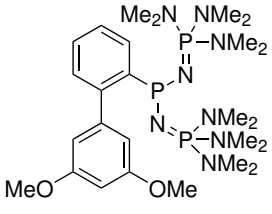

13

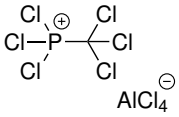

14

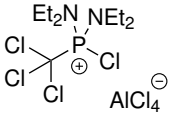

15

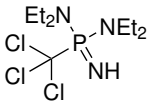

16

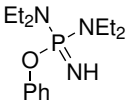

17

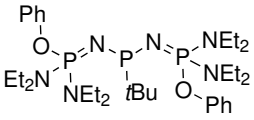

18

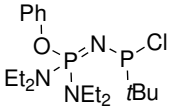

19

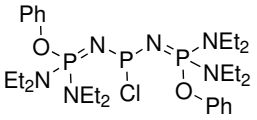

20

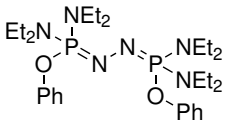

21

Selenides and nickel carbonyl complexes

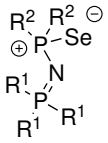

$R^1 = NMe_2$, $R^2 = t$Bu	**22a**
R^1 = pyrr, $R^2 = t$Bu	**22b**
R^1 = cy, $R^2 = t$Bu	**22c**
$R^1 = R^2 = t$Bu	**22d**
$R^1 = R^2 = NMe_2$	**22e**
$R^1 = R^2$ = pyrr	**22f**

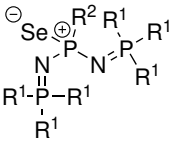

$R^1 = NMe_2$, $R^2 = t$Bu	**23a**
R^1 = pyrr, $R^2 = t$Bu	**23b**

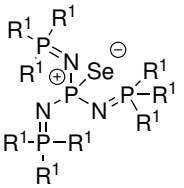

$R^1 = NMe_2$	**24a**
R^1 = pyrr	**24b**

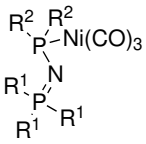

$R^1 = NMe_2$, $R^2 = t$Bu	**25a**
R^1 = pyrr, $R^2 = t$Bu	**25b**
R^1 = cy, $R^2 = t$Bu	**25c**
$R^1 = R^2 = t$Bu	**25d**
$R^1 = R^2 = NMe_2$	**25e**
$R^1 = R^2$ = Pyrr	**25f**

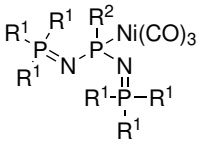

$R^1 = NMe_2$, $R^2 = t$Bu	**26a**
R^1 = pyrr, $R^2 = t$Bu	**26b**

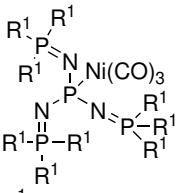

$R^1 = NMe_2$	**27a**
R^1 = pyrr	**27b**

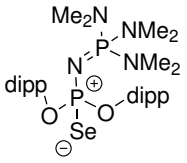

28

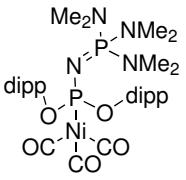

29

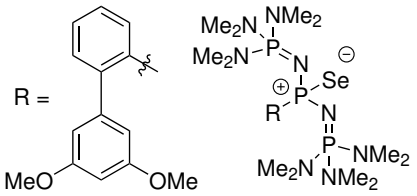

30

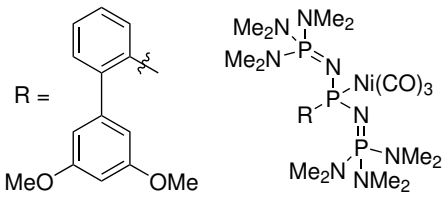

31

Gold and palladium complexes and CO_2 adducts

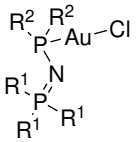

$R^1 = NMe_2$, $R^2 = t$Bu **32a**
R^1 = pyrr, $R^2 = t$Bu **32b**
R^1 = cy, $R^2 = t$Bu **32c**
$R^1 = R^2 = t$Bu **32d**

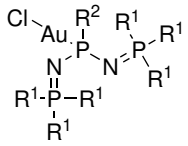

$R^1 = NMe_2$, $R^2 = t$Bu **33a**
R^1 = pyrr, $R^2 = t$Bu **33b**

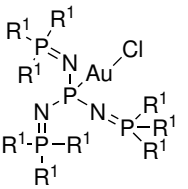

$R^1 = NMe_2$ **34a**
R^1 = pyrr **34b**

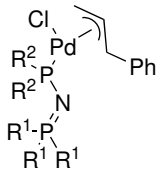

$R^1 = NMe_2$, $R^2 = t$Bu **35a**
R^1 = pyrr, $R^2 = t$Bu **35b**
R^1 = cy, $R^2 = t$Bu **35c**
$R^1 = R^2 = t$Bu **35d**

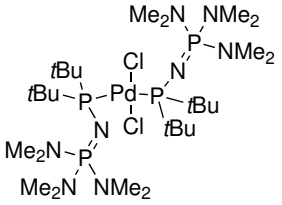

36

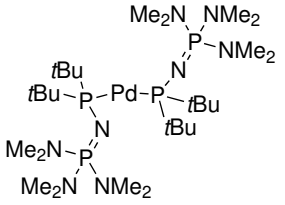

37

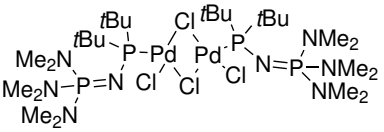

38

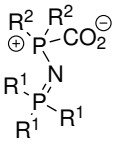

$R^1 = NMe_2$, $R^2 = t$Bu **39a**
R^1 = pyrr, $R^2 = t$Bu **39b**
R^1 = cy, $R^2 = t$Bu **39c**
$R^1 = R^2 = t$Bu **39d**

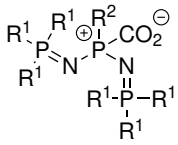

$R^1 = NMe_2$, $R^2 = t$Bu **40a**
R^1 = pyrr, $R^2 = t$Bu **40b**

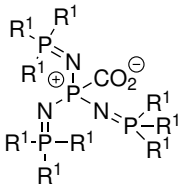

$R^1 = NMe_2$ **41a**
R^1 = pyrr **41b**

Contents

1 Introduction

1.1 Acids and Bases

The concept of acids and bases is fundamental to our understanding of modern chemistry and as such, it is one of the first concepts taught in the curriculum of most schools.[1] Traditionally S. Arrhenius is credited with the first modern definition of acid base theory for which he received the Nobel Prize in chemistry in 1903.[2–4] He defined an acid as a substance that dissociates in water to form hydrogen (H^+) ions (1) and a base a substance that dissociates in water to form hydroxide (OH^-) ions (2). Salts are the result of the neutralization reaction between an acid and a base (3) (Scheme 1.1).

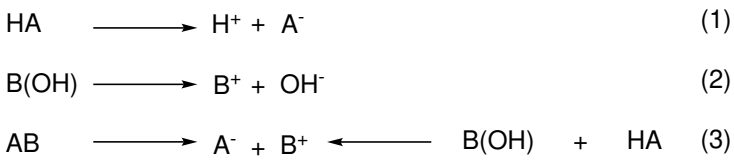

Scheme 1.1: Definition of acids (1), bases (2) and salts (3) according to Arrhenius.

This model is constricted only to aqueous solutions and substances that can release OH^- ions. To accommodate these issues,Brønsted and Lowry defined in 1923 an acid as a substance that can donate a proton and bases as substances that can accept a proton.[5,6] This definition can be applied to non-aqueous systems by the generation of corresponding conjugated acid base pairs (Scheme 1.2).

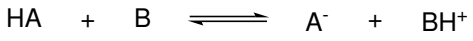

Scheme 1.2: Reaction of an acid (HA) and a base (B) to form the corresponding conjugate acid base pair (BH^+ and A^-).

Lewis proposed a different definition of acids and bases in the same year.[7] He defined acids as substances with empty orbitals capable of accepting an electron pair from a base and bases as donors of said electron pairs. Together, they form an acid-base adduct pair. Therefore, the Brønsted concept can be interpreted as a special case of the Lewis concept. Chemistry is the study of matter and the Arrhenius concept can be viewed with the matter (protons in aqueous media) as a focus, while Brønsted-Lowry and Lewis both fundamentally describe a process, the donation, or acceptance, of a proton or electron pair. Therefore, they can be seen as a process driven concept (Figure 1.1).[8]

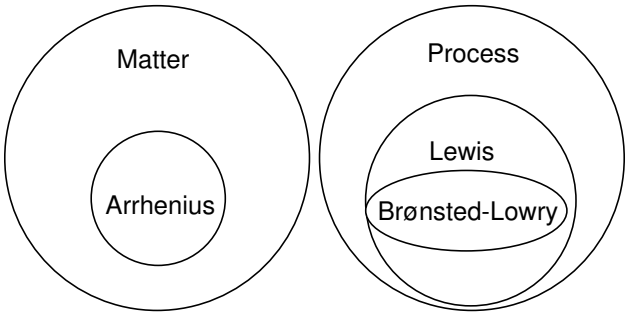

Figure 1.1: Relationship between different definitions of acid-base concepts.

An extension to these concepts is the HSAB (hard and soft acid and base) principle, popularized by Pearson in 1943.[9] He proposes a distinction between hard and soft acids and bases, where hard refers to small, highly charged and weakly polarizable species, while soft refers to big, low charged and easily polarizable species. Soft acids will form more stable bonds with other soft bases than they will with hard bases all other factors being equal. This means, that hard acids and bases will form more ionic bonds and soft acids and bases will form more covalent bonds. This concept can be useful for determining the strength of a Lewis acid-base adduct. Other methods for categorizing the relationship between acids and bases by Usanovich, Lux and Flood exist, but are limited by their niche applicability.[10–12]

1.1.1 Quantifying the Strength of Acids and Bases

In order to quantify the strength of Brønsted acids the pK_a value is typically utilized. It can be obtained by calculating the equilibrium constant K_a from the dissociation reaction of an acid into a proton and its conjugate base (Scheme 1.3).

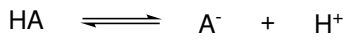

Scheme 1.3: Dissociation of an acid (HA) into a proton (H^+) and its conjugate base (A^-).

The equilibrium constant is defined as:[a]

$$K_a = \frac{[A^-][H^+]}{[HA]} \tag{1.1}$$

The pK_a value is defined as the negative decadic logarithm of this equilibrium constant:

$$pK_a = -\log K_a \tag{1.2}$$

It is related to the pH value with the following equation:

$$pH = pK_a + \frac{[A^-]}{[HA]} \tag{1.3}$$

[a] Brackets correspond to the molar concentrations of the substances.

The strength of bases is commonly defined by the pK_{BH^+} value which is the pK_a value of the conjugate acid. In principle it can be said, that the lower the pK_a value the stronger the acid and the higher the pK_{BH^+} value the stronger the base. Table 1.1 shows an overview of several acids and bases and their respective pK_a values in water.

Table 1.1: Overview of pK_a values of different substances in water.[13–15]

Entry	Compound	pK_a [H_2O]	Entry	Compound	pK_a [H_2O]
1	H_3PO_4	2.2	5	$PhNO_2H^+$	-12.4
2	*t*-BuOH	20	6	CF_3SO_3H	-14.7
3	HCN	9.1	7	$MeCNH^+$	-10.7
4	$PyrH^+$	5.2	8	HCl	-2.2

Experimentally, these values can be obtained by competition reaction of one reactant of known pK_a value and one reactant of unknown pK_a value (Scheme 1.4).

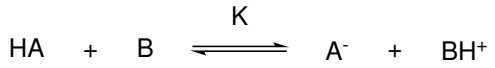

Scheme 1.4: Competition reaction between two reactants with equilibrium constant K.

In an equilibrium, the protochemical potentials of these two reactants are identical. Therefore, the equilibrium constant can be calculated and with it the pK_a value of the unknown reactant. Experimentally, the equilibrium constant can be determined by NMR spectroscopy[16], UV-Vis spectroscopy[17] or potentiometry[18] and the pK_a value of the unknown compound may be calculated according to equation 1.4. In order to guarantee the accuracy of these experimental methods, the pK_a value of the reference base should be within one pK_a unit of the unknown base.

$$pK_a = pK_a(ref) - \log K = pK_a(ref) - \log \frac{[A^-] * [BH^+]}{[HA] * [B]} \tag{1.4}$$

The scale in water begins to show its limitations when strong acids or bases are employed, because they will completely disassociate in water to form H_3O^+ or OH^- ions. It is not possible to differentiate among the relative strengths or weaknesses of stronger acids or bases than the solvents conjugate acid or base. This is called the leveling effect of water.[19] Self-consistent solvent scales have been adapted by the scientific community to alleviate this issue. Commonly used scales are DMSO[20], MeCN[21] and THF.[22] Because of intramolecular hydrogen bonding and other solvatisation effects, these scales can not be directly compared with each other. They can, however, be correlated if the solvents are comparable like THF and MeCN with values in MeCN being generally higher than in THF.[23]

1.1.2 Gas Phase Basicity and Proton Affinity of Bases

In order to assess the strengths of bases independent of solvent effects, the gas phase basicity and the proton affinities can be quantified. The gas phase basicity (GB) is calculated as the Gibbs free energy of the reaction:

$$B + H^+ \rightarrow BH^+$$

so that:

$$\Delta G = G_{(BH)} - [G_{(B)} + G_{(H^+)}] \tag{1.5}$$

Proton affinities can be calculated as the enthalpy of the aforementioned reaction.

$$PA = H_{(BH^+)} - [H_{(B)} + H_{(H^+)}] \tag{1.6}$$

The GB can be experimentally measured by Fourier-transform ion cyclotron resonance (FT-ICR) mass spectrometry of an analyte and a reference base (Scheme 1.5).[24,25]

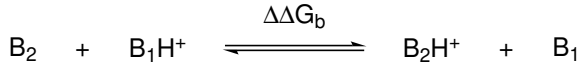

Scheme 1.5: Competition reaction between two bases in the gas phase.

With

$$\Delta\Delta G_b = \Delta G_b(B_2) - \Delta G_b(B_1) = -RT * \ln K \tag{1.7}$$

$$K = \frac{p(B_1) * I(B_2H^+)}{p(B_2) * I(B_1H^+)} \tag{1.8}$$

The ratio of the partial pressures of the neutral species can be measured by a pressure gauge and the mixture of the charged gases can be measured by comparing the intensities of the ions in the mass spectrum after a sufficient equilibrium has been reached.[24,25] Other methods such as high pressure mass spectrometry (HPMS) have also been successfully employed.[26]

1.2 Different Types of Bases

A preparative chemist performing a reaction requiring a base can choose between three different substance classes: a) Ionic metal bases such as NaOH, b) Organometallic bases such as *n*-BuLi and c) organic bases such as diisopropylethylamine (DIPEA). Ionic metal bases are convenient in their usage as they are usually cheap and easy to handle. NaOH for example is a byproduct of the generation of chlorine gas from the electrolysis of NaCl.[27] They perform reasonably well for most applications but have limited solubility in most common organic solvents such as THF and DCM, often resulting in heterogeneous reaction conditions.[28] Organometallic bases in contrast are very soluble in organic solvents, however they are also very reactive leading to a decrease in selectivity. *n*-BuLi for example will deprotonate THF at room temperature, releasing butane and ethylene as well as generating acetaldehyde. Reactions with *n*-BuLi in THF are therefore carried out at low temperatures.[29] They are often pyrophoric, which requires additional precautions, especially when used in large quantities. The third type of bases are organic bases with the simplest being substituted amines like the already mentioned DIPEA or triethylamine (NEt_3). They are versatile and easily soluble in most solvents but are limited in their applicability and have to be selected for a specific purpose. They can range from lightly basic amines to superbasic guanidines (Figure 1.2).[30]

Some organic bases are also prone to side reactions as they may react as nucleophiles, however this can be remedied by modifications on the amine backbone by increasing their steric hindrance and inhibiting nucleophilic attacks. Their nucleophilicity can also be exploited by employing them as nucleophilic catalysts instead of a base.[31] They are easily handled as they are not pyrophoric and easily removed from the reaction mixture by precipitation as a salt.

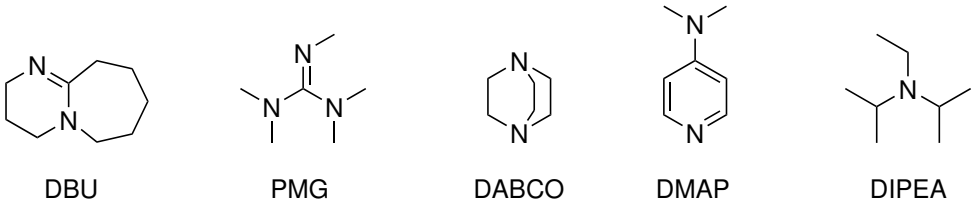

Figure 1.2: Overview of different organic amine and amidine bases.

1.3 Superbases

1.3.1 Definition of Superbases

The scientific community has not yet reached a consensus of what constitutes a superbase, though several attempts to define them have been made. Caubère applies the term superbases only to bases resulting from the mixing of two or more bases leading to a new species with inherently new properties. His definition does not mean that a base is thermodynamically or kinetically stronger than another base, it only means that the properties of the new basic species surpasses that of its parts.[32] Schlosser complements this by defining two types of superbases, Caubère's unimetal super bases and his own multimetal super bases (Scheme 1.6).[33] This definition generally is applied to ionic metal containing bases which react under irreversible proton abstraction.[30] IUPAC defines superbases as bases that possess a pK_{BH^+} value of LDA or higher.[34] Sundermeyer proposes a threshold in the gas phase of 237.8 kcal/mol (DMAN) and of a pK_{BH^+} value of 25 in MeCN or 17 in THF (based on the value for TMGN).[35,36] In this work we will use this definition going forward and pK_{BH^+} values will be, unless otherwise stated, given in MeCN.

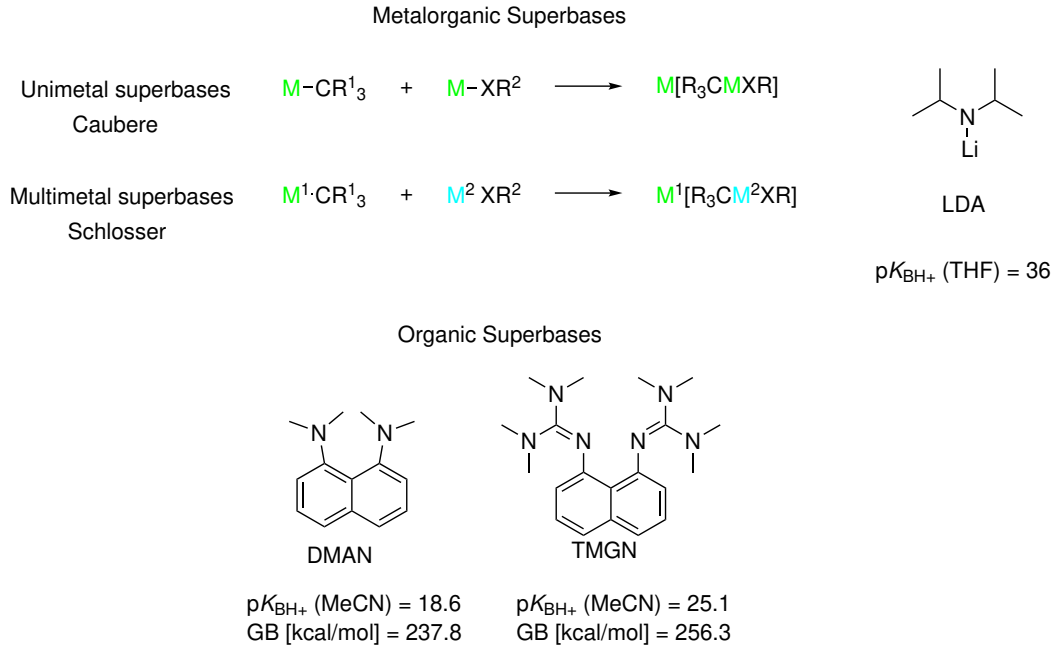

Scheme 1.6: Different definitions for superbases. Unimetal[32] and multimetal[33] superbases and LDA[37] (top) and structures of DMAN[38], TMGN[36] (bottom).

1.3.2 Nitrogen Superbases

1.3.2.1 Schwesinger Bases

Nitrogen centered superbases are the most commonly known and most established class of superbases. Schwesinger's phosphazene bases are the most readily commercially available representatives of this class of compounds. First introduced by Issleib in 1973 and later improved by Schwesinger these peralkylated (poly)iminophosphoranes are able to delocalize a positive charge over the whole of the phosphorus and nitrogen backbone.[39] They are referred to by a shortened notation $(R^1)P_x - R^2$ where R^1 is the substituent on the phosphazene core,

and R^2 is the substituent on the terminal imine group and X is the number of phosphorus atoms attached to phosphazenyl groups. The simplest of these bases (dma)P_1−Me was already synthesized by ISSLEIB and shows a remarkable pK_{BH^+} value of 27.6. SCHWESINGER improved upon this by substituting a *N*-*t*-butyl unit to the basic nitrogen site (Figure 1.3).[17] The increase of basicity by substitution of dimethylamino groups to pyrrolidino groups can be attributed to the higher electron density of the pyrrolidino nitrogen atom compared to the dimethylamino nitrogen. A more intense increase in basicity can be seen by the *battery cell* principle of SCHWESINGER. Each additional phosphazenyl unit increases the basicity by approximately 4 units, leading to the extremely basic (pyrr)P_5−*t*Bu with a pK_{BH^+} value of 46.9. SCHWESINGER remarks that including additional phosphazene units from (dma)P_5−*t*Bu to (dma)P_7−*t*Bu (not isolated) does not correspond to an increase in basicity, and indicates a levelling effect due to resonance saturation.[40] SCHWESINGER bases are not only remarkably basic, they are also easily stored as HBF_4 salts. As such, they are insensitive to oxidation and hydrolysis. They are also not prone to react as nucleophiles because of their bulky backbone, unlike other organic amidine bases such as DBU. However, due to their extreme basicity, it can be challenging to liberate the free bases from their HBF_4 salts. Another noteworthy aspect of these bases is, that through their big core, the resulting cations that are formed from protonation of these compounds are so large and sterically hindered, that it allows the generation of almost naked anions that are highly reactive.[41–43]

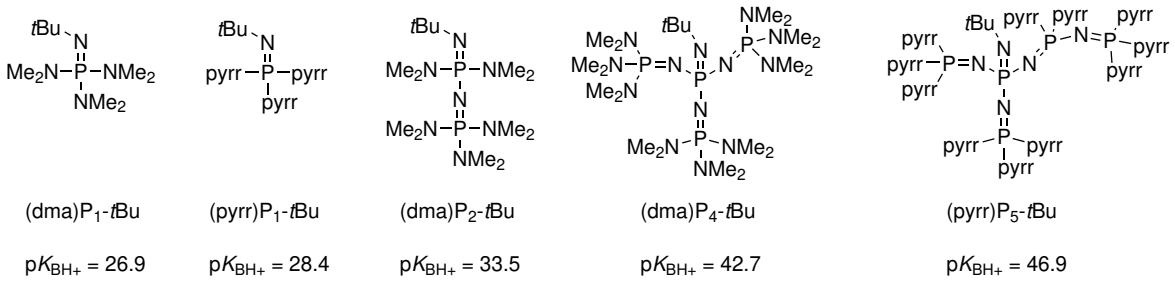

Figure 1.3: Overview of different SCHWESINGER bases (pK_{BH^+} values in MeCN).

The astounding basicity of SCHWESINGER bases comes mostly through its iminophosphorane units, which are inherently hypercoordinated phosphorus (V) compounds. Because of the octet rule, they are only able to form four bonds. Additional bonds have to be formed from negative hyperconjugation. If we look at the MO scheme of a trisubstituted phosphine, the HOMO represents the lone pair of the phosphorus atom which undergoes a covalent σ-bond with the substituent. This represents the zwitterionic structure of R_3P-X. Additionally, the antibonding π^* orbitals of the LUMO can bond with non-bonding p orbitals of the substituent, which corresponds to a formal double bond $R_3P{=}X$ (X = O, NR, CHR) (Figure 1.4). This double bond character is decreased with increasing σ- and π-donor ability of the substituent. If one compares the anionic charge of R_3P^+-NR'$^-$ and R_2C^+-NR'$^-$ (for R = Me and R' = Me) the anionic charge is less efficiently stabilized on the iminophosphorane, because it is only stabilized by negative hyperconjugation of the empty σ^*- or π^*-orbitals of the phosphonium ion. The iminium is, in contrast, stabilized by π-conjugation to the π-acceptor of the carbenium center. This means, that imines have inherently higher zwitterionic character than iminophosphoranes. If one substitutes the amino substituents on the iminophosphorane with further iminophosphorane groups however, the increase of σ- and π-donor ability of the substituent decreases the polarizability of the $R_3P{-}NR'$ bond and therefore decreases the double bond character. This leads to an increase in the zwitterionic character, which in turn

stabilizes the positively charged phosphonium ion, leading to a higher basicity. The double degenerate LUMO of 2e* symmetry (a linear combination of P-C σ*- and P 3d-orbitals) may act as an π-acceptor orbital for π-backbonding in complexes of the form $PR_3{-}M$.[44]

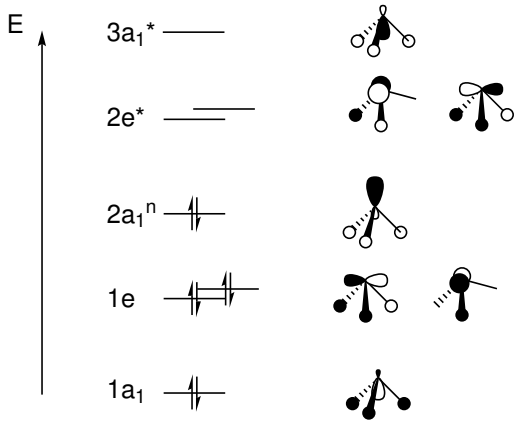

Figure 1.4: MO scheme of a -PR_3 fragment.[45]

Synthetically, SCHWESINGER's bases can be derived from two building blocks, both starting from PCl_5. By reaction of PCl_5 with gaseous Me_2NH in DCM a trisubstituted phosphonium chloride is generated which reacts with ammonia to yield the hydrochloride salt of the iminophosphorane (Scheme 1.7). Through subsequent deprotonation with KOMe in MeOH and distillation, the free iminophosphorane can be generated. The second building block PCl_3-N*t*Bu is generated by a condensation reaction of *t*-$BuNH_2$ with PCl_5. Combination of these two building blocks in THF and subsequent reaction with gaseous Me_2NH yields the hydrochloride (dma)P_2-*t*Bu · HCl. Another deprotonation step with KOMe in MeOH yields the final product.[17]

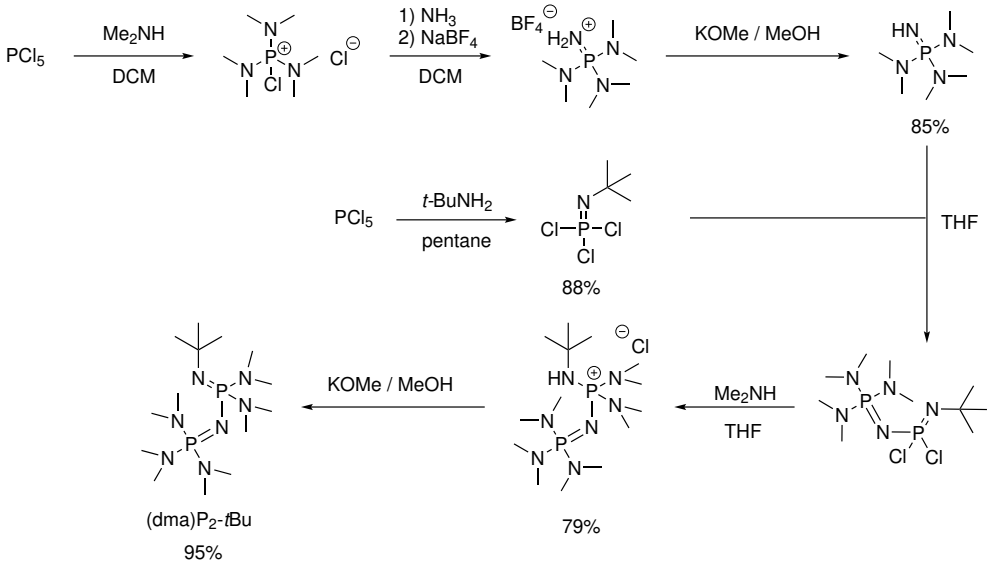

Scheme 1.7: Synthetic pathway to (dma)$P_2{-}t$Bu.

1.3.2.2 Guanidines, Amidines and Proton Sponges

Another popular structural feature of many superbases are guanidines. Their basicity can be traced due to their resonance stability of the three nitrogen core from their conjugate acids.[46–48] The most commonly known guanidine superbase is *N*,*N*,*N*',*N*',*N*"-pentamethylguanidine (PMG) with a pK_{BH^+} of 25.0 (Figure 1.5). Another example is 7-methyl-1,5,7-triazabicyclo(4.4.0)dec-5-ene (MTBD, pK_{BH^+} = 25.4) which, through its cyclic constraint, forces the two tertiary amino groups into conjugation with the imino basicity center. Proton sponges such as DMAN (1,8-bis(dimethylamino)naphthalene) have been known since 1968 when Alder first reported a huge increase in basicity through the methylation of 1,8-diaminonaphtalene. The basicity increased from a pK_{BH^+} of 6.4 to 12.3 (in water) for the final methylation step, which prompted an investigation into the nature of this phenomenon.[49] It was discovered, that the two basicity centers which are closely positioned near each other allow for an intramolecular exchange of protons. Additionally, the free base form of DMAN benefits from electronic repulsion of the nitrogen lone pairs which leads to a slight torsion of the naphtalene core and a subsequent reduction in its aromatic character. Through protonation this repulsion is removed, which makes it kinetically favored. Later on, Alder, Schwesinger and Verkade improved on this theory by a combination of steric strain, stronger intramolecular hydrogen bonding (IHB) or destabilization of the neutral molecule.[50–53] Through the implementation of a guanidine moiety, a proton sponge that can be considered a superbase was obtained in TMGN (pK_{BH^+} = 25.1) which outpaces planar amidines like DBU (pK_{BH^+} = 24.3).[36] Schwesinger's vinadimine type superbases outpace this by several orders of magnitude (pK_{BH^+} = 31.9) by forcing more nitrogen atoms into conjugation with the *N*-alkylimino functionality.[35] Variations of the TMGN proton sponge by substitution of the guanidine moiety with a phosphazene moiety lead to even higher basicities (pK_{BH^+} = 40.2).[54]

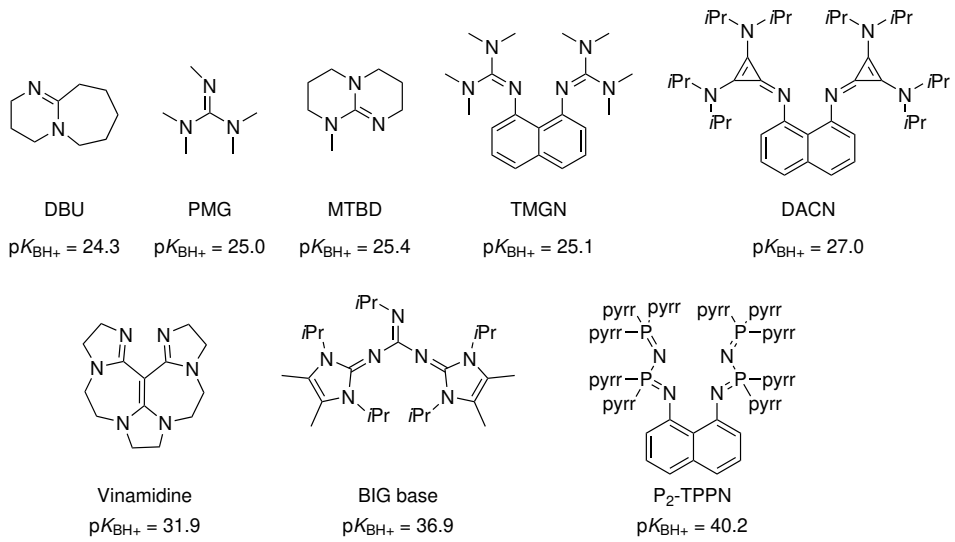

Figure 1.5: Overview of different superbases with guanidine, cyclopropenimine functions. (pK_{BH^+} in MeCN)

Proton sponges with a cyclopropenimine moiety have also been reported with basicities comparable to TMGN.[55] *N*,*N*'-bis(imidazolyl)guanidine bases (BIG bases) have also been reported that possess a fusion of guanidine and imidazol moieties. These bases are very large, which enable an efficient delocalization of the positive charge over the whole molecule, leading to

high basicities ($pK_{BH^+} = 36.9$).[56] DACN can be prepared by a simple two-step procedure by the reaction of four equivalents of diisopropylamine with one equivalent of tetrachlorocyclopropene followed by the addition of one equivalent of naphthalene-1,8-diamine to generate the hydrochloride salt (Scheme 1.8). This hydrochloride can be recrystallized and subsequently deprotonated with KHMDS in toluene to generate the free base DACN. Alternatively, the hydrochloride salt may be ion exchanged to the HBF_4 salt to allow for better storage, as the tetrafluoroborate is less hygroscopic.[57,58]

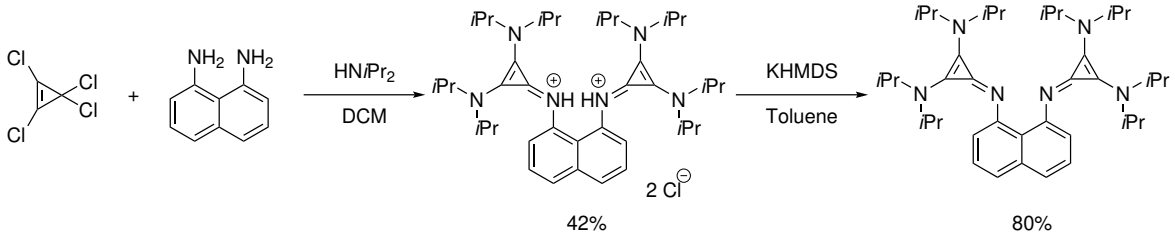

Scheme 1.8: Synthetic pathway to DACN starting from naphtalene-1,8-diamine and tetrachlorocyclopropene.

The guanidine proton sponge TMGN is prepared similarly. First, the VILSMEYER salt $(NMe_2)_2CCl$ has to be prepared from phosgene and tetramethylurea. Afterward, it is reacted with naphthalene-1,8-diamine to generate the hydrochloride salt of the bisguanidine (Scheme 1.9). This resulting solution is treated with aqueous NaOH to deprotonate and separate triethylammoniumchloride from the reaction mixture. The bisguanidinium hydrochloride can then be deprotonated and isolated by treatment with aqueous KOH (30 %), extraction with MeCN and washing with hexane.[36]

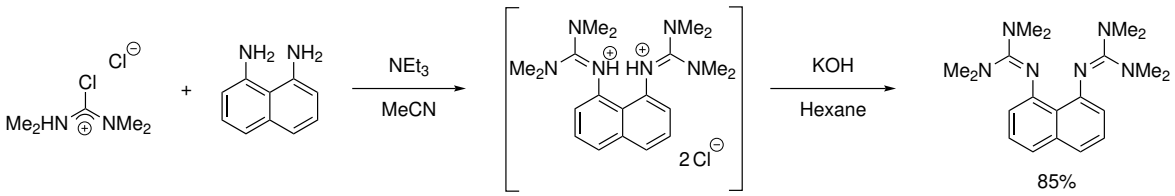

Scheme 1.9: Synthetic pathway to TMGN starting from naphtalene-1,8-diamine and $(NMe_2)_2CCl$.

For the preparation of BIG bases, *N*-alkylguanidinium iodides have to be prepared by reaction of an isothiouronium salt ($[MeS{-}C(NH_2)_2]I$) with the corresponding amine. These are then reacted with a 2-chloroimidazolium salt and KF in MeCN (Scheme 1.10). The resulting salt is subsequently treated with aqueous $NaBF_4$ to isolate the tetrafluoroborate salt. By treatment with KO*t*Bu the free base form can be generated.[56]

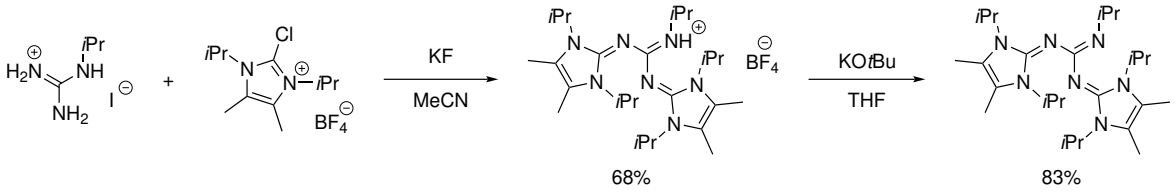

Scheme 1.10: Synthetic pathway to *i*Pr-BIG from $[MeS{-}C(NH_2)_2]I$ and 2-chloro-1,3-diisopropylimidazolium tetrafluoroborate.

1.3.3 Carbon Superbases

Molecules with a carbon atom as a basicity center like *N*-heterocyclic carbenes (NHC), P-ylide substituted phosphines (YPhos)[59] and carbodiphosphoranes (CDP) have been established mostly as strong donor ligands for various applications such as gold catalyzed aminations of alkynes[60] and palladium catalyzed[59,61,62] cross couplings or their usage as chelating ligands for OLED emitters (Figure 1.6).[63]

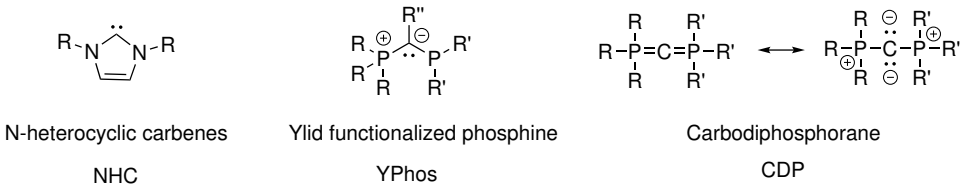

Figure 1.6: Different superbases with a carbon as basicity center.

Since the inception of CDPs by Ramirez *et al.* in 1961 with the synthesis of hexaphenylcarbodiphosphoran[64] (Ph_6-CDP) and subsequent synthesis of Me_6-CDP[65] and dma_6-CDP[66] the chemistry of CDPs grew in focus of the scientific community. Frenking describes the bonding situation of CDPs as "divalent carbon(0) compounds in which the valence electrons of carbon remain as two lone pairs of electrons".[67] In 2015 Leito *et al.* postulated a theoretical gas phase basicity of 350 kcal/mol for guanidino phosphorus carbenes.[68] This prompted an investigation to apply Schwesinger's *battery cell* principle to CDPs. In 2019 Ullrich *et al.* succeeded in synthesizing the to date strongest CDP bases $(pyrr)_6$-CDP and $sym(tmg)_2(dma)_4$-CDP (Figure 1.7) with a GB of 282.2 kcal/mol and 287.2 kcal/mol for the first protonation step respectively.[69] Ylidic basicity centers were also applied to the concept of proton sponges. 1,8-Bis(methanyliden(hexamethyltriamino)- phosphoranyl)naphthaline (MHPN) was synthesized and possesses a GB of 277.8 kcal/mol and a pK_{BH^+} of 33.2. The theoretical analogue P_2-MHPN exhibits a GB of 294.7 kcal/mol, but was not yet isolated.[70] Gessner's ylide substituted phosphines have not been thoroughly investigated about their basic properties. The spotlight for these compounds lies more in their ability to effectively donate electron density in a ligand role. They have excelled in this role in various applications and surpass NHCs and classical tertiary phosphines.[71–73]

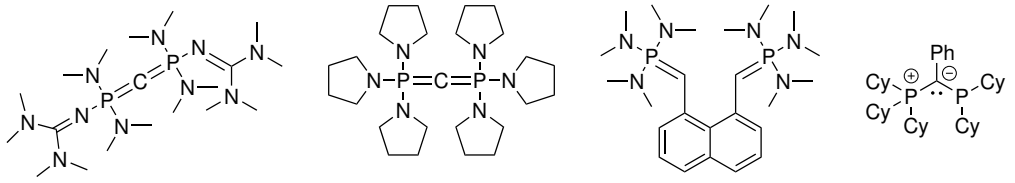

Figure 1.7: Overview of different carbon superbases (pK_{BH^+} in MeCN).[69–71]

Synthetically, these superbasic CDPs are prepared according to a modified procedure first published by Appel for the synthesis of dma_6-CDP.[66] The synthesis of bis(di(pyrrolidin-1-yl)phosphaneyl)methane (Scheme 1.11) was accomplished in a one pot reaction from one equivalent of bis(dichlorophosphino)methane with eight equivalents of pyrrolidine. This compound is unstable toward vacuum distillation and was therefore used without further purification in an oxidative imination with CCl_4 and three more equivalents of pyrrolidine. Afterward, the resulting hydrochloride was transformed to its HBF_4 salt. Deprotonation was accomplished by reaction with KHMDS in THF. For the bisylidic proton sponge MHPN, first 1,8-bis(bromomethyl)naphthalene was reacted with two equivalents of tris(dimethylamino)-phosphine to generate the hydrobromide salt of the bisylide. Through deprotonation with benzyl potassium in THF the bisylide MHPN could be generated. Gessner's YPhos ligands are generated from commonly available alkylphosphonium bromides by deprotonation with a metal base such as *n*-BuLi and subsequent reaction with a dialkylchlorophosphine. This bisylide can then be deprotonated by KO*t*Bu to generate the ylide substituted phosphine.

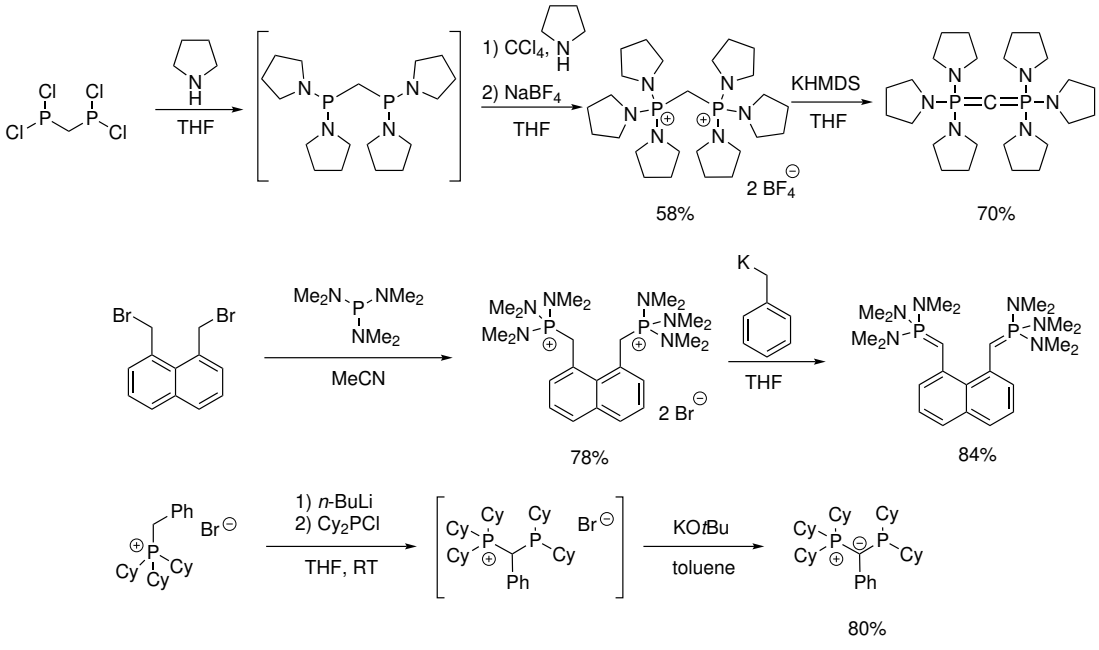

Scheme 1.11: Synthetic pathway to $pyrr_6$-CDP[69], MHPN[70] and joYPhos.[71]

1.3.4 Phosphorus Superbases

The earliest representatives of superbases, where the phosphorus atom acts as the basicity center, are VERKADE's proazaphosphatranes.[74] Originally intended as double ended ligands for connecting metal species *via* the bridgehead atoms, they found considerable success in the field of organocatalysis.[75] They are bicyclic, non-ionic bases which, when protonated are stabilized by a *trans*-annular PN bond formation as well as through negative hyperconjugation of the NR groups (Figure 1.8). These bases are stronger than P_1 phosphazenes with pK_{BH^+} values of 33.3 but weaker than P_2 phosphazenes.[76] This *trans*-annular PN bond formation can be observed by comparing the NMR spectra of the free base and its protonated counterpart. While in the free base no axial $^3J_{(P,H)}$ $PNCH_2$ coupling is observed in the ^{1}H-NMR, it is clearly visible with a coupling constant of 4.7 *Hz* in the protonated form. Similar observations can be made for the $^2J_{(P,C)}$ coupling constant of $PN_{ax}C$ of 6.7 *Hz*.[74] Iminophosphoranes of VERKADE's proazaphosphatranes also exist, but exhibit a considerably lower pK_{BH^+} of 29.0.[77] VERKADE also reports the synthesis of an analogue of P*t*Bu$_3$ where one *tert*-butyl substituent was replaced by a proazaphosphatrane.[b] The resulting phosphines are very electron rich and can be utilized as ligands for palladium catalyzed cross coupling reactions.[79,80] DIELMANN and coworkers recently published the synthesis of a series of pyridinylidenaminophosphines (IAP).[81] They approach, not from a desire to design superbasic compounds, but from the viewpoint of designing highly electron rich donor ligands for various applications. They offer cheap and simple synthetic routes (Scheme 1.8) with an easily tune-able selection of R substituents at the pyridine *N*-atom as well as offer different degrees of substitution at the central phosphorus atom. In 2022, they were able to synthesize the previously elusive tris(tetramethylguanidinyl)phosphine (P(tmg)$_3$) which possesses a pK_{BH^+} of 32.7.[82] They also report the synthesis of dialkyl(1,3-diarylimidazolin-2-ylidenamino)phosphines that possess an aromatic backbone similar to BUCHWALD's famous phosphine ligands.[83,84] ULLRICH *et al.* reported the synthesis of the to date strongest uncharged phosphorus bases with trisphosphazenyl phosphines.[85,86] They are derived from SCHWESINGER's phosphazene bases but have undergone a formal reductive elimination of a nitrene.

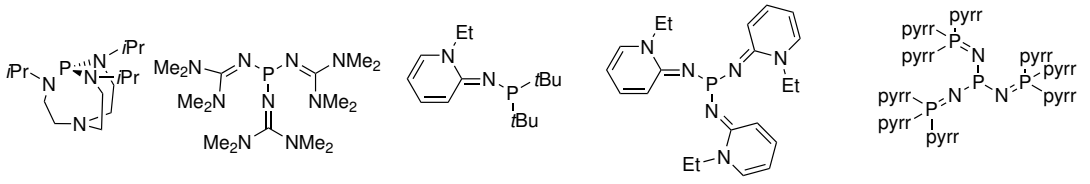

Figure 1.8: Proazaphosphatrane (left), Pyridinylidenaminophosphines, tristetramethylguanidinylphosphine (middle) and trisphosphazenylphosphines (right).

[b] For more information about VERKADE bases consult these excellent reviews.[75,78]

These phosphazenyl phosphines (PAP) are even stronger than SCHWESINGER's phosphazene bases with the same number of phosphorus atoms, as was previously theoretically predicted.[87] With a pK_{BH^+} value of 37.2 in THF, dmaP_4P is one of the strongest uncharged superbases, closely followed by dmaP_3P with a pK_{BH^+} value of 34.9 (Corresponding to 43.1 in MeCN for dmaP_3P and 45.6 for the asymmetric dmaP_4P).[23] Synthetically, VERKADE's proazaphosphatranes are prepared by reaction of an alkylaldehyde with *N*',*N*'-bis(2-aminoethyl)ethane-1,2-diamine and subsequent reduction of the intermediate aldimine with $NaBH_4$ (Scheme 1.12). The ring closure was achieved by reaction with $PCl(NMe_2)_2$ to afford the hydrochloride salt. The free base can be liberated by reaction with KO*t*Bu.[88]

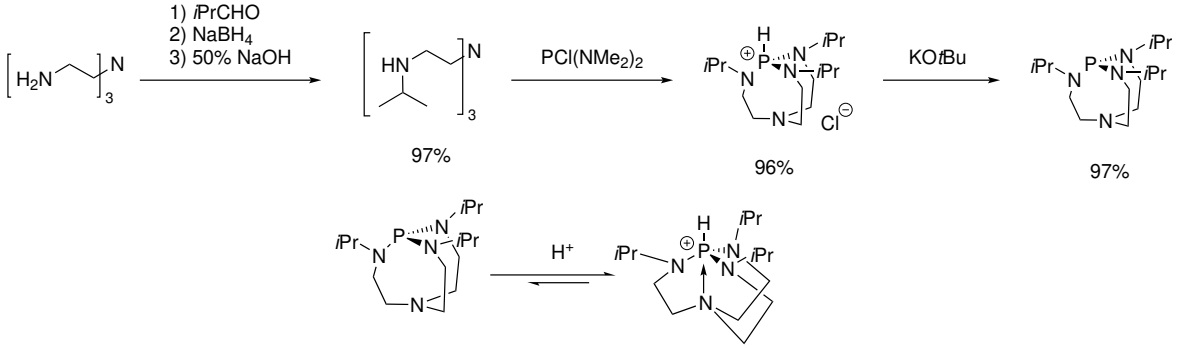

Scheme 1.12: Synthetic pathway to a proazaphosphatrane (top) and *trans*-annular P-N bonding (bottom).[88]

Trisphosphazenyl phosphines are prepared similarly. $PCl(NEt_2)_2$ reacts with an iminophosphorane to generate the trisubstituted hydrochloride $P_3P \cdot HCl$ which is converted to its HBF_4 salt with $NaBF_4$ (Scheme 1.13). $PCl(NEt_2)_2$ is used as both an auxiliary base as well as the phosphorus source for this reaction. Liberation of the free base by deprotonation with KHMDS yields the final PAP in 88% yield. VERKADE's proazaphosphatrane phosphines are synthesized by KIRSANOV reaction with iodide to generate the phosphonium iodide and subsequent reaction with ammonia to the iminophosphorane. Deprotonation and reaction with a chlorophosphine generates the final phosphine.[85] DIELMANN's IAP can be synthesized by alkylation of the aminopyridine and subsequent reaction with a chlorophosphine to generate monoIAPs. TrisIAPs are prepared by reaction of the aminopyridine with PCl_3 and subsequent generation of the IAP-HBF_4 salt (Scheme 1.14, top). Deprotonation with KHMDS results in the free base IAP. Trisubstituted $P(tmg)_3$ was prepared by a mixture of tmg-H, PCl_3 and $P(NMe_2)_3$ in a 3:2:1 ratio. This generates $PCl(NMe_2)_2$ *in situ*, which acts as both an auxiliary base and the phosphorus source and yields the hydrochloride $P(tmg)_3 \cdot HCl$ in quantitative yield (Scheme 1.14, bottom). Subsequent deprotonation with KHMDS yields the free base.[82]

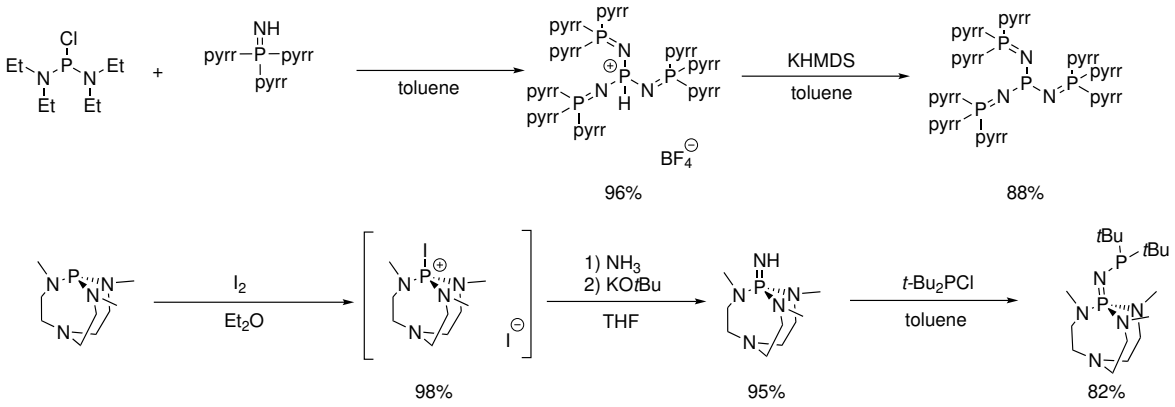

Scheme 1.13: Synthetic pathway to a tris(phosphazenyl)phosphine pyrrP_3P[85] (top) and a proazaphosphatrane phosphine (bottom).[79]

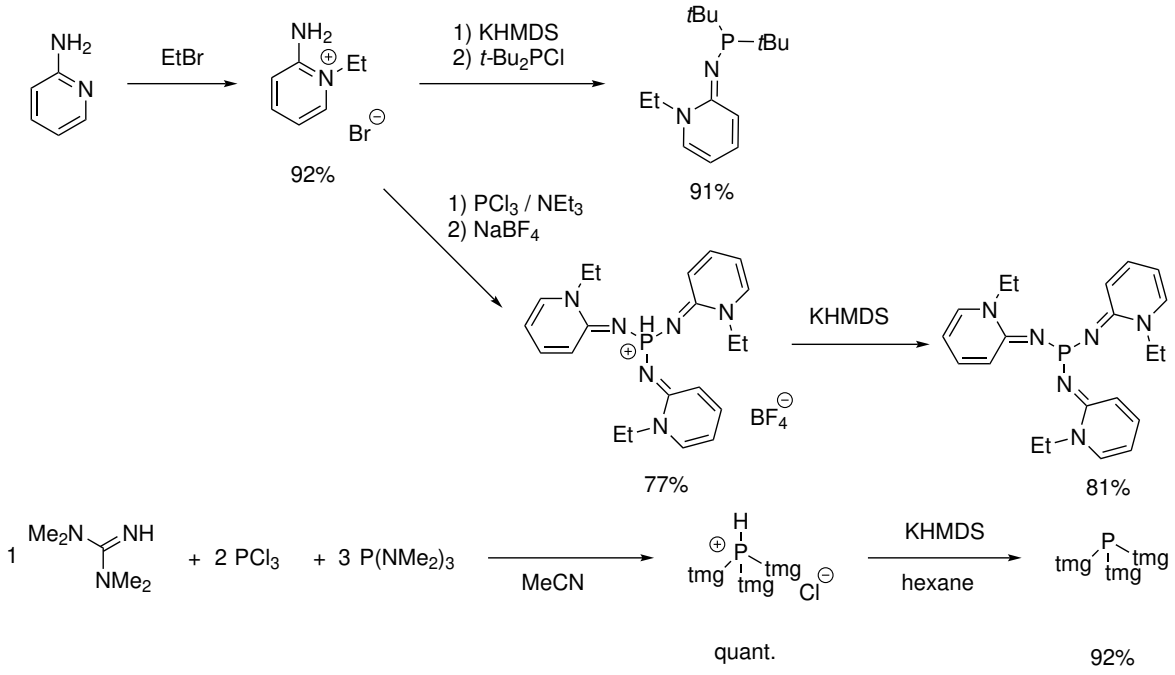

Scheme 1.14: Synthetic pathway to a mono- and trisIAP[81] (top) and $P(tmg)_3$ (bottom).[82]

1.4 Measuring Donor Abilities of Ligands

Basicity is only one aspect of a molecule's properties, and there are other quantifiable parameters that can be considered. Phosphines especially have been utilized mostly as ligands for transition metal catalysis and as such several metrics to measure and compare these compounds have been developed. The Tolman electronic parameter (TEP) describes the donor-acceptor ability of a ligand as a measure of the A_1 vibrational mode of the carbonyl bond of a tetrahedral complex of the form [L−Ni(CO)$_3$] (Figure 1.9).[89,90] The shift in the frequency of this vibrational mode upon coordination from free CO to [L−Ni(CO)$_3$] can be explained by π-backbonding from the ligand to the metal. The metal forms a π bond by donating electron density from its d-orbitals into the anti-bonding π^* orbital of CO. This

strengthens the metal-carbonyl bond and thus weakens the carbon-oxygen bond. Therefore, less energy is needed to excite the A_1 vibrational mode, thus decreasing the frequency. If the electron density on the metal is increased through σ-donation from a ligand, this density is transferred into the antibonding π^*(CO) orbitals, thus increasing the CO bond length and decreasing the CO stretching mode even more. If the electron density is decreased by ligands acting as competing π-backdonors to CO, the frequency of the A_1 vibrational mode is increased instead.

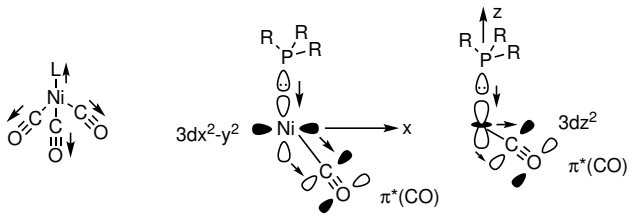

Figure 1.9: A_1 vibrational mode (left) and an example of σ-donation of a ligand.

The TEP does, however, have its limitations.[c] Some compounds won't form a tetraedral [L−Ni(CO)$_3$] complex and as such cannot be directly compared. Additionally, because of the extremely high toxicity of nickel carbonyls alternatives have been sought out. For NHCs there have been TEP analogues with complexes of the type [L−M(CO)$_2$Cl] for M = Rh, Ir.[92] Huynh proposed a ligand electronic parameter based on ^{13}C-NMR chemical shifts for NHC complexes of palladium (II).[93,94] Bertrand utilizes the ^{31}P-NMR chemical shifts of carbene-phosphinidine adducts as an indicator instead.[95] Ganter utilizes the chemical shift of ^{77}Se-NMR in NHC-Se adducts, as well as the $^1J_{(C,Se)}$ coupling constants of azolium selenide salts.[96,97] The TEP also suffers from inconsistencies because of mode-mode coupling between M-C and CO vibrations that can range up to 200 cm^{-1}[98] and because the electronic bonding mechanism is more complicated than described by Tolman[d].[90] Nonetheless, the TEP is a popular parameter because it is easily measured and gives a good approximation of donor abilities, although it is often coupled with other methods. Similarly to NHCs, selenides of phosphines are easily obtainable by reaction of the free phosphine with gray selenium. The resulting $^1J_{(P,Se)}$ coupling constants as well as the chemical shifts of the ^{31}P-NMR and ^{77}Se-NMR can be used to determine the donor ability of ligands. The $^1J_{(P,Se)}$ coupling constant is mostly influenced by the s-character of the phosphorus selenium bond, which can be correlated to the electronic properties of the phosphine.[100] Electron withdrawing groups increase the s-character of the phosphorus lone pair, therefore increasing the coupling constant according to Bent's rule.[101] Electron rich groups in turn, decrease the coupling constant.[102] This correlation is not without faults, as increased sterical hindrance on the phosphorus atom may also result in a decrease of s-character of the lone pair.[103,104] Additionally, it is known that intramolecular hydrogen bonding may affect the coupling constant and bulky aryl substituents on phosphorus atoms have been known to cause an increase in $^1J_{(P,Se)}$ coupling constants that do not necessarily correlate with its electronic properties.[105–107] Sterical properties of ligands can be described by the cone angle θ of a ligand, originally described by Tolman for nickel phosphine complexes.[89] The cone angle is the apex angle of a cylindrical cone

[c] For an excellent review of electronic properties of NHCs and the limitations of the TEP consult these references.[91]

[d] Recently the introduction of the metal ligand electronic parameter (MLEP) has been popularized as far infrared spectroscopy becomes more available. This parameter derives from the M-L vibrational mode. For further information, consult the following review.[99]

centered 2.28 Å from the center of the phosphorus atom which touches the van-der-Waals radii of the outermost atoms.[90] It is, however, limited by the restriction of the M-L bond length being fixed at 2.28 Å and inaccuracies occur for non-phosphine or asymmetric ligands. Closely related is the solid angle ω, which can be described as a measure of the 'shadow' cast by an atom or group of atoms when placed relative to an apex atom, 'a light source'.[108] They are not bound by a fixed L-M bond length and can be calculated from a crystal or a computationally generated structure. The disadvantage of the solid angle approach is, that it treats the ligand as 'frozen', which induces inaccuracies, as ligands are often able to almost freely rotate along low rotational barriers.[109,110] Another metric that can be calculated is the percent of buried volume of a ligand in a transition metal complex, which can be described as the amount of space occupied by a ligand inside a sphere of a predefined radius (3.5 Å for this work) centered on the metal atom. This can be useful for the determination of catalytic pockets and the generation of space mapping for ligands.[111,112]

1.5 Applications of Organic Superbases

Organic superbases can be utilized in a variety of ways. In this section we will examine a host of examples that can be categorized broadly in stochiometric transformations, where the base is employed in a quantity of at least 1.0 equivalents as a base or a nucleophile (Section 1.5.1), catalytic transformations, where the base is employed in substochiometric quantities (Section 1.5.2) and applications where the base is employed as a ligand for transition metal catalyzed reactions (Section 1.5.3).[e]

1.5.1 Stochiometric Transformations

Phosphazene bases have been utilized in stochiometric application for the synthesis of C-annelated pyrroles from unreactive nitroquinolines (Scheme 1.15). The usage of a phosphazene base was imperative for these transformations, as DBU did not yield the desired product. This is achieved by deprotonation of an isocyanoacetate ester, which attacks the nitroarene. Intramolecular nucleophilic attacks on the terminal carbon of the isocyano group generates the five membered ring. Through 1,2-elimination of the nitro group, the product is generated.[114]

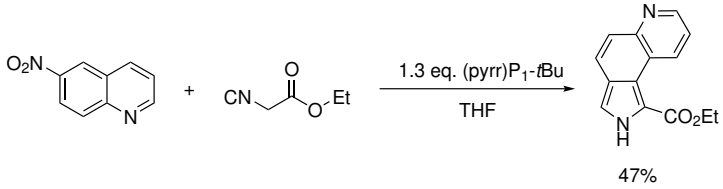

Scheme 1.15: Alkylation of 6-nitroquinoline with ethyl isocyanoacetate.[114]

They are also able to couple aryl iodides with thiophenols with a catalytic amount of CuBr in an Ullmann coupling to biarylthioethers (Scheme 1.16). The generation of a 'naked' thiol anion by deprotonation is a key step in this transformation. While DBU was also used successfully for these transformations it did perform worse, while other bases such as triethylamine and *N*,*N*-dimethylaminopyridine did not produce the desired product. Aryl

[e]For an overview over different usages of various superbases consult the following book [113].

chlorides did not react, and aryl bromides were only able to couple while bearing electron withdrawing groups on the aryl core.[42]

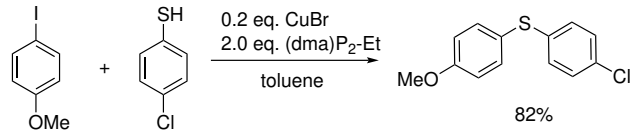

Scheme 1.16: Nucleophilic aromatic substitution reaction between 1-iodo-4-methoxybenzene and 4-chlorobenzenethiol.[42]

Amidines like DBU as well as guanidines like MTBD can be utilized for the base promoted addition of chloroform to benzaldehyde (Scheme 1.17). It can be applied to a range of aromatic and aliphatic aldehydes and ketones, but large aldehydes like mesitylaldehyde may hinder the reaction.[115]

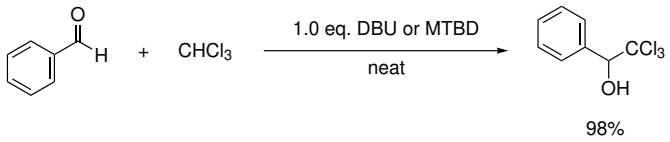

Scheme 1.17: Base promoted addition of chloroform to benzaldehyde.[115]

Schwesinger's P_4-*t*Bu base allows for the Julia-Kocienski olefination reaction in one pot between alkyl 3,5-bis(trifluoromethyl)phenylsulfones and aldehydes with excellent stereoselectivities (Scheme 1.18). It surpasses the performance of traditional bases like KHMDS and KOH in both yield and selectivity.[116]

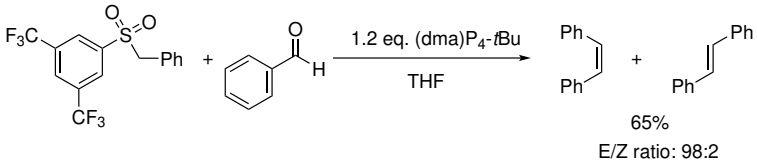

Scheme 1.18: Julia-Kocienski olefination reaction between 1-(benzylsulfonyl)-3,5-bis(trifluoromethyl)benzene and benzaldehyde.[116]

Dielmann *et al.* recently published a one pot method for the degradation of SF_6 into non-volatile solids by reaction with a superbasic IAP (Scheme 1.19, top). Depending on the basicity of the utilized IAP, either an ionic IAP−SF_5 salt or complete degradation into a mixture of phosphine sulfides and difluorophosphines is reported.[117] Shibata *et al.* were able to utilize Schwesinger's P_4-*t*Bu base to deprotonate fluoroform (CHF_3) and react the resulting trifluoromethyl anion with carbonyl compounds (Scheme 1.19, bottom).[43] This is accomplished through the highly active 'naked' CF_3 anion that is generated by deprotonation. Weaker bases like DBU, TMG and P_1-*t*Bu were not strong enough for this transformation.

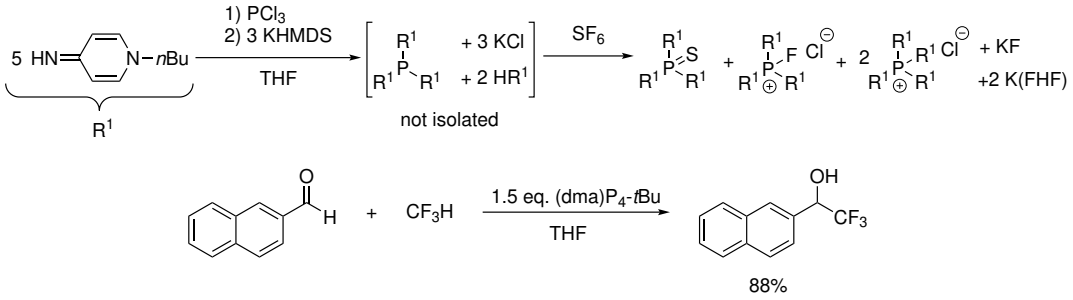

Scheme 1.19: Synthesis of superbasic IAP and subsequent degradation of SF_6[117] (top) and P_4-*t*Bu mediated trifluoromethylation of 2-naphthaldehyde (bottom).[43]

1.5.2 Organocatalytic Applications

Catalytically, Schwesinger's phosphazene bases have been employed in a number of transformations. For example, a nucleophilic substitution reaction between difluoroalkenes and ketene silyl acetals has been performed with excellent yields and selectivities.[118] (Scheme 1.20, top) With catalytic loads of 10 mol%, it outperformed both TBAF as well as Verkade's proazaphosphatrane bases. The functionalization of aryltrimethylsilanes with aldehydes with the use of P_4-*t*Bu has also been reported (Scheme 1.20, middle).[119] It is interesting to note, that weaker bases like DBU and P_2-*t*Bu did not show any conversion, suggesting that the extreme basicity of P_4-*t*Bu is imperative for this reaction. The superbase acts as a nucleophile in this reaction by abstracting the TMS group. Bae *et al.* published a thia-Michael addition of alkenyl sulfonyl fluorides with thiols catalyzed by P_4-*t*Bu with an impressive catalyst loading of only 0.01 to 0.5 mol% (Scheme 1.20, bottom).[120] The authors state, that the reaction shows almost no reactivity in organic solvents such as THF, but by utilizing a mixture of THF and brine the yield is increased to almost quantitative quantities. They attribute this to hydrophobic hydration of the components, where the reaction takes place in a hydrophobic pocket surrounded by a highly polar aqueous $H_2O \cdot NaCl$ sphere.[121,122]

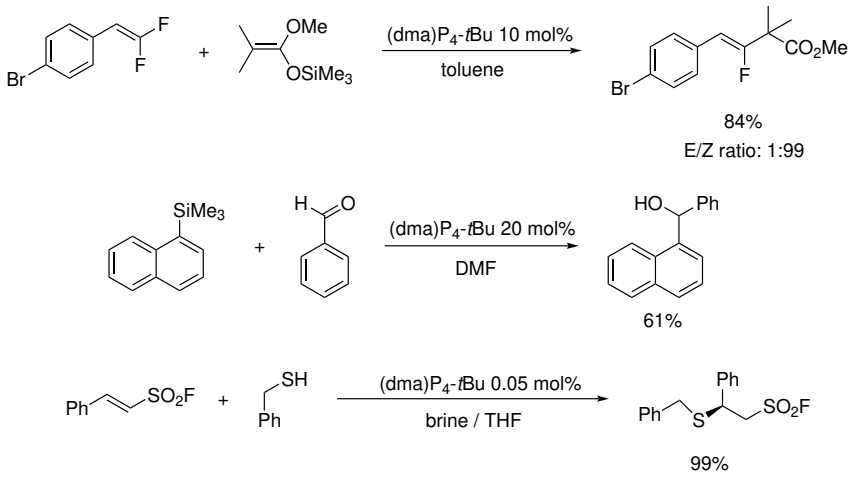

Scheme 1.20: Nucleophilic substitution of difluoroalkenes with ketene silyl acetals (top),[118] desilylation reaction of aryltrimethylsilanes with aldehydes (middle)[119] and thia-michael addition of alkenyl sulfonyl fluorides with phenylmethanthiol.[120] (bottom)

Terada *et al.* reports the Aza-Henry reaction of ketimines using guanidine as well as phosphazene bases (Scheme 1.21, top). The addition of nitromethane to *N*-phosphinoyl ketimines is achieved by addition of 10 mol% of base. They report, that TMG, P_1-*t*Bu as well as MTBD achieve good results.[123] Pollini *et al.* report the addition of primary nitroalkanes to aldehydes and ketones with the help of catalytic amounts of TMG (Scheme 1.21, middle).[124] They also reported the TMG catalyzed addition of dialkylphosphites to alkenenitriles, aldehydes and ketones (Scheme 1.21, bottom). These phosphonates can be used as intermediates for their application in the Wadsworth-Emmons reaction.[125]

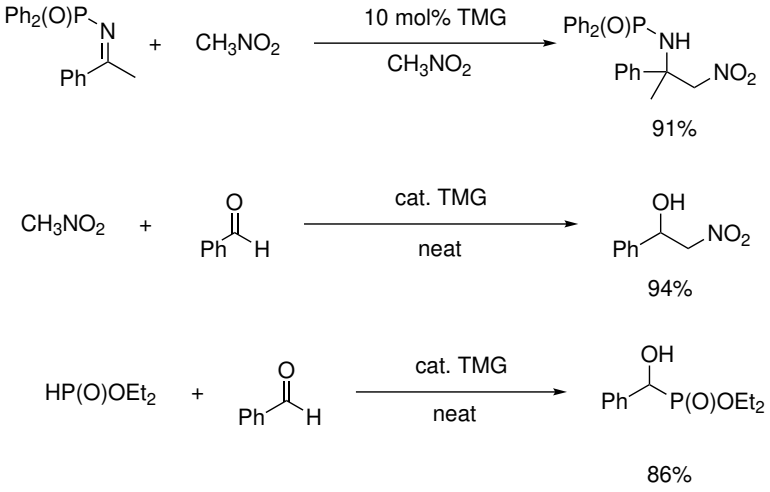

Scheme 1.21: Aza-Henry reaction of ketimines (top)[123], reaction of nitromethane with aldehydes (middle)[124] and addition of nitromethane to diethylphosphite (bottom).[125]

Verkade reports the base catalyzed reaction of aldehydes with allyltrimethylsilanes to yield homoallylic alcohols (Scheme 1.22, top).[126] They suggest, that the reaction proceeds by coordination of the base with allyltrimethylsilane to form an anionic allyl and Base-TMS. An attack on the carbonyl yields an anionic allylalcohol which in turn attacks the TMS group located on the base, regenerating it. A subsequent aqueous workup liberates the desired allyl alcohol. Similarly, they report the trimethylsilylcyanation of aldehydes with 10 mol% of base which proceeds similarly.[127] First abstraction of the TMS group onto the base and generation of an anionic species and subsequent attack on the carbonyl compound (Scheme 1.22, bottom).

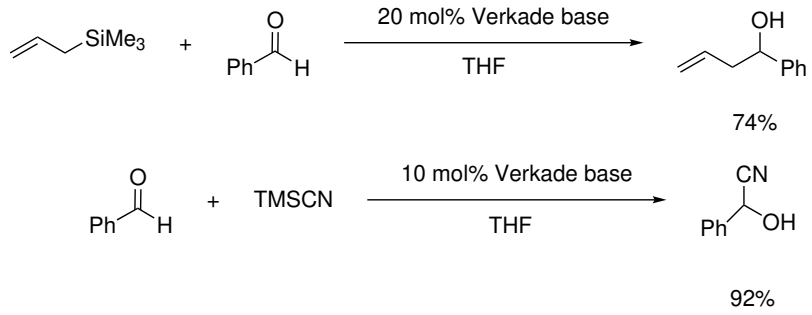

Scheme 1.22: Reaction of proazaphosphatrane catalyzed reaction of allyltrimethylsilane with benzaldehyde (top)[126] and reaction of trimethylsilylcyanide with benzaldehyde (bottom).[127]

1.5.3 Applications as Ligands for Transition Metal Catalysis

Another field of applications for superbasic compounds, especially for phosphines and carbenes, is their usage as ligands for transition metal catalysis. Verkade reported the usage of their proazaphosphatrane phosphines in palladium catalyzed C-C and C-N coupling reactions (Scheme 1.23, top).[79] They report the coupling of aryl bromides and chlorides with arylboronic acids with catalyst loads of 2 mol% of palladium and 4 mol% of ligand. They achieve good tolerances for a variety of functional groups like OMe, CF_3, CN and NO_2. Similarly, they reported the palladium catalyzed Buchwald-Hartwig amination reaction of aryl chlorides and bromides with secondary amines (Scheme 1.23, bottom).[80] They achieve good yields with catalyst loads as low as 0.25 mol% for electron rich and neutral amines with both electron withdrawing as well as electron rich aryl halides.

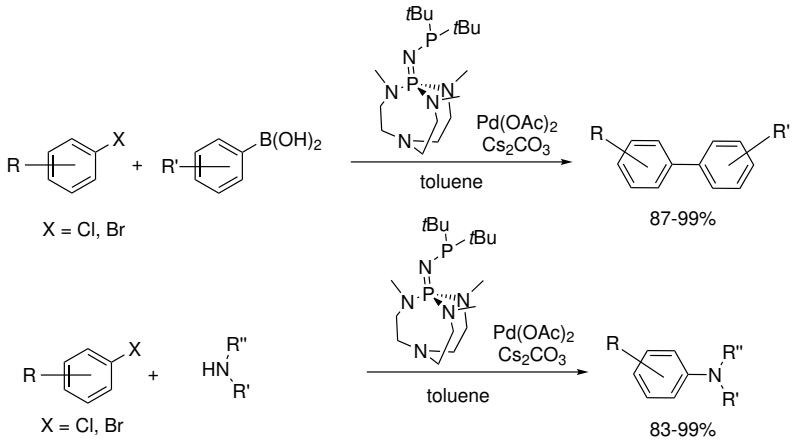

Scheme 1.23: Palladium catalyzed cross coupling reactions with proazaphosphatrane phosphine ligands.[79,80]

Dielmann reports the usage of [Au(IAP)BF_4] complexes for the gold catalyzed hydroamination of acetylenes with anilines (Scheme 1.24).[128] They outperform Buchwald-type ligands like JohnPhos with catalyst loads of 2 mol%. Gessner reports the same reaction with ylide functionalized phosphines as ligands instead.[73] They can be employed in extremely low catalyst loads of only 5 ppm and still achieve high yields of 72%.

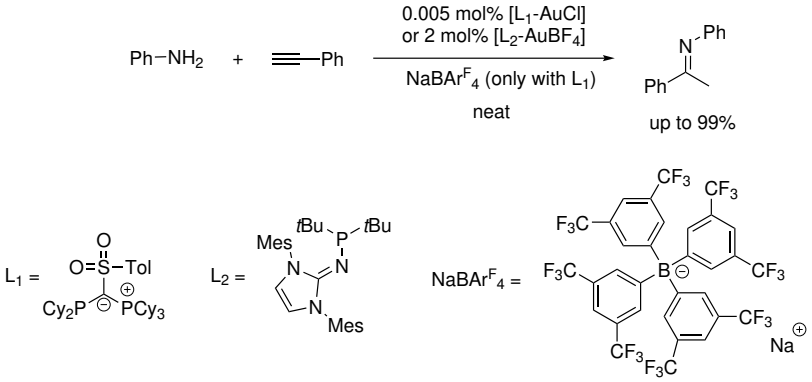

Scheme 1.24: Gold catalyzed hydroamination of phenylacetylene with aniline using YPhos[73] (L_1) and IAP[128] (L_2) ligands.

2 Aim of this work

The aim of this thesis can be separated into three different topics. The first topic was to complement the series of already known trisphosphazenyl phosphines by lower substituted mono- and bisphosphazenyl phosphines, related to the work of Ullrich.[86] These new mono- and bisPAPs were designed to be related to the famous ligand P*t*Bu$_3$. By substitution of one or two *t*-butyl groups with phosphazenyl groups, the electron donating capabilities of these ligands could be increased while their sterical and weak π-acceptor properties could be preserved (Scheme 2.1).

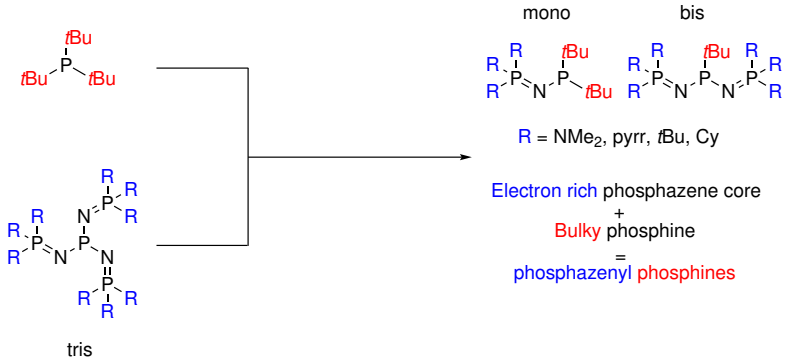

Scheme 2.1: Combination of electron rich phosphazenyl phosphines (bottom left) and bulky alkyl groups (top left) for new mono- and bisphosphazenyl phosphine hybrids.

In order to further the understanding of this class of compounds, the electronic, sterical and chemical properties should be investigated. The electronic character can be quantified by the Tolman parameter *via* the synthesis of a row of nickel tricarbonyl complexes and measurement of the A_1 vibrational mode of the carbonyl bond. Further insight can be gained by the synthesis of PAP selenides and the measurement of the phosphorus selenium coupling constant $^1J_{(P,Se)}$. Additionally, the solution basicity should be determined by measurement of a competition experiment of a base of known pK_{BH^+} value. Through quantitative ^{31}P-NMR spectroscopy and integration of the product peaks the basicity can be determined by the ratio of protonated species.[a] To support these findings, DFT calculations of the solution and gas phase basicity as well as proton affinity should be performed. Additionally, the donor properties were supposed to be calculated by analyzing the change in Mulliken charges of the ligands upon addition of a nickel tricarbonyl fragment. Sterical parameters like the exact cone angle and the solid angle can be calculated from both XRD and DFT optimized structures, as well as the buried volume of the ligand sphere. This allows for the prediction of the behavior of these ligands upon coordination to substrates for catalytic applications. The chemical properties can be investigated by the execution of stability tests upon hydrolysis

[a] Unless otherwise stated, when referring to ^{31}P-NMR spectroscopy, the spectra were measured with proton decoupling.

in acidic, basic and neutral media. The nucleophilicity can be measured by reaction of a base with ethyl iodide and the determination of the ratio of protonated to alkylated base by quantitative ^{31}P-NMR spectroscopy. Additionally, CO_2 adducts as well as a number of metal complexes were supposed to be synthesized in order to investigate the reactivities of the PAPs (Scheme 2.2).

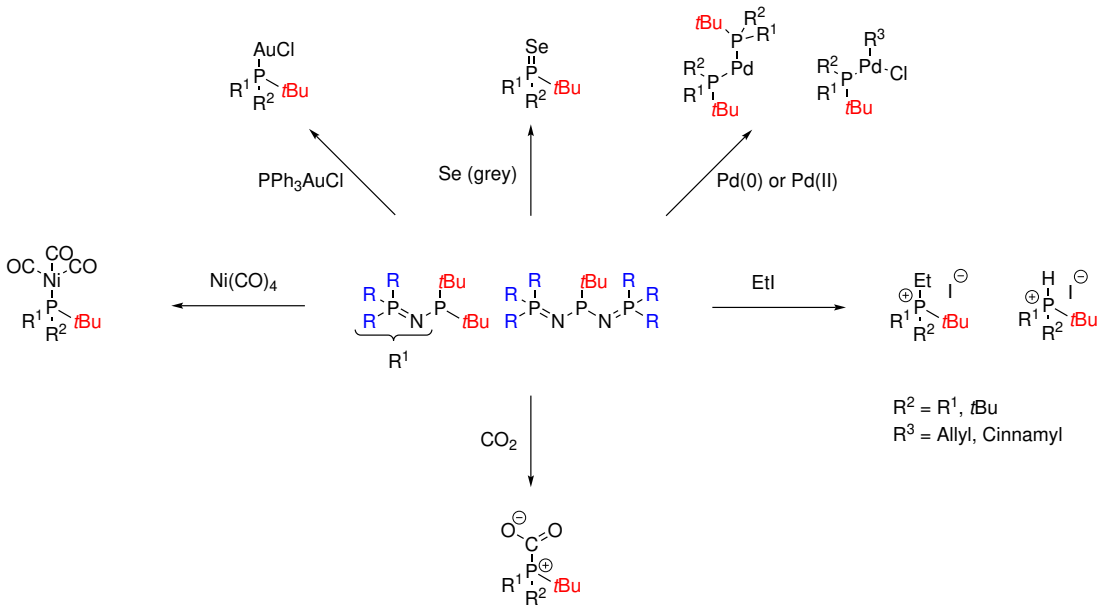

Scheme 2.2: Reactions to determine the electronic, steric and chemical properties of novel mono- and bis PAPs.

The second topic of this thesis was the application of trisPAPs and newly synthesized mono- and bisPAPs as ligands in transition metal catalysis. Similar ligands such as IAPs, YPhos, Verkade or the Fu catalyst can be utilized in palladium catalyzed cross coupling reactions, so the application opportunities of PAPs in these reactions was of great interest.[59,79,129,130] They should be tested for Suzuki-Miyaura, Buchwald-Hartwig aminations, Kumada and Negishi couplings as well as nickel catalyzed Suzuki-Miyaura and Buchwald-Hartwig couplings (Scheme 2.3). Additionally, gold catalyzed aminations of acetylenes should be attempted.

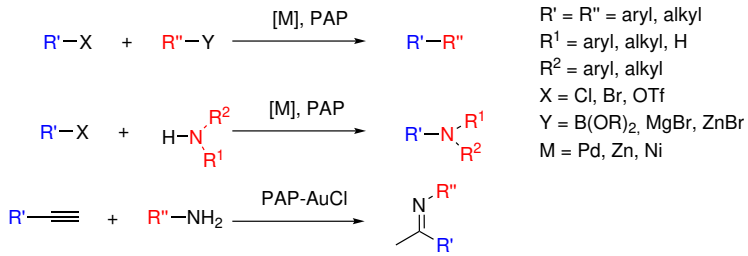

Scheme 2.3: Proposed metal catalyzed cross coupling reactions with PAP ligands.

The third area of interest for these newly synthesized PAPs were supposed to be organocatalytic applications. Spurred by the discovery of the ability of trisPAPs to deprotonate

acetonitrile, the catalytic applications of this reaction should be explored by the transfer of a -CH_2CN group to carbonyl compounds. Related to this is the catalytic alkylation of indoles that can be performed by other strong metal containing bases such as KO*t*Bu and cyclopropenimine superbases.[131–133] The addition of CO_2 to epoxides is known to be catalyzed by NHCs, leading to cyclic carbonates.[134,135] The question if this principle can be applied to superbasic PAPs was another task that was supposed to be investigated (Scheme 2.4).

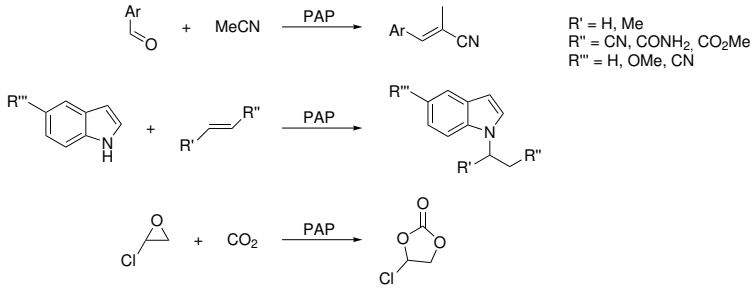

Scheme 2.4: Proposed organocatalytic transformations of PAP catalysts.

3 Synthesis and Characterization of Phosphazenyl Phosphines

3.1 Results and Discussion

Trisphosphazenyl phosphines are the to date strongest P-bases known in chemistry, demonstrating an even higher proton affinity, gas phase and solution basicity than the corresponding polyphosphazene *N*-bases containing the same number of phosphorus atoms.[85] Relatively little is known of the easier accessible mono- and bisPAP ($R_xP(N{=}PR'_2R'')_y$; $x, y \neq 0$, $x + y = 3$).[85,86] Schmidbaur *et al.* reported the synthesis of the simplest monoPAP from the reaction of TMS-$NPMe_3$ and $MePCl_2$ and the synthesis of the corresponding bisPAP from TMS-$NPMe_3$ and Me_2PCl.[136] Flindt reports the synthesis of a monoPAP from TMS-$NPMe_3$ and a phosphinic ester (Ph_2P-OCH_2CF_3) (Scheme 3.1).[137] Other representatives of this substance class are phosphazenyl phosphines based on Verkade's proazaphosphatrane cage, as already mentioned in the introduction.[79,80]

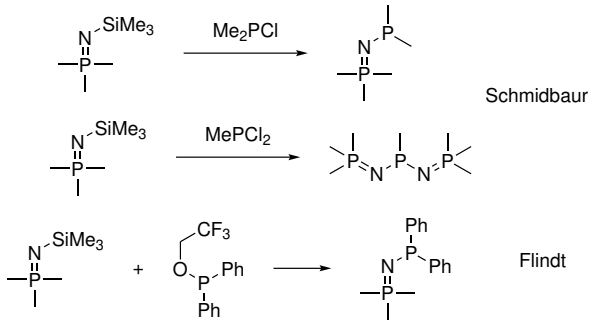

Scheme 3.1: Known synthesis of mono- and bisPAP.

Based upon this, a range of target ligands was developed that would allow the systematic exploration of the electronic and sterical parameters of this substance class. The evaluation of the chemical behavior was another goal that should lead to the utilization of this substance class in a number of transformations. The target ligands are displayed in Figure 3.1. A manuscript describing most of the results herein has been prepared, but has as yet not been submitted. The synthesis and characterization of **5e** and **5f** has been published.[138]

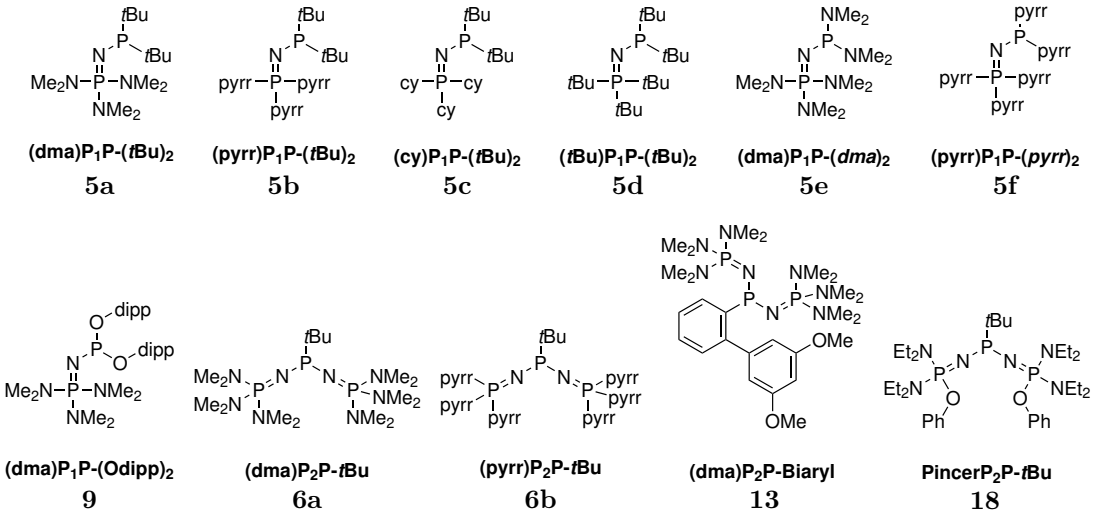

Figure 3.1: Overview over the target ligands for this work.

3.1.1 Synthesis of monoPAP 5a to 5f and 9

To synthesize **5a** to, **5f** a strategy starting from a P(III)-amide or a tertiary phosphine by STAUDINGER reaction with $TMSN_3$ was chosen. The reaction proceeds by nucleophilic attack of the phosphorus lone pair onto the azide (a) (Scheme 3.2). The negatively charged terminal nitrogen atom then attacks the central phosphorus atom (b) by formation of a four membered triazaphosphete ring (c). Through elimination of molecular nitrogen, the products **3a** to **3d** are formed (d).[139]

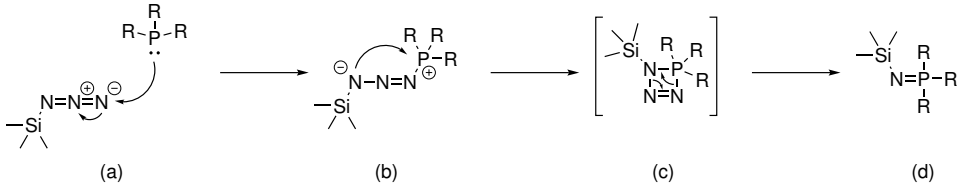

Scheme 3.2: STAUDINGER reaction between TMS azide and a tertiary phosphine.

These are subsequently reacted with PCl_3 to form monophosphazenyl phosphorus dichlorides **4a** to **4d** through elimination of TMSCl. These phosphorus dichlorides are alkylated by *t*-BuLi to form the final target ligands **5a** to **5d** in excellent yields. The all amine substituted monoPAPs **5e** and **5f** are synthesized by reaction of the monophosphazenyl phosphorus dichlorides with gaseous dimethylamine or potassium pyrrolidide and subsequent distillation (Scheme 3.3).[138]

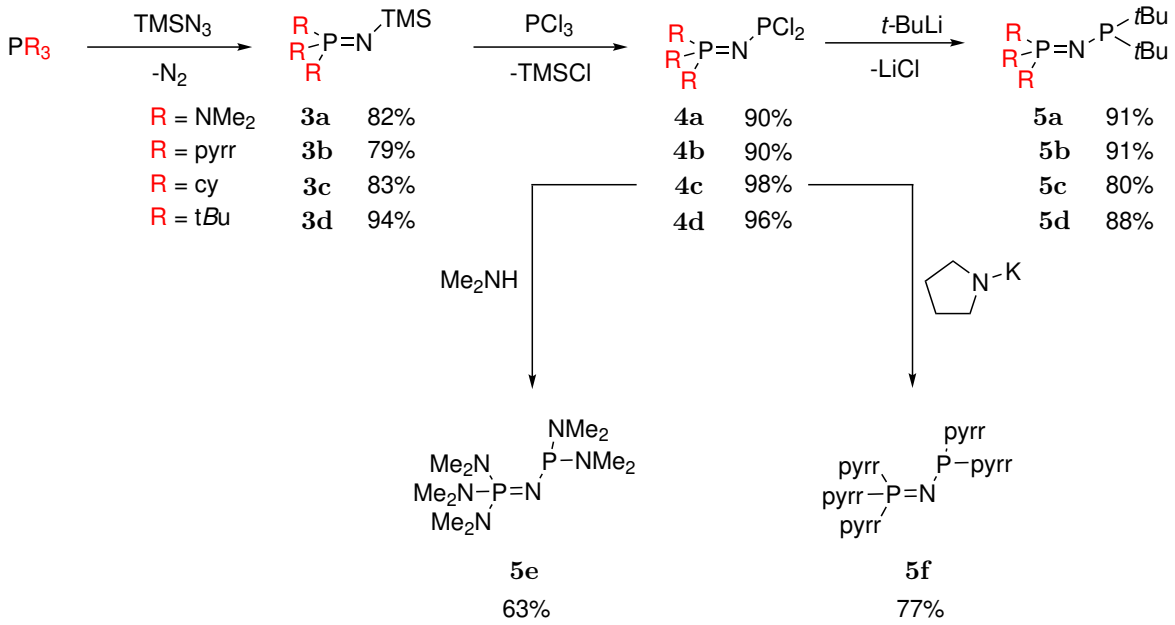

Scheme 3.3: Performed synthetic route towards monoPAPs **5a** to **5f**.

This described synthetic strategy allows the introduction of other sterically demanding groups at intermediates **4a** to **4d**, although *tert*-butyl groups have proven to be the most selective. The choice of Et_2O as the solvent turned out to be essential. The lattice energy of precipitating LiCl is an essential driving force in order to obtain LiCl free pure superbasic monoPAPs. In THF, even at low temperatures, a significant amount of side products were formed, most likely through some type of radical Wurtz reactions or ether cleavage. Additionally, it turned out that a much better conversion could be achieved, if the lithium organyl was added to the phosphorus dichloride and not *vice versa*. The speed of this addition was also a factor, as a slow addition proved superior. If these factors are considered, the conversion is highly selective and can easily be tracked by ^{31}P-NMR spectroscopy, as seen in Figure 3.2 for the transformation of **1a** to **5a**. **5a** to **5d** are white solids that are soluble in pentane, THF and toluene while possessing limited solubility in MeCN and DMSO. Single crystals suitable for *X-Ray* analysis were obtained by dissolving monoPAPs in DMSO at 150 °C and slowly cooling to room temperature. **5e** and **5f** are viscous oils at room temperature.[138] They are all air and moisture sensitive and should be stored in a glovebox.

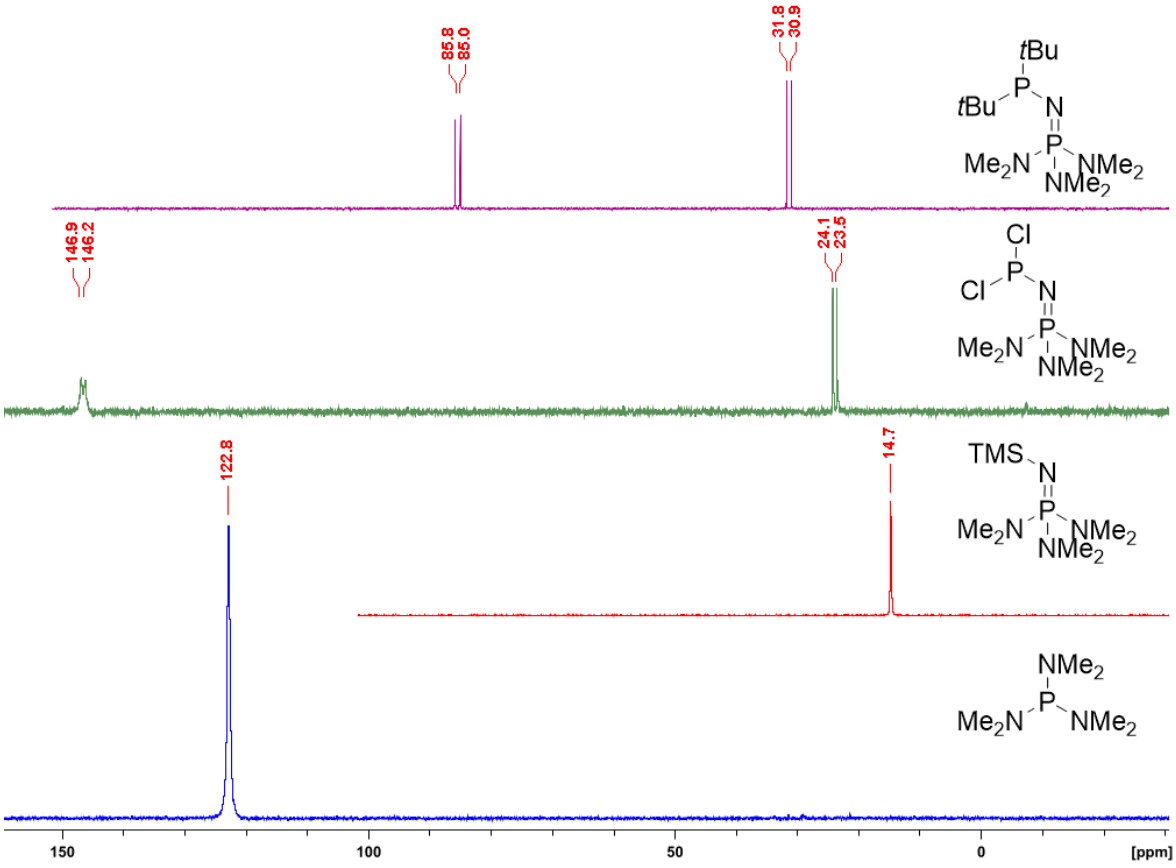

Figure 3.2: ^{31}P-NMR (121 MHz, C_6D_6) spectra of the transformation from **1a** to **5a**.

As seen in Figure 3.2 the ^{31}P-NMR signal of **1a** shifts from 122.8 ppm to 14.7 ppm in **3a** through STAUDINGER reaction with TMS azide. After reaction with PCl_3 two phosphorus signals can be detected as expected. The new doublet at 146.5 ppm corresponds to the trivalent phosphorus atom of **4a** with two chloride substituents. Alkylation shifts this signal to 85.4 ppm with a coupling constant of 100.5 Hz. monoPAPs **5a** to **5f** all exhibit similar chemical shifts. It is noteworthy, that the coupling constant for alkyl substituted **5c** and **5d** is significantly lower than that of their amine substituted analogues with 57.3 Hz and 26.7 Hz respectively. It is likely that this decrease is at least partially attributed to a decrease of the electronegativity of the substitutents on the phosphazene core.[140,141] monoPAP **9** was designed to act as an π-acceptor in addition to being a σ-donor, in contrast to the overwhelming σ-donors **5a** to **5f**. For this synthesis a different approach was needed, it consisted of the reaction of a chlorophosphite **8** with *N*-lithiated iminophosphorane **2a-Li**.[142] **8** is readily available by reaction of 2,6-diisopropylphenol (dippOH) with PCl_3 and a catalytic amount of NMP (Scheme 3.4).[143]

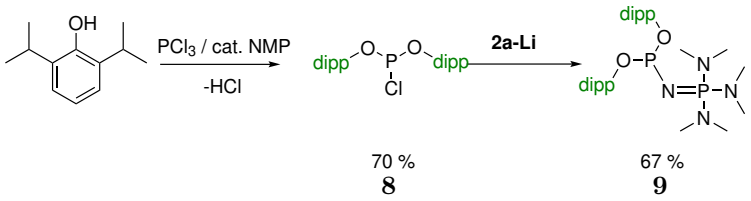

Scheme 3.4: Synthesis of monoPAP **9** from **8** and PCl_3.

The reaction can be observed by ^{31}P-NMR spectroscopy through the shift of the signal of **8** from 174.3 ppm to 150.2 ppm. A new signal at 24.5 ppm corresponds to the pentavalent phosphorus center with a coupling constant of 64.5 Hz, which is significantly lower than **5a** which possesses the same phosphazene core (Figure 3.3). This can be attributed to the increased steric hindrance of this PAP induced by the added dipp groups. The chemical shift of the trivalent phosphorus center is notable compared to **5a**, this is due to lower electron density induced by -Odipp which causes a lower shielding of the nucleus resulting in a downfield shift. **9** is a white solid that is sensitive to air and moisture. Single crystals suitable for XRD were obtained in the already described way.

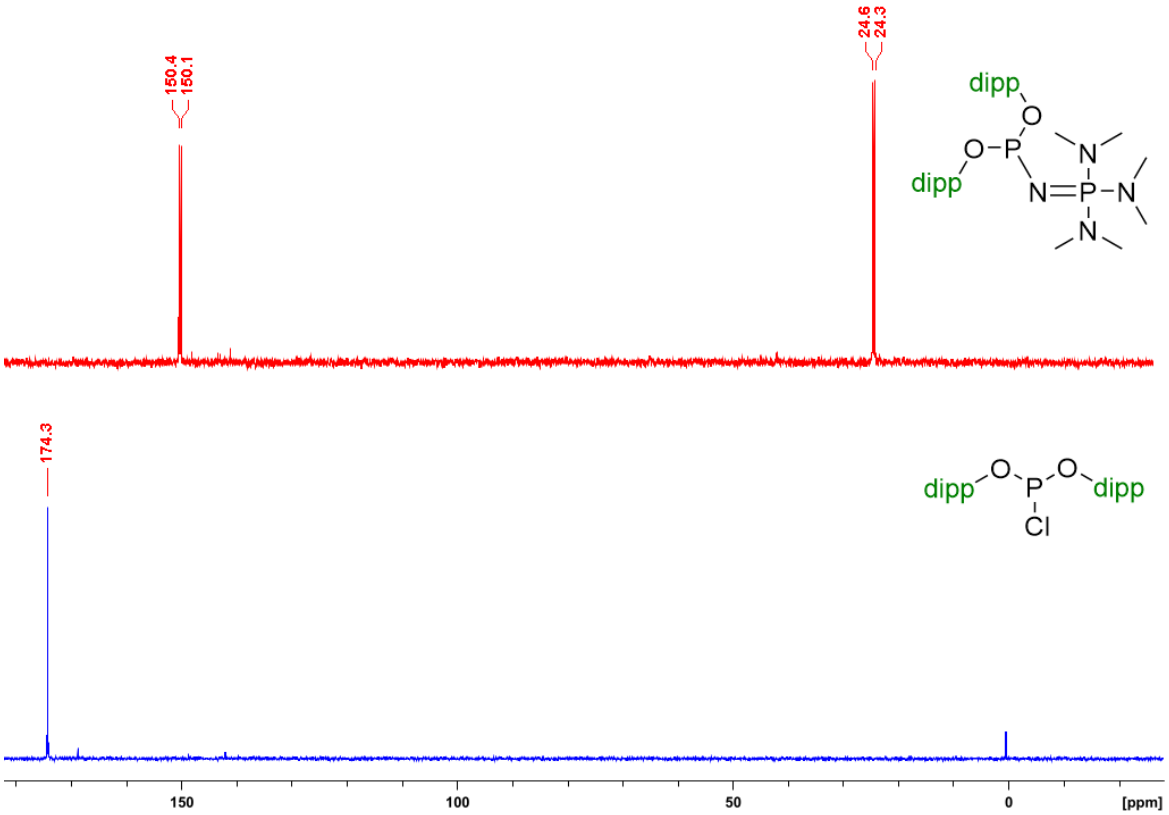

Figure 3.3: ^{31}P-NMR (121 MHz, C_6D_6) spectra of the reaction from **8** to **9**.

3.1.2 Synthesis of bisPAP 6a, 6b and 13

To complete the series of alkyl-substituted PAP, bisPAPs **6a** and **6b** were synthesized. For this a new strategy had to be employed because the theoretical intermediate Cl-P(N=PR_3)$_2$ is known to be unstable and prone to decomposition.[144] Instead, alkyl-PCl_2 compounds were reacted with lithiated iminophosphoranes. The lithiation of iminophosphoranes proceeds in quantitative yields at low temperatures in Et_2O. By careful addition of alkyl-PCl_2, the desired bisPAPs could be generated (Scheme 3.5). Again, the rate and order of addition is important, as a too fast addition leads to the generation of side products, specifically Cl-P(*t*Bu)(N=PR_3) as evident by ^{31}P-NMR spectroscopy.

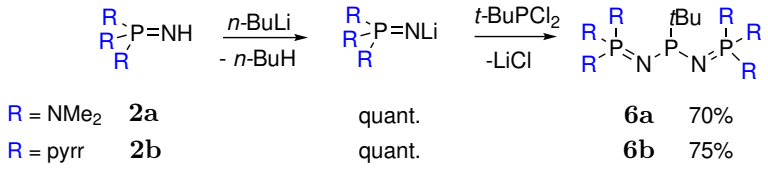

Scheme 3.5: Used synthetic route towards bisPAPs **6a** and **6b**.

When comparing the ^{31}P-NMR spectra of monoPAP, bisPAP and trisPAP a clear trend is visible in the chemical shifts of the pentavalent phosphorus atoms as evident by Figure 3.4. The signal shifts upfield for each added phosphazenyl group, from 31.4 ppm (**5a**) to 20.4 ppm (**6a**) to 14.4 ppm (**7a**). A similar trend can be observed when comparing the $^2J_{(P,P)}$ coupling constants. Each added phosphazenyl group decreases the coupling constants from 100.5 Hz (**5a**) to 59.3 Hz (**6a**) to 19.6 Hz (**7a**). **6a** is a viscous liquid, while **6b** is a white solid. Both compounds are extremely air and moisture sensitive and should be stored in a glovebox. They are soluble in apolar solvents such as pentane, as well as more polar solvents like THF. Single crystals of **6b** could be obtained in the same matter as its monoPAP analogues, while even at −30 °C no crystals could be obtained for **6a**. Their structural parameters will be discussed in a later section. In order to diversify this class of ligands another target, **13**, was designed with a biaryl backbone that resembles the famous Buchwald ligands commonly used in transition metal catalyzed cross couplings.[84] This biaryl backbone may undergo π-arene interactions that stabilize the intermediate after oxidative addition of a substrate. The starting point for this synthesis was 2-bromo-3',5'-dimethoxy-1,1'-biphenyl, which would allow further functionalization on the 2 position of the biaryl moiety. It was synthesized according to literature procedures by a Suzuki-Miyaura cross coupling reaction.[145] The next step involved a bromine-lithium exchange reaction at low temperatures with *n*-BuLi and a subsequent trapping step with Cl-P(NEt_2)$_2$. A direct reaction of PCl_3 with this lithiated biaryl led to the generation of a variety of side products, and therefore this protecting group strategy was employed. Subsequent reaction of **11** with HCl in dioxane, which cleaved the diethylamino groups, liberated the aryl-PCl_2 compound **12**. **12** was recrystallized from a mixture of toluene and Et_2O and stored at −30 °C as it decomposed at room temperature over time even under inert atmosphere. Afterward, reaction with **2a-Li** yielded target ligand **13** (Scheme 3.6).

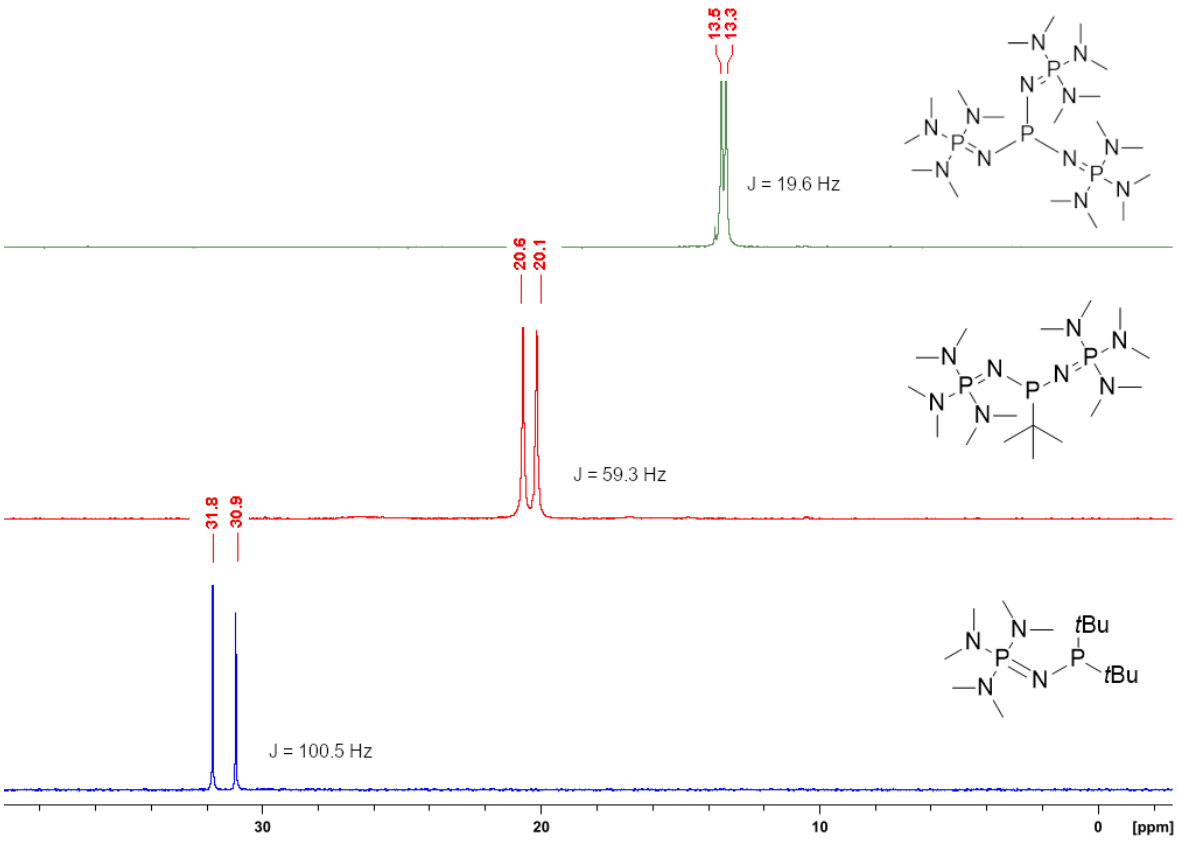

Figure 3.4: ^{31}P-NMR shift and $^{2}J_{(P,P)}$ coupling constants of the pentavalent phosphorus atoms of **5a** (bottom), **6a** (middle) and **7a** (top).

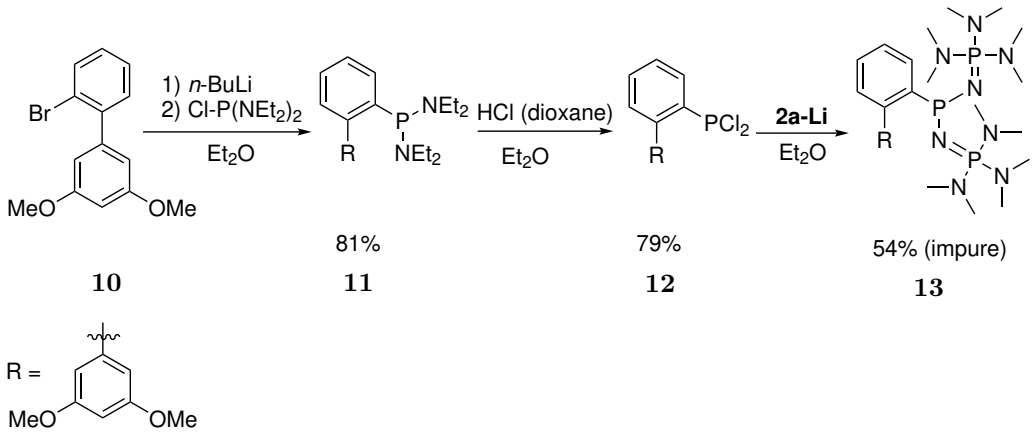

Scheme 3.6: Employed synthetic route to **13**.

This reaction was extremely sensitive to temperature and addition rate, as reported before for **6a** and **6b**. **13** could not be obtained free of contaminants, mainly **2a**, which inhibited further applications such as the measurement of its basicity (see Section 3.1.4).

Another target ligand **18** was designed to possess multiple coordination sites for metals and to provide π-arene interactions with possible substrates. The synthesis is based upon the reaction of $AlCl_3$, PCl_3 and CCl_4 to generate **14** according to a literature procedure.[146] Through reaction with gaseous diethylamine under abstraction of diethylammonium chloride **15** is generated.[147] Subsequent reaction with gaseous ammonia yields the free iminophosphorane **16**.[148] Through elimination of $CHCl_3$, **16** reacted with phenol to yield **17**.[149] A subsequent reaction with *n*-BuLi yielded the lithiated iminophosphorane **17**-Li, which would react with *t*-BuPCl_2 to form the target ligand **18**. However, only mono-substituted product ($R_3P{=}NP(t\text{Bu})Cl$, **19**) could be isolated. Therefore, it was decided if it would be possible to first, generate the bis-substituted chlorophosphine and afterward react this compound with *t*-BuLi to yield the target ligand. The first reaction did prove successful, however the subsequent alkylation with *t*-BuLi did not proceed. The whole reaction sequence is displayed in Scheme 3.7.

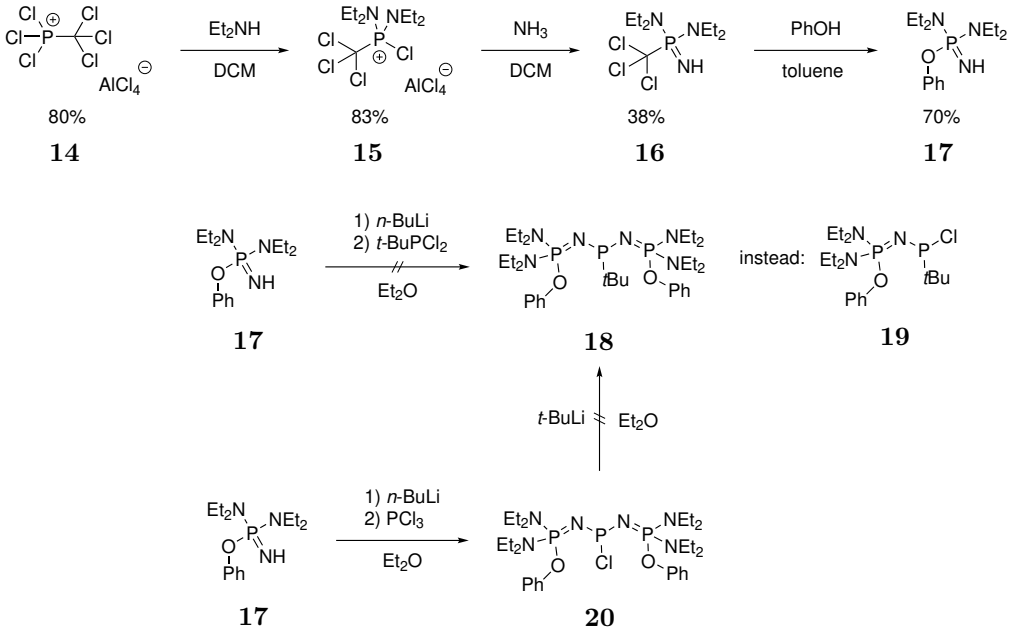

Scheme 3.7: Attempted synthesis for target ligand **18**.

An overview over the ^{31}P-NMR chemical shifts and the $^{2}J_{(P,P)}$ coupling constants of all synthesized PAPs in this chapter is shown in Table 3.1.

Table 3.1: Overview over the ^{31}P-NMR chemical shifts and the $^{2}J_{(P,P)}$ coupling constants of PAP.

MonoPAP	**5a**	**5b**	**5c**	**5d**	**9**
δ [ppm][a]	85.4; 31.4	82.4; 15.8	85.6; 22.2	90.4; 39.3	150.3; 23.7
$^{2}J_{(P,P)}$ [Hz]	100.5	94.8	57.3	26.7	68.0
Bis- and trisPAP	**6a**	**6b**	**13**	**7a**[85]	**7b**[85]
δ [ppm][a]	87.3; 20.4	84.0; 6.8	61.1; 20.2	84.4; 14.4	81.1; 1.4
$^{2}J_{(P,P)}$ [Hz]	59.3	59.5	68.5	19.0	10.0

[a] P^{III};P^{V}, measured in C_6D_6.

3.1.3 Structural Features of PAP

Single crystals of monoPAPs **5a** to **5d** (Figure 3.5) as well as phosphoramidite **9** and bisPAPs **6b** (Figure 3.6) could be obtained by dissolving the corresponding PAP in DMSO at 150 °C. Slowly cooling to RT yielded crystals suitable for X-Ray diffraction.[a] MonoPAPs **5a** to **5c** contain P1-N1 distances that lie between 1.67 Å (**5c**) and 1.68 Å (**5a**). This is shorter than the reported bond lengths for $P(tmg)_3$ (1.70 Å).[82]

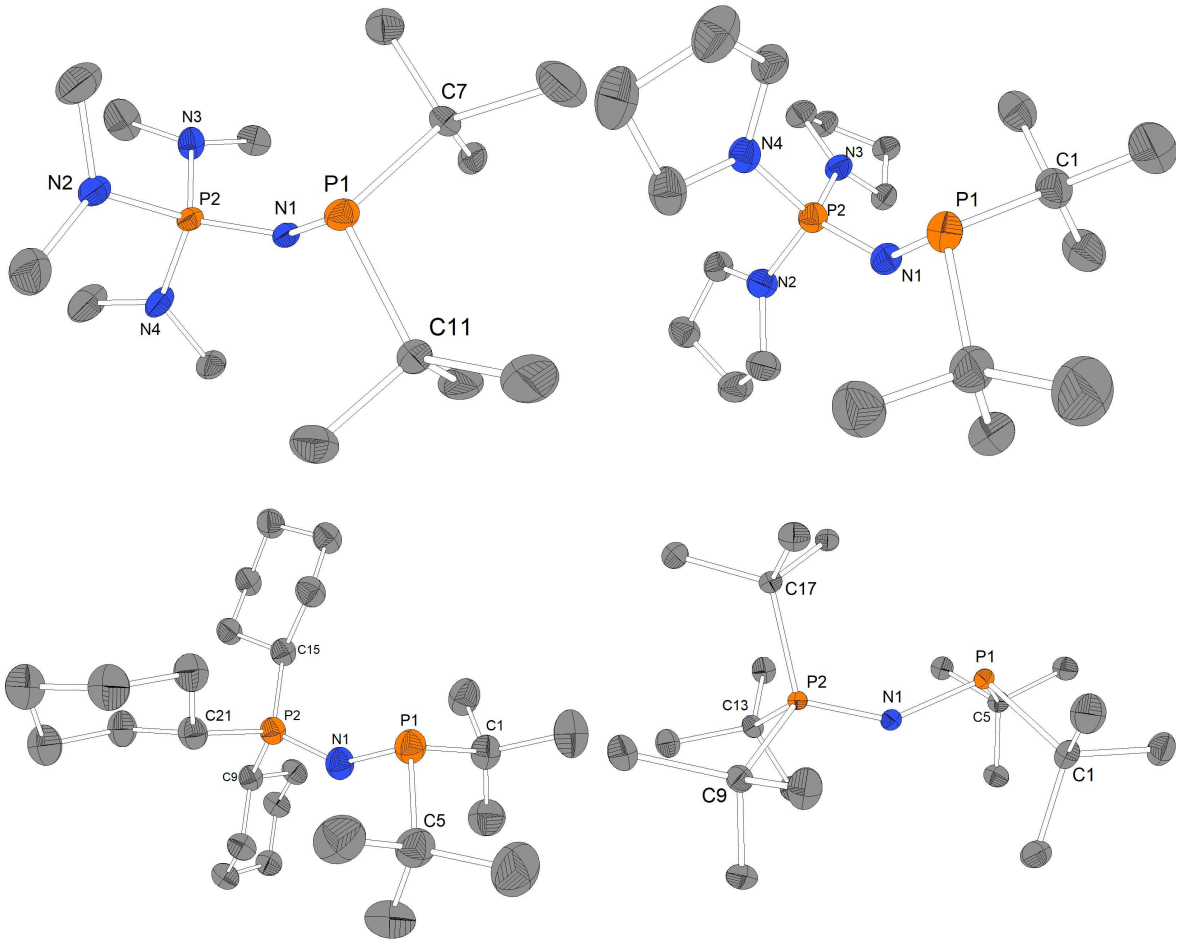

Figure 3.5: Molecular structure of **5a** (top, left), **5b** (top, right), **5c** (bottom, left) and **5d** (bottom, right). Ellipsoids are set at 50% probability. Hydrogen atoms have been omitted for clarity. Notable bond lengths [Å] and angles [°]: **5a**: C11–P1 1.89(3), N1–P1 1.68(2), N1–P2 1.55(2), N4–P2 1.65(2), P2–N1–P1 125.0(1), N1–P1–C11 101.0(1), N1–P2–N2 121.8(1). **5b**: N1–P1 1.68(2), N1–P2 1.57(2), C5–P1 1.90(3), P2–N1–P1 126.8(1), 126.8(1) N1–P2–N4 121.6(1). **5c**: N1–P1 1.67(2), C5–P1 1.91(2), C9–P2 1.83(2), N1–P2 1.56(2), P2–N1–P1 137.9(1), N1–P1–C5 101.3(1). **5d**: P1–C1 1.92(1), N1–P1 1.68(1), N1–P2 1.57(1) 1.57(1), P2–N1–P1 143.3(7), N1–P1–C5 103.0(6), N1–P2–C13 109.6(6).

[a]From here on, the central phosphorus(III)-atom will be denoted P1 and phosphazenyl phosphorus atoms will be denoted P2-P4.

This can be attributed to a lower contribution of negative hyperconjugation as evidenced by its inherent lower basicity. The P2-N1 bond lengths are between 1.55 Å (**5a**) and 1.59 Å (**5b**) and are characteristic for P(V)=N formal double bonds strengthened *via* negative hyperconjugation.[150,151] The P1-N1-P2 bond angles are between 125° and 143°, with the bulkier **5c** and **5d** at the higher end of this spectrum. This can be attributed to increased steric demand of the cyclohexyl and *t*-butyl groups. The crystals of **5a** and **5b** are in the same range as the trisPAPs (**7a** and **7b**) while **5c** and **5d** are much higher. For monoPAP **9** the P1-N1 bond length of 1.62 Å is shorter than in monoPAPs **5a** to **5d**. The N1-P2 bond length is 1.57 Å and therefore comparable to usual P-N double bonds. The P1-N1-P2 bond angle of **9** is 133.4° and is therefore on the higher end of the spectrum because of the bulky dipp groups. P1-O1 and P1-O2 bond lengths average 1.68 Å and are comparable to typical P-O single bonds. BisPAP **6b** features P1-N1 and P1-N5 bond lengths of 1.66 Å and 1.69 Å respectively and are very similar to its monoPAP analogues. The bond angle of P2-N1-N1 is comparable to bulky **5d** with 141.7°.

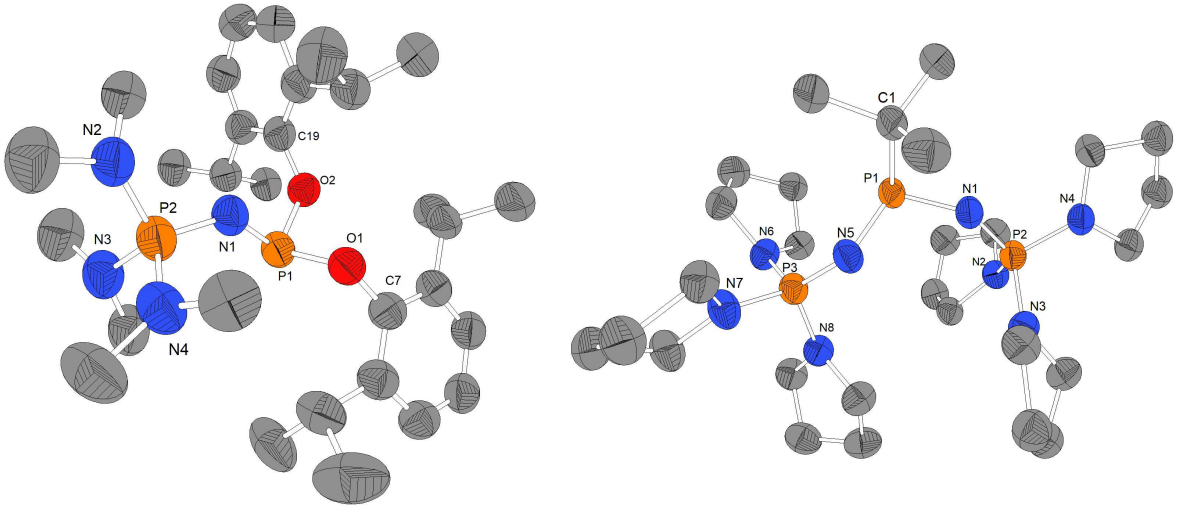

Figure 3.6: Molecular structure of **9** (left) and **6b** (right). Ellipsoids are set at 50% probability. Hydrogens are omitted for clarity. Notable bond lengths [Å] and angles [°]: **9**: N1–P1 1.62(4), N1–P2 1.57(3), O1–P1 1.69(3), O2–P1 1.68(3), C19–O2–P1 125.3(2), N1–P1–O1 100.7(2), P2-N1-P1 133.4(2). **6b**: N5–P3 1.58(6), N5–P1 1.69(6), N1–P1 1.66(6), C1–P1 1.89(6), N1–P2 1.54(6), N5–P3–N6 123.8(4), P2–N1–P1–141.7(4).

Single crystals of iminophosphorane hydrochloride salt **17**-HCl could be obtained by decomposition of the free iminophosphorane in Et_2O. The hydrochloride possesses a P1-N3 bond length of 1.61 Å which is comparable to $[(NMe_2)_3P{=}NH_2]^+$ and a P1-N1 bond length of 1.62(2) Å which is slightly shorter than $[(NMe_2)_3P{=}NH_2]^+$ with 1.63(2) Å.[86] The P1-O1 bond length of 1.56 Å is shorter than that of $P(O)(NH_2)_2OPh$ (1.59 Å).[152] The bond angles around P1 suggest a slightly disordered tetrahedral structure, as is expected. Although it could not be synthesized, the structure of **18** in the gas phase was calculated utilizing the PBE functional with a basis set of def2/tzvpp in order to obtain an idea of the molecular structure (Figure 3.7).[153,154]

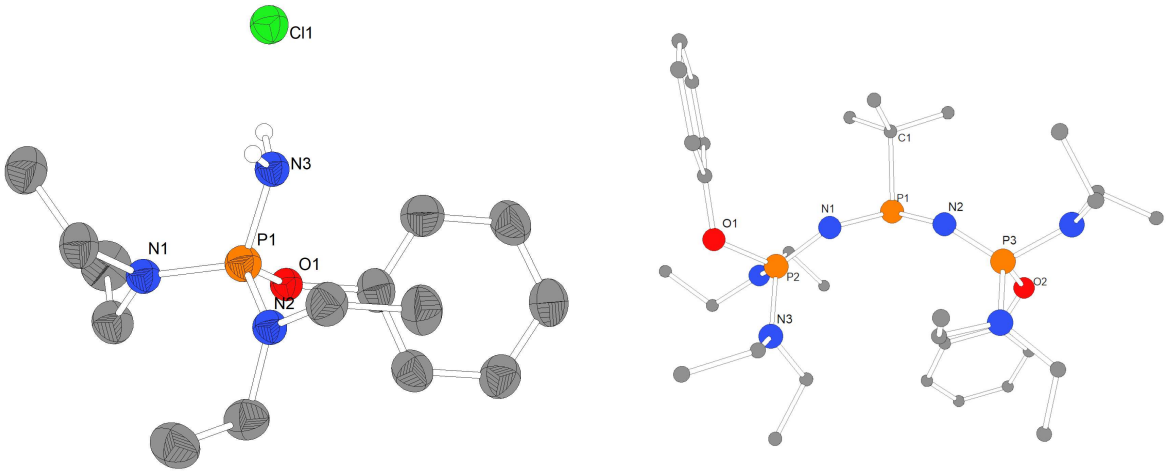

Figure 3.7: Molecular structure of **17**-HCl (left) and calculated structure of **18** (right). Ellipsoids are set at 50% probability. Structure was calculated with PBE def2/tzvpp.[153,154] Hydrogens are omitted for clarity except for those located on the terminal NH_2 group. Notable bond lengths [Å] and angles [°]: **17**-HCl: P1-N1 1.62(2), P1-O1 1.58(2), P1-N3 1.61(2), N3-P1-N1 117.3(1), O1-P1-N3 108.8(9), N2-P1-N1 111.6(9).

3.1.4 Evaluation of the Nucleophilicity

In order to evaluate the nucleophilicity of these new PAP ligands, they were reacted with an excess of dried ethyl iodide. There are two possible mechanisms for this reaction, either the PAP reacts as a nucleophile and forms a P-ethylated phosphonium PAP *via* S_N2 reaction or the PAP reacts as a base in a E_2 reaction and is protonated (Scheme 3.8).

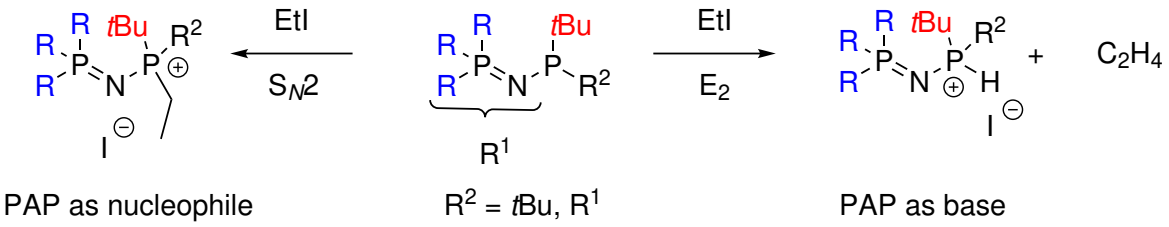

Scheme 3.8: Evaluation of the nucleophilicity of different PAP by reaction with EtI.

The ratio of products was determined by quantitative ^{31}P-NMR measurement by inverse gated decoupling method with an increased relaxation delay (in relation to standard ^{31}P measurement) in order to guarantee complete relaxation between pulses. Therefore, the ratio of PAP-Et^+ to PAP-H^+ could be determined by the integration of the corresponding P(III) or P(V) signals. The results of these experiments can be seen in Table 3.2.

Table 3.2: ^{31}P-NMR chemical shifts of PAP-Et$^+$ to PAP-H$^+$ and their ratio.

MonoPAP	**5a**	**5b**	**5c**	**5d**	**9**
PAP-Et: δ [ppm][a]	45.5; 23.0	40.8; 8.3	56.1; 50.5	46.3; 40.5	24.3; −16.7
PAP-H$^+$: δ [ppm][a]	46.0; 21.0	44.5; 5.4	42.3; 27.6	55.0; 45.5	22.3; −12.0
Nucleophilicity [%][b]	60.9	51.7	12.0	18.8	7.0[c]

Bis- and trisPAP	**6a**	**6b**	**13**	**7a**[86]	**7b**[86]
PAP-Et: δ [ppm][a]	17.0; 19.7	14.1; 3.7	n/a	13.2; −10.1	−0.7; −10.3
PAP-H$^+$: δ [ppm][a]	12.9; 14.9	16.3; 1.3	n/a	21.5; −28.9[d]	7.9; −29.3[d]
Nucleophilicity [%][b]	45.4	1.0[e]	n/a	83.0	88.0

[a] P^{III};P^V, measured in MeCN-d_3.
[b] Ratio of the integrals of PAP-Et/PAP-H$^+$.
[c] Only 27% reacted with EtI, of these 27% only 7% of PAP-Et was found.
[d] Measured in C_6D_6 from $P_3P \cdot HBF_4$ salt.
[e] Measured in THF-d_8 due to low solubility of the isolated reaction mixture.

As expected, both protonation as well as alkylation induce a significant upfield shift of the formerly trivalent phosphorus nucleus: e.g., **5a** to **5a**-H, 85.4 ppm to 46.0 ppm; **5a** to **5a**-Et 85.4 ppm to 42.5 ppm (Figure 3.8). The coupling constant also decreases drastically: **5a** to **5a**-H, 100.5 Hz to 29.4 Hz; **5a** to **5a**-Et, 100.5 Hz to 3.7 Hz. In fact, the $^2J_{(P,P)}$ coupling disappears completely for some P-ethylated PAPs. It is observed, that both trisPAPs **7a** (83.0%) and **7b** (88.0%) react predominantly as C-nucleophiles, forming [PAP-Et]$^+$.[86] MonoPAPs **5a** (60.9%) and **5b** (51.7%) show a lower ratio towards ethylation. Interestingly, all PAPs with sterically demanding alkyl substituents (**5c** and **5d**) display predominantly the character of a base: only 12.0% (**5c**) and 18.8% (**5d**) of the [PAP-Et]$^+$ cations are formed next to [PAP-H]$^+$. This can be attributed to their difference in sterics as the alkyl core hinders an attack of the electrophile by the P(III) center. BisPAP **6a** falls in between mono- and trisPAPs with 45.4%. Surprisingly, sterically demanding bisPAP **6b** presents as a pure base: When reacted under the same conditions as **6a** in THF, only 1% [PAP-Et]$^+$ and 99% [PAP-H]$^+$ cations are formed. The high selectivity towards dehydrohalogenation is most likely due to steric hindrance introduced by the combination of P-pyrrolidino and P-*tert*-butyl groups. MonoPAP **9** is another example of high selectivity towards elimination by steric hindrance, as it is only ethylated by 7%. It can be concluded, that PAP superbases have a considerable and competing P-nucleophilicity towards soft C-electrophiles such as alkyliodides. Bulky groups decrease their nucleophilic behavior and can, if introduced at the phosphazene core, even inhibit nucleophilicity. As nucleophilicity towards soft carbon electrophiles is qualitatively correlated to donor strength towards soft transition metal Lewis acids, PAP P-bases will display a different spectrum of applications compared to Schwesinger's N-bases.

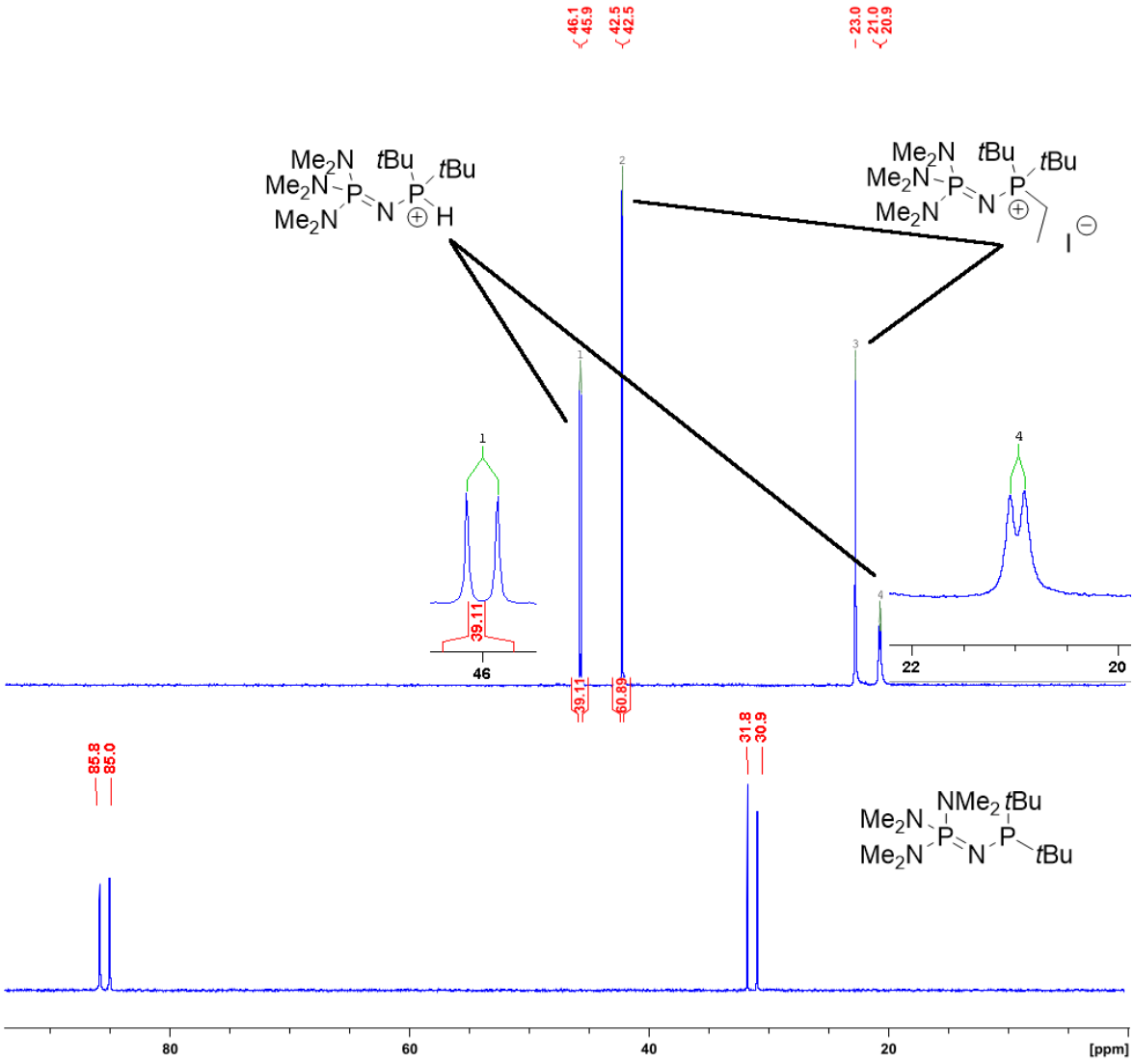

Figure 3.8: ^{31}P-NMR (121 MHz, MeCN-d_3) spectrum of **5a** before (bottom) and after (top) reaction with EtI.

3.1.5 Chemical Stability of PAP

The stability of PAPs towards hydrolysis in acidic and basic environments is of relevance because the phosphazene core can be hydrolyzed to form hexamethylphosphorous acid trisamide (HMPA) which is highly toxic and is known to cause cancer in rats.[155–157] In order to investigate this risk, three different reactions for each PAP were performed. PAP was dissolved in a small quantity of dioxane and subsequently 1 mL of a) 1 M HCl, b) 1 M NaOH or c) H_2O was added and heated to reflux overnight. Afterward the solvent was removed, and the residue dissolved in $CHCl_3$ and NMR spectra as well as MS measurements were taken. All synthesized PAP were stable under these conditions except for **5c** which decomposed in acidic and basic media to form several phosphorus species, though none of them could be attributed to HMPA. In basic conditions, most monoPAPs reacted to form a mixture of protonated PAP $[PAP\text{-}H]^+$ and PAP oxides [PAP=O] as detected by MS (Figure 3.9). In acidic media more

$[PAP\text{-}H]^+$ is formed and in neutral media more [PAP=O] is formed. Higher substituted bis-PAPs (**6a** and **6b**) and trisPAPs (**7a** and **7b**) reacted almost exclusively to form $[PAP\text{-}H]^+$ no matter the media. All synthesized PAPs are thermally stable in DMSO at 150 °C with minimal decomposition. This method was used to grow single crystals for X-ray diffraction upon cooling of these saturated solutions. As already mentioned, all PAPs are sensitive towards water and oxygen and will eventually decompose into the corresponding PAP oxides or phosphonium salts. However, all these PAPs can be stored without decomposition even at humid conditions in form of their PAP-HBF_4 salts, allowing storage of these compounds under ambient conditions. Deprotonation with a strong base such as KHMDS liberates the free bases for further use.

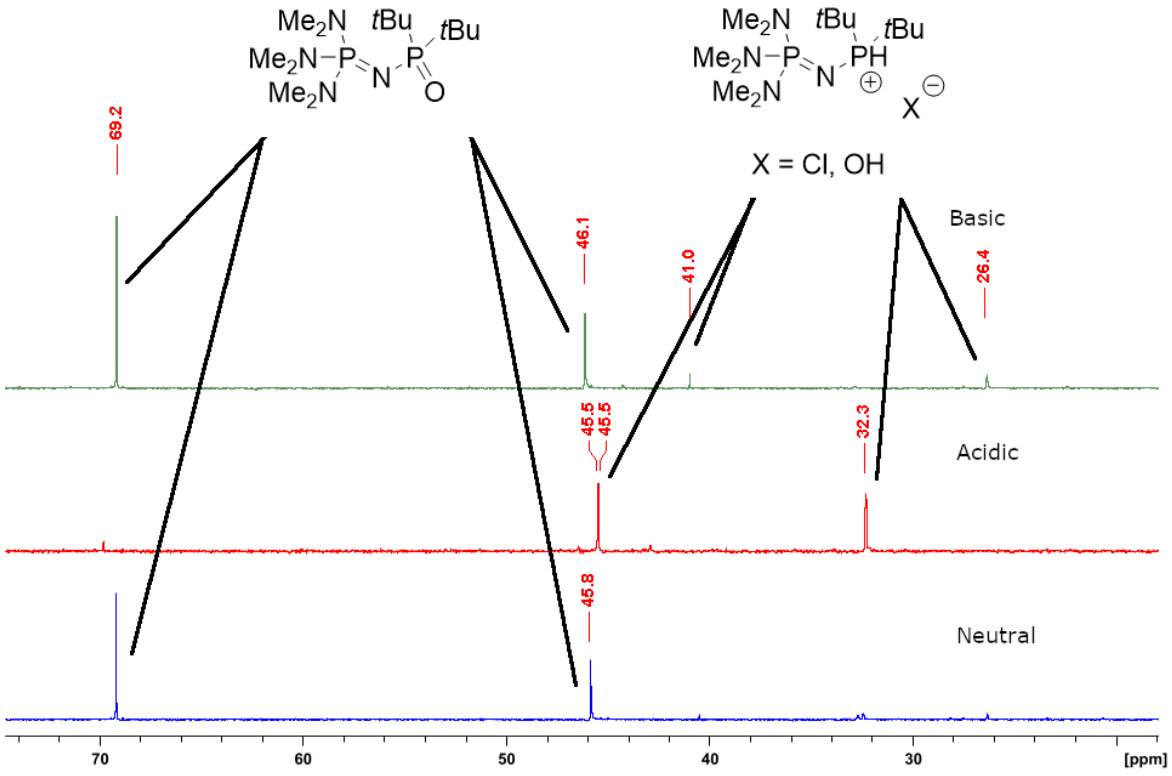

Figure 3.9: ^{31}P-NMR (121 MHz, $CDCl_3$) spectrum of **5a** after reaction with H_2O (bottom), HCl (middle) and NaOH (top).

3.1.6 Evaluation of the Tolman Electronic Parameter and PAP Selenides

To investigate the electronic properties of the ligands, the Tolman electronic parameter (TEP) was measured as mentioned in Section 1.4. The TEP corresponds to the frequency of the A_1 C-O vibrational mode of [L-Ni(CO)$_3$] type complexes. This can be used to determine the electron donor capabilities of a ligand. For this purpose each ligand was reacted with [$Ni(CO_4)$], the resulting nickel complex was isolated and an IR spectrum of the solid compounds was measured. Additionally, the structure of each complex was calculated with DFT using the PBE functional and the def2/tzvpp basis set.[153,154] PAP selenides allow a similar assumption about donor capabilities and have been prepared by reaction of each ligand with gray selenium. The synthesized and discussed compounds for this section are shown in Figure 3.9.

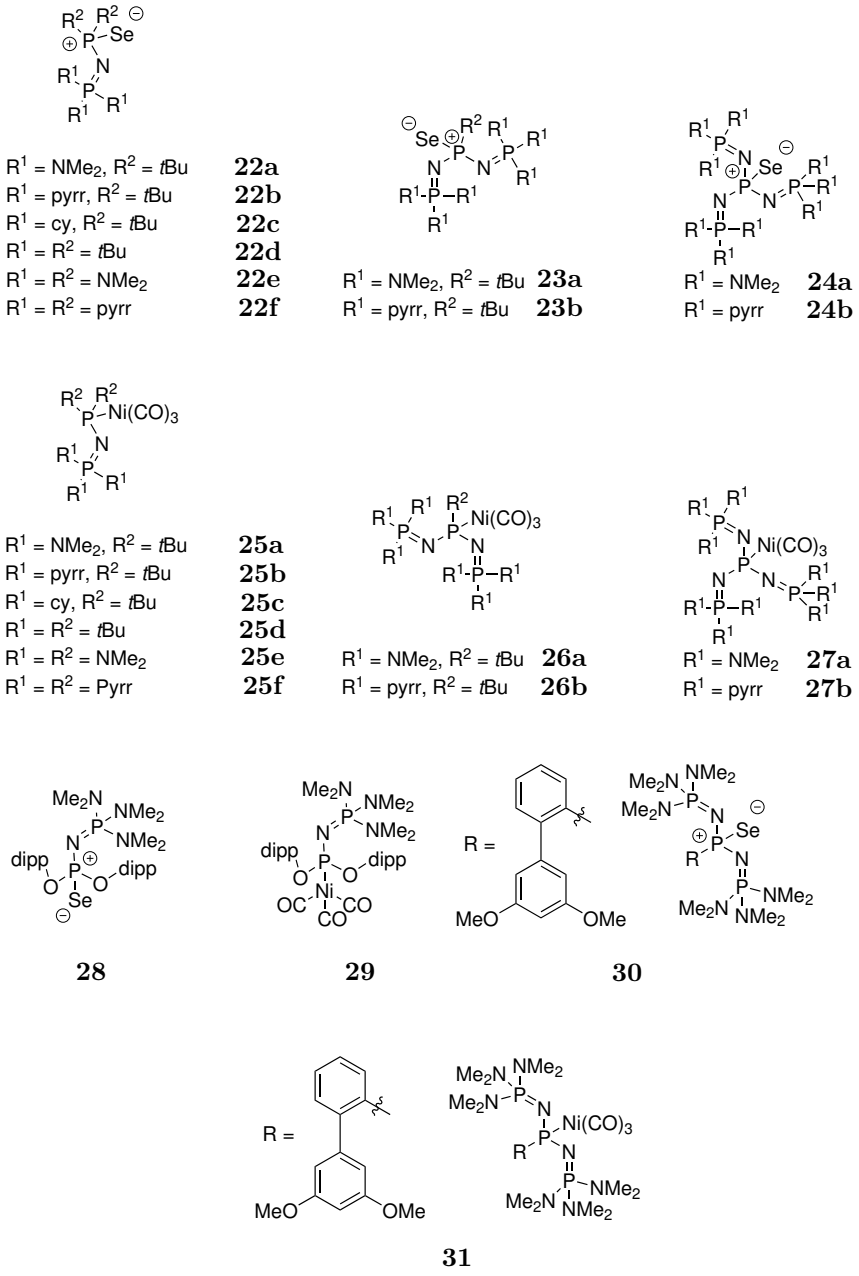

Scheme 3.9: Overview over the synthesized and discussed molecules for this section.

An overview over the measured TEP is shown in Table 3.3. It can be deduced that monoPAPs **25a** to **25d** all possess TEPs of 2040±2 which is lower (electron richer) than popular NHCs such as IMes (2050.5)[158] and $ImNMe_2$ (2054.1)[158] or phosphines like $PtBu_3$ (2056.1)[90] and to modern ylidenaminophosphines (IAP)[81,159] (Figure 3.10) of Dielmann and ylide functionalized phosphines (YPhos)[59,71,73] of Gessner. Interestingly, they are also lower than all amino substituted analogues **25e** (2047.4) and **25f** (2042.4).[138] This suggests, that alkyl substituents contribute more to the electron donating capabilities of a ligand than amino groups. **29**, which shows a TEP of 2104.6, lies in the realm of PF_3 which suggests, that it may compete with CO as an π-acceptor ligand.[90] Unsurprisingly, **26a** and **26b** lie between monoPAPs **25a**-**25b** and trisPAPs **27a**-**27b** with TEP values of 2032.0 and 2033.5 respec-

tively. Biaryl PAP **31** fits in with these bisPAPs with a TEP value of 2036.7. With these values, they surpass even some of the strongest NHCs in donor capability.[85,158] ^{13}C-NMR signals for these carbonyls can all be found around 200 ppm. The $^{2}J_{(P,C)}$ constants increase for each added phosphazenyl unit from ca. 2.0 Hz for monoPAP, to 4.6 Hz for bisPAP to 9.0 Hz for trisPAP. Phosphoramidite **29** displays a singlett as its bulky dipp groups shield the phosphorus atom from coupling with the carbonyl units. A linear dependency between the calculated average bond lengths of the CO fragments of [PAP-Ni(CO)$_3$] complexes could be correlated to their calculated A_1 C-O vibrational mode, as has been established by Gusev for a series of two electron ligands.[160] This dependency was replicated for PAP as evident by Figure 3.11 with a R^2 value of 0.995.

Table 3.3: Measured and calculated TEP, ^{13}C-NMR chemical shifts and $^{2}J_{(P,C)}$ of the carbonyl carbon of PAP and similar ligands.

monoPAP	**25a**	**25b**	**25c**	**25d**	**29**
TEP[a]	2040.0	2042.1	2042.8	2039.4	2104.5
TEP calc.[b]	2047.0	2036.7	2047.6	2043.6	2062.6
^{13}C (CO) δ[c]	200.0	200.5	200.0	200.1	195.8
$^{2}J_{(P,C)}$ [Hz]	2.3	2.6	1.9	2.2	0

Bis, trisPAP	**26a**	**26b**	**31**	**27a**[85]	**27b**[85]
TEP[a]	2032.1	2030.4	2036.7	2022.4	2018.6
TEP calc.[b]	2036.7	2030.2	2038.7	2016.7	2022.2
^{13}C (CO) δ[c]	202.0	201.9	–[d]	203.4	203.9
$^{2}J_{(P,C)}$ [Hz]	4.6	5.0	–[d]	9.0	9.0

Ligand[e]	P(R$_1$)$_2$iPr[161]	P(R$_1$)$_3$[161]	Y*o*TolPCy$_2$[60]	cy-YPhos[162]	IMes[158]
TEP[a]	2038.6	2029.7	2051.7[b]	2057.1	2050.7

[a] Measured *via* ATR-IR spectroscopy of neat substance.
[b] Calculated using PBE/def2tzvp.[153,154]
[c] Measured in C_6D_6.
[d] Due to low signal-to-noise ratio, no signal could be assigned unambiguously.
[e] Structures for these compounds can be found in Figure 3.10.

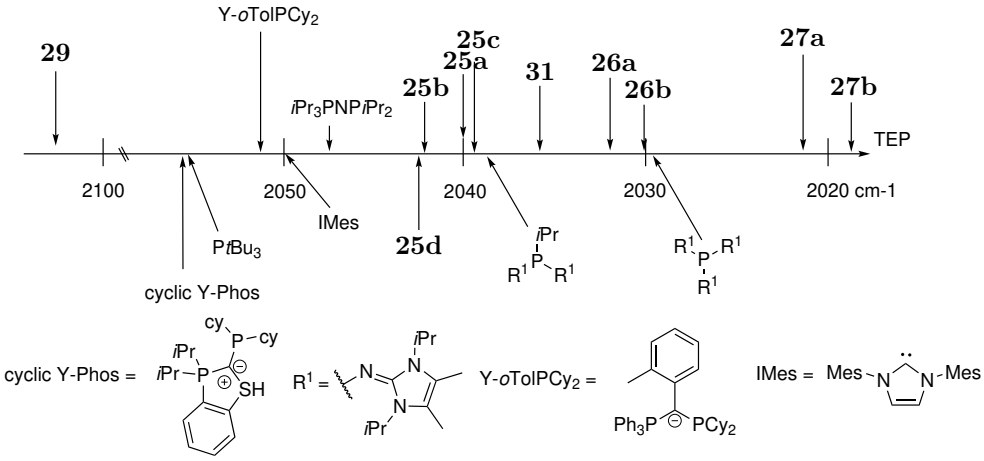

Figure 3.10: TEP values of the nickel tricarbonyl complexes of PAP and various other ligands. Exact values for these examples are given in Table 3.3.

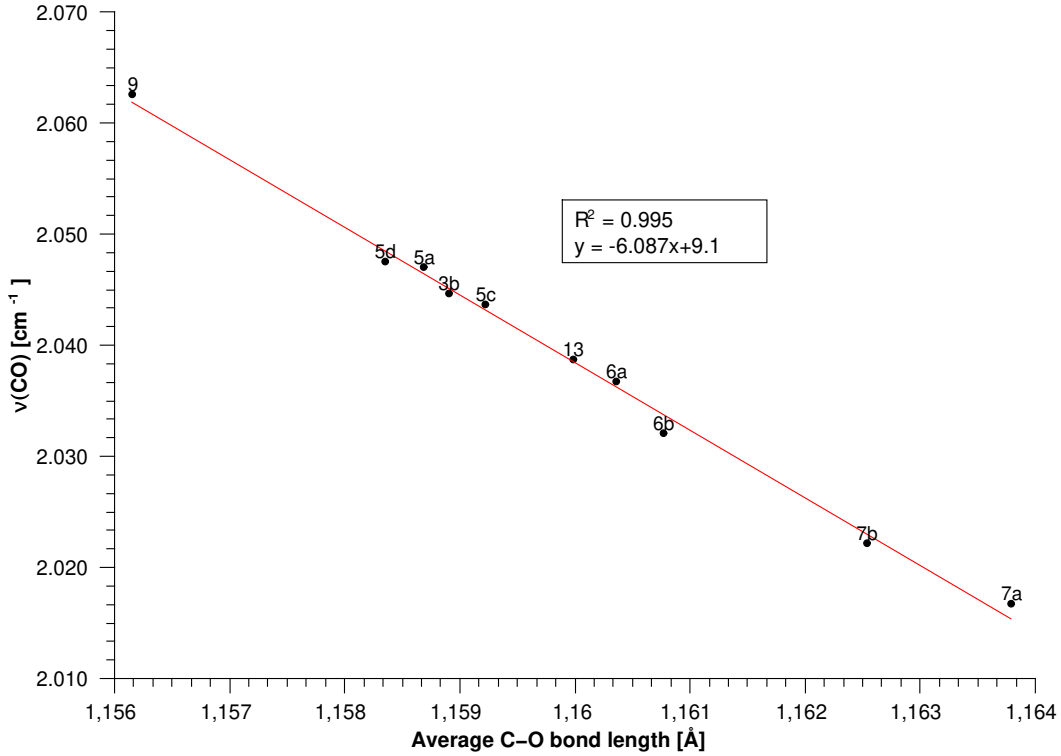

Figure 3.11: Correlation of the average calculated CO bond lengths and A_1 C-O vibrational mode of [PAP-Ni(CO)$_3$] complexes. Molecules numbered according to their parent PAP.

Single crystals suitable for XRD for **25a** and **25d** were obtained by slow cooling of a saturated pentane solution to −30 °C. The structures are shown in Figure 3.12. **25a** possesses an average C-O bond length of 1.15 Å and **25d** of 1.14 Å which is, as expected, shorter than the average C-O bond length in **27a** with 1.19 Å.[86] This corresponds to their lower TEP value as the A_1 C-O vibrational mode is harder to exite the shorter the bond length. The P1-Ni bond

lengths are similar with 2.298 Å for **25d** and 2.263 Å for **25a** compared to 2.259 Å for **27a**. The higher bond length of **25d** clearly stems from its increased sterical hindrance introduced by *t*-butyl groups on the phosphazenyl core.

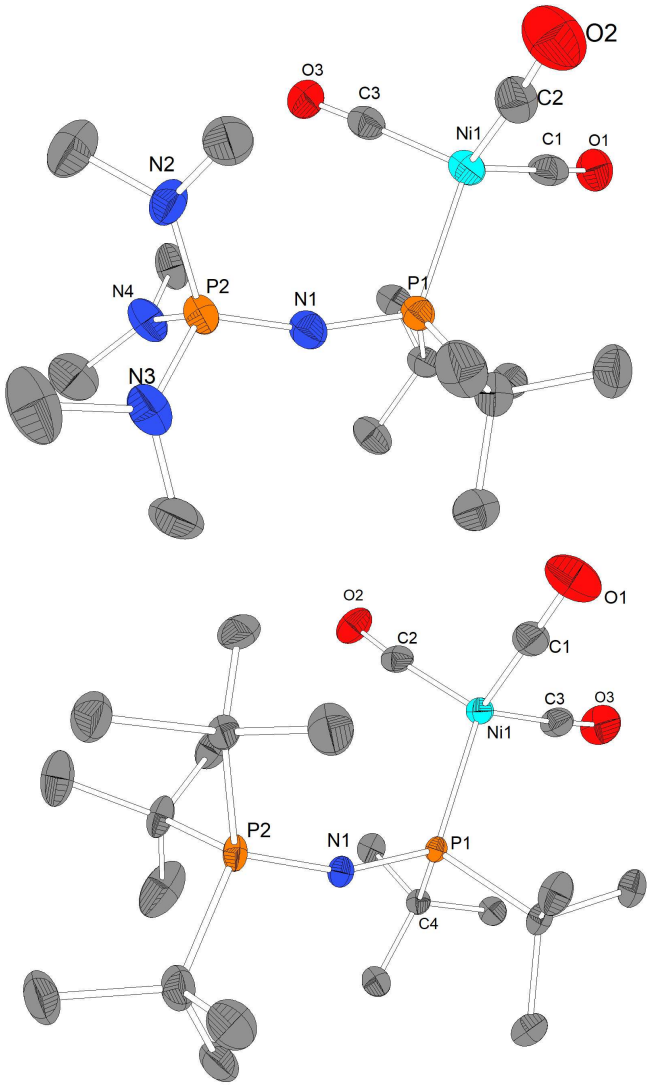

Figure 3.12: Molecular structure of **25a** (top) and **25d** (bottom). Ellipsoids are set at 50% probability. Hydrogen atoms have been omitted for clarity. Notable bond lengths [Å] and angles [°]: **25a**: N1-P1 1.628(5), N1-P2 1.531(5), N2-P2 1.642(5), N3-P2 1.654(5), N3-P2 1.654(5), P1-C4 1.894(6), P1-Ni1 2.2626(2), Ni1-C1 1.792(7), C1-O1 1.148(8), O1-C1-Ni1 179.0(6), P2-N1-P1 161.3(4), C1-Ni1-P1 109.8(2), N1-P1-Ni1 116.8(2); **25d**: N1-P1 1.644(2), N1-P2 1.563(2), P2-C12 1.899(2), P2-C16 1.897(2), P1-C4 1.917(2), P1-Ni1 2.298(6), Ni1-C1 1.797(3), C1-O1 1.136(3), O1-C1-Ni1 176.7(2), P2-N1-P1 159.2(1), C1-Ni1-P1 109.9(8), N1-P1-Ni1 120.7(7).

A similar evaluation of the donor capabilities can be made from the $^{1}J_{(P,Se)}$ coupling constant of corresponding PAP selenides, their chemical shifts as well as their $^{1}J_{(P,Se)}$ coupling constants are shown in Table 3.4.[102,107]

Table 3.4: ^{31}P and ^{77}Se-NMR chemical shifts of PAP selenides and their $^{1}J_{(P,Se)}$ coupling constants.

monoPAP	**22a**	**22b**	**22c**	**22d**	**28**
^{31}P δ [ppm][a]	75.4	73	76.2	74.2	38.5
^{77}Se δ [ppm][b]	−273.4	−257.4	−250.6	−222.5	−119.9
$^{1}J_{(P,Se)}$ [Hz][b]	696.2	695.4	692.4	695.4	902.2

Bis, trisPAP	**23a**	**23b**	**30**	**24a**[85]	**24b**[85]
^{31}P δ [ppm][a]	34.2	31	13.2	−6.7	−5.5
^{77}Se δ [ppm][b]	−97.5	−71.3	26.7	137.9	190.9
$^{1}J_{(P,Se)}$ [Hz][b]	676.6	665.5	672.4	654	628

[a] $R_3P{=}N\underline{P}R_2$-Se; Measured in C_6D_6.
[b] Measured in C_6D_6.

22a-22d all exhibit similar coupling constants of 694± Hz. This is in the magnitude of 50 Hz lower than all amine substituted monoPAPs **22e** and **22f**.[138] This difference can be attributed at least partly to the higher electron donor capabilities of **22a-22d** as evidenced by their TEP values. Sterical hindrance at the central phosphorus atom may also result in a decrease in s-character of the lone pair.[103] In the row of **22a**, **23a** to **24a** a clear trend in the decreasing of the coupling constant by about 20 Hz per phosphazene unit can be observed. This corresponds with their TEP. This prompted an investigation to determine if a linear correlation between the TEP and the $^{1}J_{(P,Se)}$ coupling constants is possible, as was shown by Gessner.[163] Such a dependency was confirmed with a R^2 value of 0.987 (Figure 3.13, top). Notably, the fitted function was very similar to the one used by Gessner with only a variance of 1±0.5% between our obtained values and values obtained by Gessner's method. Phosphoramidite **28** presents a clear outlier to its electron rich monoPAP analogues, with a $^{1}J_{(P,Se)}$ coupling constant of 902.2 Hz. This stems mostly from the electron withdrawing -Odipp groups, but bulky aryl substituents have been known to cause an increase in $^{1}J_{(P,Se)}$ coupling constants that do not necessarily correlate to its electronic properties.[105,106] It can be said, that **9** is the ligand with the lowest donor and highest π-acceptor abilities within these PAPs. Betrand and Hudnall discovered a dependency of ^{31}P-NMR and ^{77}Se-NMR signals for phosphinidines and NHCs.[95,96,164] This dependency extends to PAP as shown in Figure 3.13 (bottom) with a R^2 value of 0.962.

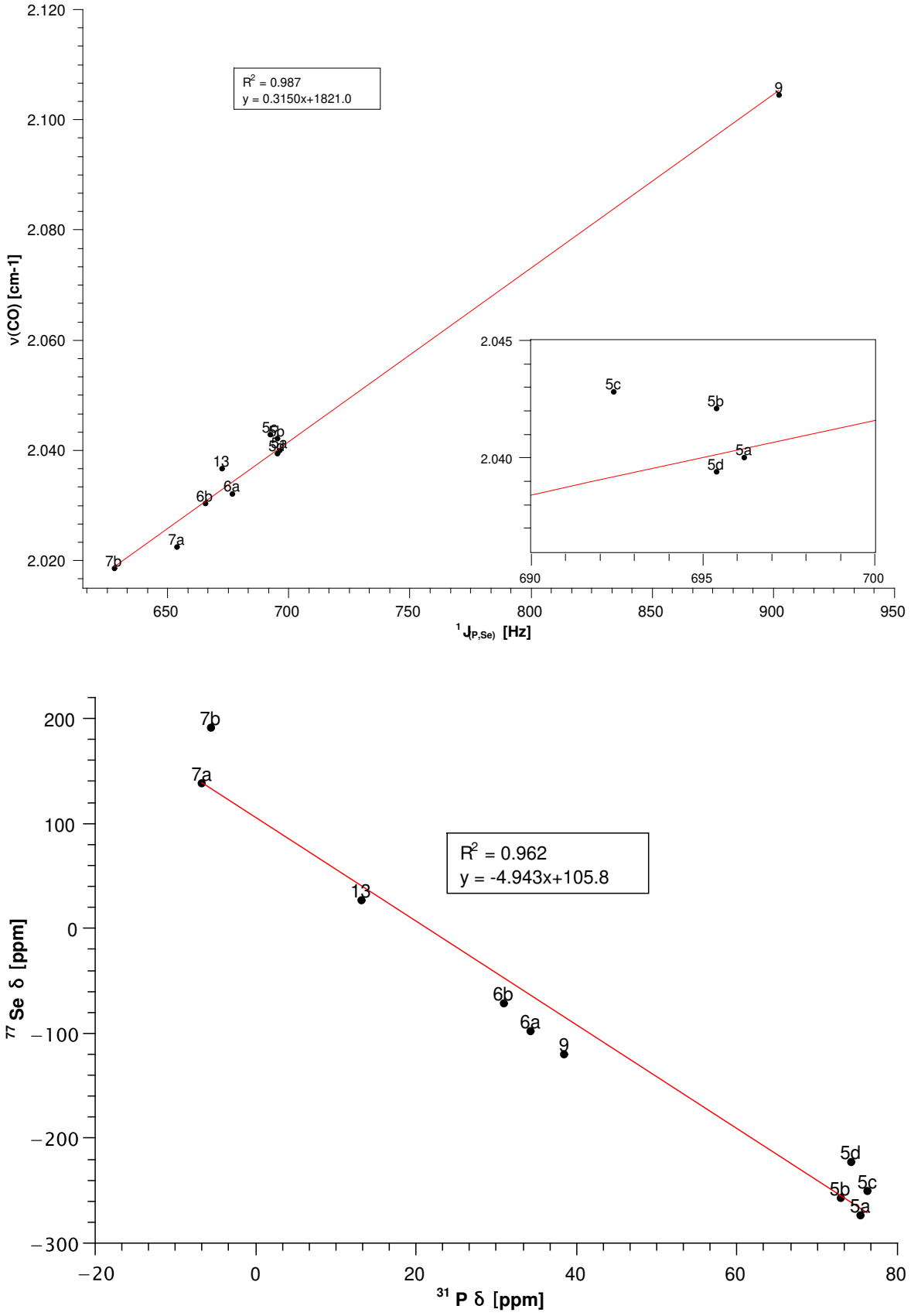

Figure 3.13: Linear dependence of the $^{1}J_{(P,Se)}$ NMR (57 MHz, C_6D_6) coupling constant with the TEP (top). Linear dependence of the ^{31}P (121 MHz, C_6D_6) and ^{77}Se-NMR (57 MHz, C_6D_6) chemical shifts of PAP selenides (bottom). Molecules numbered according to their parent PAP.

Single crystals suitable for XRD for **22a**, **23b** and **30** were obtained by slow cooling of a saturated pentane solution to −30 °C. **22a** features a P1-Se1 bond length of 2.140 Å which is shorter than **23b** with 2.156 Å, **30** with 2.163 Å and **24a** 2.167 Å. It can be concluded, that added phosphazenyl groups increase this bond length. The length is additionally increased by the sterically demanding biaryl substituent of **30**. The second phenyl ring of **30** is twisted by 59.6° in relation to the first phenyl ring. This may enable the parent ligand **13** to stabilize possible metal adducts *via* π-arene interactions, as shown by BUCHWALD's biaryl ligands.[84] The N1-P1-Se1 bond angles are between 112-115°, suggesting a slightly disordered tetrahedral coordination of P1.[86]

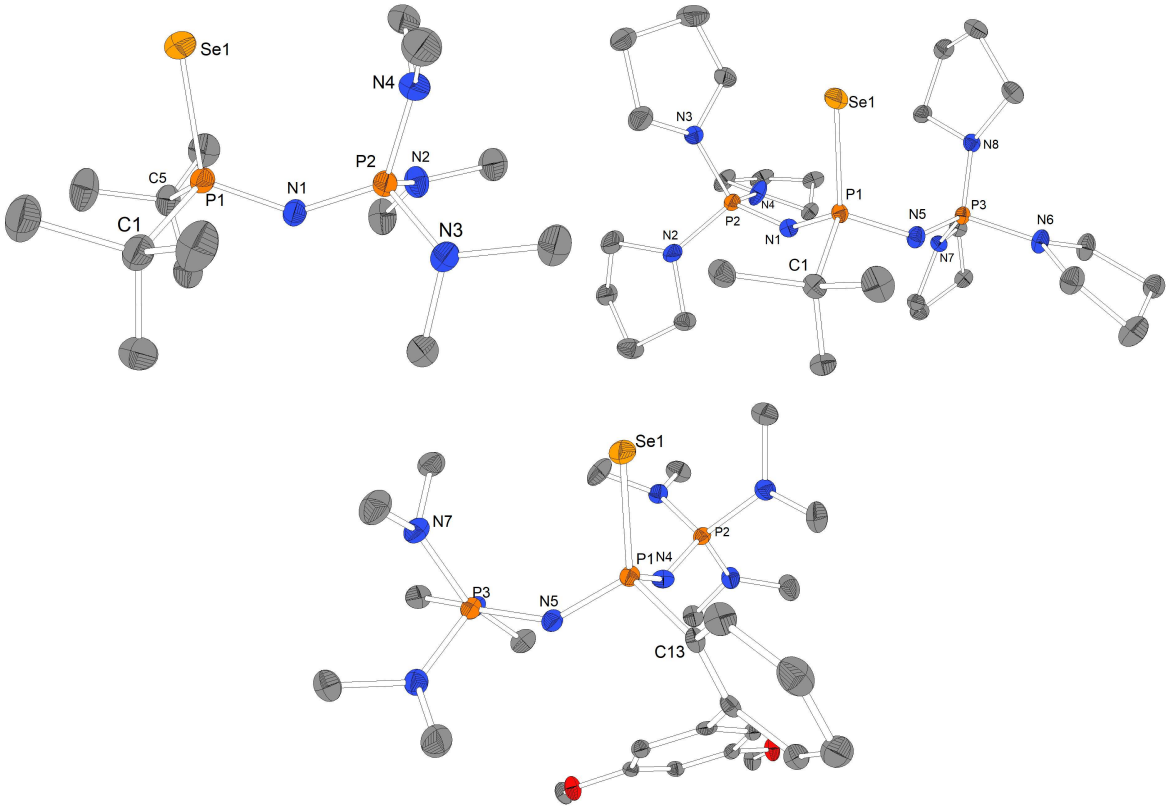

Figure 3.14: Molecular structure of **22a** (left), **23b** (right) and **30** (bottom). Ellipsoids are set at 50% probability. Hydrogen atoms have been omitted for clarity. Notable bond lengths [Å] and angles [°]: **22a**: Se1-P1 2.140(6), P1-N1 1.613(2), N1-P2 1.565(0), P2-N2 1.653(2), P1-C1 1.879(2), N1-P1-Se1 118.3(7), P1-N1-P2 137.3(1), N1-P2-N3 112.2(9); **23b**: P1-Se1 2.156(5), P1-N1 1.623(2), N1-P2 1.553(2), P2-N2 1.659(2), P1-C1 1.857(2), N1-P1-Se1 115.4(6), P1-N1-P2 142.2(1), N1-P2-N3 123.4(8); **30**: P1-Se1 2.163(7), P1-N4 1.614(2), N4-P2 1.560(2), P1-C13 1.847(2), N4-P1-Se1 113.8(7), P1-N4-P2 137.3(1), N5-P3-N7 121.7(1), C13-C18-C19-C24 -59.3(3).

Overall, it can be concluded that these measures are a reliable way to quantify the donor capabilities of PAP.

3.1.7 Experimental Determination of the Basicity

The basicity of PAP was determined experimentally as well as theoretically. Additionally, the gas phase basicity and proton affinity were calculated using DFT methods. Experimentally, the basicity could be determined by the competition reaction between a PAP and a reference base with a similar pK_{BH^+} value by measurement of quantitative ^{31}P-NMR spectra as described in Section 3.1.4. An example for the determination of pK_{BH^+} values is shown here:

5a (8.57 mg, 26.6 µmol), MTBD (4.66 mg, 30.4 µmol) and bistriflimidic acid $HNTf_2$ (5.78 mg, 26.6 µmol) were dissolved in THF-d_8, transferred to an NMR tube and shaken. The integrals of the resulting mixture of **5a** and **5a**-H^+ were 0.67 and 0.33 (Figure 3.15). Therefore, the molarity of **5a** and MTBD can be calculated as 17.7 µmol and 12.7 µmol. The molarities of **5a**-H^+ and $MTBDH^+$ are the differences of the starting molarity to the calculated molarity. The rate constant K can now be calculated by equation 3.1:

$$K = \frac{n[(\mathrm{dma})\mathrm{P}_1\mathrm{P} - (t\mathrm{Bu})_2] * n[\mathrm{MTBDH}^+]}{n[\mathrm{MTBD}] * n[(\mathrm{dma})\mathrm{P}_1\mathrm{P} - (t\mathrm{Bu})_2\mathrm{H}^+]} \tag{3.1}$$

The pK_{BH^+} can be calculated by subtraction of the logarithm of K with the pK_{BH^+} of the reference base (MTBD = 18.6 in THF).[23]

$$\mathrm{p}K_{BH^+} = 18.6 - \log(K) = 18.6 - \log 2.80 = 18.15 \tag{3.2}$$

pK_{BH^+} values of the THF scale (measured) can be correlated to the MeCN scale using correlation equation 3.3 reported by Leito *et al.*[23]

$$\mathrm{p}K_{BH^+}(THF) = (0.92 \pm 0.02) * \mathrm{p}K_{BH^+}(MeCN) - (5.15 \pm 0.51) = 24.8 \pm 0.1 \tag{3.3}$$

These measurements were repeated for all PAPs except for **9** because its basicity proved to be lower than NEt_3 and therefore wasn't pursued further. The measurements for **13** could not be taken, as impurities of **2a** inhibited the competition reaction. The gas phase basicities (GB) and proton affinities (PA) were determined by the calculation of the gas phase structures of PAP and protonated PAP. They can be calculated as follows:[165]

$$\Delta G = G_{(LH)} - [G_{(L)} + G_{(H^+)}] \tag{3.4}$$

$$PA = H_{(LH^+)} - [H_{(L)} + H_{(H^+)}] \tag{3.5}$$

The values for the gas phase enthalpy and entropy of protons are:
$H_{(H^+)} = 1.48\ kcal/mol$
$S_{(H^+)} = 26.02\ kcal/(mol * K)$
$G_{(H^+)} = -6.28\ kcal/mol$.[166]

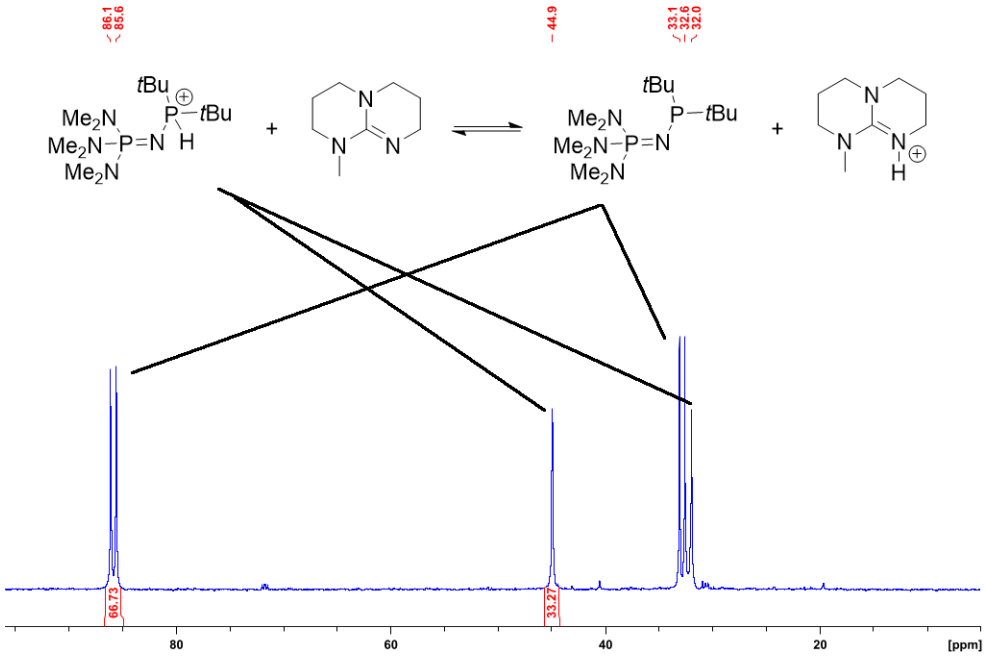

Figure 3.15: ^{31}P-NMR (121 MHz, THF-d_8) spectra of the experimental evaluation of **5a** by competition reaction with MTBD and integration of the protonated and free PAP.

To calculate the pK_{BH^+} value, the compounds were optimized in the gas phase and their vibrational frequencies were calculated in order to ensure that the optimized structure was a global minimum. Next, the compounds were calculated using a conductor-like polarizable continuum model (CPCM) to simulate solvent interactions.[167] By inserting the GIBBS energies of these PAPs into the thermodynamic cycle by SHIELDS *et al.* (Figure 3.16 and Equation 3.6) the pK_{BH^+} value could be calculated.[153]

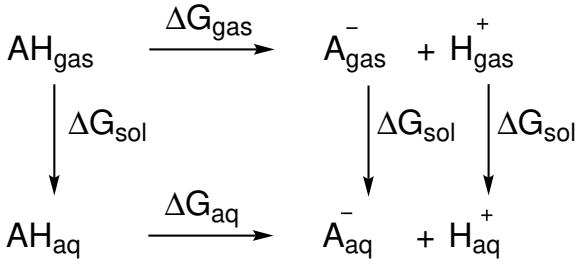

Figure 3.16: Thermodynamic cycle for estimating basicity in solution by SHIELDS and coworkers.[153]

The basicity can therefore be described by the following equation:

$$\begin{aligned} pK_{(BH^+)} = pK_{(AH^+)} + [&G_{gas}(B) - G_{gas}(A) - G_{gas}(BH^+) + G_{gas}(AH^+) + \\ &\Delta G_{sol}(B) - \Delta G_{sol}(A) - \Delta G_{sol}(BH^+) + \Delta G_{sol}(AH^+)] \ / \ 2.303\ RT \end{aligned} \tag{3.6}$$

The results of these experiments and calculations are displayed in Table 3.5.

Table 3.5: Gas phase basicity (GB), proton affinity (PA), measured and calculated pK_{BH^+} values of PAP.

monoPAP	**5a**	**5b**	**5c**	**5d**	**5e**[138]	**5f**[138]	**9**
GB [kcal/mol][a]	258.1	259.6	258.6	258.2	257.4	267.9	243.7
PA [kcal/mol][a]	265.6	267.2	266.2	265.2	265.8	274.7	251.4
pK_{BH^+}[b]	24.8	25.7	25.1	24.8	-	-	>18
pK_{BH^+} (calc.)[c]	25.2	25.8	26.2	25.6	26.4	31.5	-

Bis, trisPAP	**6a**	**6b**	**13**	**7a**[85]	**7b**[85]	**PMe_3**[138]
GB [kcal/mol][a]	270.3	276.0	274.4	291.3	300.2	223.6
PA [kcal/mol][a]	278.7	283.6	282.0	297.4	307.5	230.9
pK_{BH^+}[b]	33.7	35.1	-	41.7	43.1	15.5
pK_{BH^+} (calc.)[c]	34.3	36.7	30.7	43.8	45.1	15.5

[a] Proton affinities and gas phase basicities were calculated using PBE/def2tvp[153,154] and calculated according to equation 3.4 and 3.5.
[b] Measured in THF-d_8 and correlated to the MeCN scale according to Leito *et al.*[23]
[c] Calculated using PBE/def2tzvp[153,154] and calculated according to equation 3.6.[153]

From these experiments it can be concluded, that monoPAPs **5a-5d** all exhibit similar pK_{BH^+} (MeCN) values of 25±1 with **5b** being stronger than **5a** and **5f** being overall the strongest of these as would be expected. Also, as expected, **6a** and **6b** are stronger than their monoPAP analogues **5a** and **5b** and weaker than their trisPAP analogues **7a** and **7b**. This is further supported by the calculated pK_{BH^+} values, which match the experimental values. This trend can also be seen in the GB and PA of these compounds. monoPAPs **5a-5f** have GB of 257-267 kcal/mol and PA of 265-274 kcal/mol with **5f** being the strongest of this series. In the row of **5a** to **6a** to **7a** the GB increases by 10-15 kcal/mol per phosphazene unit corresponding to an increase in basicity of 6–7 units which matches with Schwesinger's *battery cell* principle.[17]

3.1.8 Sterical Parameters

In order to investigate the steric properties of these PAPs, the buried volume as well as the solid and exact cone angles were calculated. The buried volume ($\%V_{Bur}$) is the amount of space that is occupied by a ligand inside a sphere of a predefined radius (3.5 Å) centered on the metal atom. It was calculated by the use of an online tool SambVca by Cavallo *et al.*[111,112] It also allows for the generation of steric maps of the ligands. Other steric parameters that were calculated were the exact cone angle and the solid cone angle developed

by Bilbrey *et al.*[109,110] The exact cone angle is the apex angle of a cylindrical cone centered on the metal atom of a [PAP-Ni] complex. This angle is different to Tolman's definition of a cone angle, as it allows for flexibility on the bond length of [PAP-Ni]. Closely related is the solid angle ω, which can be described as a measure of the 'shadow' cast by an atom or group of atoms when placed relative to an apex atom, 'a light source'.[109,110] They are not bound by a fixed L-M bond length and can be calculated from a crystal or computationally generated structure. The disadvantage of the solid angle approach is, that it treats the ligand as 'frozen' which induces inaccuracies, as ligands are often able to almost freely rotate along low rotational barriers.[108–110] For the sake of completeness, both cone angles were included. An overview over the cone and solid angles as well as the buried volumes of PAPs can be seen in Table 3.6. The inputs for these calculations were optimized gas phase structures of PAP-Ni complexes for cone angles and [PAP-AuCl] complexes for buried volumes.[b] Notably, the values for **32a** and **33a** only differ by 0.5% and 0.1% from XRD to DFT optimized structures, showing that this method is a reliable measure to compare their buried volumes.

Table 3.6: Calculated cone and solid angles, as well as buried volumes of PAP.

monoPAP	**5a**	**5b**	**5c**	**5d**	**9**
Cone Angle [°][a]	193.5	207.9	203.5	194.8	214.2
Solid Angle [°][a]	182.2	186.7	202.9	185.6	203.8
$\%V_{Bur}$[b]	44.1	45.6	45.9	43.1	55.1

Bis, trisPAP	**6a**	**6b**	**13**	**7a**	**7b**
Cone Angle [°][a]	194.9	216.9	237.6	203.2[85]	198.9[85]
Solid Angle [°][a]	193.5	201.3	258.7	-	-
$\%V_{Bur}$[b]	47.4	46.5	54.2	48.7[86][c]	40.9[86]

[a] Cone angles were calculated according to a method developed by Bilbrey *et al.*[110] A Mathematica package FindConeAngle or FindSolidAngle developed by the authors was used.[168] The inputs were optimized geometries of L-Ni complexes at the PBE/def2tvp level.[153,154]

[b] Calculated using [L-AuCl] complexes at the PBE/def2tvp[153,154] level with SambVca 2.0 (r = 3.50 Å, Bond radii scaled with 1.17, Hydrogens omitted).[111,112]

[c] Calculated using the crystal structure of [L-Ni(CO)$_3$] complex.

PAPs exhibit very high cone angles of around 200°, which surpasses P*t*Bu$_3$ (182°)[89] and lies in the same range as Gessner's YPhos (199°).[60] The higher end of cone angles for these compounds can be found on the pyrrolidino and cyclohexyl substituted PAPs **5b**, **5c** and **6b**. Interestingly, the substitution of dimethylamino groups by *t*-butyl groups from **5a** to **5d** does not increase the cone angles by a huge amount. **9** and **13** both exhibit extremely high cone angles, as was expected because of their bulky dipp or biaryl substituents. The buried volume follows a similar trend and ranges from 44-55%. **9** and **13** are the exceptions again with extremely high buried volumes which are similar to Buchwald's biarylphosphines (50.9% for JohnPhos)[169] and Gessner's YPhos (48.5%).[72] PAPs are also sterically more demanding than Dielmann's IAPs (35.3%; 36.2%)[81,169], P(Ad)$_3$ (40.5%)[170] and P*t*Bu$_3$

[b]For computational details, refer to section 8.6.

(38.1%).[169] As already mentioned, steric maps of these PAPs were obtained by the use of *SambVca* which allows some insight into the catalytic pockets that may be formed with these compounds. Figure 3.17 shows the sterical maps of **5a** to **5d** which represent the filled space of a sphere with a radius of 3.5 Å. The P-Au axis is oriented into the plane and defined as the z-axis. From this, the difference between monoPAPs can be seen clearly as both **5c** and **5b** have more bulky substituents on the phosphazene core, resulting in a higher hindrance in the western sectors of these sterical maps.

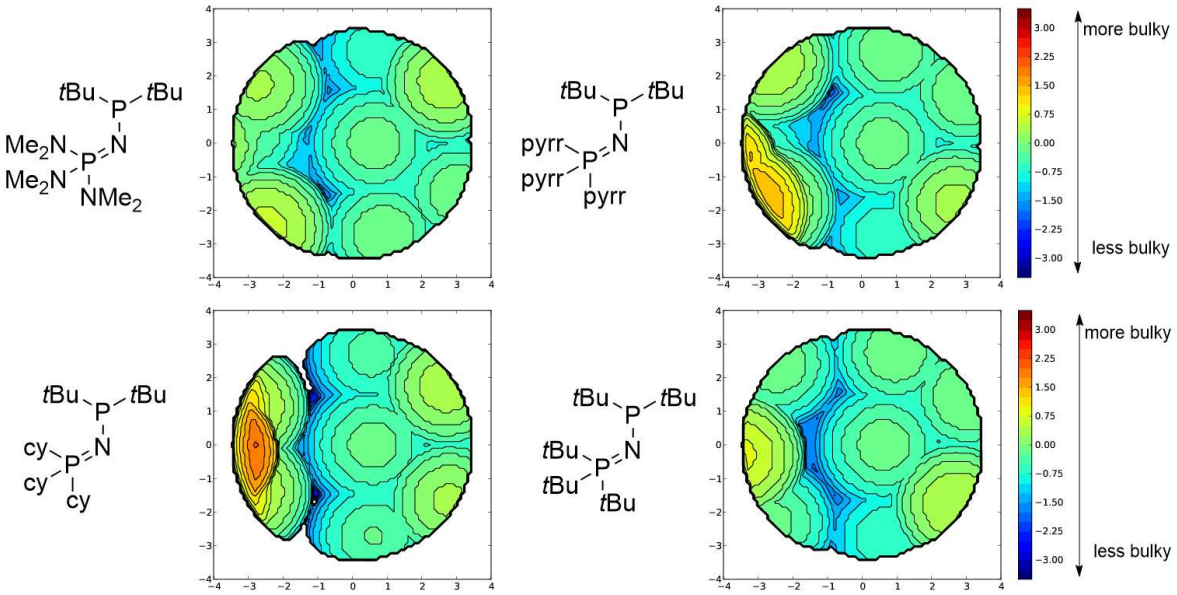

Figure 3.17: Sterical maps of **5a** (top left), **5b** (top right), **5c** (bottom left) and **5d** (bottom right). The trivalent phosphorus atom is centered in the middle of the sterical map and the molecule is viewed along the P-Au (z) axis.

Figure 3.18 shows the sterical maps of bisPAPs **6a** and **6b**. The increase in steric demand from mono- to bisPAP is clearly visible. Again, the pyrrolidino substituents of **6b** are more sterically demanding than the dimethylamino substituents of **6a**.

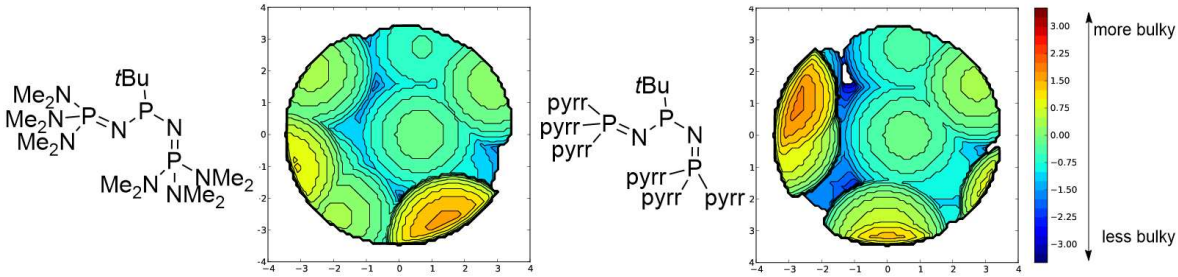

Figure 3.18: Sterical maps of **6a** (left), **6b** (right). The trivalent phosphorus atom is centered in the middle of the sterical map and the molecule is viewed along the P-Au (z) axis.

Figure 3.19 shows the sterical maps of **9** and **13**. These two PAPs show very blatantly their difference in sterics in comparison to other PAPs. Phosphoramidite **9** features very high

sterical demand, stemming from its dipp groups in the eastern sector of the map. Bisaryl **13** is even more extreme, both the northern as well as the southern sector are sterically shielded by the phosphazenyl and biaryl substituents. However, good accessibility from the eastern and western side of the ligand can be seen. This is the catalytic pocket stabilized by π arene interactions. The same can be said for **9** to a lesser extent.

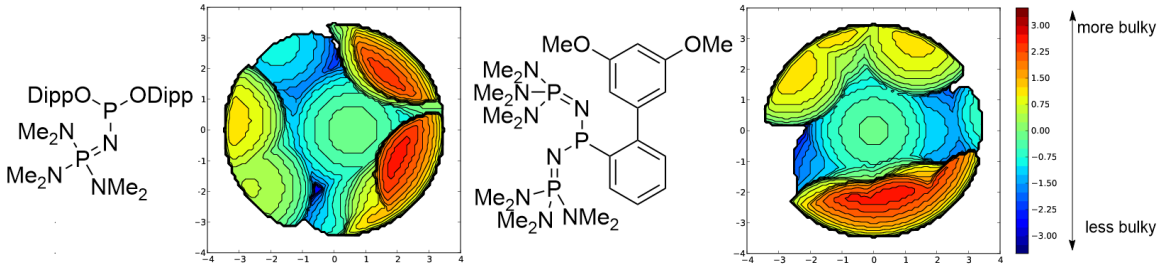

Figure 3.19: Sterical maps of **9** (left) and **13** (right). The trivalent phosphorus atom is centered in the middle of the sterical map and the molecule is viewed along the P-Au (z) axis.

Synthetically, [AuClPxP] (x = 1,2) compounds were obtained by addition of [PPh_3AuCl] or [SMe_2AuCl] under the exclusion of light after stirring for one hour or overnight (Scheme 3.10). Through removal of the solvent *in vacuo* and subsequent redissolving in hot pentane, the compounds were isolated. It is noteworthy to add, that slow cooling to −30 °C is required in order to ensure the product is free of PPh_3.

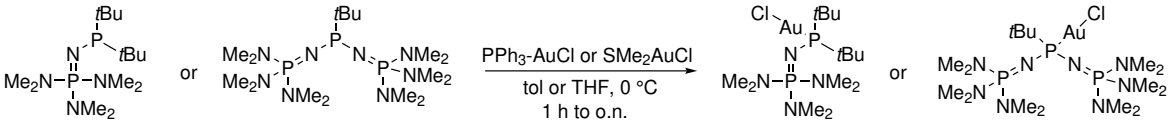

5a **6a** **32a** **33a**

Scheme 3.10: Synthesis of **32a** and **33a**.

Single crystals suitable for XRD of **32a** and **33a** (Figure 3.20) were obtained by slowly cooling a saturated pentane solution to −30 °C. **32a** features a P1-Au1 bond length of 2.253 Å and **33a** of 2.256 Å. This is shorter than PPh_3-AuCl with 2.231 Å[171] and comparable to Gessner's *o*TolYPCy_2 with 2.254 Å.[72] The Cl1-Au1-P1 bond angles are all close to the expected 180°. The P1-N1 bonds are shortened relative to their free base forms.

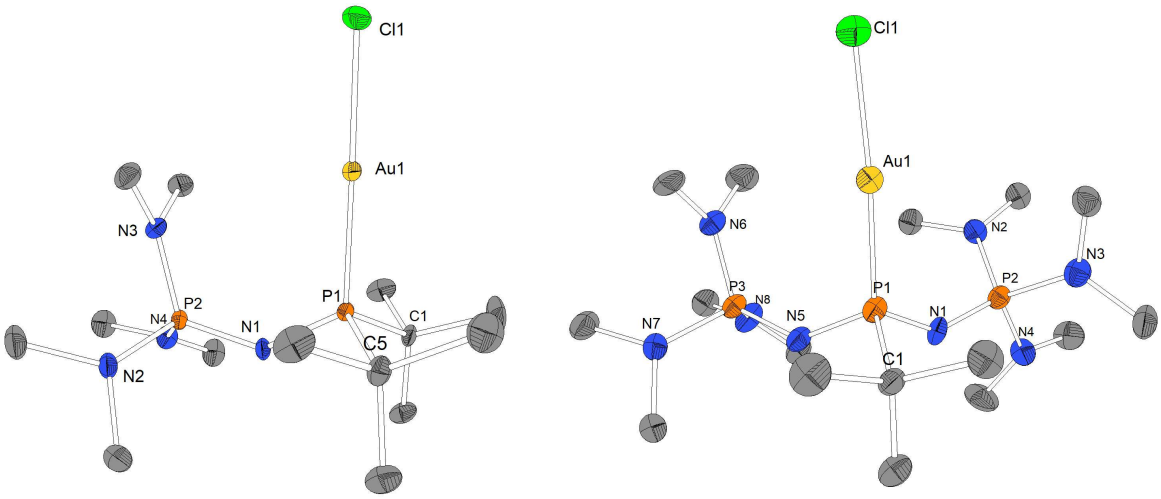

Figure 3.20: Molecular structures of **32a** (left) and **33a** (right). Ellipsoids are set at 50% probability. Hydrogen atoms have been omitted for clarity. Notable bond lengths [Å] and angles [°]: **32a**: N1–P1 1.62(3), N1–P2 1.57(3), P1–Au1 2.25(9), Cl1–Au1 2.31(1), P1–Au1–Cl1 179.2(4), **33a**: N1–P2 1.57(7), Cl1–Au1 2.34(2), N1–P1 1.61(7), P1–Au1 2.26(2), P1–Au1–Cl1 175.6(9).

3.1.9 Mulliken Orbital Charge Population Analysis

For a closer investigation into the nature of the donor capabilities, a series of calculations was performed to determine the strength of σ-donation and π-acceptance for these ligands. This was previously done for the heavier analogues of NHCs: heterocyclic tetrylenes (Ar_2NENAr_2 with E = Ge, Sn, Pb).[172] [PAP-Ni$(CO)_3$] complexes were calculated using PBE/def2tvp and the P(III)-Ni axis was oriented along the z-axis.[153,154] The σ-donation may be measured as the change of the Mulliken charges in s(P) and p_z(P) orbitals from free ligand to nickel complex. The π-acceptance can likewise be calculated by the differences in p_x(P) and p_y(P) orbitals. The fragmentation as well as the bond energy were calculated as the breakage of the P-Ni bond along the z-axis with unrelaxed (non-optimized) and relaxed (optimized) fragments, respectively. An overview of these results is given in Table 3.7.

Table 3.7: Overview over the changes in the Mulliken orbital charge population in π and σ orbitals of PAPs as well as the fragmentation and bond energy of [PAP-Ni(CO)$_3$] fragments.

Ligand[a]	ΔS[b]	$\Delta P\sigma$[b]	$\Delta P\pi$[b]	$\sum \mid \Delta \mid$[c]	π/σ[d]	E_{frag} [kcal/mol][e]	E_{bond} [kcal/mol][e]
5a	0.06	0.47	−0.08	0.44	0.16	54.1	42.9
5b	0.08	0.47	−0.11	0.45	0.19	54.3	43.8
5c	0.09	0.49	−0.06	0.52	0.10	54.9	40.2
5d	0.06	0.48	−0.07	0.48	0.13	52.7	42.8
9	0.15	0.11	0.03	0.23	−0.11	52.3	40.9
6a	0.10	0.49	−0.09	0.49	0.16	59.4	45.9
6b	0.16	0.42	−0.09	0.49	0.15	61.5	47.1
13	0.19	0.39	−0.07	0.52	0.11	56.4	42.7
7a	0.17	0.37	0.01	0.54	0.02	68.4	48.8
7b	0.24	0.33	0.00	0.56	0.00	66.4	54.7
P*t*Bu$_3$	0.06	0.50	−0.04	0.52	0.07	46.7	38.5

[a] The inputs were optimized geometries of [PAP-Ni(CO)$_3$] complexes at the PBE/def2tvp level.[153,154]

[b] ΔS, $\Delta P\sigma$ and $\Delta P\pi$ values are the differences in Mulliken charge populations of the orbitals between PAP and [PAP-Ni(CO)$_3$] at the central phosphorus atom. $\Delta P\sigma$ orbitals are defined as p_z orbitals along the axis of P-Ni; $\Delta P\pi$ orbitals are defined as the sum of p_x and p_y orbitals perpendicular to said axis.

[c] $\sum \mid \Delta \mid$ is the sum of ΔS+$\Delta P\sigma$ and $\Delta P\pi$ values.

[d] π/σ is the ratio of $\Delta P\pi$ / (ΔS+$\Delta P\sigma$).

[e] E_{frag} is the difference in energy of the unrelaxed fragments of PAP and Ni(CO)$_3$; E_{bond} is the energy of the relaxed fragments.

It can be deduced, that the introduction of alkyl groups into PAPs (**5a-5d**) increases their π-acceptance character, however it is still very low, about double that of P*t*Bu$_3$, a ligand known as an almost pure σ-donor. TrisPAPs (**7a** and **7b**) are pure σ-donors and display virtually no π-acceptance. The sum of donation increases for each added phosphazenyl group, as does the bond and fragmentation energy. Donation abilities of **5a-5d** are comparable, but a substitution of amines to alkyl groups on the phosphazene core seems to increase σ-donation by a small amount. σ-Donor and π-acceptor characteristics are consistent across monoPAPs. **9** is a much weaker σ-donor, but is a better π-acceptor than **5a-5d**. This is also reflected in its very high TEP as discussed earlier. Fragmentation as well as bond energy lie in the range of its mono substituted analogues **5a-5d**. BisPAPs (**6a** and **6b**) lie between its mono- and trisPAP analogues, as expected. Biaryl PAP **13** behaves similarly to its bisPAP analogues despite its obvious sterical differences, suggesting that the electronic properties are mostly set by the phosphazenyl core.

3.2 Summary

The class of phosphazenyl phosphines (PAP) was extended to readily available monoPAPs $R_3P{=}N{-}PtBu_2$ (**5a-5d**) which exhibit similar cone angles and buried volumes as $PtBu_3$ while simultaneously exceeding it in terms of donor ability. A mono phosphazenyl phosphoramidite ligand **9** was introduced in order to provide a PAP with higher π-acceptor character compared to **5a-5d**. With bisPAP representatives $(R_3P{=}N)_2PtBu$ (**6a-6b**), the missing gap to trisPAPs was established. An analogue to BUCHWALD's biarylphosphines **13** could be synthesized and characterized (Figure 3.21). The synthetic strategies allow the extension of the PAP construction kit *via* readily available, easily modifiable building blocks. Electronic properties of all new PAP ligands were investigated and correlated according to their experimental and calculated TEPs of [PAP-Ni(CO)$_3$] complexes and $^1J_{(P,Se)}$ coupling constants of corresponding P-selenides. Their P-basicity was calculated and experimentally measured with the help of a reference bases. Basicity and donor characteristics of monoPAPs are in the same range as prominent ligands from the substance classes of NHCs and YPhos. P-basicity of monoPAPs is comparable to N-basicity of classical Schwesinger-P$_2$ bases. BisPAPs are superior with respect to their basicity and donor character and are comparable to IAP ligands. A computational MULLIKEN population study analyzing the σ-donor and π-acceptor metal ligand bond interactions added additional insight for all these findings. Stability of PAPs towards acidic and basic aqueous conditions was evaluated and a study revealing their potential to act as C-nucleophiles versus as a base was performed.

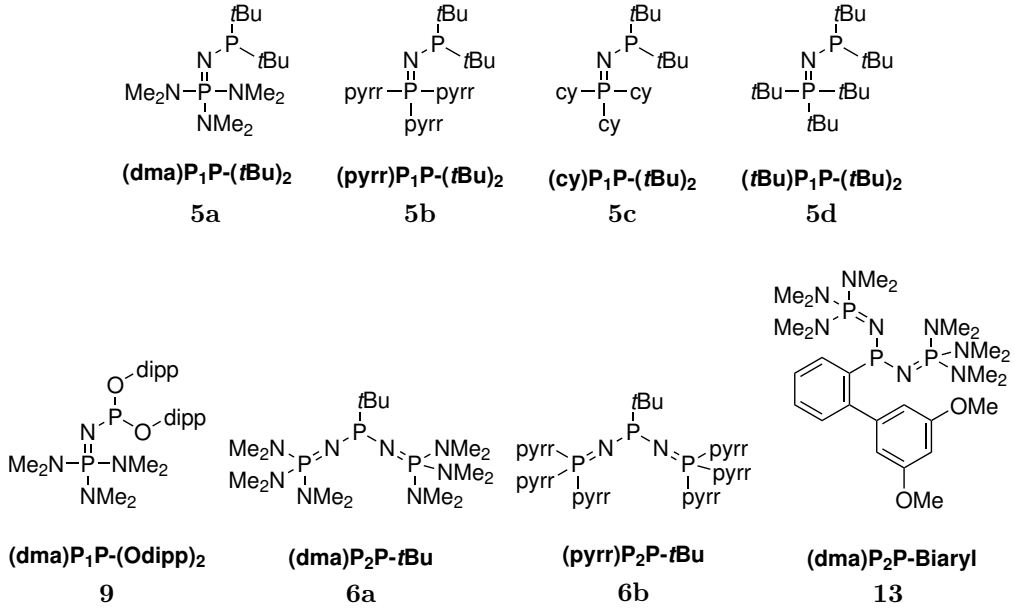

Figure 3.21: Overview over the synthesized and characterized ligands in this chapter.

4 Transition Metal Catalysis with PAP Superbases

4.1 Results and Discussion

Transition metal catalyzed cross coupling reactions have been in the focus of the scientific community for many years. Since their first iteration, there have been huge advancements both in ligand design and understanding of the underlying mechanisms.[173] The Suzuki-Miyaura reaction has been widely used for the synthesis of natural products, liquid crystals and pharmaceuticals.[174–177] Similarly, the palladium catalyzed Buchwald-Hartwig amination reaction can be used for a wide variety of substrates and can be performed on an industrial scale.[178–180] Another reason for the continued popularity of these reactions is the comparably low toxicity of its products and byproducts by avoiding for example tin organyls.[181,182] Mechanistically, these cross coupling reactions function quite similarly. The first step generally involves the generation of the active metal species by reduction of a precatalyst (Figure 4.1). This [L_nPd] (n = 1 or 2) complex undergoes oxidative addition with ArX (X = Cl, Br, I, OTf) leading to $L_nPd(Ar)X$. Through transmetallation with RM (M = $B(OH)_2$, Mg, Sn, Zn) $L_nPd(Ar)R$ is generated. Reductive elimination liberates ArR and regenerates [L_nPd].[183]

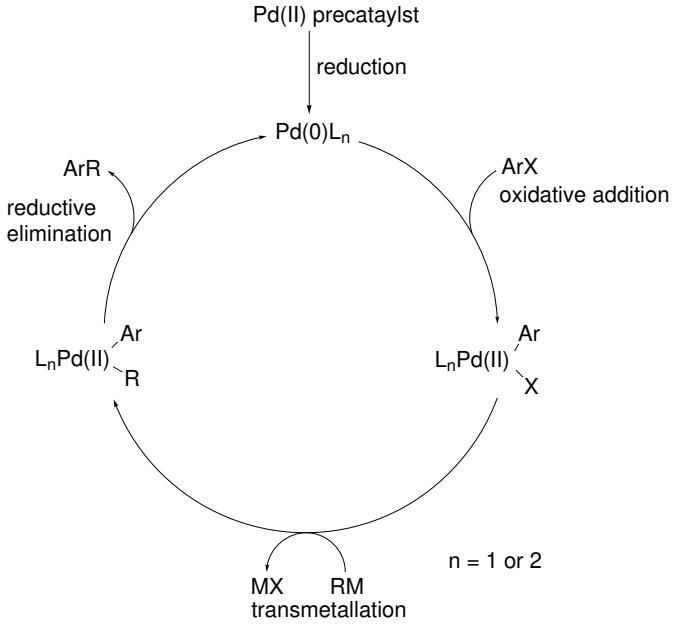

Figure 4.1: General mechanism for a palladium catalyzed cross coupling reaction.[183]

One of the most dominant ligand classes for these transformations are bulky electron rich phosphines. Buchwald *et al.* showed that the introduction of a biaryl moiety offers the

needed sterical hindrance to promote ligand dissociation into 14 VE [L_2Pd] and 12 VE [L-Pd] complexes, while the electron rich phosphine promotes the oxidative addition step.[184–187] Furthermore, the use of precatalysts with a ligand to palladium ratio of 1:1 promotes the formation of a highly active monoligated [L-Pd] species.[188] Buchwald's fourth generation (G4) of precatalysts demonstrate this concept very well (Scheme 4.1). These metallacycles release [L-Pd] and a carbazole derivative under basic conditions with a weak base at low temperatures.[189,190] Several groups make use of these monoligated species like Nolan with NHC complexes of the type [Pd(NHC)(η^3−allyl)Cl][191–193], Fu with [Pd(P*t*Bu$_3$)$_2$][130] as well as Gessner with YPhos [Pd(YPhos)(η^3−*t*Bu−ind)Cl] (*t*Bu-ind = 1-*tert*-butylindenyl).[71,194–196] Dielmann and Verkade show that IAPs and phosphazenes can be utilized as ligands for these transformations as well.[79,80,129] With the intention to expand the scope of available ligands to include phosphazenyl phosphines as an example of highly electron rich and bulky ligands, screening reactions were performed.

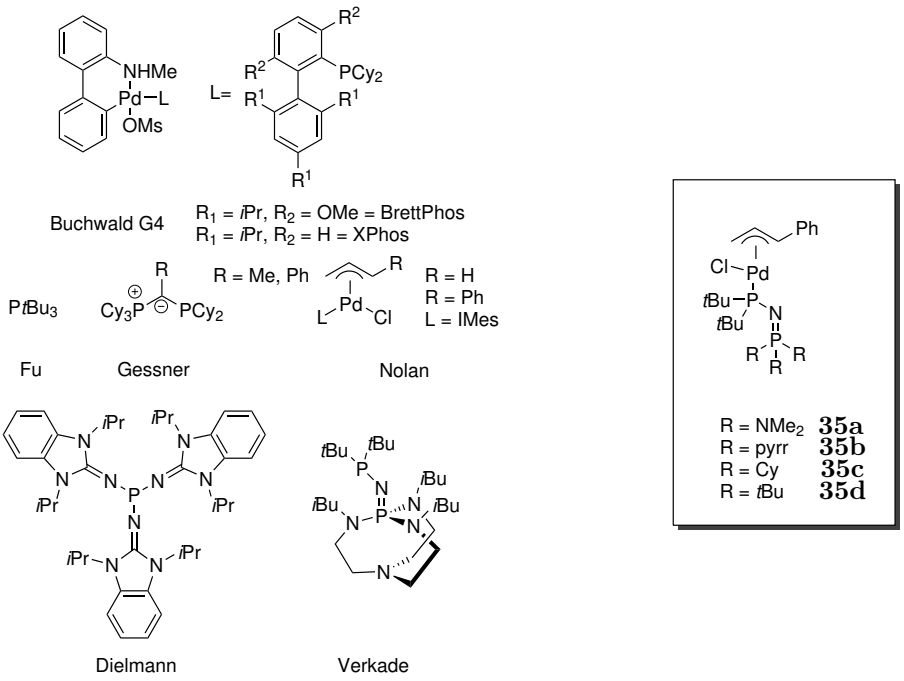

Scheme 4.1: Survey of electron rich ligands used in transition metal catalysis.

4.1.1 Palladium Complexes of PAP

To understand the behavior of these ligands towards different palladium sources, a range of palladium (0) and (II) sources were reacted with various mono-, bis- and trisPAPs in toluene at room temperature. As evident from Scheme 4.2, reactions with $PdCl_2$ and [$(MeCN)_2PdCl_2$] yielded the chlorophosphonium PAP chlorides ([Cl-PAP]Cl) as well as palladium black and a variety of side products (Reactions 1,2 and 8). MonoPAP **5a** yielded, when Na_2PdCl_4 is employed, the palladium complex [$(PAP)_2PdCl_2$] (**36**) as well as a variety of side products. These include the chlorophosphonium PAP as well as palladium black (Reaction 9). If $PdCl_2$ was used, only chlorophosphonium PAP and palladium black were isolated (Reaction 8). The reaction between trisPAP **7a** and [Pd(PPh_3)$_2$$Cl_2$] yielded a mixture of [PAP−Pd−PPh_3], chlorophosphonium PAP and PPh_3 (Reaction 3). The reaction between trisPAP **7a** and [Pd(P*t*Bu$_3$)$_2$] yielded a mixture of [PAP−Pd−P*t*Bu$_3$] and P*t*Bu$_3$ (Reactions 4 and 5).[86]

TrisPAP **7a** reacted with $[Pd(\eta^3\text{−allyl})Cl]_2$ to form the corresponding allyl complex (Reaction 6) and a variety of side products. $[Pd(\pi\text{−cinn})Cl]_2$ reacted, in the case of bisPAP **6a** to palladium black and chlorophosphonium PAP (Reaction 7). If monoPAP **5a** was employed, a quantitative conversion to the corresponding [PAP-Pd(η^3−cinn)Cl] complex could be observed (Reaction 10). It is reasonable to assume, that the reason no $(PxP)_2$-Pd (X = 2 or 3) complexes could be isolated, is that the complexes do not possess a sufficient amount of π-backbonding capabilities to stabilize Pd(0) and therefore hinder the generation of palladium black. The fact that [P_3P-Pd-L] (L = PPh_3, P*t*Bu_3) complexes exist, supports this hypothesis, as the π-acidity of PPh_3 or P*t*Bu_3 may compensate the extreme σ-donor character of the PAP ligand. This is also the reason, why monoPAP reacts much more selectively with palladium precursors, especially $[Pd(\pi\text{−cinn})Cl]_2$ as it possesses better π-backbonding capabilities, as was shown in a previous section.

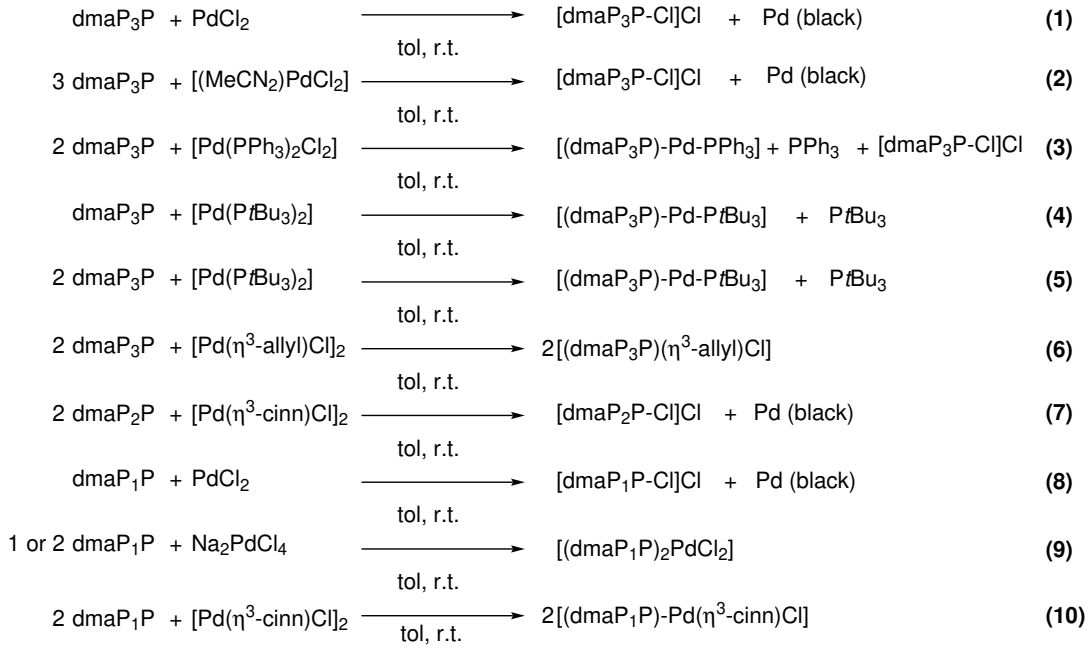

Scheme 4.2: Reaction of various palladium sources with various PAPs. **7a** is referred to as dmaP$_3$P, **6a** as dmaP$_2$P and **5a** as dmaP$_1$P as a shortened notation.

The reaction progress of monoPAP **5a** with $[Pd(\pi\text{−cinn})Cl]_2$ to **35a** can be observed by ^{31}P-NMR spectroscopy as the signals for **5a** shift from 85.4 (P^{III}) and 31.4 ppm (P^V) to 96.6 (P^{III}) and 13.4 ppm (P^V) in **35a**. This is accompanied by a reduction in the $^2J_{(P,P)}$ coupling constant from 100.5 Hz to 6.5 Hz (Scheme 4.3). In order to investigate the activation of this palladium (II) precatalyst an NMR experiment was designed to simulate cross coupling conditions. The complex was reacted with an excess of KO*t*Bu and ^{31}P-NMR spectra were taken. No changes could be detected at room temperature after 1 h indicating an activation barrier in order to generate the active Pd(0) species. Heating of this mixture to 80 °C for 30 min generated a new set of signals in the ^{31}P-NMR spectrum. A set of virtual triplets at 95.3 and 20.7 ppm with a coupling constant of 16.5 Hz appeared, which correspond to a homoleptic [L_2Pd] complex analogous to the Fu catalyst [Pd(P*t*$Bu_3)_2$] (Figure 4.2). Virtual coupling may appear between two nuclei, in this case phosphorus, when the difference in the chemical shift is comparable to their coupling constants. It appears as if in this AA'XX' spin system, X or X' (the trivalent phosphorus atoms) couple to both A and A' (the pentavalent phosphorus atoms), while in

fact, they only couple to A or A' respectively. These two doublets overlap to form this virtual triplet. The Pd(0) species was quenched by addition of phenyl iodide to induce the oxidative addition, resulting in a new set of doublets at 98.0 and 14.0 ppm.

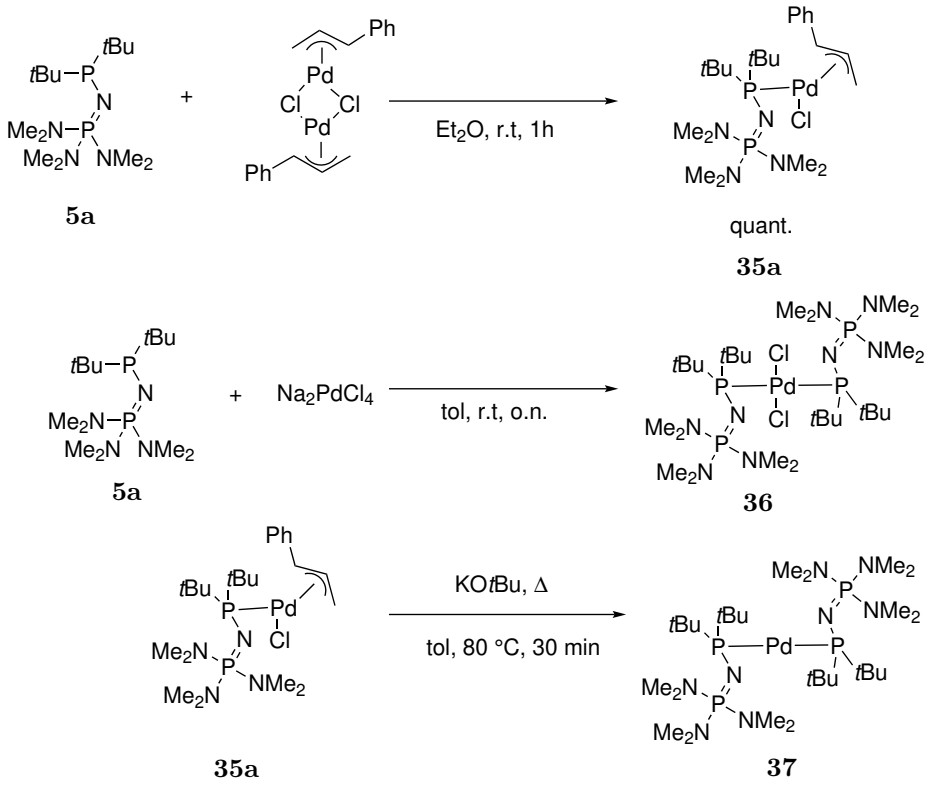

5a **35a** **36** **37**

Scheme 4.3: Synthesis of **35a**, **36** and **37**.

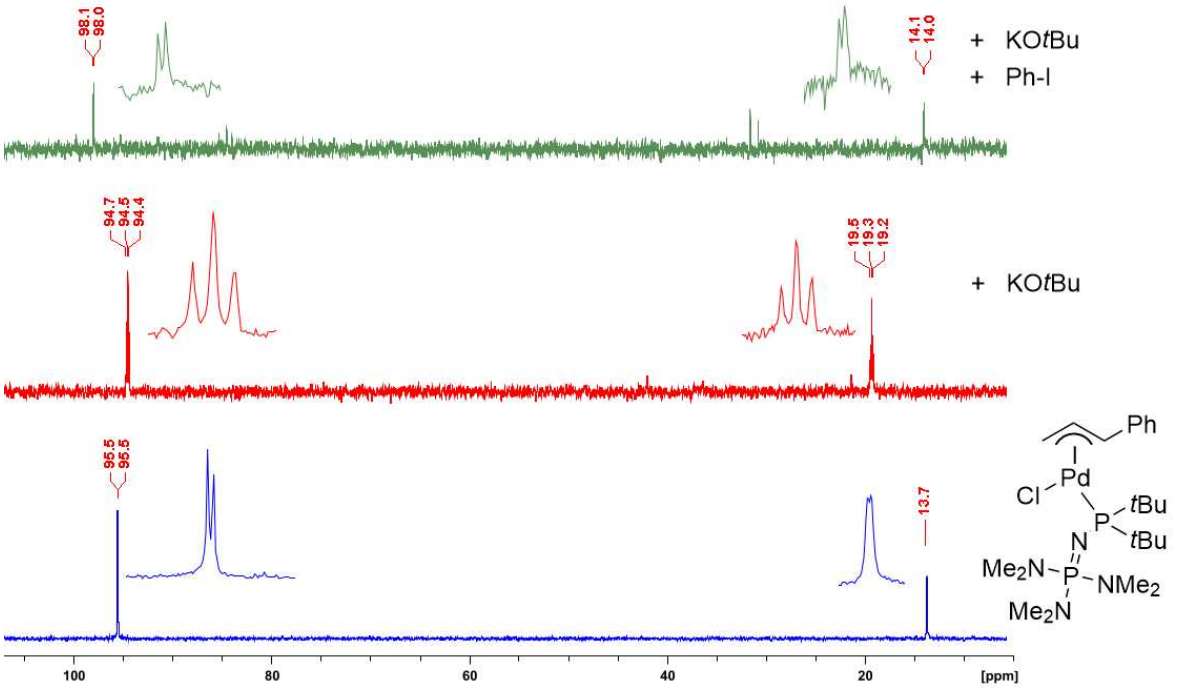

Figure 4.2: ^{31}P-NMR (121 MHz, toluene) spectrum of the reaction of **35a** (bottom) with KO*t*Bu (middle, excess) and phenyl iodide (top, excess).

35a is stable as a solid under air for several months. **38** was obtained as a decomposition product of **35a** with bridging chloride ligands under elimination of the cinnamyl moiety (Scheme 4.4). It was reported by Sigman *et al.* that a solution of [(IMes)-Pd(η^3–allyl)Cl] reacted to form [(IMes)PdCl(μ-Cl]$_2$ upon addition of an ethereal HCl solution.[197] This explains the formation of **38** as a solution of **35a** was most likely hydrolyzed by traces of HCl or onium chlorides.

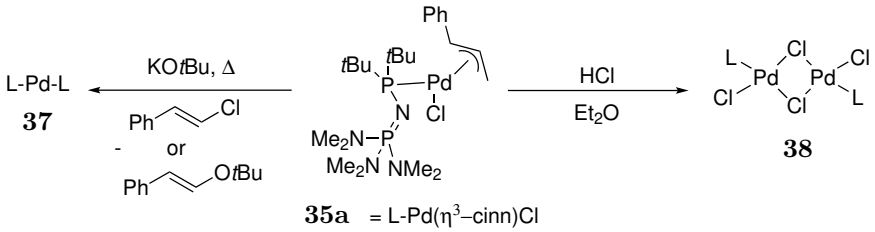

Scheme 4.4: Synthesis of **37** and possible decomposition pathway of **35a** to **38**.

Depending on the ligand, two possible active catalytic species can be generated, either a 14 electron [L$_2$Pd] or a 12 electron [L-Pd] complex.[a] The 12 electron complex has been proven to be kinetically more active than the thermodynamically more stable 14 electron complex.[199] These 12 electron complexes are generated by sterically demanding ligands.[200,201] Due to their electronically unsaturated nature, they cannot be generated *in situ* in the reaction mixture, but must be generated from precatalysts with a 1:1 ratio of ligand to palladium by reductive elimination.[202] Various groups have exploited these 12 electron complexes by the

[a]For more information on the mechanistic aspects, see references [188] and [198].

utilization of a variety of precatalysts. Nolan and Gessner have been employing complexes of [L-Pd(η^3–allyl)Cl] for NHCs[203] and YPhos respectively.[71] The introduction of bulkier groups on the allyl core such as phenyl and *t*-butylindenyl by Hazari has proven to facilitate the reductive elimination towards the [L-Pd] species by hindering the generation of unwanted Pd(I) dimers.[183,204–206] Buchwald phosphines follow a different route towards the generation of these 12 electron complexes *via* the reduction of palladacycles.[207] Organ introduced PEPPSI (**p**yridine-**e**nhanced **p**recatalyst **p**reparation **s**tabilization and **i**nitiation) precatalysts featuring a [NHC-PdCl$_2$-pyridine] unit.[202,208] While each of these precatalysts undergoes a different mechanism for the generation of the active species, a similar mechanism to the ones suggested by Nolan or Poater who investigated [Pd(NHC)(η^3-R-allyl)Cl] complexes is plausible for monoPAPs (Scheme 4.5, path b).[209]

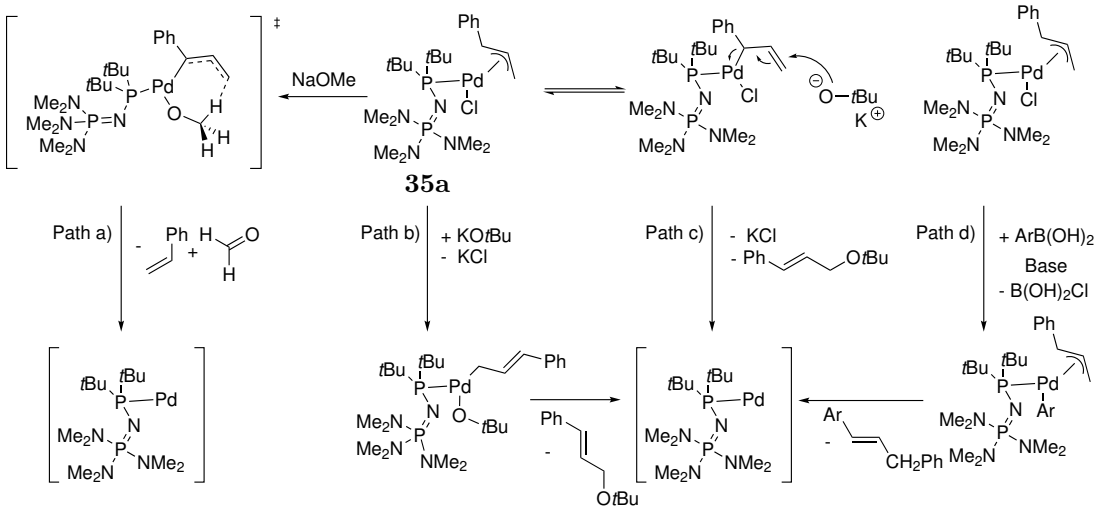

Scheme 4.5: Plausible mechanistic pathways for the generation of [monoPAP-Pd] *via* reductive elimination at precatalyst **35a**.[209]

Four mechanistic pathways a), b), c) and d) towards activation of the precatalyst are suggested. Path a) describes first, a ligand exchange between Cl^- and an alkoxide capable of β-H elimination, in this case OCH_3^-. According to Hazari *et al.* this may occur in an associative or dissociative pathway, depending on the substitutents on the allyl moiety.[206] A H-atom migration, followed by a β-H elimination generates the desired [L-Pd], an alkene and formaldehyde. This was described in alcoholic solvents, but may be applicable if primary or secondary alkoxides are employed as the base. Nolan reports a mechanism where the base, in this case KO*t*Bu, attacks at the coordinated allyl moiety as a nucleophile. Subsequent reductive elimination generates [L-Pd] and allyl-O*t*Bu (Path b).[210] Melvin *et al.* suggests a different route, where a direct attack of an alkoxide nucleophile (RO^-, R = allyl, H) at the Pd-activated allyl moiety followed by reductive elimination generates the free [L-Pd] (Path c).[211] Poater *et al.* calculated the mechanism for this activation with a series of [Pd(NHC)(η^3-R-allyl)Cl] (R = H, Me, Me$_2$, Ph) precatalysts with a variety of substituents on the allyl moiety.[209] They concluded, that the concerted pathway c) is unlikely as they were unable to find a transition state. This does not mean that this pathway is not possible, it only means that in their specific case it was unlikely. Pathway b) is initiated by the substitution of the chloride substituent by -O*t*Bu, but they note, that this step is not rate determining, as the energy barrier is minimal. Much more impact towards the thermodynamic stability

of the intermediates is determined by the allyl backbone, with cinnamyl being the most stable intermediate of the set. The rate determining step was determined to be the reductive elimination, which means, that the stabilization of the transition state has the highest effect on the overall generation of [L-Pd]. Path d) describes the transmetallation of the precatalyst with an arylboronic acid under SUZUKI-MIYAURA reaction conditions. The subsequent reductive elimination yields the desired [L-Pd] complex and the olefin ArCH=CHCH$_2$R (R = Ph).[212,213] This pathway does require the usage of a base, but does allow the option to employ mild bases such as K_2CO_3 which are compatible with most organic substrates, unlike paths a) to c) which need stronger bases. All four mechanistic pathways are possible, depending on the ligand and the substituents on the allyl moiety, as well as the solvent. However, the reductive elimination is the rate determining step in all four cases and the stabilization of the corresponding transition states should be imperative in the design of new systems. It should be noted, that the generated [L-Pd] complexes may coordinate to the eliminated olefins to [LPd(olefin)] type complexes but, upon entry into the catalytic cycle, these olefins are easily released.

4.1.2 Crystal Structures of Palladium Complexes

Single crystals of four different palladium complexes of monoPAP **5a** could be obtained. Firstly, **35a** was obtained by reaction of **5a** with $[Pd(\eta^3\text{–cinn})Cl]_2$ in Et_2O and slow cooling of the ethereal solution to −30 °C (Figure 4.3). The second structure, **36**, was obtained by reaction of **5a** with Na_2PdCl_4 in toluene and subsequent slow evaporation of the solvent (Figure 4.4). Thirdly, the Fu analogue **37** was obtained by slow cooling of an ethereal solution of **35a** after reaction with KO*t*Bu at 60 °C for 1 h (Figure 4.5). Lastly, **38**, a compound with bridging chlorides was obtained as a decomposition product of an ethereal solution of **35a** after several months (Figure 4.6).

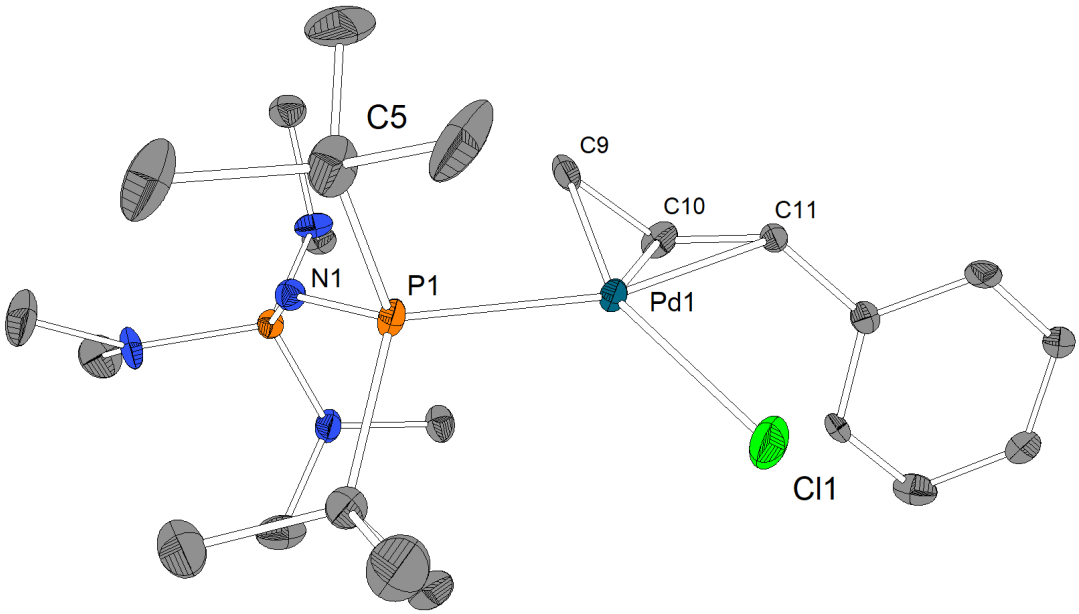

Figure 4.3: Molecular structure of **35a**. Ellipsoids are set at 50% probability. Hydrogen atoms have been omitted for clarity. Notable bond lengths [Å] and angles [°]: P1-Pd1 2.314(5), P1-N1 1.635(16), N1-P2 1.562(17), Pd1-Cl1 2.370(5), Pd1-C11 2.312(18), Pd1-C10 2.174(19), Pd1-C9 2-11(2); P1-N1-P2 145.5(12).

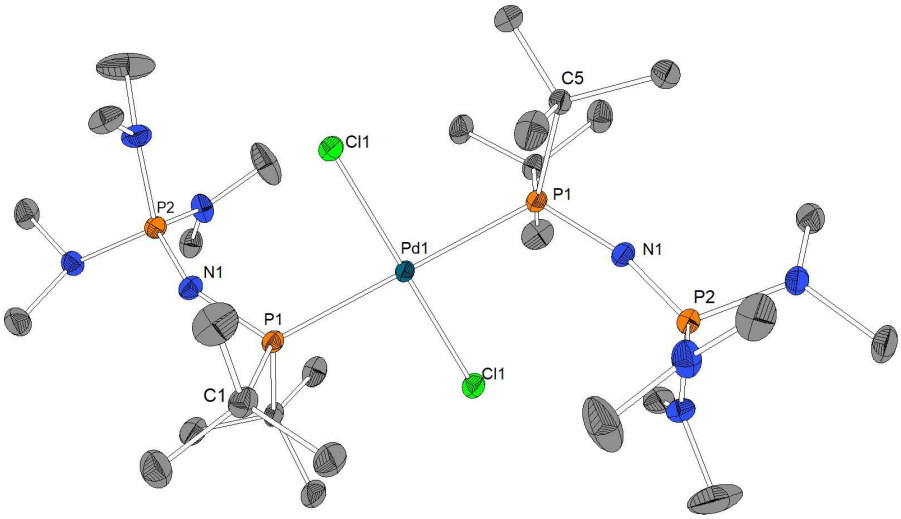

Figure 4.4: Molecular structure of **36**. Ellipsoids are set at 50% probability. Hydrogen atoms have been omitted for clarity. Notable bond lengths [Å] and angles [°]: Pd1-P1 2.4168(5), Pd1-Cl1 2.3008(5), P1-N1 1.6224(16), P2-N2 1.6559(19); P1-Pd1-P1 180.0, Cl1-Pd1-P1 87.066(18).

35a features a P-Pd bond length of 2.314 Å and a Pd-Cl bond length of 2.370 Å which is comparable to similar [Pd(L)(η^3-cinn)Cl] complexes (L = PCy_3 P-Pd: 2.299 Å, Pd-Cl 2.373 Å;[214] L = $PCy_3C(Me)PCy_2$ = keYPhos, P-Pd: 2.317 Å, Pd-Cl: 2.386 Å).[71] **36** crystallizes in the orthorhombic space group P_{bca}. It features a Pd1-P1 bond length of 2.417 Å while in $[(PPh_3)_2PdCl_2]$ it is 2.337 Å and Pd1-Cl1 distances of 2.301 Å compared to 2.291 Å in $[(PPh_3)_2PdCl_2]$.[215] The central palladium atom is, as expected, in a square planar arrangement with bond angles of 180° for P1-Pd1-P1 and Cl1-Pd1-Cl1. The phosphazenyl substituents exhibit a torsion angle N1-P1-P1-N1 of 180°.

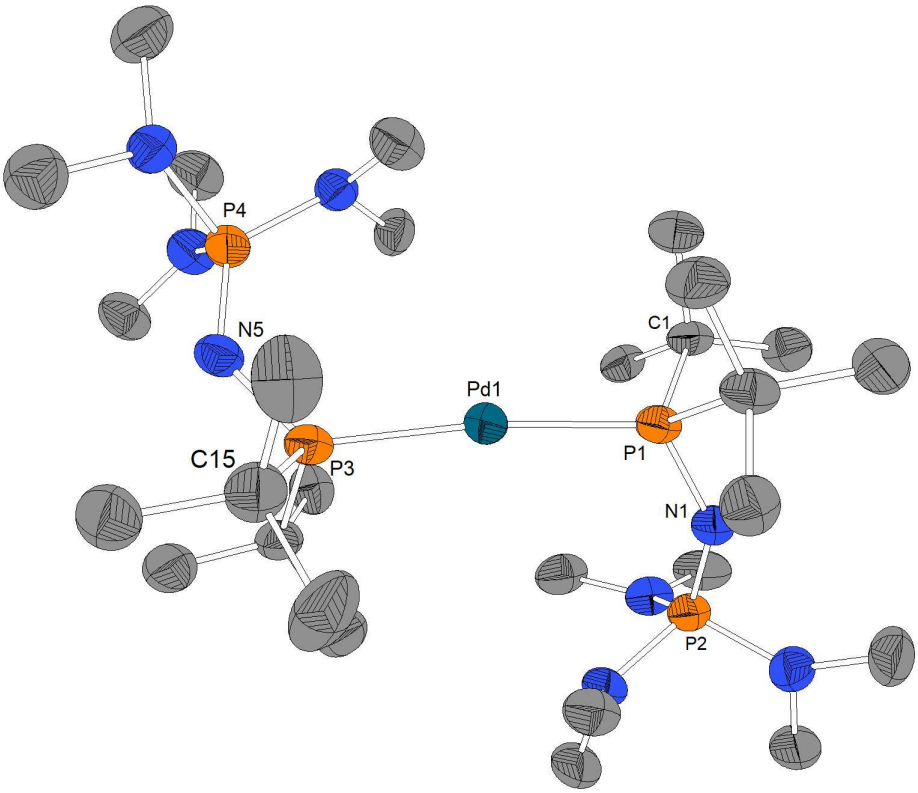

Figure 4.5: Molecular structure of **37**. Ellipsoids are set at 50% probability. Hydrogen atoms have been omitted for clarity. Notable bond lengths [Å] and angles [°]: P1-N1 1.652(5), P2-N1 1.544(5), P1-Pd1 2.2910(17), Pd1-P3 2.3031(18), P3-N5 1.666(6), N5-P4 1.549(5); P3-Pd1-P1 171.49(6), N5-P3-P1-N1 −152.53(4).

The P1-Pd bond length of **37** of 2.291 Å and the P2-Pd bond length of 2.303 Å is slightly longer than the P-Pd bond in [Pd(P*t*Bu$_3$)$_2$] (2.280 Å) and shorter than in the heteroleptic complex [dmaP$_3$P−Pd−PPh$_3$] (2.357 Å).[86,216] The P1-Pd-P2 bond angle of 171.5° is distorted compared to the 180° of the aforementioned structures. The P1-C1 bond length of 1.893 Å is lower than the Fu analogue (1.915 Å). The two phosphazenyl substituents exhibit a torsion angle N1-P1-P3-N5 of 152° in comparison to the torsion angle of the *t*-butyl groups of [Pd(P*t*Bu$_3$)$_2$] with 60°. These differences may be attributed firstly, because **5a** is a better σ-donor than P*t*Bu$_3$ (see Section Donor Properties) and secondly because of the increased sterical strain that is introduced into the structure by the two phosphazenyl substituents.

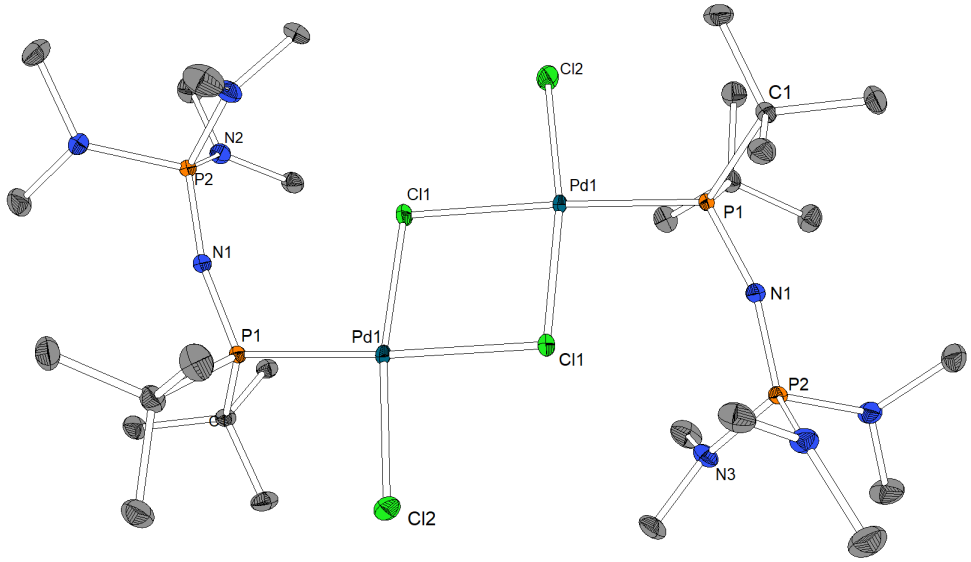

Figure 4.6: Molecular structure of **38**. Ellipsoids are set at 50% probability. Hydrogen atoms have been omitted for clarity. Notable bond lengths [Å] and angles [°]: Pd1-P1 2.2596(3), P1-N1 1.5964(1), N1-P2 1.5522(1), Pd1-Cl2 2.2976(3), Pd1-Cl1 2.4798(3); P1-Pd1-Cl1 176.590(1).

38 crystallizes in the monoclinic space group $P_12_{1/c}$. It possesses a P1-Pd1 bond length of 2.260 Å and a Pd1-Cl2 bond length of 2.298 Å. The bond length of the bridging chlorides Pd1-Cl1 is 2.313 Å. In comparison, an IMes analogue of this crystal ([(IMes)PdCl(μ-Cl]$_2$) possesses a C1-Pd1 bond length of 1.955 Å and Pd1-Cl1 bond length of 2.276 Å while the bond length of the bridging chlorides to Pd1 is 2.332 Å.[197] **38** is completely planar along the P-Pd-Cl-Pd-P axis and exhibits C_{2h} symmetry. In contrast to this, its IMes analogue is twisted along this axis by 27° and is asymmetric. The palladium atoms are distanced 3.6258 Å apart from each other, while in IMes they are only 3.298 Å apart. An overview over some bond lengths of various palladium (0) and palladium (II) complexes is given in Table 4.1.

Table 4.1: An overview over some bond lengths of various palladium (0) and palladium (II) complexes.

Pd(0)	[Pd(P*t*Bu$_3$)$_2$][216]	[Pd(CH$_2$P*t*Bu$_3$)$_2$][217]	[dmaP$_3$PPdPPh$_3$][86]	**37**
P1-Pd1 [Å]	2.280	2.282	2.357	2.291
P1-Pd1-P3 [°]	180	180	180	171.5
Pd(II)	Pd(PPh$_3$)$_2$Cl$_2$[215]	**36**	keYPhos[71]	**35a**
P1-Pd1 [Å]	2.337	2.417	2.317	2.314
Pd1-Cl1 [Å]	2.291	2.301	2.386	2.370

4.1.3 Suzuki-Miyaura reactions

In order to test these ligands about their applicability in cross coupling reactions, they were employed in a palladium catalyzed Suzuki-Miyaura coupling of phenylboronic acid with *p*-toluyl chloride. The halide was chosen consciously as chloride in order to provide a bet-

ter comparison to its parent ligand P*t*Bu$_3$, which is able to catalyze this transformation.[130] Phenylboronic acid was chosen for its simplicity, atom efficiency and high reactivity in the transmetalation. They are more prone to protodeboronation or oxidation compared to other commonly used boron reagents like boronic esters, *N*-coordinated boronates or trifluoroborates, but these require prior hydrolysis to the boronic acid (Figure 4.7).[213] Most often this is achieved by addition of water to the reaction mixture, which was to be avoided with PAPs.[218]

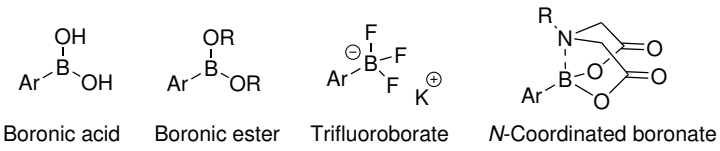

Figure 4.7: Overview over different boron reagents for the Suzuki-Miyaura coupling.

Every ligand was screened under the same conditions with palladium cinnamyl chloride as the palladium source, which was premixed with the ligand before addition (Scheme 4.6). It can be concluded, that monoPAPs **5a**-**5d** perform reasonably well under these conditions, with **5a** providing an almost quantitative yield. Interestingly, **9** also performed well with a yield of 73%, suggesting that not only the donor ability of these ligands is important. A certain degree of π-backbonding has to be present to stabilize Pd(0) intermediates to avoid decomposition to palladium black. With higher substituted PAPs **6a** and **6b** this phenomenon can be observed, as no conversion to the desired product could be detected, only the generation of palladium black. The same can be said for trisPAPs **7a** and **7b**. In direct comparison, P*t*Bu$_3$ did not yield any biaryl product, however, if Cs_2CO_3 was used as the base and dioxane as the solvent, a yield of 85% could be achieved, which is in line with the reported literature.[130] Based upon these promising results, further investigations into these reactions were made. Screening reactions to determine the best base, solvent, palladium source and ligand were performed to optimize this reaction.

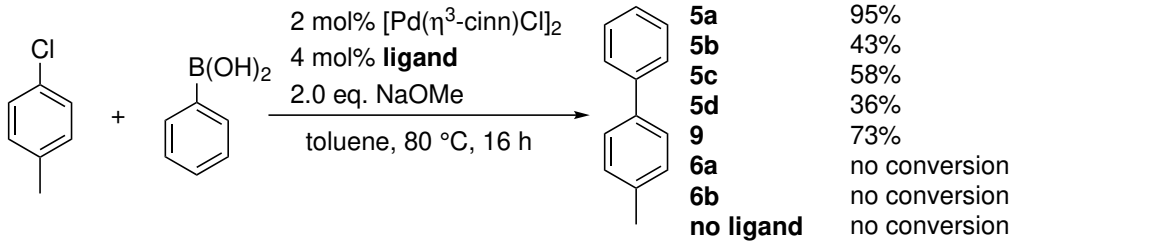

Scheme 4.6: Screening of different PAP ligands in a Suzuki-Miyaura cross coupling reaction with *p*-toluyl chloride and phenylboronic acid.[130]

4.1.3.1 Screening and Optimisation Reactions

The screening of the ligands (Table 4.2) revealed that **5a** outperformed other monoPAPs significantly under the same conditions, as it was able to generate the biaryl product in 99% yield. Lower yields of 36% and 59% were obtained for **5d** and **5c** respectively (Entries 1, 9 and 10). This may be due to their increased steric hindrance at the phosphazene core, which makes them bulkier than **5a**. **9** performed well with 73% yield (Entry 11). The yield did drop significantly to 61% when the catalyst load was reduced to 0.5 mol% (Entry 8). Interestingly,

if weaker bases such as Cs_2CO_3 and Na_2CO_3 were used, the impact on the yield was enormous (Entry 4). This may be due to the inherent need to regenerate the [L-Pd] species through reductive elimination in the catalytic cycle. Due to the ligands intrinsic high basicity, weaker bases may not be able to sufficiently regenerate these. Another plausible reason is, that CO_2 which is generated when metal carbonates are employed, can react with the free base PAP to form reversible PAP-CO_2 adducts which are stable in contrast to PtBu$_3$-CO_2 adducts which require stabilization by a Lewis acid like BCF (tris(pentafluorophenyl)borane).[219] Solvent screening showed that coordinating solvents such as DME and THF slowed down the reaction, while toluene favored it (Entries 6 and 7). When compared under these optimized conditions, both SPhos as well as IMes yielded less product, with 16% and trace amounts only (Entries 12 and 13). However, it is reported that with K_3PO_4 as base and $[(MeCN)_2PdCl_2]$ as precatalyst SPhos can couple with 90% yield in 5 h at 100 °C.[220] IMes may also achieve these yields if microwave assisted or a $[Pd(\pi{-}t\text{Bu}{-}\text{ind})Cl]_2$ precursor is employed.[220,221] The increased performance of IMes with $[Pd(\pi{-}t\text{Bu}{-}\text{ind})Cl]_2$ as opposed to its cinnamyl equivalent can be attributed to a more stabilized transition state for the reductive elimination of the allyl moiety to form [L-Pd] as described earlier. Since these ligands are sensitive to air but can be converted to their HBF_4 salts to allow their storage, it was of interest, if it was possible to employ these salts and *in situ* deprotonate them for usage as ligands. It turned out, that by including a simple deprotonation step by the base, followed by premixing with the Pd source **5a**-HBF_4 performed similarly with a yield of 87% (Entry 5).

Table 4.2: Overview over the performed screening reactions for the SM coupling of toluyl chloride with phenylboronic acid.

Entry	Ligand	Pd source[a]	Base	Solvent	Yield [%]
1	**5a**	DBA	NaOMe	toluene	48
2	**5a**	cinn	NaOMe	toluene	99
3	**5a**	cinn	NaO*t*Bu	toluene	71
4	**5a**	cinn	Cs_2CO_3	toluene	33
5	**5a**-HBF_4	cinn	NaOMe	toluene	87
6	**5a**	cinn	NaOMe	THF	78[c]
7	**5a**	cinn	NaOMe	DME	74
8	**5a**	cinn[b]	NaOMe	toluene	61
9	**5c**	cinn	NaOMe	toluene	59
10	**5d**	cinn	NaOMe	toluene	36
11	**9**	cinn	NaOMe	toluene	73
12	Sphos	cinn	NaOMe	toluene	16[d]
13	Imes	Allyl	NaOMe	toluene	traces[e]
14	-	Fu catalyst	NaOMe	toluene	traces[f]

[a] DBA = Bis-(dibenzylidenaceton)-palladium(0); cinn = Palladium-(π-cinnamyl)-chloride dimer; Allyl = Allylpalladium(II) chloride dimer; Fu catalyst = Bis(tri-*tert*-butylphosphine)palladium(0).
[b] 0.5 mol%
[c] Room temperature
[d] Yield of 90% can be achieved by usage of K_3PO_4 as a base.[220]
[e] Yield of 80% can be achieved in dioxane.[221]
[f] Yield of 85% could be achieved with Cs_2CO_3.[130]
Reaction conditions: 1.0 eq. toluylchloride, 1.5 eq. phenylboronic acid, 2.0 eq. NaOMe, 4 mol% ligand, 4 mol% [Pd], 80 °C for 16 h. Yields are isolated.

Next, the kinetic profile of this reaction was investigated by monitoring of the yield in timed intervals by removal of an aliquot from the reaction mixture and quantifying it by NMR spectroscopy with the help of an internal standard. From Figure 4.8 it can be deduced, that after an initial induction period, the highest activity is detected in the first 90 minutes of the reaction after which it begins to slow down until it has quantitatively proceeded after 4 h. The induction period can be rationalized as the time it takes to generate the active [L-Pd] species through reductive elimination of the cinnamyl moiety by the base and the subsequent oxidative addition of the aryl chloride, as described earlier. In fact, it has been proposed, that the initial generation of [L-Pd] may be the rate determining step.[209] The conversion rate was determined at the amount of time it takes to convert the first 20% of substrate to the desired biaryl product.[222] The conversion rate adjusted for the induction period was also determined, where the rate from the time where conversion is first detected is measured. This results in a rate of 0.63 mol/h and 0.37 mol/h for a concentration of 0.33 M and 0.033 M respectively. Adjusted for the induction period, this corresponds to a rate of 0.84 mol/h and 0.70 mol/h.

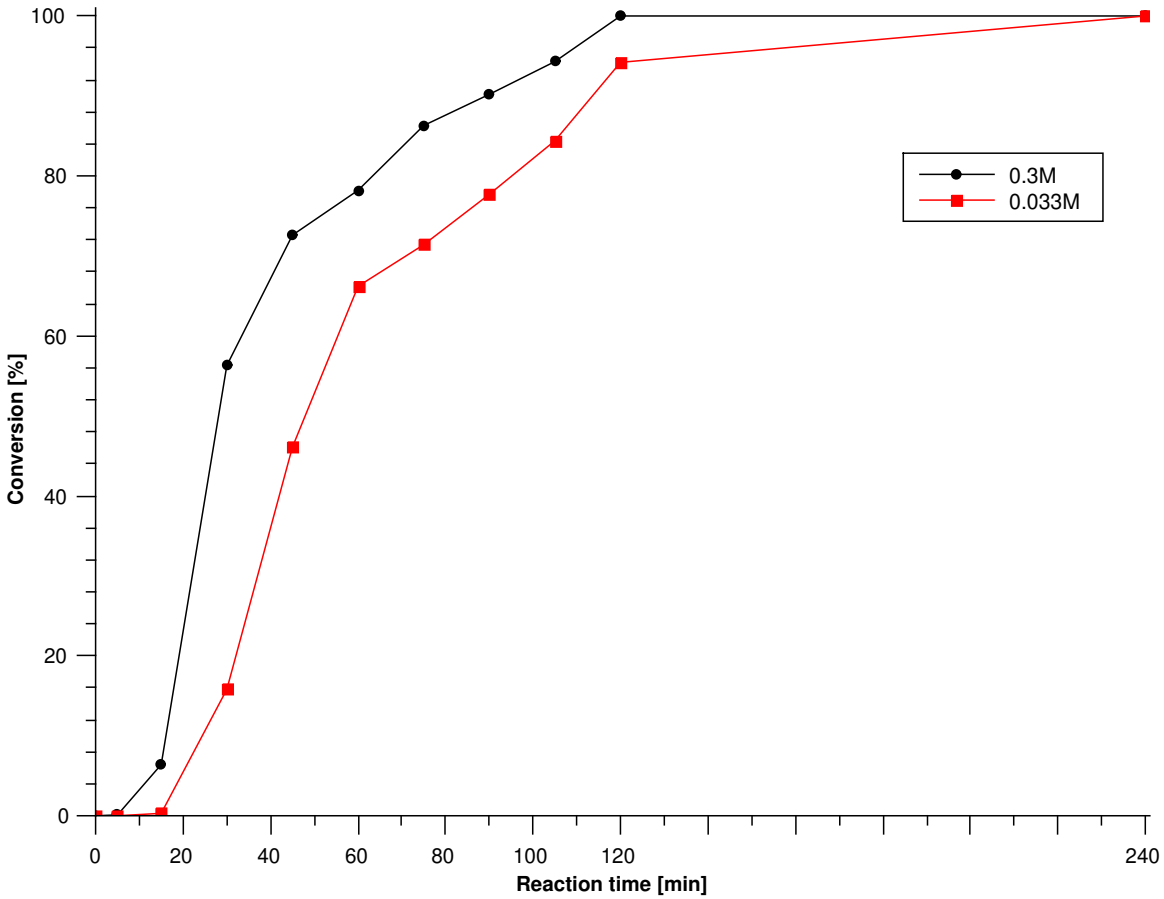

Figure 4.8: Reaction rate of SUZUKI-MIYAURA coupling of 4-chlorotoluene and phenylboronic acid. Conditions: 1.0 eq. ArCl, 1.5 eq. $PhB(OH)_2$, 2.0 eq NaOMe, 4 mol% **5a**, 2 mol% $[Pd(\pi{-}cinn)Cl]_2$. Yields are determined by integration and comparison of product peak to internal standard (1,3,5-trimethoxybenzene).

4.1.3.2 Scope

Satisfied with these reaction conditions, the scope of this new ligand was investigated (Figure 4.9). Electron rich as well as electron poor arenes were coupled in excellent yields. Sterically demanding mesitylboronic acid was coupled with chloroanisole successfully with 78% yield. Chlorobenzenes with *ortho*-substitution were also coupled with both neutral and electron rich boronic acids. Electron poor arylchlorides with *p*-cyanido and trifluoromethyl groups also yielded good results. Mixtures of electron rich and electron poor substrates led to almost quantitative yields. Notably, it was possible to successfully couple a primary amino substituted aryl substrate, demonstrating the functional group tolerance of this system. While it must be conceded, that these ligands may not perform as well as some of the more specialized BUCHWALD ligands at very low catalyst loads, they are at least capable of delivering similar outputs to industry standards such as IMes, SPhos or the Fu Catalyst.[223]

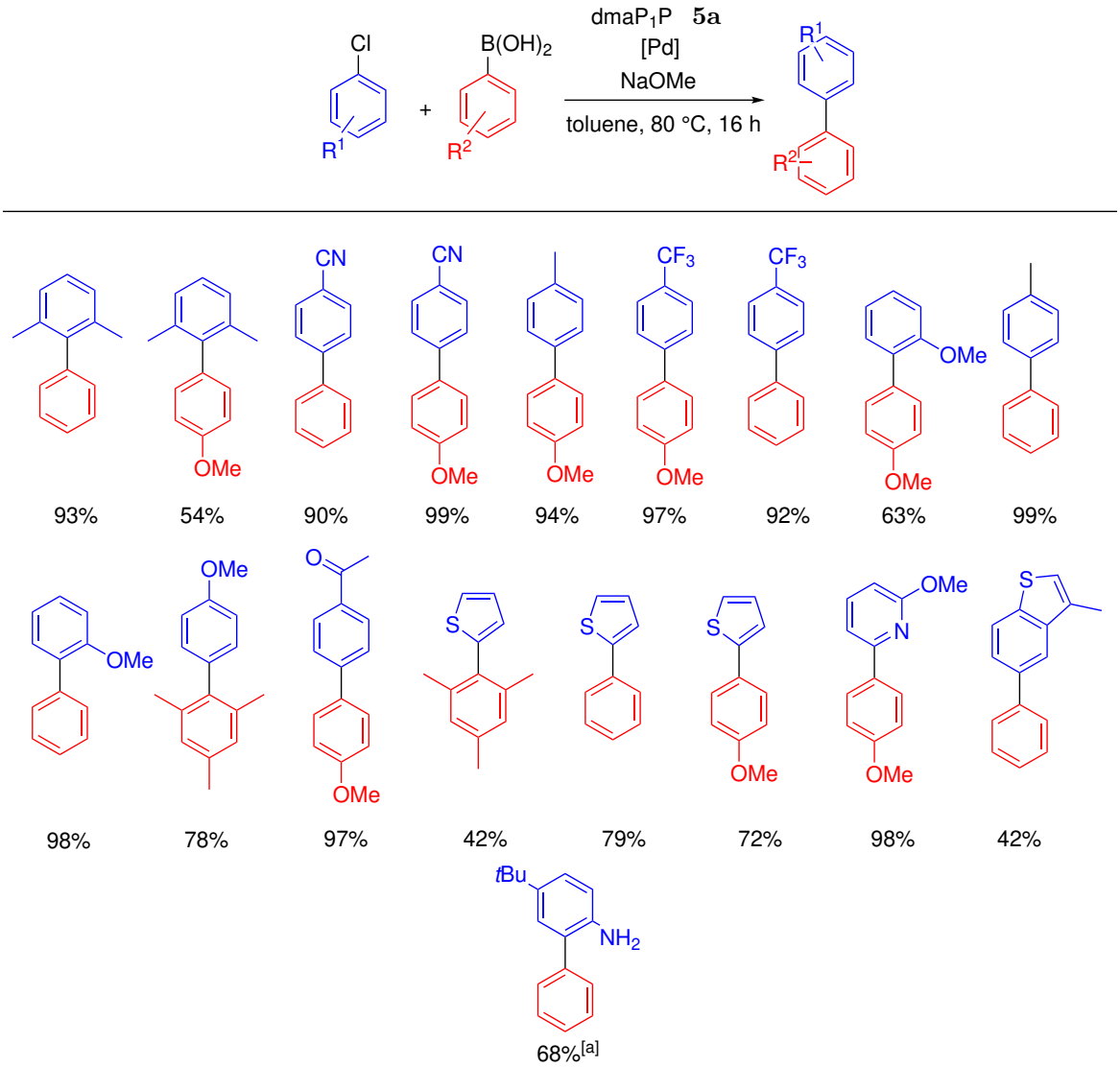

Figure 4.9: Scope of palladium catalyzed SUZUKI-MIYAURA couplings. Reaction conditions: 1.0 eq. ArCl, 1.5 eq. $ArB(OH)_2$, 2.0 eq. NaOMe, 4 mol% **5a**, 2 mol% $[Pd(\pi\text{–cinn})Cl]_2$. Yields are isolated. [a] From Ar-Br.

4.1.4 Buchwald-Hartwig Amination

4.1.5 Screenings and Optimization Reactions

Similarly, it was of interest, if monoPAPs could be utilized as ligands for palladium catalyzed BUCHWALD-HARTWIG amination reactions. The model reaction of 4-methylbromobenzene and morpholine was chosen to evaluate the reactivity of these ligands (Scheme 4.7).

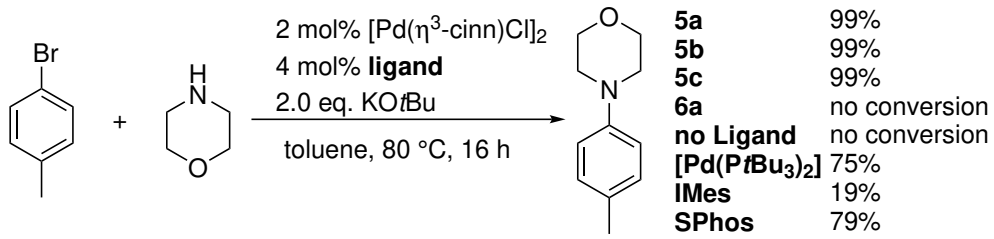

Scheme 4.7: Screening of different PAP ligands in a BUCHWALD-HARTWIG amination reaction with *p*-toluyl bromide and morpholine.[130]

5a, **5c** and **5d** performed very well, achieving quantitative results in all three cases (Table 4.3).

Table 4.3: Overview over the screening conditions for the BUCHWALD-HARTWIG amination of 4-bromotoluene with morpholine.

Ligand	Pd source[a]	Base	Solvent	Yield [%]
5a	DBA	KO*t*Bu	toluene	86
5a	cinn	KO*t*Bu	toluene	99
5d	DBA	KO*t*Bu	toluene	99
5d	cinn	KO*t*Bu	toluene	99
5d	cinn	Cs_2CO_3	toluene	20
5d	cinn	KO*t*Bu	THF	37
5d	cinn	KO*t*Bu	DME	79
5c	DBA	KO*t*Bu	toluene	99
5c	cinn	KO*t*Bu	toluene	99
5c	cinn[b]	KO*t*Bu	toluene	99
SPhos	cinn	KO*t*Bu	toluene	78 (77)[c]
IMes	Allyl	KO*t*Bu	toluene	19 (98)[d]
-	Fu catalyst	KO*t*Bu	toluene	75[e]

[a] DBA = Bis-(dibenzylidenaceton)-palladium(0); cinn = Palladium-(π-cinnamyl)-chloride dimer; Allyl = Allylpalladium(II) chloride dimer; FU catalyst = Bis(tri-*tert*-butylphosphine)palladium(0).
[b] 0.5 mol%
[c] From $Pd(OAc)_2$ and NaO*t*Bu in dioxane.[224]
[d] From (SIPr)Pd(η^3-1-Me-allyl)Cl (SIPr = *N*,*N*'-bis(2,6-diisopropylphenyl)-4,5-dihydroimidazol-2-ylidene) and LiHMDS in toluene.[225]
[e] Isolated yield of 67% is reported in the literature.[223]
Reaction conditions: 1.0 eq. 4-bromotoluene, 1.5 eq. morpholine, 2.0 eq. KO*t*Bu, 4 mol% ligand, 4 mol% [Pd], 80 °C for 16 h. Yields are calculated using an internal standard of 1,3,5-trimethoxybenzene and are obtained by integrating the product peaks compared to the standard.

As seen with the SUZUKI-MIYAURA reaction, when weaker bases were employed, the yields dropped significantly. The reaction proceeded well in toluene and worse in THF or DME. In

the case of **5c** a reduction in catalyst load to 0.5 mol% did not decrease the yield. Therefore, it was decided to focus on this ligand for subsequent reactions. **5c** outperforms SPhos (78% yield at 4 mol%, literature value: 77%)[224] and similar to optimized conditions for IMes (19.2% yield at 4 mol%, literature value: 98%)[225] and shows, at least for electron rich secondary amines, a comparable reactivity to GESSNER's YPhos ligands.[72] In analogue to the SUZUKI-MIYAURA coupling reaction, the kinetic profile of this reaction was investigated by removal of aliquots from the reaction mixture and determination of the yield using an internal standard (Figure 4.10). Notably, the conversion was completed in only ten minutes when utilized at high concentrations. No induction period was identified for this reaction, this may be due to the higher reactivity of aryl bromides compared to their chloride analogues. To better study the reaction kinetics, the concentration of substrates was lowered tenfold. This allowed the generation of a much better kinetic profile. With a conversion rate of about 0.04 mol/min or 2.2 mol/h the reaction proceeded much faster than the SUZUKI-MIYAURA coupling while operating at 1/8th the catalyst load.

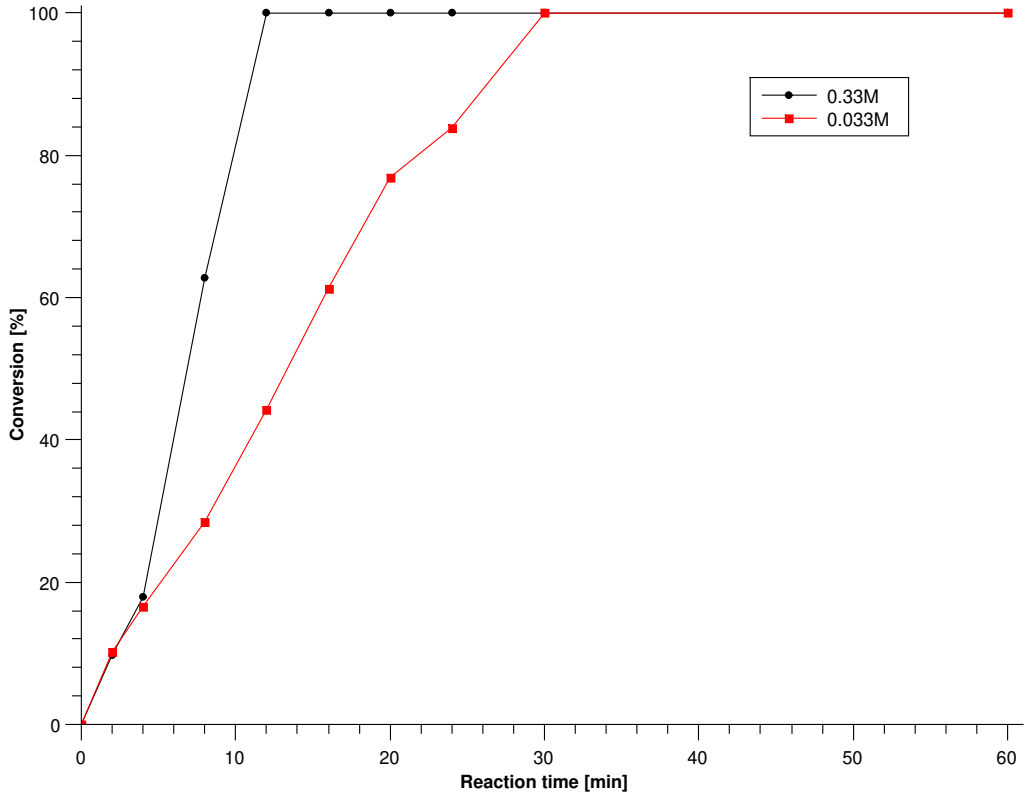

Figure 4.10: Reaction rate of BUCHWALD-HARTWIG amination of 4-bromotoluene and morpholine. Reaction conditions: 1.0 eq. 4-bromotoluene, 1.5 eq. morpholine, 2.0 eq. KO*t*Bu, 0.5 mol% ligand, 0.25 mol% $[Pd(\pi\text{-cinn})Cl]_2$, 80 °C for 16 h. Yields are calculated using an internal standard of 1,3,5-trimethoxybenzene.

4.1.5.1 Scope

To explore the scope of this reaction several compounds were prepared, as evidenced by Figure 4.11. Utilizing **5c** at a catalyst load of 0.5 mol% electron rich and sterically demanding bromoarenes with various anilines were efficiently coupled. The employment of electron poor arenes is accompanied by a large decrease in the yield. Notably, if the aniline is electron poor,

the coupling proceeds satisfactorily with sterically demanding, as well as electron rich arenes. Secondary amines couple efficiently but need, in the case of pyrrolidine, a higher catalyst load. With this higher catalyst load, it was also possible to couple aryl chlorides with electron rich anilines with excellent yields, while the coupling with pyrrolidine proceeded in only 27%. Coupling reactions with primary amines such as *n*-butyl amine were also performed, but did not lead selectively to the desired products. For **5a** the product could only be isolated in trace amounts. For **5c** a satisfactory yield of 69% could be achieved, however a significant amount of homocoupling (about 20%) could also be detected. The reason for this better performance of **5c** compared to **5a** may be attributed to agostic interactions between the ligand backbone and the oxidative addition product [L-Pd-(Ar)Br].

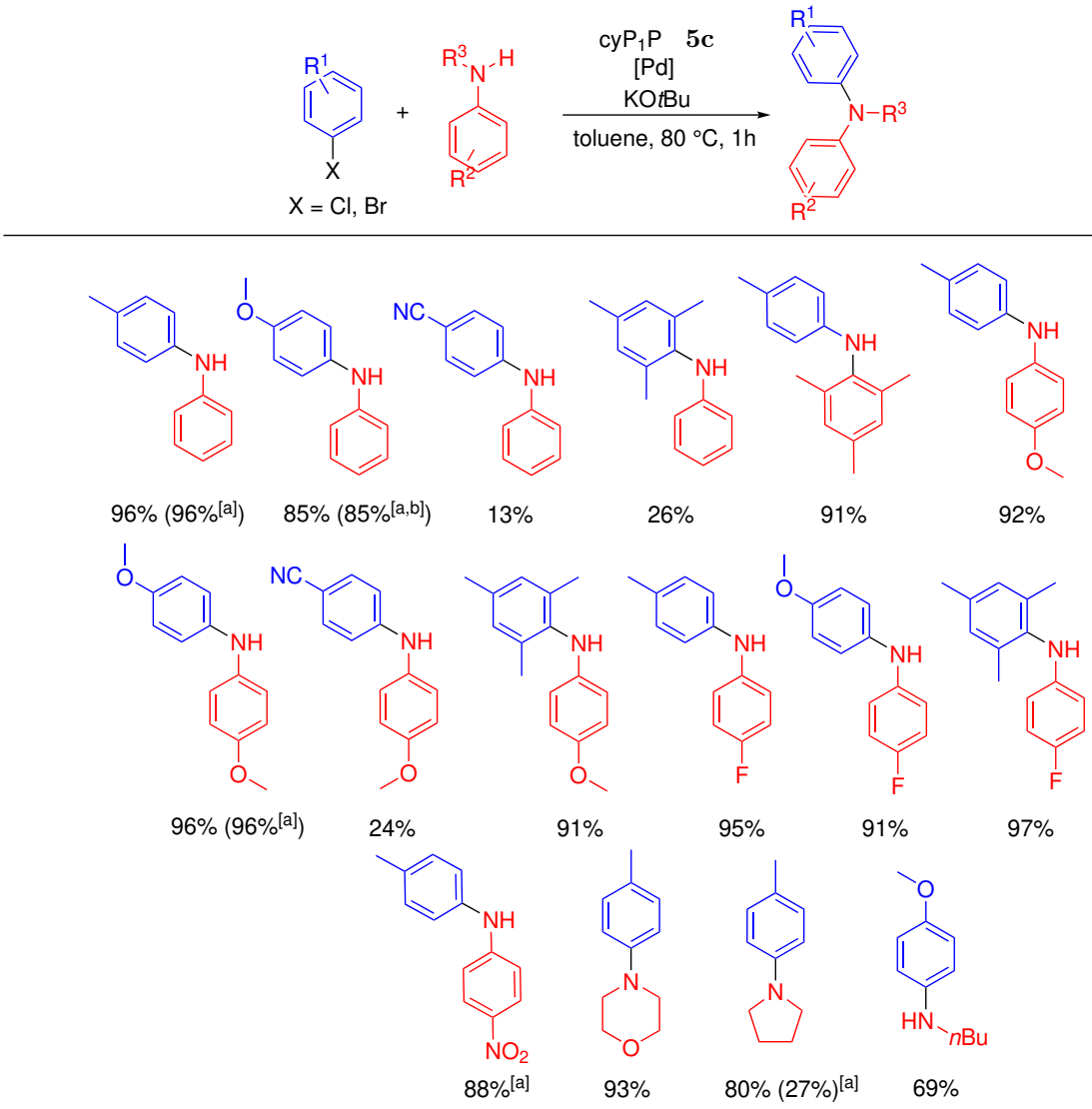

Figure 4.11: Scope of palladium catalyzed BUCHWALD-HARTWIG amination. Yields are isolated. Yields in brackets correspond to the yield from the aryl chloride. Reaction conditions: 1.0 eq. ArBr, 1.5 eq. amine, 2.0 eq. KO*t*Bu, 0.5 mol% **5c**, 0.25 mol% $[Pd(\pi\text{-cinn})Cl]_2$. Yields are isolated. [a] 4 mol% **5d**, 2 mol% $[Pd(\pi\text{-cinn})Cl]_2$. [b] NMR yield.

4.1.6 Gold complexes

Spurred by a recent surge in interest of the scientific community in gold catalyzed coupling reactions, it was decided, that the usage of PAPs in these transformations should be investigated. Of particular interest were cationic Au(I)-complexes which can be used for coupling reactions of alkynes, alkenes and allenes with various nucleophiles.[226,227] Gessner and Dielmann report the hydroamination of acetylenes with low catalyst loads for YPhos and IAP ligands, respectively.[60,128] Bertrand reports the cyclic-alkylaminocarbene (CAAC) supported addition of ammonia to allenes and alkynes[228] while Espines reports the usages of nitrogen acyclic carbenes (NAC) for hydroarylation reactions.[229] Zhang reports a ligand design concept for ligand-directed anti-nucleophilic attacks of alkynes with catalyst loads as low as the ppm level.[230] These ligands utilize Buchwald-type biaryl directing groups to allow for stabilizing arene interactions. Gessner's and Dielmann's ligands utilize these interactions too. An overview over different ligands employed in gold catalysis is given in Figure 4.12.

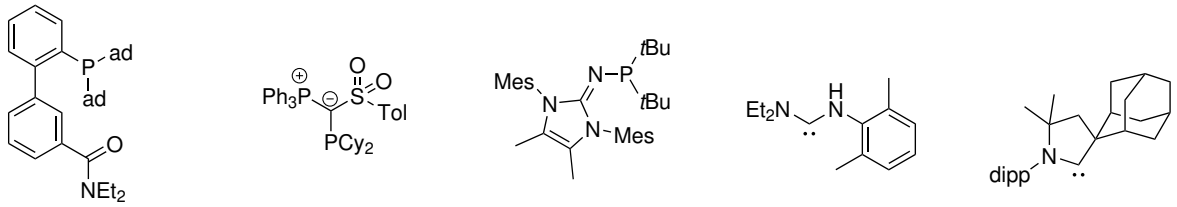

Zhang Gessner Dielmann Espinet Betrand

Figure 4.12: Various ligands employed in gold catalysis.

4.1.7 Hydroamination of Acetylenes

To explore the ability of PAPs to catalyze the hydroamination of acetylenes a model reaction of phenylacetylene and aniline was selected. The ligand (dma)P_3P (**7a**) was chosen as a highly electron rich example. The gold complex of **7a**, **34a**, was isolated and added to the reaction mixture together with sodium-tetrakis-[3,5-bis-(trifluormethyl)-phenyl]-borate ($NaBAr^F$) as a chloride scavenger.[230] The yield was determined by direct integration of the acetylene proton to the methyl group of the product (Scheme 4.8).

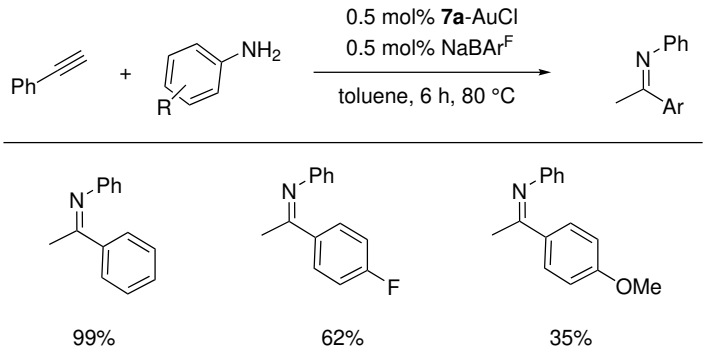

Scheme 4.8: Overview over the performed hydroaminations of phenylacetylene with **7a**. Reaction conditions: 1.0 eq. phenylacetylene, 1.5 eq. aniline, 0.5 mol% **34a**, 0.5 mol% $NaBAr^F$. Yield determined by direct integration of the acetylene proton to the methyl group of the product.

This reaction shows the potential for this type of coupling as it proceeds, in the case of the coupling of phenylacetylene and aniline, in quantitative yields. For electron rich as well as electron poor anilines, the yield decreases. Notably, the reaction may also be performed solvent free without loss in performance.

4.2 Summary

It was successfully demonstrated, that easily synthesized monophosphazenyl phosphines **5a-5d** could be employed as ligands in transition metal catalyzed cross coupling reactions such as the palladium catalyzed Suzuki-Miyaura coupling and the Buchwald-Hartwig amination. These sterically demanding and extremely electron rich phosphines with TEPs of around 2040 can be used to form an air stable precatalyst of the type [PAP-Pd(η^3−cinn)Cl] or as PAP-HBF_4 salts that can be deprotonated and mixed with the palladium source. The applicability of these ligands was shown by preparation of a relevant substrate scope, showcasing its strengths and limitations in both the Suzuki-Miyaura coupling as well as the Buchwald-Hartwig amination. Additionally, the abilities of **7a** in gold catalyzed alkyne hydroaminations was explored in a preliminary study.

5 Organocatalytic Applications of PAP Superbases

5.1 Results and Discussion

5.1.1 *N*-Alkylation of Indoles

The important role of heterocycles, especially *N*-alkylated indoles and pyrroles, has been established by the scientific community in particular in the field of pharmacologic research.[231] They can be utilized in a wide array of pathophysiological conditions such as inflammation, depression, and cancer.[232–235] As such, the synthesis of these compounds is of interest. The alkylation can be achieved through several means. Base promoted alkylation by the addition of stochiometric or several equivalents of an inorganic base such as cesium carbonate yields the desired product.[236] Other methods include the use of *n*-BuLi in THF[237] or KOH in ionic liquids.[238] Recently, the catalytic *N*-alkylation of indoles by KO*t*Bu in solvent free conditions was reported.[239] The catalytic *N*-alkylation of indoles by monomeric phosphates has also been reported.[240] Most impressively, the cyclopropenimine superbase catalyzed *N*-Alkylation of indoles was reported as a completely metal free alternative by Lambert *et al.*[241]

5.1.2 Alkylation of Indoles with PAP

Spurred by this discovery of Lambert *et al.*, the applicability of PAPs for these base catalyzed Michael reactions came into focus. The model reaction of indole with (*E*)-but-2-enenitrile was chosen with bases **5a** and **7a** at 2.5 mol% in THF at 60 °C (Scheme 5.1). It is evident, that the base strength is imperative for this transformation, as the weaker base **5a** showed no reaction. This is in line with Lambert's discoveries, as his weaker mono cyclopropeneimine bases did not react as well.[241] Therefore, the focus was put on trisPAPs **7a** and **7b** which showed promising results.

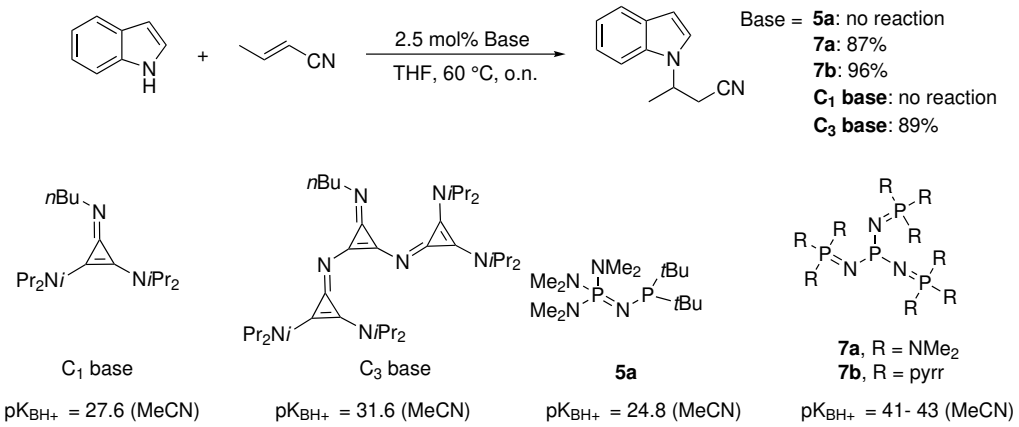

Scheme 5.1: Screening of different PAP ligands and cyclopropeneimine ligands for the *N*-alkylation of indole with (*E*)-but-2-enenitrile.[85,241]

Next, the influence of different catalyst loads on the reaction was investigated. The reaction was performed with catalyst loads of 1 to 20 mol% for **7a** and **7b** (Table 5.1).

Table 5.1: Screening of the influence of the catalyst loading on the *N*-alkylation of indoles with **7a** and **7b**.

Catalyst load [mol%]	Base	Yield [%]	Base	Yield [%]
20	**7a**	55	**7b**	41
10	**7a**	76	**7b**	62
5	**7a**	84	**7b**	75
2.5	**7a**	87	**7b**	94
1	**7a**	10	**7b**	29 (51)[b]

[a] Reaction conditions: 1.0 eq. alkene, 1.5 eq. indole, THF, RT, 16h. Yields are determined with the help of an internal standard of 1,3,5-trimethoxybenzene by integration of the methyl group of the product to the internal standard.
[b] 60 °C

A proposed mechanism for this reaction is shown in Scheme 5.2. The reaction is initiated by deprotonation of the indole by the superbase which generates protonated PAP and an anionic indole (I). This anionic species may attack the alkene (II) to form a carbanionic intermediate (III). This intermediate reacts with another molecule of indole to form the product and another anionic indole (IV). It is necessary for this reaction, that the superbase is strong enough to deprotonate the NH functionality of the indole ($pK_a = 32.6$ in MeCN)[242]. Additionally, the carbanionic intermediate (III) needs to be strong enough to deprotonate another equivalent of indole. Table 5.1 shows, that a lower catalyst load yields (up to a point) to a higher yield. This may be attributed to an increase in side reactions between the superbase and the alkene, like the nucleophilic attack on the alkene by the base (V). This could be confirmed by the deliberate reaction between **7a** and acrylnitrile, which yielded the adduct.

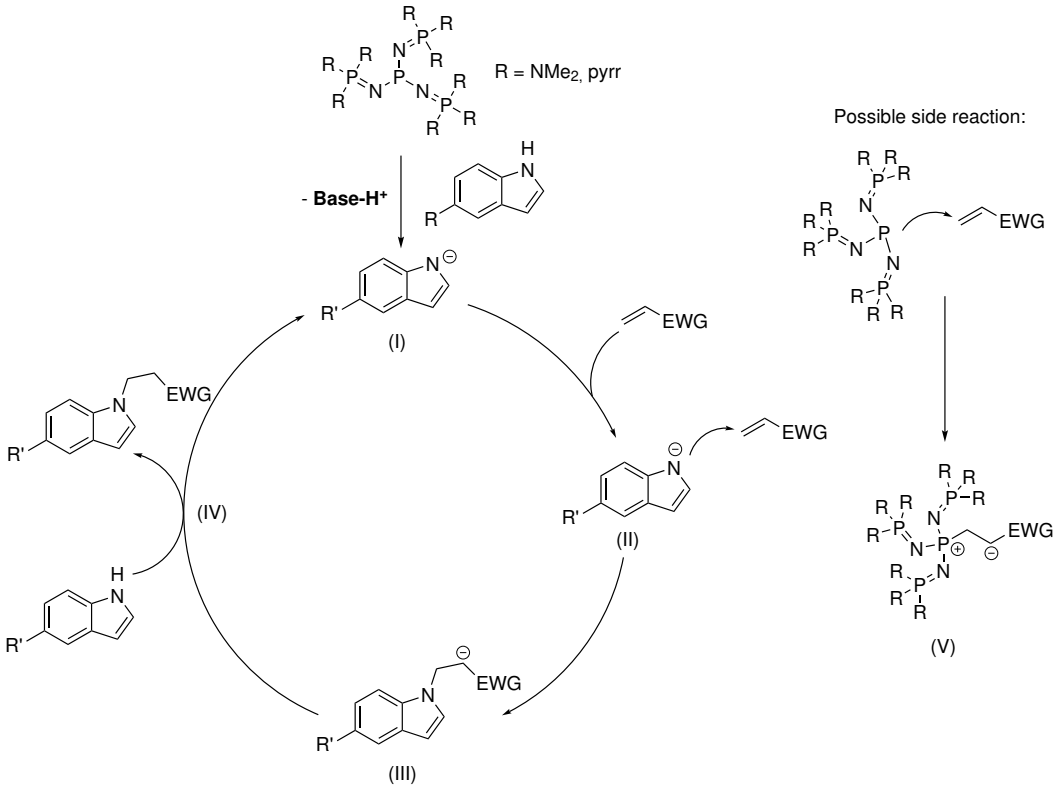

Scheme 5.2: Proposed catalytic cycle for the *N*-alkylation of indoles catalyzed by PAP bases.

Additionally, according to the proposed catalytic cycle, the superbase does not react with the alkene directly. To further support this hypothesis, another experiment was performed. By the addition of 5 mL of 'wet' hexane (100 ppm H_2O) the superbase was quantitatively protonated which eliminates any possibility of a reaction between base and alkene. Instead, the indole is deprotonated by the resulting OH^- anion. This succeeded with a yield of 88%.

The kinetic profile of this reaction was investigated by monitoring of the yield in timed intervals by removing an aliquot from the reaction mixture and quantifying it by NMR spectroscopy with the help of an internal standard (Figure 5.1).

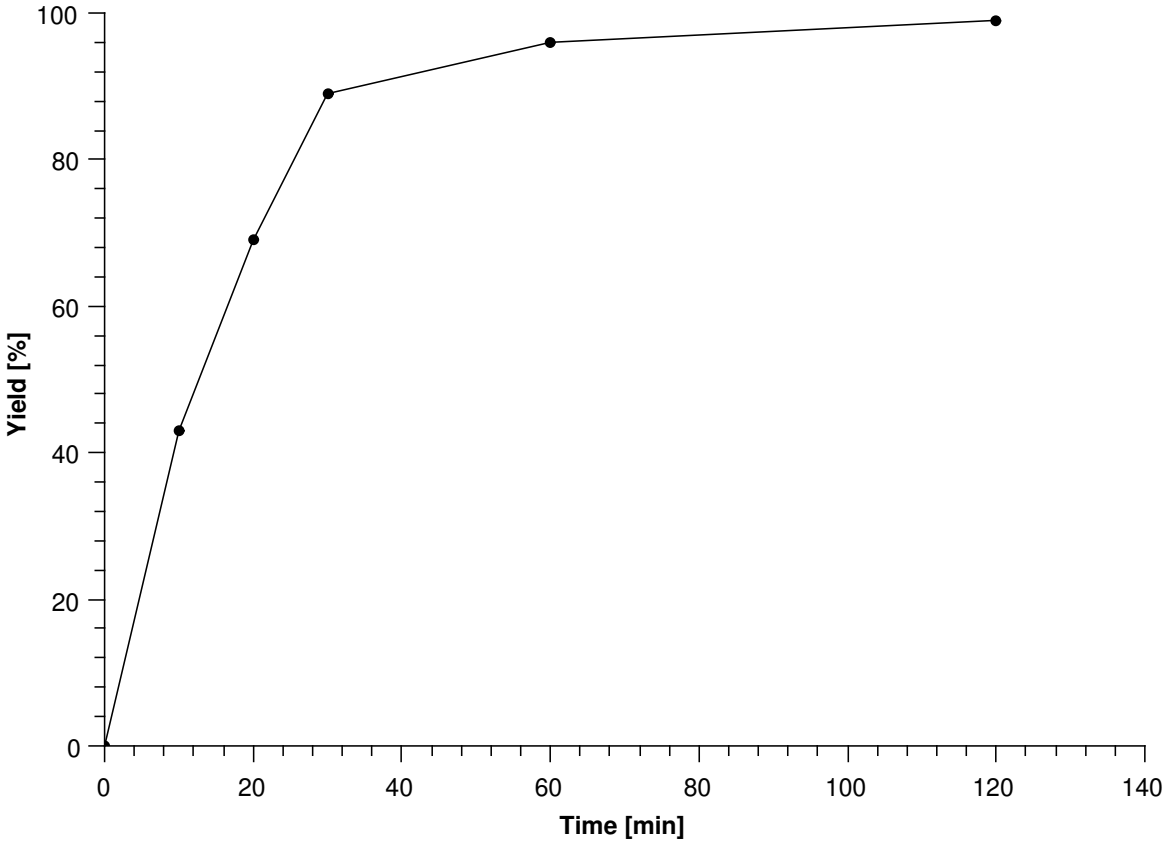

Figure 5.1: Kinetics of *N*-alkylation of indoles. Reaction conditions: 1.0 eq. alkene, 1.5 eq. indole, THF, RT, 16h. Yields are determined with the help of an internal standard of 1,3,5-trimethoxybenzene by integration of the methyl group of the product to the internal standard.

5.1.2.1 Scope

Satisfied with these reaction conditions, the scope of this reaction was explored. A small array of electron poor alkenes was coupled with electron rich and electron poor indoles (Figure 5.2).

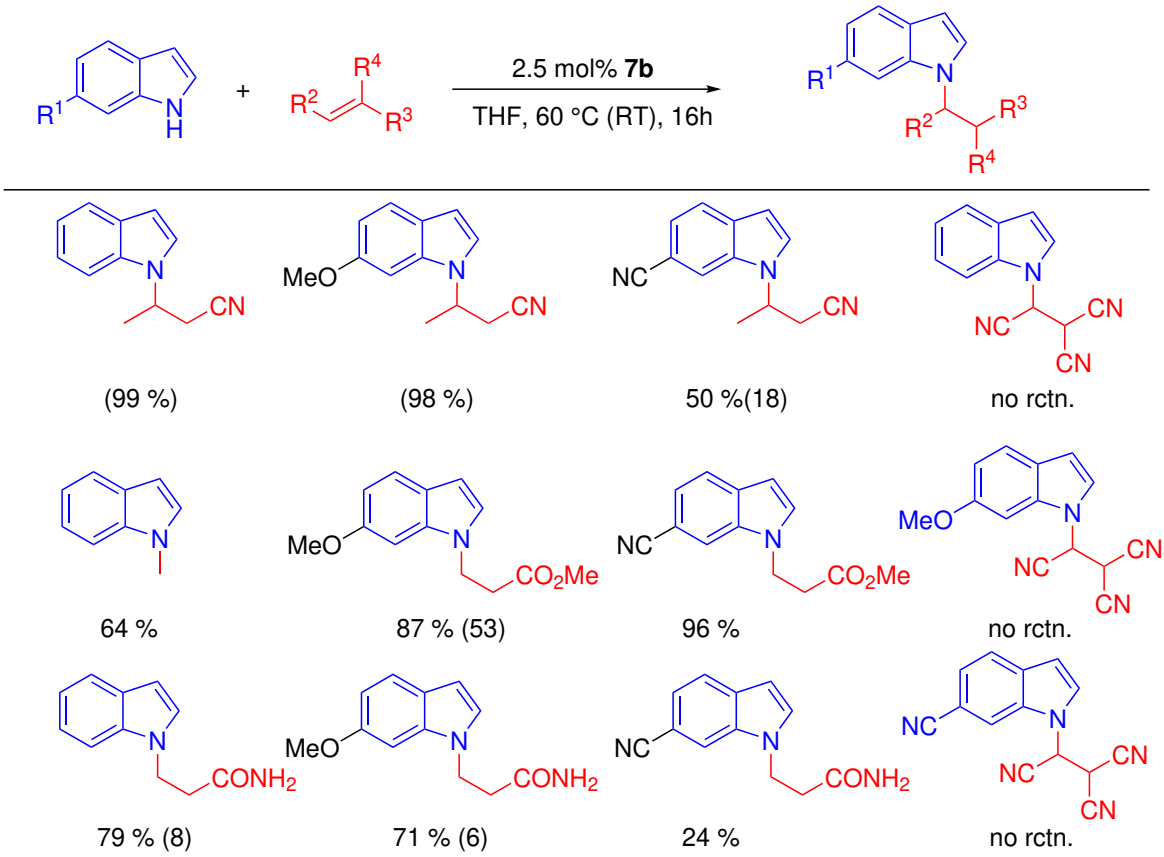

Figure 5.2: Scope of *N*-alkylation of indoles. Reaction conditions: 1.0 eq. alkene, 1.5 eq. indole, THF, 60 °C or RT, 16h. Yields are determined with the help of an internal standard of 1,3,5-trimethoxybenzene by integration of the methyl group of the product to the internal standard.

This screening demonstrates, that electron rich and electron poor indoles couple efficiently with electron poor Michael acceptors. Unsubstituted acrylamide requires additional heating to 60 °C to react efficiently with indoles. Trisubstituted ethene-1,1,2-tricarbonitrile did not react, presumably because its corresponding carbanion is unable to deprotonate the starting indole.

5.1.3 Organic Bases as Catalysts for the Coupling of CO_2 and Epoxides

5.1.3.1 CO_2 adducts of Organic Bases

Carbon dioxide is a valuable and easily accessible C_1 building block that can be utilized in chemical synthesis. CO_2 can form stable adducts with a variety of non-protic organic bases. Already in 1966 Matthews[243] *et al.* described the formation of a phosphorus ylide-CO_2 adduct (Figure 5.3) while Kuhn[244] *et al.* describes the formation of a stable NHC-CO_2 adduct. Villiers *et al.* describes the successful isolation and structure determination of TBD-CO_2 (TBD = 1,5,7-triazabicyclo[4.4.0]dec-5-en).[245] In recent years, Dielmann *et al.* describes the synthesis of bis and trisIAP-CO_2 adducts.[161,246]

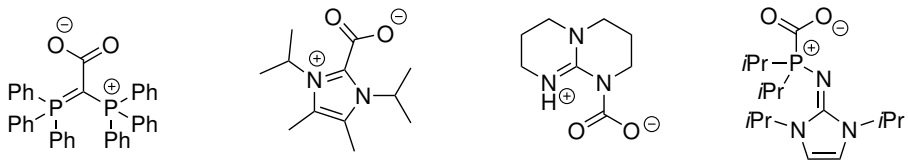

Figure 5.3: Different adducts of organic bases with CO_2.

These compounds have been investigated toward their thermal stability by various groups. Dielmann was able to establish a clear correlation between the decomposition temperature of his IAP-CO_2 adducts and the TEP.[161,246] The lower the TEP and the higher the electron donating ability of the base, the higher the decomposition temperature. Louie *et al.* reports similar findings for NHC-CO_2 adducts.[247] They also argue, that an increased steric bulk on the *N*-substituent of the NHC contributes to the stability of the adduct. Ji *et al.* reports a linear correlation of the basicity of NHCs and the thermal stability of NHC-CO_2 adducts.[248] Dielmann makes use of this by the synthesis of photoswitchable *N*-heterocyclic imines (NHI) with a photochromic dithienylethene unit which undergoes reversible cycloisomerisation by irradiation with UV light which is accompanied by a large decrease of basicity by 8.7 units.[249] The ring closed base isomer releases the CO_2 and therefore enables light controlled capture and release of CO_2.

5.1.3.2 CO_2 Adducts of PAP

Spurred by these discoveries, the availability of PAP-CO_2 adducts was investigated. PAPs **5a-5d**, **6a-6b** and **7a-7b** were reacted with CO_2. The findings of these experiments mostly correlate with the aforementioned literature. MonoPAP adducts **39a-39d** were unstable at room temperature and decomposed almost immediately. BisPAP adducts **40a-40b** as well as trisPAP adducts **41a-41b** were stable at room temperature and only decarboxylated after heating to 80 °C over 30 minutes. An overview over the ^{13}C-NMR chemical shifts, the $^{1}J_{(P,C)}$ coupling constants as well as the $\tilde{\nu}(CO_2)$ IR band is given in Table 5.2 as well as the structures in Figure 5.4.

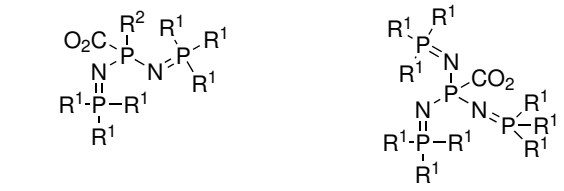

Figure 5.4: Overview over the synthesized PAP-CO_2 adducts.

Table 5.2: Overview over the ^{13}C-NMR chemical shifts, the $^{1}J_{(P,C)}$ coupling constants as well as the $\tilde{\nu}(CO_2)$ IR band.

BisPAP-CO_2	δ ^{13}C [ppm][a]	$^{1}J_{(P,C)}$ [Hz][a]	$\tilde{\nu}(CO_2)$ [cm^{-1}][b]
40a	166.7	130.1	1632.9
40b	169.2	130.4	1630.8

TrisPAP-CO_2	δ ^{13}C [ppm][a]	$^{1}J_{(P,C)}$ [Hz][a]	$\tilde{\nu}(CO_2)$ [cm^{-1}][b]
41a	172.3	191.9	1611.7
41b	173.2	194.4	1609.0

[a] Measured in C_6D_6 (75 MHz).

[b] Measured *via* ATR-IR spectroscopy of the neat substance.

From this table, a clear correspondence between the basicity of the parent PAP and the $^{1}J_{(P,C)}$ coupling constant can be determined. The $\tilde{\nu}(CO_2)$ IR band behaves similarly. Thermogravimetric analysis to determine the exact decomposition temperature of these adducts has been performed, but did not lead to conclusive results and are therefore not included herein. It should be noted, that after heating, the parent PAP is regenerated and no decomposition or metathesis products could be detected by ^{31}P-NMR spectroscopy.

5.1.3.3 Crystal Structure of PAP-CO_2 adducts.

Single crystals suitable for XRD analysis were obtained for **40a** (Figure 5.5), **41a** (Figure 5.6) and **41b** (Figure 5.7) by slow cooling of a saturated solution in pentane to −30°C. The P1-C1 bond length of trisPAPs **41a** and **41b** of 1.88 Å are comparable to the bond lengths of Dielmann's trisIAP.[246] The O2-C1-O1 bond angle of the CO_2 fragment of 128.5° is also almost exactly the same.[246] BisPAP **40a** possesses a P1-C1 bond length of 1.90 Å which is slightly longer than the length of the P1-C1 bond in bisIAP with 1.88 Å. The O2-C1-O1 bond angle of the CO_2 fragment of 129.5° is very similar to the 129.6° in bisIAP.[249] Villier's TBD-CO_2 adduct also possesses a similar bond angle of 128.6°.[245]

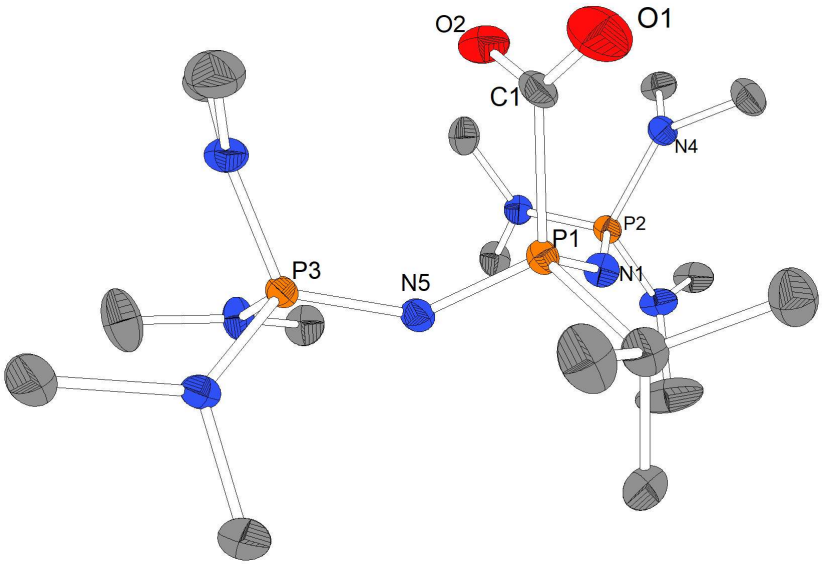

Figure 5.5: Molecular structure of **40a**. Ellipsoids are set at 50% probability. Hydrogen atoms have been omitted for clarity. Notable bond lengths [Å] and angles [°]: C1-O1 1.234(6), C1-O2 1.237(5), C1-P1 1.900(4), N1-P1 1.592(4), N5-P1 1.601(3), N1-P2 1.557(4), N5-P3 1.557(3); O2-C1-O1 129.5.

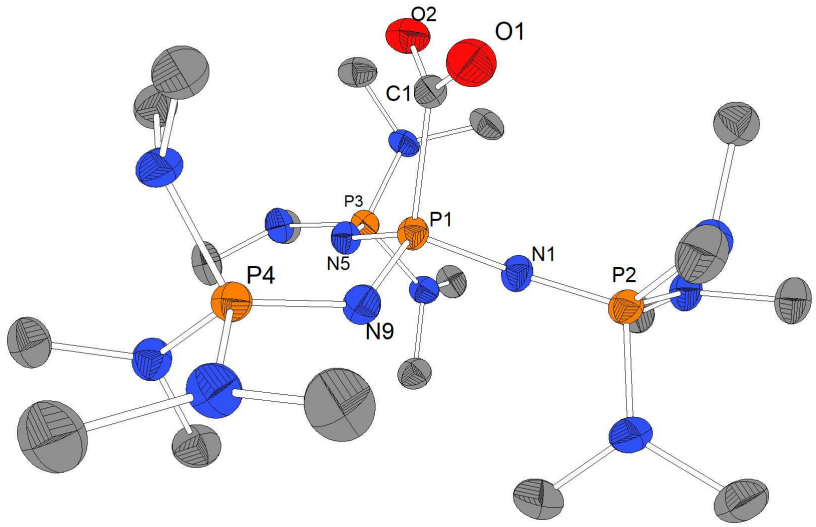

Figure 5.6: Molecular structure of **41a**. Ellipsoids are set at 50% probability. Hydrogen atoms have been omitted for clarity. Notable bond lengths [Å] and angles [°]: C1-O1 1.255(3), C1-O2 1.239(3), C1-P1 1.885(3), N5-P1 1.613(2), N1-P1 1.605(2), N1-P2 1.555(2), N5-P3 1.561(2); O2-C1-O1 128.7.

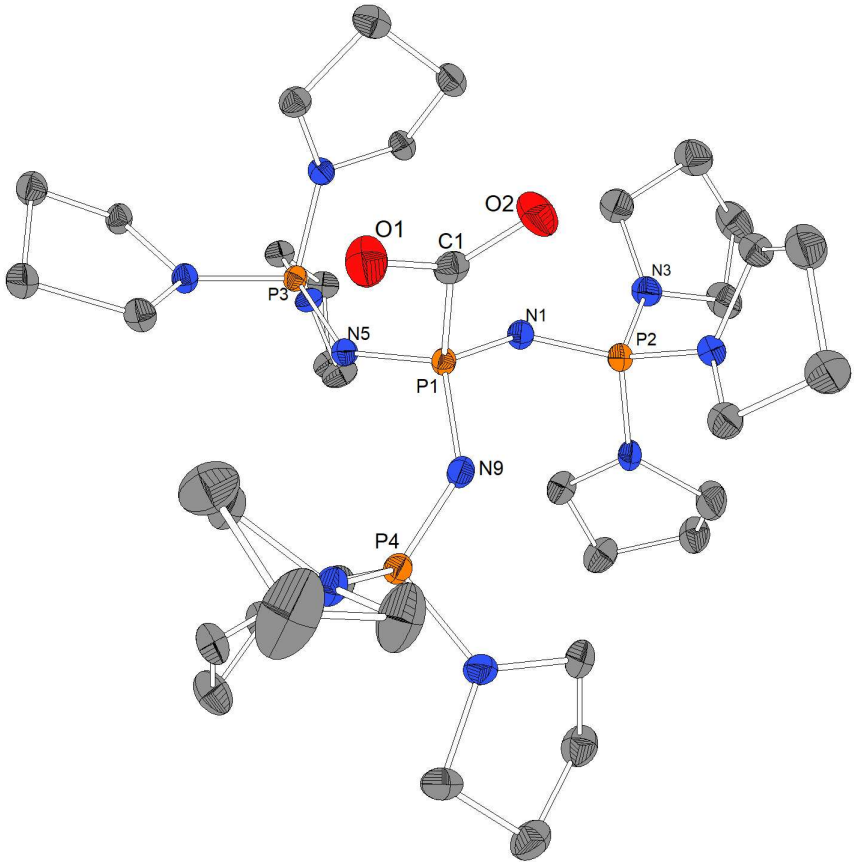

Figure 5.7: Molecular structure of **41b**. Ellipsoids are set at 50% probability. Hydrogen atoms have been omitted for clarity. Notable bond lengths [Å] and angles [°]: C1-O1 1.244(3), C1-O2 1.245(3), C1-P1 1.882(2), N1-P1 1.6171(18), N9-P1 1.6111(18), N5-P1 1.6090(17), N1-P2 1.5562(18), N5-P3 1.5513(18).

5.1.3.4 Catalytic Applications of PAP-CO_2 Adducts.

The catalytic potential of organobase-CO_2 adducts for the carboxylation of epoxides has been demonstrated in the past. Lu *et al.* demonstrated in 2008 the NHC-CO_2 catalyzed carboxylation of propylene oxides with excellent yields at CO_2 pressures of 20 bar at 120 °C (Figure 5.8).[135] Mechanistically, they propose a nucleophilic attack of the zwitterionic NHC-CO_2 as the first step. In 2015 the same group reported the cyclic addition of CO_2 with phosphorus ylide-CO_2 adducts.[250] They propose a different mechanism, where first the P-ylide-CO_2 adduct activates a free CO_2, forming a zwitterionic species which is more nucleophilic than the P-ylide-CO_2 acetate anion because of reduced steric hindrance. Based on the work of Dufaud, the group of Martinez utilized fluoroazaphosphatranes as effective catalysts for the carboxylation of epoxides.[251,252] They propose a coordination of the oxygen atom of the epoxide to the azaphosphatrane which enables a nucleophilic attack of the chloride anion to open the epoxide. Next, a CO_2 molecule inserts into the P-NCH_2CH_2 bond of the azaphosphatrane. The cyclic carbonate is generated by nucleophilic attack of the open epoxide on this species, which regenerates the fluoroazaphosphatrane. Schwesinger's phosphazene bases have been successfully utilized in the catalytic hydrosilylation of carbon dioxide.[253]

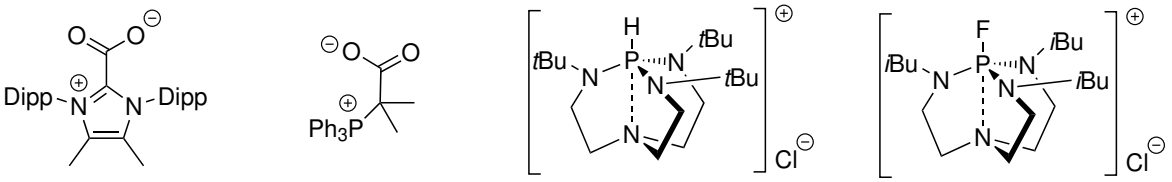

Lu 2008 Lu 2015 Dufaud 2013 Martinez 2022

Figure 5.8: Examples of organobases utilized for the carboxylation of epoxides.

These findings prompted an investigation in the applicability of phosphazenyl phosphine (PAP) and carbodiphosphorane (CDP) bases in these transformations. The following results have been prepared as an internal group cooperation with Igor Martin, who investigated the applicability of CDPs, and Morten Dittmar, who performed the screenings (Table 5.3).[254] This section will focus only on the performance of PAP bases. For an initial screening of bases the coupling of butylene oxide with CO_2 was selected (Scheme 5.3).

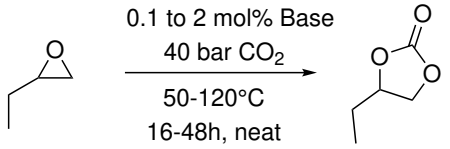

Scheme 5.3: Screening reaction for the coupling of butylene oxide with CO_2 with different PAP. Conditions: 20 mmol butylene oxide, 40 bar CO_2, yields determined by GC FID, no oligomers were detected by ^{1}H-NMR spectroscopy.

Table 5.3: Results of the coupling of butylene oxide with CO_2 with various PAP catalysts.

Base	T [°C]	t [h]	Cat. load [mol%]	Conversion [%][a]	Selectivity [%][a]	Yield [%][a]
5a	120	16	2	93	>99	93
5a	50	16	2	-	>99	-
5a	120	48	0.1	62	>99	62
5b	120	48	1	84	>99	84
5c	120	48	1	65	>99	65
5d	120	48	1	45	>99	45
9	120	48	1	-	>99	-
41a	120	48	1	42	>99	42

All reactions were performed by Morten Dittmar in an internal group cooperation. Bases were provided by Sebastian Wagner.[254]

[a] Conditions: 20 mmol butylene oxide, 40 bar CO_2, yields determined by GC FID, no oligomers were detected by ^{1}H-NMR spectroscopy.

Except for **9**, all monoPAP bases were able to catalyze the formation of butylene carbonate (Table 5.3). The lack of reactivity of **9** most likely stems from its lack of basicity and nucleophilicity, which hinders the formation of CO_2 adducts as described earlier.[248] **5a** performed well, even at low catalyst loadings of 0.1 mol%. The lack of reactivity at 50 °C compared to 120 °C may be due to the kinetic barrier of the epoxide opening. Bulkier **5c** and **5d** performed worse than **5a** and **5b** as they are less nucleophilic. **7a** could not be employed as its free base form for this reaction as it underwent rapid and exothermic polymerization with the epoxide. Therefore, the CO_2 adduct **41a** was isolated prior to the reaction. This makes it unlikely, that the mechanism for this transformation undergoes a nucleophilic attack of the superbase on the epoxide. ^{31}P-NMR spectra after the reaction show protonated **7a**-H^+ as the only species, which leads to the assumption, that, through trace moisture from the epoxide, the base gets protonated and a highly reactive unsolvated HCO_3^- anion is formed. This is probable, taking into account the extreme moisture sensitivity of **7a** and the limited availability of drying agents for epoxides.[135,255] The reduced yield of **41a** compared to **5a** coincides with the observation of Lu *et al.* that higher thermal stability corresponds to lower catalytic activity.[135] Similar observations were made, when hexaphenylcarbodiphosphorane (CDP-Ph_6) was employed. After the reaction only protonated CDP-H^+ was detected by ^{31}P-NMR and, after addition of additional substrate, the reaction would continue confirming the role of the bicarbonate anion.[254] Taking these findings into account, the following catalytic cycle is proposed, derived from one previously reported by Park *et al.* (Scheme 5.4).[256] First, the bicarbonate anion is generated by reaction of trace moisture with the PAP and CO_2 (I). The bicarbonate anion then attacks the epoxide, leading to a ring opening (II). This adduct reacts with a second molecule of CO_2 (III). Through an intramolecular nucleophilic attack, the cyclic carbonate is liberated, and the bicarbonate anion regenerated (IV). An alternative mechanism, first proposed by Suresh *et al.*, is initiated by the generation of the Base-CO_2 adduct (Ib).[257] This adduct may open the epoxide *via* nucleophilic attack (IIb). The ring is closed by an intramolecular nucleophilic attack on the carbonyl carbon atom by the alkoxide (IIIb). This liberates the cyclic carbonate and the free base (IVb).

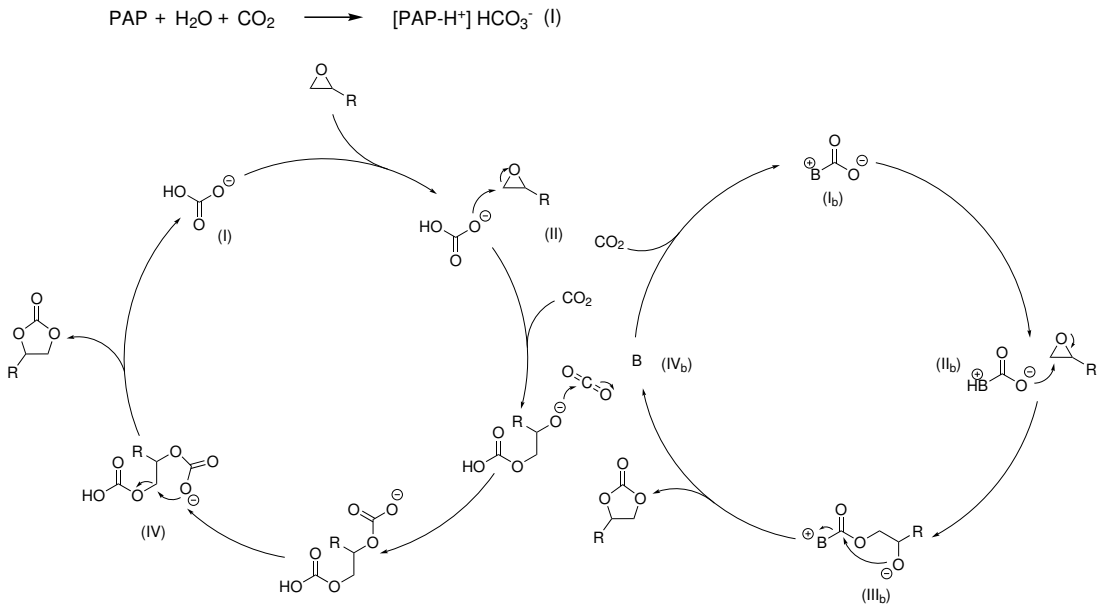

Scheme 5.4: Proposed catalytic cycle for the carboxylation of epoxides with PAP bases (left) and alternative cycle (right).

5.2 Summary

It was shown, that highly basic trisPAP can act as efficient, completely metal free catalysts for the alkylation of indoles with low catalyst loadings. These reactions were performed under mild conditions, in most cases in only two hours. The scope of this reaction ranges from electron rich to electron poor indoles with challenging acrylamide substrates. Furthermore, the synthesis, stability, characteristics, and applicability of PAP-CO_2 adducts was investigated. These adducts can be categorized according to their basicity, which is manifested in the $^1J_{(P,C)}$ coupling constant of the central phosphorus atom and the CO_2 carbon atom as well as in the $\tilde{\nu}(CO_2)$ vibrational mode. Single crystals of many of these adducts were obtained and described. PAP were employed as efficient catalysts in the coupling of butylene oxide with CO_2 in low catalysts loadings. The mechanism of this reaction was investigated, and a catalytic cycle was proposed.

6 Summary and Outlook

6.1 Summary

Trisphosphazenyl phosphines (trisPAP), first introduced by S. Ullrich from our group, are the strongest uncharged metal free bases known in Chemistry.[85,86] With these compounds in hand, the application potential in a variety of transition metal and organocatalytic transformations were of interest. The question if it was possible to substitute one or two of the phosphazenyl groups by alkyl groups and the influence this would have was also of interest (Figure 6.1). These new compounds should be investigated towards their basicity, nucleophilicity, chemical stability, donor capabilities and coordination behavior.

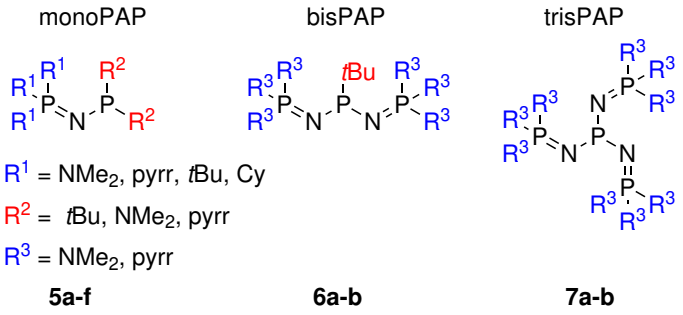

Figure 6.1: Overview over various phosphazenyl phosphine compounds.

6.1.1 Synthesis and Characterisation of PAP

The topical superbase class of phosphazenyl phosphines (PAPs) was extended to include several novel mono- and bisphosphazenyl phosphines. They were synthesized from tertiary P(III)-amides or a tertiary phosphine by Staudinger reaction with $TMSN_3$ (Scheme 6.1). By reaction of these *N*-silyl P(V)-imides with PCl_3 and subsequent elimination of TMSCl, monophosphazenyl phosphorus dichlorides **4a-4d** were generated. At this step, a variety of different functional groups may be added *via* substitution. However, *t*-butyl groups have proven to be the most selective. MonoPAPs **5a-5f** were synthesized in this manner.

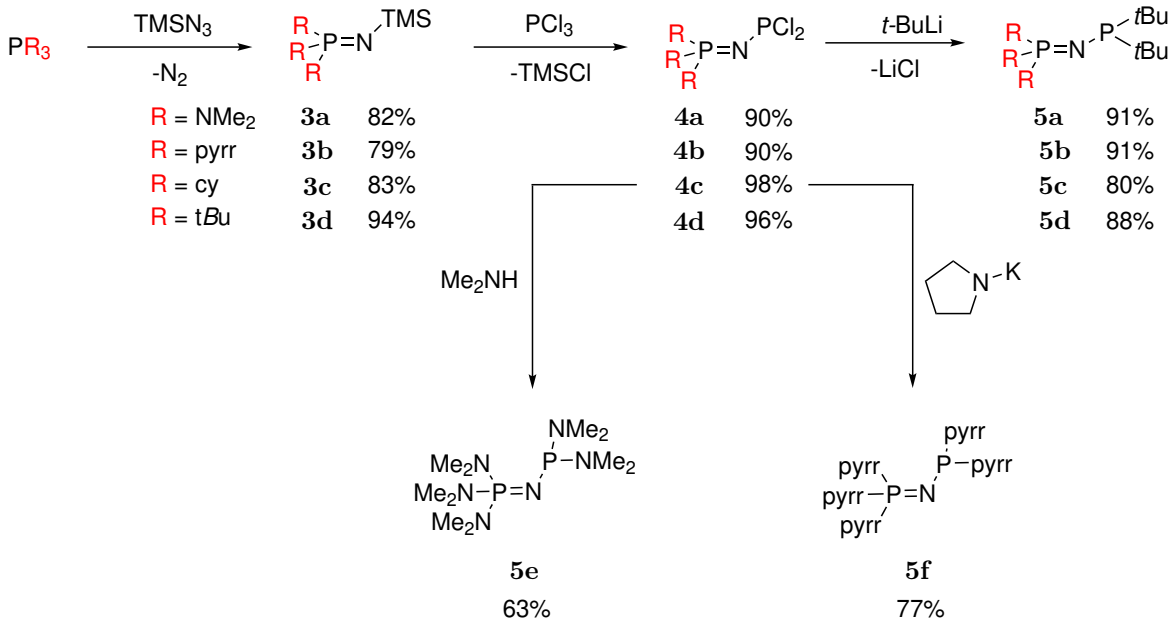

Scheme 6.1: Synthesis of monoPAP **5a** to **5f**.

Additionally, phosphoramidite **9** was synthesized as a potentially better π-acceptor ligand in contrast to the overwhelmingly high σ-donor character of **5a**-**5f**. The synthesis involved the reaction of 2-6-diisopropylphenol (dippOH) with PCl_3 and subsequent reaction with **2a**-Li to yield **9** (Scheme 6.2).

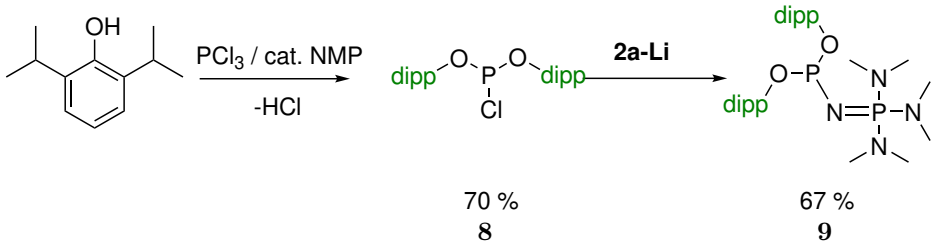

Scheme 6.2: Synthesis of monoPAP **9** from **8** and PCl_3.

Additionally, the first amino substituted bisPAPs **6a**-**6b** were synthesized by reaction of the corresponding phosphazenes **2a**-**2b** with *n*-BuLi and subsequent reaction with *t*-BuPCl_2 (Scheme 6.3).

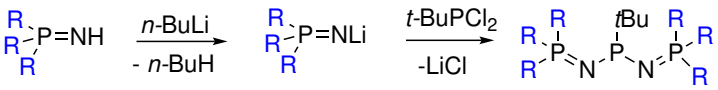

R = NMe_2	**2a**	quant.	**6a**	70%
R = pyrr	**2b**	quant.	**6b**	75%

Scheme 6.3: Synthesis of bisPAP **6a** and **6b**.

BisPAP **13** was designed with a biaryl backbone that resembles the famous Buchwald ligands.

It was synthesized by reaction of bromobiaryl **10** with *n*-BuLi and $P(NEt_2)_2Cl$ to yield **11** (Scheme 6.4). **12** is liberated *via* cleavage of the P-N bonds with HCl. Subsequent reaction with **2a**-Li generates the biaryl substituted bisPAP **13**.

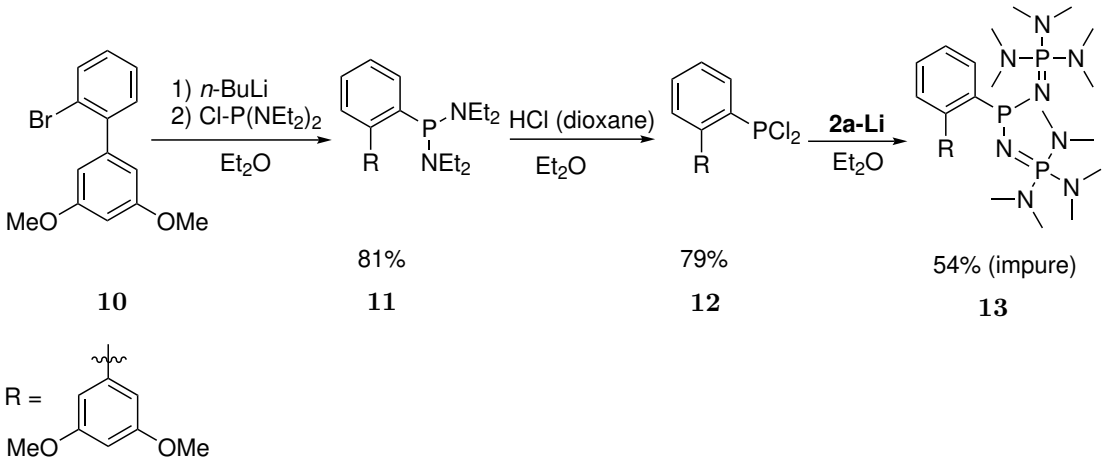

Scheme 6.4: Synthesis of **13** by reaction of **2a**-Li with **12**.

In order to evaluate the nucleophilicity of these new PAP ligands, they were reacted with an excess of dried ethyl iodide. There are two possible mechanistic paths for this reaction, either the PAP reacts as a nucleophile and forms a P-ethylated phosphonium PAP *via* S_N2 reaction or the PAP reacts as a base in a E_2 reaction and is protonated (Scheme 6.5).

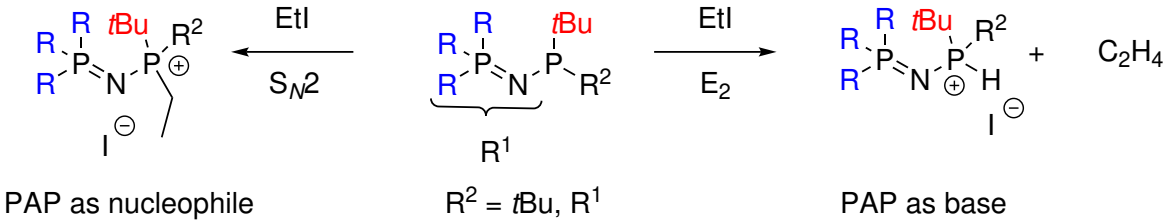

Scheme 6.5: Evaluation of the nucleophilicity of different PAP bases.

Through quantitative ^{31}P-NMR measurements, it was possible to determine the ratio of PAP-Et to PAP-H^+ by integration of the corresponding P(III) or P(V) signals and therefore measure the nucleophilicity of these PAPs. The electronic properties of the ligands were determined by the TOLMAN electronic parameter (TEP) as well as the $^1J_{(P,Se)}$ coupling constant of the corresponding phosphazenylphosphine selenides. It was found, that monoPAP possess TEPs of 2040±2 which is lower (electron richer) than popular NHCs such as IMes (2050.5)[158] and $ImNMe_2$ (2054.1)[158] or phosphines like P*t*Bu$_3$ (2056.1)[90] and similar to ylidenaminophosphines (IAP)[81,159] (Figure 6.2) of DIELMANN and ylide functionalized phosphines (YPhos)[59,71,73] of GESSNER. Structural parameters of these [PAP-Ni(CO)$_3$] complexes were investigated by XRD analyses.

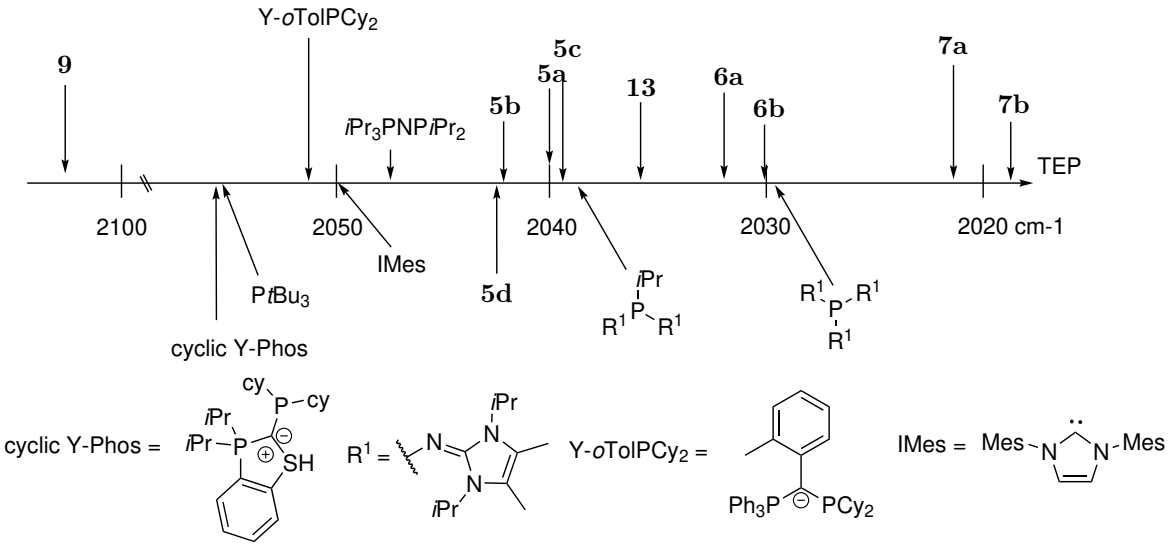

Figure 6.2: TEP values of the nickel tricarbonyl complexes of PAP and various other ligands. Exact values for these examples are given in Table 3.3.

The basicity of PAPs was determined by competition experiments with a comparable base of known pK_{BH^+} value. Additionally, the gas phase basicity (GB), proton affinity (PA) and solution basicity was calculated using DFT methods. MonoPAPs **5a-5f** all exhibit similar pK_{BH^+} (MeCN) values of 25±1. As expected, **6a** and **6b** are stronger than their monoPAP analogues **5a** and **5b** and weaker than their trisPAP analogues **7a** and **7b**. This is further supported by the calculated pK_{BH^+} values, which match the experimental values. This trend can also be seen in the GB and PA of these compounds. For the steric properties of PAPs the cone and solid angles as well as the buried volumes have been calculated. Mono and bisPAPs possess very high cone angles of around 200°, which surpasses PtBu$_3$ (182°)[89] and lies in the same range as Gessner's YPhos (199°).[60] The buried volumes follow a similar trend and range from 44-55%. For a closer investigation into the nature of the donor capabilities, a series of calculations was performed to determine the strength of σ-donation and π-acceptance by the change of Mulliken charges. This study established PAPs as strong σ-donors. Their π-acceptance character is increased by the introduction of alkyl groups on the central phosphorus atom, but is still very low. It can be said, that each added phosphazenyl group (by replacing a t-butyl group) increases the σ-donor and decreases the π-acceptor character of the ligand.

6.1.2 PAP as Ligands in Transition Metal Catalysis

The nature of PAPs as ligands in transition metal catalysis was investigated by reaction with a variety of palladium sources. The resulting palladium complexes were analyzed *via* XRD and compared to similar ligands (Figure 6.3).

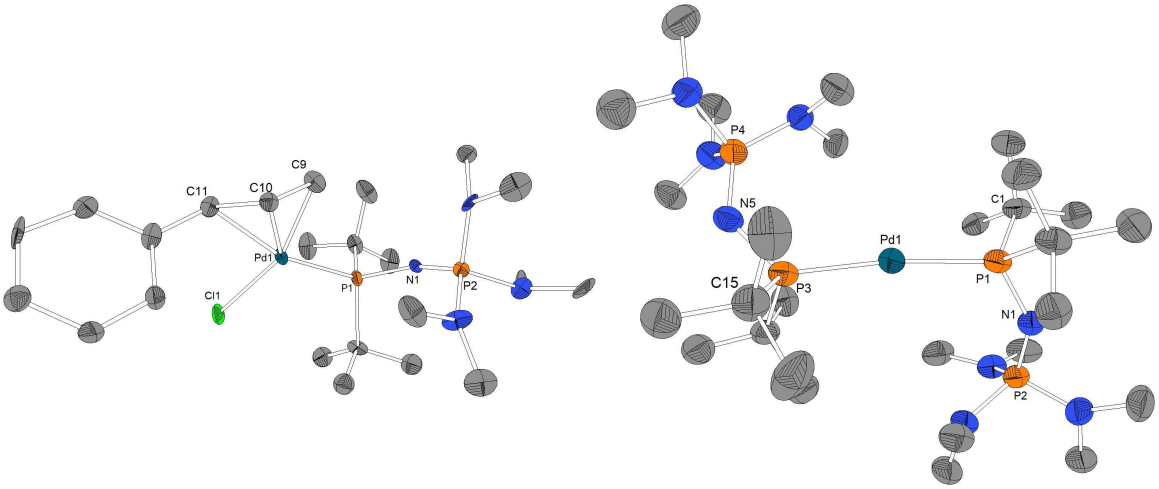

Figure 6.3: Molecular structure of [Pd(dma)P_1P-(tBu)$_2$-(η^3−cinn)Cl] (left, **35a**) and [Pd((dma)P_1P-(tBu)$_2$)$_2$] (**37**, right). Ellipsoids are set at 50% probability. Hydrogen atoms have been omitted for clarity.

In order to test these ligands with respect to their applicability in cross coupling reactions, they were employed in palladium catalyzed Suzuki-Miyaura coupling reaction of a variety of boronic acids with aryl chlorides (Scheme 6.6). After optimization of the reaction conditions and an investigation of the kinetic reaction profile, an extensive scope of aryl-aryl' coupling products was established. It was possible to couple electron rich and neutral boronic acids with electron poor, electron rich and sterically demanding aryl chlorides with catalyst loads of 4 mol%. The system was also successfully used for the coupling of heterocyclic aryl chlorides and showed tolerance to a variety of functional groups.

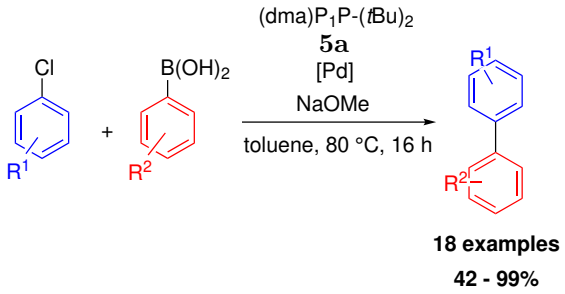

Scheme 6.6: Palladium catalyzed Suzuki-Miyaura couplings. Reaction conditions: 1.0 eq. ArCl, 1.5 eq. ArB(OH)$_2$, 2.0 eq. NaOMe, 4 mol% **5a**, 2 mol% [Pd(π−cinn)Cl]$_2$. For scope see Figure 4.9 in Chapter 4.

A similar approach was taken in the investigation in the applicability of palladium catalyzed Buchwald-Hartwig aminations with PAPs **5c** and **5d** (Scheme 6.7). It was possible to couple electron rich as well as electron neutral anilines to aryl bromides with low catalyst loads of 0.5 mol%. However, the usage of electron poor aryl bromides impeded the yield tremendously. Sterically demanding anilines like mesitylaniline were efficiently coupled to 1-bromo-4-methylbenzene in 91% yield. The C-N coupling of secondary electron rich amines like morpholine yielded almost quantitative results.

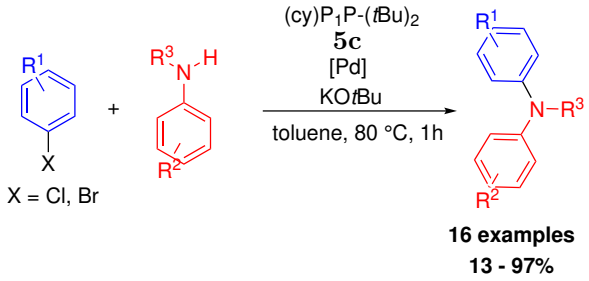

Scheme 6.7: Palladium catalyzed BUCHWALD-HARTWIG amination. Reaction conditions: 1.0 eq. ArBr, 1.5 eq. amine, 2.0 eq. KO*t*Bu, 0.5 mol% **5c** or **5d**, 0.25 mol% $[Pd(\pi\text{–cinn})Cl]_2$. For scope see Figure 4.11 in Chapter 4.

6.1.3 Organocatalytic Applications of PAP

The superbase catalyzed *N*-alkylation of indoles was explored by the reaction of indole with *E*-but-2-enenitrile with various PAP catalysts. After an initial screening of reaction conditions and an investigation into the kinetic profile of the reaction a suitable reaction protocol was established (Scheme 6.8). With catalyst loads of 2.5 mol%, **7b** was able to efficiently catalyze the *N*-alkylation of electron rich as well as electron poor indoles with a variety of Michael acceptors such as acrylamide and methyl acrylate with good to excellent yields.

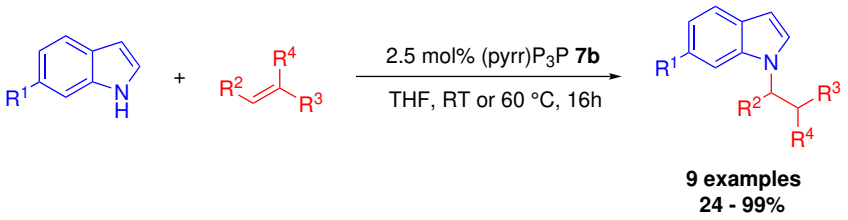

Scheme 6.8: PAP catalyzed *N*-alkylation of indoles. Reaction conditions: 1.0 eq. alkene, 1.5 eq. indole, THF, RT, 16h. For scope see Figure 5.2 in Chapter 5.

The reactivity, stability, and structure of PAP-CO_2 adducts was investigated and several XRD structures were obtained. It was possible to establish a distinct correlation between the basicity of the parent PAP and the $^1J_{(P,C)}$ coupling constant of the adduct. These findings prompted an investigation into the catalytic applications of such PAP-CO_2 adducts for the carboxylation of epoxides (Scheme 6.9). Through screening of different P-bases (PAP) and C-bases (carbodiphosphoranes, CDP) in cooperation with MORTEN DITTMAR and IGOR MARTIN a set of conditions could be established. Investigations into the mechanistic aspects revealed a high probability of the involvement of a 'naked' weakly solvated bicarbonate anion species in the catalytic cycle.

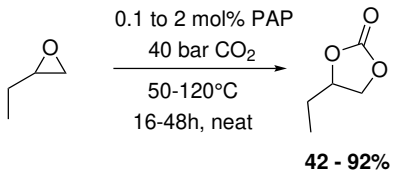

Scheme 6.9: Coupling reaction of butylene oxide with CO_2 catalyzed by different PAPs. For details see Table 5.3 in Chapter 5.

6.2 Outlook

The potential applications of PAPs in the field of transition metal- and organocatalysis could be further investigated in a variety of ways. The ligand **13** might be modified to monoPAP **45** which should improve its stability and ease of synthesis (Scheme 6.10). This could be achieved by the lithiation of a biaryl bromide **43** with *n*-BuLi and subsequent reaction with *t*-BuPCl$_2$.[258] Through reaction with a lithiated phosphazene **45** could be generated. The resulting compounds could be tuned *via* variation of the organic substituents R^1-R^4.

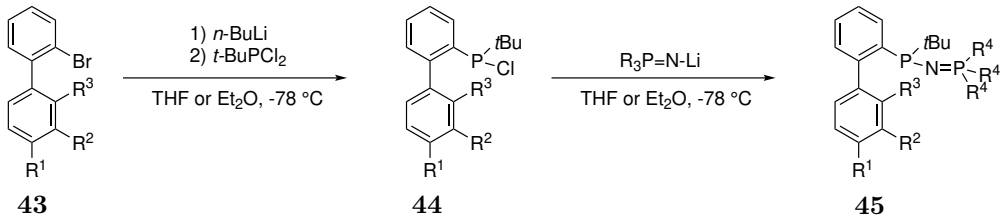

Scheme 6.10: Suggested synthesis for monoPAP analogues of Buchwald's biaryl ligands.

In the field of transition metal catalysis, an interesting reaction to explore would be the Kumada cross coupling reaction of magnesium organyls with aryl chlorides. Preliminary results (Scheme 6.11) suggest reactivity of both mono- and trisPAPs for this type of reaction. Notably, it is possible to utilize nickel instead of palladium for this transformation. The compatibility of a **7a** or **7b** / Ni(COD)$_2$ system has also proven successful for both Suzuki-Miyaura couplings as well as Buchwald-Hartwig aminations in initial screenings.

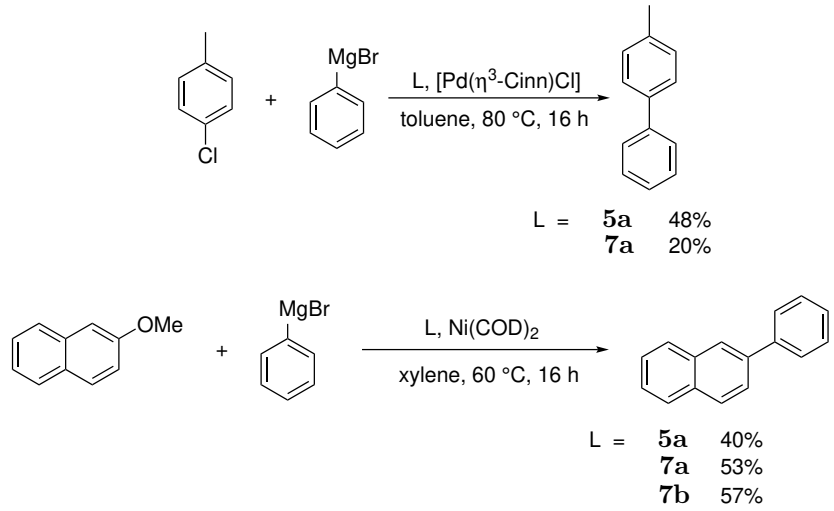

Scheme 6.11: Palladium (top) and nickel catalyzed (bottom) KUMADA cross coupling with PAP bases. Preliminary results; Conditions are not optimized.

The applicability of PAP ligands in the gold catalyzed hydroamination of alkynes should be explored more in depth by a systematic investigation of the reaction conditions, substrate scope and ligands. The organocatalytic applications of trisPAPs **7a** and **7b**, which possess the ability to deprotonate MeCN, should be explored more thoroughly. During initial studies the reaction of benzaldehyde with MeCN in the presence of 2.5 mol% of **7b** yielded the alkylnitrile condensation product in 69% yield (Scheme 6.12). This interesting reaction should be explored further with a variety of aldehydes and ketones as well as other substrates such as EtCN and $MeNO_2$, possibly in the presence of molecular sieves for the trapping of water which is liberated during the reaction.

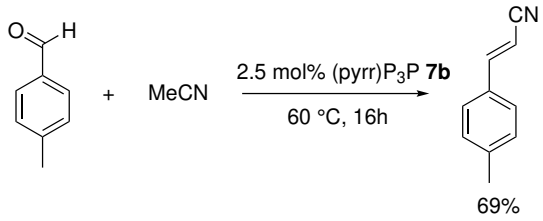

Scheme 6.12: Condensation of 4-methyl-benzaldehyde with MeCN catalyzed by **7b**.

Additionally, the ability of **7b** to rapidly polymerize epoxides, as shown earlier, should be investigated further, as this may prove to be an important application for the synthesis of polymers in the future.

6.3 Conclusion

The field of uncharged phosphorus superbases was expanded to include several new mono- and bisphosphazenyl phosphines. These novel bases have been systematically analyzed according to their basicity, nucleophilicity, chemical stability, donor capabilities and coordination behavior. They complement the missing link between extremely basic trisphosphazenyl phosphines

and traditional tertiary phosphines by combining the stability and steric properties of tertiary phosphines like P*t*Bu$_3$ with the extreme donor capabilities of phosphazenyl phosphines. The aforementioned parameters that were established during this work allow the easy classification of newly synthesized bases. Several applications of these bases were presented, as ligands in transition metal catalysis as well as organocatalysts in a variety of transformations.

7 Zusammenfassung und Ausblick

7.1 Zusammenfassung

Trisphosphazenylphosphane (TrisPAP) sind die stärksten derzeit bekannten metallfreien Basen der Chemie.[85] Sie wurden in der eigenen Arbeitsgruppe von S. Ullrich erstmals eingeführt.[86] Es stellte sich die Frage über deren Verwendung als Liganden in der Übergangsmetall- und Organokatalyse. Ebenfalls sollte untersucht werden welchen Einfluss eine Derivatisierung dieser Verbindungen durch Austausch von ein bzw. zwei der Phosphazenylgruppen durch Alkylgruppen hat (Abbildung 7.1). Diese neu synthetisierten Verbindungen wurden systematisch analysiert bezüglich ihrer Donor-Akzeptor Eigenschaften, ihrer Basizität, ihrer chemischen Stabilität und ihrem Reaktionsverhalten.

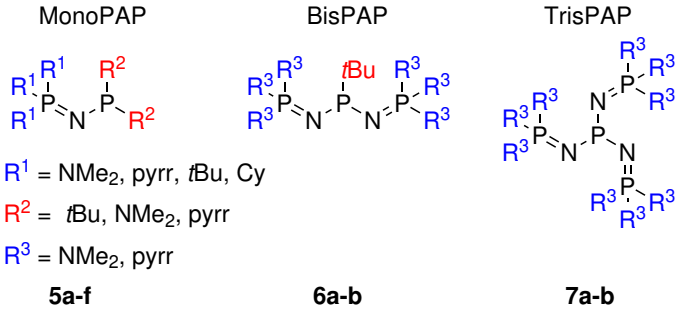

Abbildung 7.1: Übersicht über in dieser Arbeit synthetisierten und untersuchten Phosphazenylphosphanverbindungen.

7.1.1 Synthese und Charakterisierung von PAP

Die Klasse der superbasischen Phosphazenylphosphane (PAP) wurde um mehrere neue Mono- und Bisphosphazenylphosphane erweitert. Sie wurden ausgehend von einem tertiären P(III)-amid oder einem tertiären Phosphan durch Staudinger Reaktion mit TMS azid synthetisiert (Schema 7.1). Durch Reaktion dieser *N*-Silyl P(V)-imide mit PCl_3 und anschließender Eliminierung von Trimethylsilylchlorid wurden die Monophosphazenylphosphordichlorid Verbindungen **4a-4d** erhalten. An dieser Stelle ist es möglich weitere funktionelle Gruppen durch Substitution einzuführen, allerdings stellte sich die Substitution mit *t*-Butyl Gruppen als die selektivste in einer Reihe von Alkylsubstituenten heraus. MonoPAP **5a-5f** wurden auf diese Art synthetisiert.

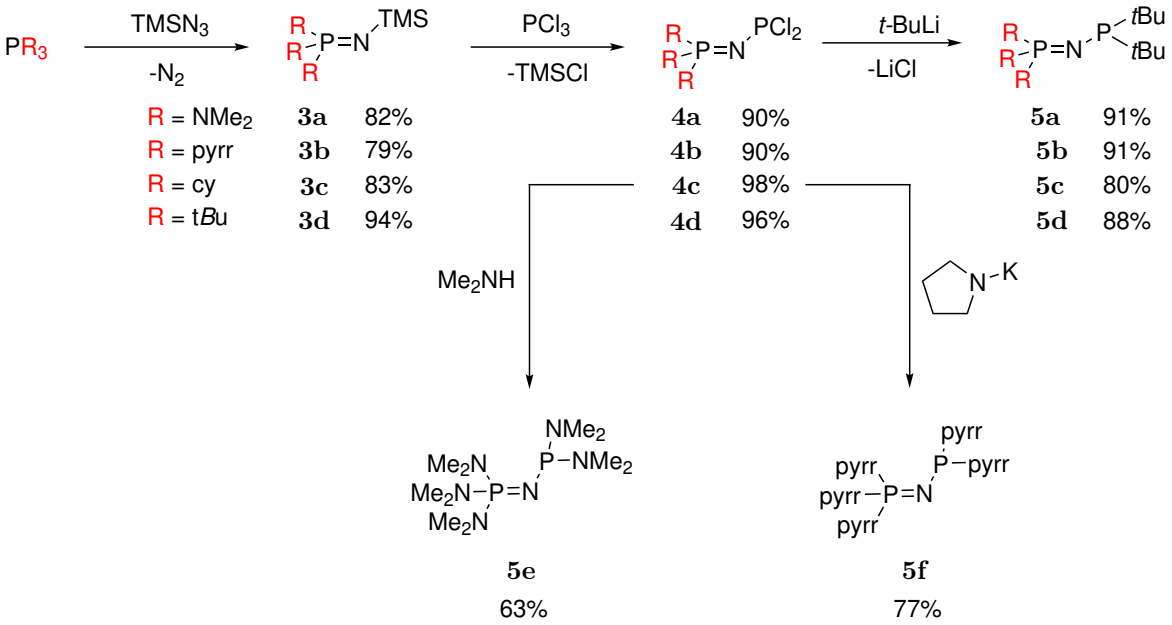

Schema 7.1: Synthese von monoPAP **5a** bis **5f**.

Als Kontrast zu den überwiegend extrem starken σ-Donoren **5a-5f** wurde das Phosphoramidite **9** als ein potentiell besserer π-Akzeptor Ligand synthetisiert. Durch Reaktion von 2-6-Diisopropylphenol (dippOH) mit PCl_3 und anschließender Reaktion mit **2a**-Li konnte **9** erhalten werden (Schema 7.2).

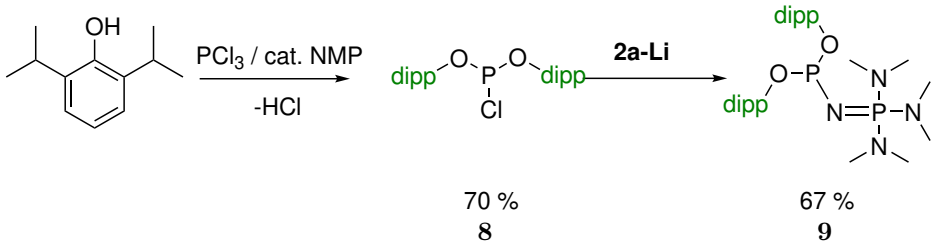

Schema 7.2: Synthese von monoPAP **9** aus **8** und PCl_3.

Ausserdem wurden die ersten Amino substituierten BisPAP **6a-6b** durch Reaktion der korrespondierenden Phosphazene **2a-2b** mit *n*-BuLi und anschließender Umsetzung mit *t*-BuPCl_2 synthetisiert (Schema 7.3).

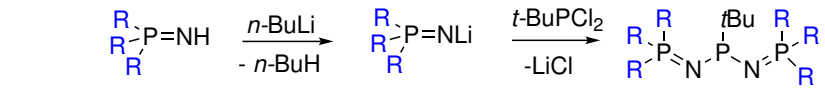

Schema 7.3: Synthese von bisPAP **6a** und **6b**.

BisPAP **13** wurde mit einem, den berühmten Buchwald-Liganden nachempfundenen, Biaryl-

Rückgrat konzipiert. **11** wurde durch die Reaktion des Bromobiaryls **10** mit *n*-BuLi und $P(NEt_2)_2Cl$ synthetisiert (Schema 7.4). **12** wurde erhalten durch Spaltung der P-N Bindungen mit HCl. Anschließend wurde das erhaltene Chlorophosphan mit **2a**-Li umgesetzt um BisPAP **13** zu erhalten.

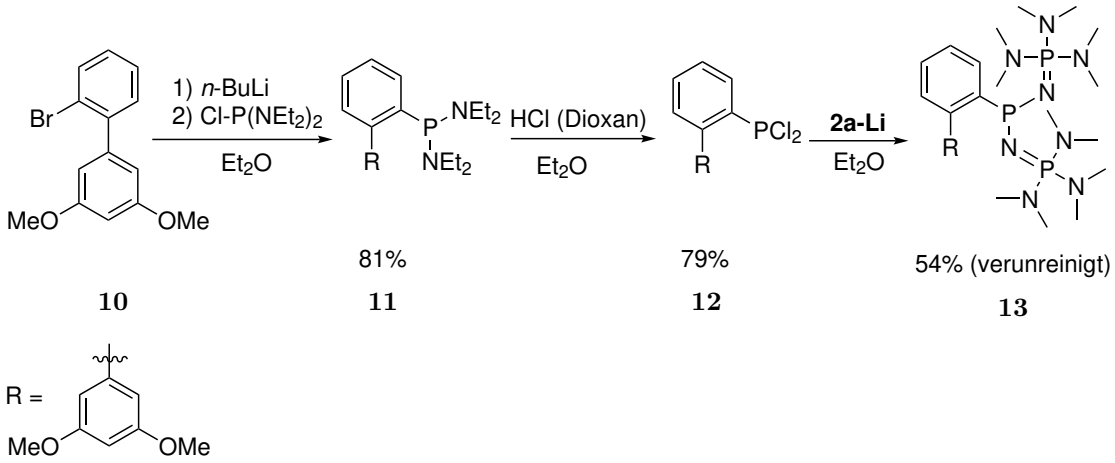

Schema 7.4: Synthese von **13** durch Reaktion von **2a**-Li mit **12**.

Um die Nukleophilie dieser neuen PAP Liganden zu untersuchen, wurden diese mit einem Überschuss an trockenem Ethyliodid umgesetzt. Zwei mögliche mechanistische Pfade können verfolgt werden: PAP reagiert entweder als ein Nukleophil und es wird durch eine S_N2 Reaktion ein P-ethyliertes Phosphonium PAP gebildet oder es reagiert als Base in einer E_2 Reaktion und wird dabei protoniert (Schema 7.5).

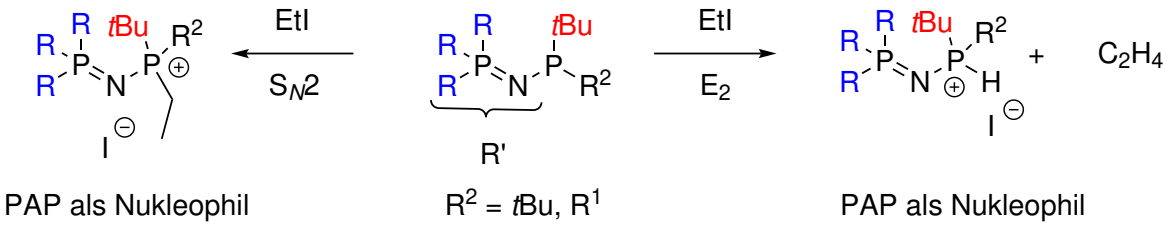

Schema 7.5: Evaluierung der Nukleophilie von PAP-Basen.

Durch quantitative ^{31}P-NMR-Messungen war es möglich, das Verhältnis von PAP-Et zu PAP-H^+ durch Integration der entsprechenden P(III)- oder P(V)-Signale zu bestimmen und somit die Nukleophilie dieser PAP zu evaluieren. Die elektronischen Eigenschaften der Liganden wurden durch den Tolman-Elektronik-Parameter (TEP) sowie die $^1J_{(P,Se)}$-Kopplungskonstante der entsprechenden Phosphazenylphosphan Selenide bestimmt. Der TEP von MonoPAP liegt im Bereich von 2040±2, was niedriger (elektronenreicher) ist als bekannte NHC's wie IMes (2050.5)[158] und $ImNMe_2$ (2054.1)[158] oder Phosphane wie P*t*Bu_3 (2056.1).[90] Der TEP ist ähnlich wie bei Ylidenaminophosphanen (IAP)[81,159] (Abbildung 7.2) von Dielmann und Ylid-funktionalisierten Phosphanen (YPhos)[59,71,73] von Gessner. Die Strukturparameter dieser [PAP-$Ni(CO)_3$]-Komplexe wurden durch XRD-Analysen untersucht.

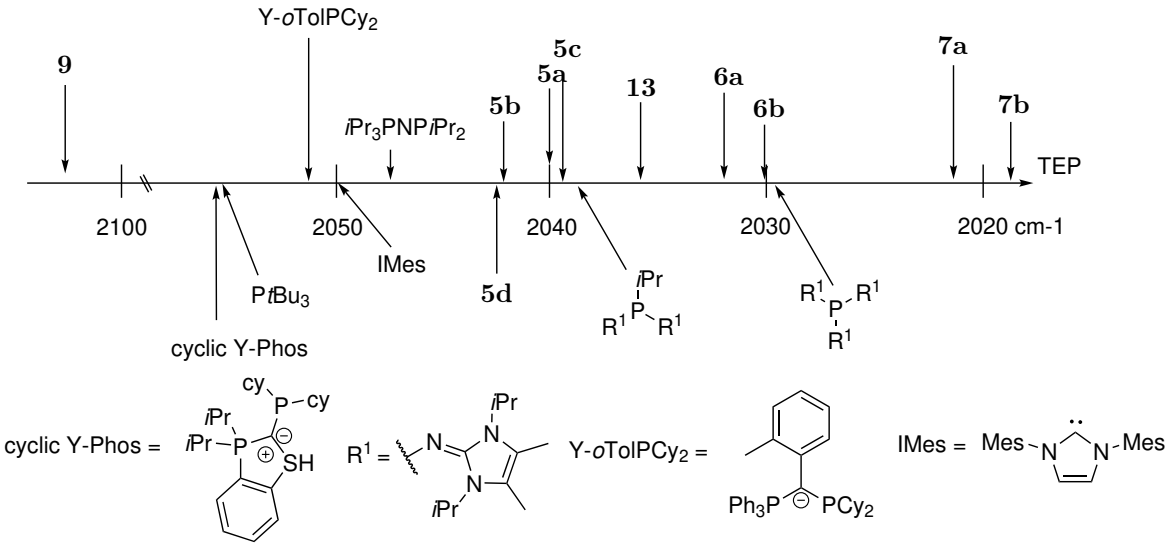

Abbildung 7.2: Tolman Elektronischer Parameter (TEP) verschiedener Liganden und PAP als Nickeltricarbonylkomplex. Die genauen Werte sind Tabelle 3.3 zu entnehmen.

Die Basizität der unterschiedlichen PAP wurde durch Konkurrenzversuche von einer Vergleichsbase mit bekanntem pK_{BH^+}-Wert bestimmt. Zusätzlich wurde die Gasphasenbasizität (GB), die Protonenaffinität (PA) und die Basizität in Lösung (MeCN) mittels DFT berechnet. MonoPAP **5a-5f** besitzen ähnliche pK_{BH^+}-Werte (MeCN) von 25±1. Wie erwartet sind **6a** und **6b** stärker als ihre MonoPAP-Analoga **5a** und **5b** und schwächer als ihre TrisPAP-Analoga **7a** und **7b**. Dies wird auch durch die berechneten pK_{BH^+}-Werte bestätigt, die mit den experimentellen Werten übereinstimmen. Dieser Trend lässt sich auch für die GB und die PA dieser Verbindungen feststellen. Um die sterischen Abschirmungseffekte von PAP zu bestimmen, wurden die Kegelwinkel sowie das "*buried volume*" berechnet. Die Molekülgeometrien für diese Berechnungen konnten mittels DFT-Methoden erhalten werden. Mono- und BisPAP besitzen sehr hohe Kegelwinkel von etwa 200°, was PtBu$_3$ (182°)[89] übertrifft und im gleichen Bereich wie Gessners YPhos (199°) liegt.[60] Das "*buried volume*" folgt einem ähnlichen Trend und liegt zwischen 44-55%. Um die Donor Eigenschaften dieser PAP genauer zu untersuchen wurde eine Reihe von quantenchemischen Berechnungen durchgeführt um die Stärke der σ-Donation und π-Akzeptanz durch die Änderung der Mulliken-Ladungen zu bestimmen. In diese Studie wurden PAP als starke σ-Donoren Liganden etabliert. Der π-Akzeptorcharakter wird durch Einführung von Alkylgruppen am zentralen Phosphoratom erhöht, ist aber immer noch sehr gering. Jeder Phosphazenylsubstitutent, der eine *tert*-Butyl Gruppe ersetzt, erhöht den σ-Donor und verringert den π-Akzeptor Charakter.

7.1.2 PAP als Liganden in der Übergangsmetallkatalyse

Der Einsatz von PAP als Liganden in der Übergangsmetallkatalyse wurde durch Reaktion mit einer Vielzahl an Palladiumpräkursoren erstmals untersucht. Die resultierenden Palladiumkomplexe wurden per XRD-Methoden analysiert und mit ähnlichen Strukuren verglichen (Abbildung 7.3).

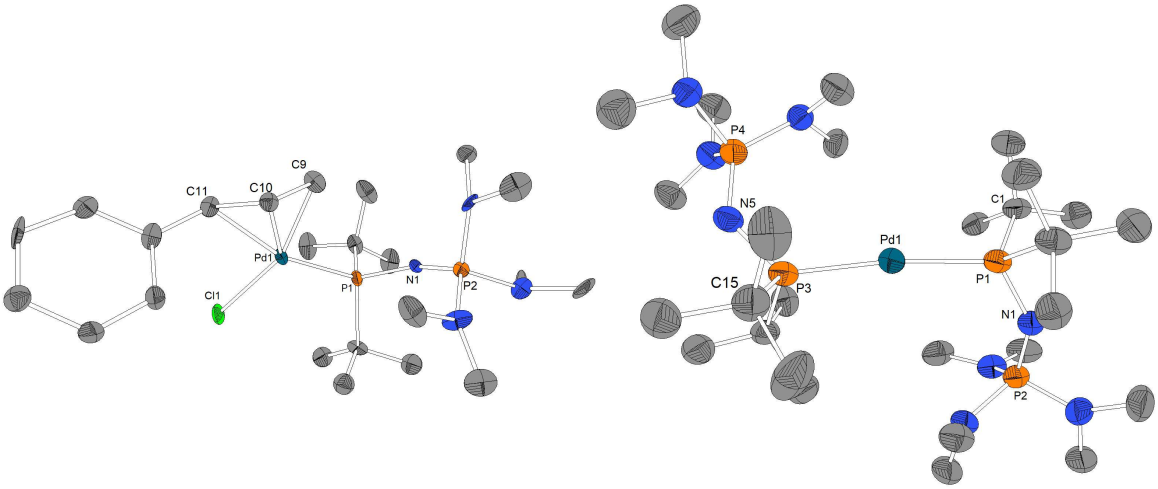

Abbildung 7.3: Molekülstruktur von [Pd(dma)P_1P-(tBu)$_2$-(η^3−cinn)Cl] (links, **35a**) und [Pd((dma)P_1P-(tBu)$_2$)$_2$] (rechts, **37**). Ellipsoide werden mit einer Wahrscheinlichkeit von 50% angenommen. Die Wasserstoffatome wurden aus Gründen der Übersichtlichkeit weggelassen.

Um die Möglichkeit der Anwendung dieser Liganden in Kreuzkupplungsreaktionen zu testen, wurden sie in einer Palladium-katalysierten SUZUKI-MIYAURA-Kupplungsreaktion mit einer Vielzahl von Arylboronsäuren und Arylchloriden eingesetzt (Schema 7.6). Nach Optimierung der Reaktionsbedingungen und einer Untersuchung des kinetischen Reaktionsprofils wurde eine umfangreiche Bibliothek von Aryl-Aryl'-Kupplungsprodukten erstellt. Es war möglich, elektronenreiche und neutrale Arylboronsäuren mit elektronenarmen, elektronenreichen und sterisch anspruchsvollen Arylchloriden mit Katalysatorbeladungen von 4 mol% zu koppeln. Das System wurde ebenfalls erfolgreich für die Kupplung von heterocyclischen Arylchloriden eingesetzt und zeigte Toleranz gegenüber einer Vielzahl von funktionellen Gruppen.

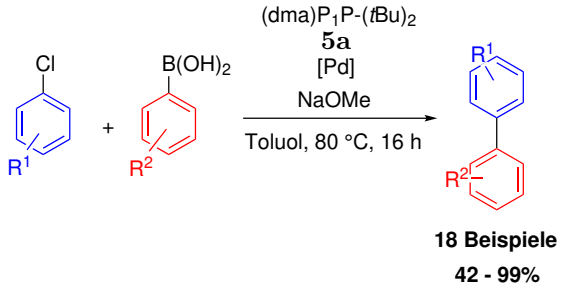

Schema 7.6: Palladium katalysierte SUZUKI-MIYAURA Kupplungsreaktionen. Reaktionsbedingungen: 1.0 Äq. ArCl, 1.5 Äq. Ar$B(OH)_2$, 2.0 Äq. NaOMe, 4 mol% **5a**, 2 mol% [Pd(π−cinn)Cl]$_2$. Für eine Übersicht siehe Abbildung 4.9 in Kapitel 4.

Ein ähnlicher Ansatz wurde für die Untersuchung palladiumkatalysierter BUCHWALD-HARTWIGAminierungen mit PAP **5c** und **5d** verfolgt (Schema 7.7). Es war möglich, Aniline mit elektronenreichen und neutralen Substituenten mit niedrigen Katalysatorbeladungen von 0.5 mol% an Arylbromide zu koppeln. Der Einsatz von elektronenarmen Arylbromiden beeinträchtigte die Ausbeute allerdings sehr stark. Sterisch anspruchsvolle Aniline wie Mesitylanilin

konnten mit 1-Bromo-4-methylbenzol in hohen Ausbeuten von bis zu 91% gekoppelt werden. Die C-N-Kupplung von sekundären elektronenreichen Aminen wie Morpholin lieferte nahezu quantitative Ausbeuten.

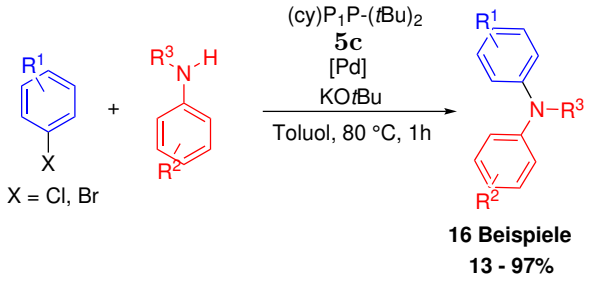

Schema 7.7: Palladiumkatalysierte BUCHWALD-HARTWIG Aminierung. Reaktionsbedingungen: 1.0 Äq. ArBr, 1.5 Äq. amine, 2.0 Äq. KO*t*Bu, 0.5 mol% **5c** oder **5d**, 0.25 mol% $[Pd(\pi\text{–cinn})Cl]_2$. Für eine Übersicht siehe Abbildung 4.11 in Kapitel 4.

7.1.3 Organokatalytische Anwendungsgebiete für PAP-Superbasen

Die Superbasen katalysierte *N*-Alkylierung von Indolen wurde durch die Reaktion von Indol mit *E*-But-2-en-nitril mit verschiedenen PAP Katalysatoren untersucht. Nach einer anfänglichen Studie der Reaktionsbedingungen und einer Untersuchung des kinetischen Reaktionsprofils wurden passende Reaktionsbedingungen ermittelt (Schema 7.8). Mit Katalysatorbeladungen von 2.5 mol% konnte **7b** die *N*-Alkylierung von elektronenreichen und elektronenarmen Indolen mit einer Vielzahl von Michael-Akzeptoren wie Acrylamid und Methylacrylat mit guten bis sehr guten Ausbeuten effizient katalysieren.

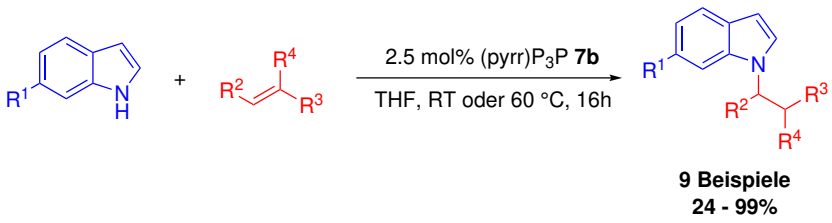

Schema 7.8: PAP-katalysierte *N*-Alkylierung von Indolen. Reaktionsbedingungen: 1.0 Äq. Alken, 1.5 Äq. Indol, THF, RT, 16h. Für eine Übersicht siehe Abbildung 5.2 in Kapitel 5.

Zusätzlich konnten, durch Reaktion von PAP mit CO_2, die ensprechenden PAP-CO_2-Addukte erhalten werden. Diese wurden hinsichtlich ihrer Reaktivitäten, Stabilitäten und Strukturparameter untersucht. Es war möglich, eine Korrelation zwischen der Basizität des PAP und der $^1J_{(P,C)}$-Kopplungskonstante des Addukts herzustellen. Diese Ergebnisse veranlassten eine Untersuchung über die katalytischen Anwendungsmöglichkeiten solcher PAP-CO_2-Addukte für die Carboxylierung von Epoxiden (Schema 7.9). Durch Umsetzung verschiedener P-Basen (PAP) und C-Basen (Carbodiphosphorane, CDP) in Zusammenarbeit mit MORTEN DITTMAR und IGOR MARTIN konnten optimierte Reaktionsbedingungen bestimmt werden. Untersuchungen zu den mechanistischen Aspekten ergaben eine hohe Wahrscheinlichkeit für die Beteiligung "nackter", schwach solvatisierter Bicarbonat-Anionen am katalytischen Zyklus.

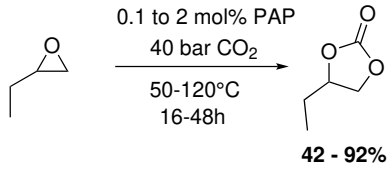

Schema 7.9: Reaktion von Butylenoxid mit CO_2 mit PAP Katalysator. Für Details siehe Tabelle 5.3 in Kapitel 5.

7.2 Ausblick

Diese erstmaligen Einblicke in das Anwendungspotential von PAP in der Übergangsmetall- sowie der Organokatalyse könnten in diversen Richtungen weiterentwickelt werden. Der Ligand **13** könnte zu MonoPAP **45** modifiziert werden, was seine Stabilität verbessern könnte und einen einfacheren Zugang zum gewünschten Biaryl-Rückgrat des Liganden gewährleisten sollte (Schema 7.10). Dies könnte durch die Lithiierung eines Biarylbromids **43** mit *n*-BuLi und anschließendes Umsetzen mit *t*-$BuPCl_2$ erreicht werden.[258] Durch Reaktion mit einem lithiierten Phosphazen würde **45** entstehen. Die Eigenschaften der resultierenden Verbindungen könnten durch Variation der organischen Substituenten R^1-R^4 abgestimmt werden.

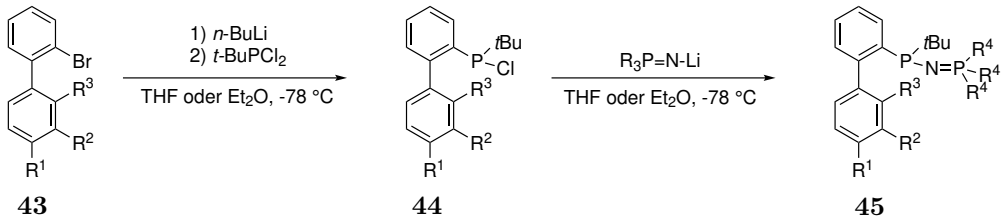

Schema 7.10: Synthesevorschlag für ein MonoPAP-Biarylliganden.

Im Bereich der Übergangsmetallkatalyse wäre eine interessante Reaktion die Kreuzkupplungsreaktion von Magnesiumorganylen mit Arylchloriden. Vorläufige Ergebnisse (Schema 7.11) deuten auf das Potential von Mono- und TrisPAP Liganden für diese Art von Reaktion hin. Insbesondere ist es möglich, Nickel anstelle von Palladium für diese Umwandlung zu verwenden. Die Kompatibilität eines **7a** oder **7b** / $Ni(COD)_2$-Systems hat sich auch für Suzuki-Miyaura-Kupplungen sowie für Buchwald-Hartwig-Aminierungen in ersten Untersuchungen als erfolgsversprechend erwiesen.

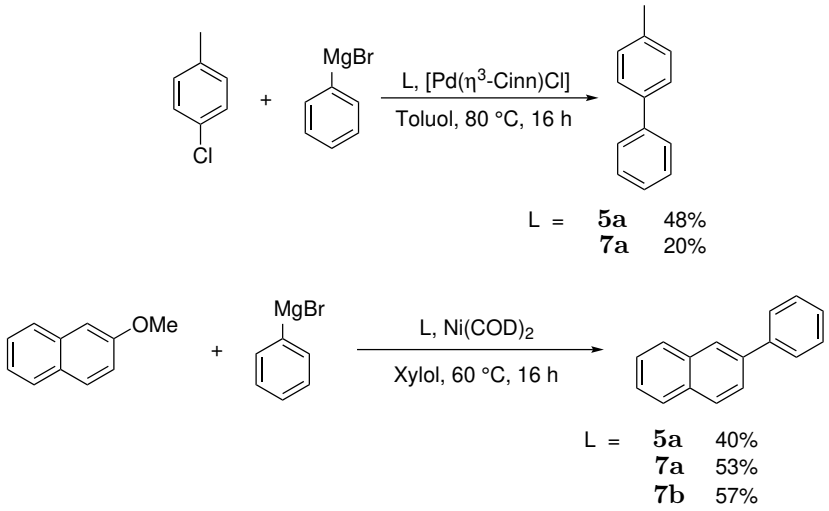

Schema 7.11: Palladium (oben) und Nickel-Katalysierte (unten) KUMADA Kreuzkupplungsreaktionen mit PAP Liganden. Vorläufige Ergebnisse; Reaktionsbedingungen nicht optimiert.

Die Nutzung von PAP-Liganden in der goldkatalysierten Hydroaminierungsreaktionen von Alkinen sollte durch eine systematische Untersuchung der Reaktionsbedingungen, Substrate und Liganden tiefgreifender erforscht werden. Die organokatalytischen Anwendungen von trisPAP **7a** und **7b** zur Deprotonierung von MeCN sollte eingehender untersucht werden. In ersten Untersuchungen ergab die Reaktion von Benzaldehyd mit MeCN in Gegenwart von 2.5 mol% **7b** das Alkylnitril-Kondensationsprodukt in 69% Ausbeute (Schema 7.12). Diese interessante Reaktion sollte mit einer Vielzahl von Aldehyden und Ketonen sowie mit anderen Substraten wie EtCN und $MeNO_2$, gegebenenfalls in Gegenwart von Molsieb, um das während der Reaktion abgespaltene Wasser abzufangen, weiter erforscht werden.

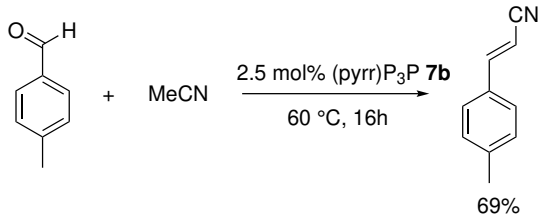

Schema 7.12: Durch **7b** katalysierte Kondensationsreaktion von 4-Methylbenzaldehyd mit MeCN.

Darüber hinaus sollte die nachgewiesene katalytische Aktivität von **7b** in der Polymerisation von Epoxiden weiter untersucht werden. Dies könnte Anwendungspotential in der Gewinnung von Polymeren finden und das Repertoir dieser Verbindungsklasse um eine weitere Anwendungsmöglichkeit ergänzen.

7.3 Fazit

Das Forschungsgebiet der ungeladenen Phosphorsuperbasen wurde um mehrere neue Mono- und Bisphosphazenylphosphane erweitert. Diese neuen Basen wurden systematisch auf ihre Basizität, Nukleophilie, chemische Stabilität, Donor-Fähigkeiten und ihr Koordinationsverhalten hin untersucht. Sie ergänzen das fehlende Bindeglied zwischen den extrem basischen Trisphosphazenylphosphanen und den traditionellen Trialkylphosphanen, indem sie die Stabilität und die sterischen Eigenschaften von tertiären Phosphanen wie P*t*Bu$_3$ mit den extremen Donor-Fähigkeiten der Phosphazenylphosphane kombinieren. Die oben genannten Parameter, die im Rahmen dieser Arbeit ermittelt wurden, ermöglichen eine einfache Klassifizierung der neu synthetisierten Basen. Es wurden mehrere Anwendungen dieser Basen vorgestellt, sowohl als Liganden in der Übergangsmetallkatalyse als auch als Organokatalysatoren in einer Vielzahl von Anwendungen.

8 Experimental Section

8.1 General Procedures

All reactions were carried out under inert argon atmosphere using standard SCHLENK techniques. Air or moisture sensitive substances were stored in a nitrogen flushed glovebox. Solvents were purified according to common literature procedures and stored under an inert atmosphere over molecular sieves (3 Å or 4 Å).[259] For chromatographic purifications Kieselgel 60 (less than 0.063 nm, CAS No. 7631-86-9) from MERCK was utilized. ^{1}H, ^{13}C, ^{31}P, ^{19}F and ^{77}Se NMR spectra were recorded on a Bruker Avance III HD 250, Avance II 300, Avance III HD 300 or Avance III HD 500 spectrometer. Chemical shift δ is denoted relatively to $SiMe_4$ (^{1}H, ^{13}C), 85% H_3PO_4 (^{31}P), $SeMe_2$ (^{77}Se) or $CFCl_3$ (^{19}F). ^{1}H and ^{13}C NMR spectra were referenced to the solvent signals. Multiplicity is abbreviated as follows: s (singlet), d (doublet), t (triplet), q (quartet), m (multiplet), sept (septet), br. (broad signal). High resolution mass spectrometry was performed on a Thermo Fisher Scientific LTQ-FT Ultra or a Jeol AccuTOF GCv. IR spectra were recorded in a glovebox on a Bruker Alpha ATR-FT-IR.

8.1.1 Precursors and chemicals

The following precursors were synthesized according to literature procedures:
$P(dma)_3$[260], $P(pyrr)_3$[261], $P(tBu)_3$[262], dma_3PNH[17], $pyrr_3PNH$[17], dma_3PNTMS[138], $pyrr_3PNTMS$[138], cy_3PNTMS[138], t-Bu_3PNTMS[138], dma_3PNPCl_2[138], $pyrr_3PNPCl_2$[138], cy_3PNPCl_2[138], t-Bu_3PNPCl_2[138], $dma_3PNPNMe_2$[138], $pyrr_3PNPNpyrr$[138], $(dma)P_3P$[85], $(pyrr)P_3P$[85], $P(Odipp)_2Cl$[143], 2-bromo3',5'dimethoxy-1,1'biphenyl[145], Ph_3PAuCl[263], $[Cl_3CPCl_3]AlCl_4$[146], $[Cl_3CP(NEt_2)_2Cl]AlCl_4$[147], $Cl_3CP(NEt_2)_2NH$[148], $[Pd(\pi\text{-cinn})Cl]_2$[191], $(NEt_2)_2OPhPNH$[149], $(NEt_2)_2PCl$[264], t-$BuPCl_2$[265].

The following precursors were purchased and utilized without further purification:

Pcy_3, KHMDS, PCl_5, $TMSN_3$, n-BuLi, t-BuLi, t-BuMgCl, $[NiCO_4]$, Se (grey), dipp-OH, $NaBF_4$, NH_4PF_6, NaOH, NaCl, LiCl, $[Pd(PPh_3)_4]$, $NiCl_2$, $PdCl_2$, $[(Me_2S)AuCl]$, phenylboronic acid, 4-methoxy boronic acid, 2,4,6-trimethylphenylboronic acid, 2,6-dimethylchlorobenzene, 4-chlorobenzonitrile, 4-chlorotoluene, 1-chloro-4-(trifluoromethyl)benzene, 1-chloro-2-methoxybenzene, 1-chloro-4-methoxybenzene, 1-(4-chlorophenyl)ethan-1-one, 1-(4-bromophenyl)ethan-1-one, 2-chlorothiophene, 2-chloro-6-methoxypyridine, 5-chloro-3-methylbenzo*[b]*thiophene, 2-bromo-4-(*tert*-butyl)aniline, aniline, 2,4,6-trimethylaniline, 4-methoxyaniline, 4-fluoroaniline, 4-nitroaniline, morpholine, 4-bromotoluene, 2-bromo-1,3,5-trimethylbenzene, 4-bromobenzonitril, indole, 5-methoxy-1*H*-indole, 1*H*-indole-5-carbonitrile, *E*-but-2-enenitrile, methyl acrylate, 1-bromo-4-methoxybenzene, acrylamide.

The following precursors were purchased and purified according to common literature procedures[259]:

Pyrrolidine, PCl_3, EtI.

8.2 Synthesis

8.2.1 Phosphazene bases and precursors

8.2.1.1 Synthesis of $(cy)_3PNPCl_2$ (4c)

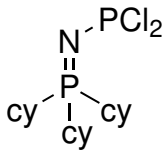

The compound was prepared analogously to literature procedures.[138] The product was obtained as a colorless solid (98%).

^{1}H-NMR (300 MHz, C_6D_6): δ (ppm) = 2.00–1.84 (m, 3H), 1.83–1.72 (m, 6H), 1.65–1.58 (m, 6H), 1.53–1.46 (m, 3H), 1.40–1.23 (m, 6H), 1.07–0.94 (m, 9H).
^{13}C{^{1}H}-NMR (75 MHz, C_6D_6): δ (ppm) = 34.5 (dd, ^1J(P,C) = 58.0 Hz, ^3J(P,C) = 6.8 Hz), 26.9 (d, ^2J(P,C) = 12.5 Hz), 26.6 (d, ^3J(P,C) = 2.8 Hz), 25.9 (d, ^4J(P,C) = 1.0 Hz).
^{31}P{^{1}H}-NMR (121 MHz, C_6D_6): δ (ppm) = 159.3 (d, ^2J(P,P) = 119.0 Hz, P(III)), 40.5 (d, ^2J(P,P) = 119.0 Hz, P(V)).

8.2.1.2 Synthesis of $(t\text{Bu})_3PNPCl_2$ (4d)

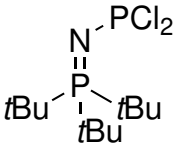

The compound was prepared analogously to literature procedures.[138] The product was obtained as a colorless solid (96%).

^{1}H-NMR (300 MHz, C_6D_6): δ (ppm) = 1.46 (d, ^3J(P,H) = 14.2 Hz, 18H, $CC\underline{H}_3$).
^{13}C{^{1}H}-NMR (75 MHz, C_6D_6): δ (ppm) = 40.3 (dd, ^1J(P,C) = 47.6 Hz, ^3J(P,C) = 5.9 Hz $\underline{C}CH_3$), 29.4 (s, $C\underline{C}H_3$).
^{31}P{^{1}H}-NMR (121 MHz, C_6D_6): δ (ppm) = 158.3 (d, ^2J(P,P) = 133.2 Hz, P(III)), 54.3 (d, ^2J(P,P) = 133.2 Hz, P(V)).

8.2.1.3 Synthesis of (dma)P_1P-(*t*Bu)$_2$ (5a)

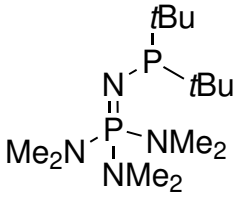

To a solution of [tris(dimethylamino)phosphazenyl] phosphorus dichloride (**4a**)
(0.77 g, 2.76 mmol, 1.0 eq.) in Et_2O (50 mL) was added *t*-BuLi (3.00 mL of 1.88 M solution in pentane, 5.66 mmol, 2.05 eq.) dropwise at −78 °C. After stirring for 1 h at this temperature, the mixture was allowed to reach RT overnight. The mixture was filtered over Celite®, the filter cake washed with Et_2O (3 x 20 mL) and the solvent removed *in vacuo*. [tris(dimethylamino)-phosphazenyl]-bis(*tert*-butyl)phosphine (**5a**) (0.81 g, 2.51 mmol, 91%) was obtained as a colorless solid.

^{1}H-NMR (300 MHz, C_6D_6): δ (ppm) = 2.52 (d, ^3J(P,H) = 9.5 Hz, 18H, NC$\underline{H}_3$), 1.37 (d, ^3J(P,H) = 10.5 Hz, 18H, CC$\underline{H}_3$).
^{13}C{^{1}H}-NMR (75 MHz, C_6D_6): δ (ppm) = 36.9 (t, ^2J(P,C) = 2.5 Hz), 33.7 (dd, ^1J(P,C) = 12.4 Hz), 27.7 (d, ^2J(P,C) = 16.2 Hz).
^{31}P{^{1}H}-NMR (121 MHz, C_6D_6): δ (ppm) = 85.4 (d, ^2J(P,P) = 100.5 Hz, P(III)), 31.4 (d, ^2J(P,P) = 100.5 Hz, P(V)).
LIFDI(+)-HRMS = 323.247 50 $[M\text{-}H]^+$ calc., 323.239 34 $[M\text{-}H]^+$ found.

8.2.1.4 Synthesis of (pyrr)P_1P-(*t*Bu)$_2$ (5b)

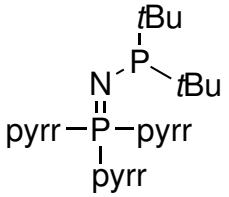

To a solution of [trispyrrolidinophosphazenyl] phosphorus dichloride (**4b**)
(2.00 g, 5.60 mmol, 1.0 eq.) in Et_2O (75 mL) was added *t*-BuLi (6.11 mL of 1.88 M solution in pentane, 11.48 mmol, 2.05 eq.) dropwise at −78 °C over 10 min. After stirring for 1 h at this temperature, the mixture was allowed to reach RT overnight. All volatile components were removed *in vacuo* and the residue redissolved in pentane (30 mL). The reaction mixture was filtered over Celite® and the filter cake was washed with pentane (3 x 10 mL). After removal of the solvent *in vacuo* [tris(pyrrolidino)phosphazenyl]bis-*tert*-butyl phosphine (**5b**) (2.10 g, 5.12 mmol, 91%) was obtained as a colorless solid.

^{1}H-NMR (300 MHz, C_6D_6): δ (ppm) = 3.20–3.10 (m, 12H, NC$\underline{H}_2$CH$_2$), 1.63–1.54 (m, 12H, NCH$_2$C$\underline{H}_2$), 1.42 (d, ^3J(P,H) = 10.4 Hz, 18H, CC$\underline{H}_3$).
^{13}C{^{1}H}-NMR (75 MHz, C_6D_6): δ (ppm) = 47.2 (dd, ^2J(P,C) = 3.2 Hz, ^4J(P,C) = 2.1 Hz, N$\underline{C}$H$_2$CH$_2$), 34.8 (dd, ^1J(P,C) = 26.8 Hz, ^3J(P,C) = 10.5 Hz, $\underline{C}$CH$_3$), 28.9 (d, ^3J(:P,C) = 7.3 Hz, NCH$_2\underline{C}$H$_2$).

^{31}P{^{1}H}-NMR (121 MHz, C_6D_6): δ (ppm) = 82.4 (d, ^{2}J(P,P) = 94.8 Hz, P(III)), 15.8 (d, ^{2}J(P,P) = 94.8 Hz, P(III)).
LIFDI(+)-HRMS = 401.296 29 [M-H]$^{+}$ calc., 401.298 23 [M-H]$^{+}$ found.

8.2.1.5 Synthesis of (cy)P_1P-(*t*Bu)$_2$ (5c)

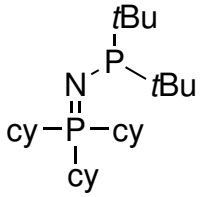

To a solution of tris(*tert*-cyclohexyl)phosphazenyl phosphorus dichloride (**4c**) (0.30 g, 0.76 mmol, 1.0 eq.) in Et_2O (50 mL) was added *t*-BuLi (0.83 mL of 1.88 M solution, 2.05 mmol, 2.05 eq.) dropwise at −78 °C over 10 min. The reaction mixture was stirred at this temperature for 1 h and afterward was allowed to reach RT overnight. The solvent was removed *in vacuo* and the residue was redissolved in pentane. The solution was filtered over Celite®, the filter cake washed with pentane (3 x 10 mL) and the solvent was removed *in vacuo*. Tris(cyclohexyl)phosphazenyl)bis-*tert*-butyl phosphine (**5c**) (0.27 g, 0.61 mmol, 80%) was obtained as a colorless solid.

^{1}H-NMR (300 MHz, C_6D_6): δ (ppm) = 2.10–1.97 (m, 3H), 1.89–1.45 (m, 24H), 1.37 (d, ^{3}J(P,H) = 10.2 Hz, 18H, CC$\underline{H}_3$), 1.20–1.00 (m, 6H).
^{13}C{^{1}H}-NMR (75 MHz, C_6D_6): δ (ppm) = 38.7 (dd, ^{3}J(P,C) = 2.0 Hz, ^{1}J(P,C) = 60.1 Hz), 34.8 (dd, ^{3}J(P,C) = 7.3 Hz, ^{1}J(P,C) = 27.3 Hz), 28.7 (d, ^{2}J(P,C) = 16.0 Hz), 27.4 (s), 27.3 (s), 27.2 (s), 26.4 (s).
^{31}P{^{1}H}-NMR (121 MHz, C_6D_6): δ (ppm) = 85.6 (d, ^{2}J(P,P) = 57.3 Hz, P(III)), 22.2 (d, ^{2}J(P,P) = 57.3 Hz, P(V)).
LIFDI(+)-HRMS = 439.349 67 [M-H]$^{+}$ calc., 439.348 91 [M-H]$^{+}$ found.

8.2.1.6 Synthesis of (*t*Bu)P_1P-(*t*Bu)$_2$ (5d)

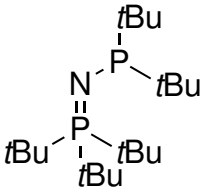

To a solution of tris(*tert*-butyl)phosphazenyl phosphorus dichloride (**4d**) (0.32 mg, 1.00 mmol, 1.0 eq.) in Et_2O (50 mL) was added *t*-BuLi (1.09 mL of 1.88 M solution, 2.05 mmol, 2.05 eq.) dropwise at −78 °C. The reaction mixture was stirred at this temperature for 1 h and afterward was allowed to reach RT overnight. The solvent was removed *in vacuo* and the residue was redissolved in pentane (20 mL). The solution was filtered over Celite® and the filter cake was washed with pentane (3 x 10 mL) before the solvent was removed *in vacuo*. Tris(*tert*-butyl)phosphazenyl)bis-tert-butyl phosphine (**5d**) (0.31 mg, 0.88 mmol, 88%) was obtained as a colorless solid.

^{1}H-NMR (300 MHz, C_6D_6): δ (ppm) = 1.40 (d, ^3J(P,H) = 10.1 Hz, 12H, P(III)CC$\underline{H}_3$), 1.32 (d, ^3J(P,H) = 12.6 Hz, 18H, P(V)CC$\underline{H}_3$).
^{13}C{^{1}H}-NMR (75 MHz, C_6D_6): δ (ppm) = 42.7 (dd, ^1J(P,C) = 50.0 Hz, ^3J(P,C) = 2.8 Hz), 35.8 (dd, ^1J(P,C) = 31.5 Hz, ^3J(P,C) = 5.8 Hz), 30.8 (d, ^2J(P,C) = 3.1 Hz), 30.1 (d, ^2J(P,C) = 16.2 Hz).
^{31}P{^{1}H}-NMR (121 MHz, C_6D_6): δ (ppm) = 90.4 (d, ^2J(P,P) = 26.7 Hz, P(III)), 39.3 (d, ^2J(P,P) = 26.7 Hz, P(V)).
LIFDI(+)-HRMS = 362.310 55 $[M\text{-}H]^+$ calc., 362.306 75 $[M\text{-}H]^+$ found.

8.2.1.7 Synthesis of P(Odipp)$_2$Cl (8)

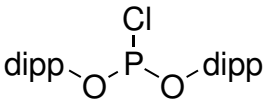

Bis(2,6-diisopropylphenyl) phosphorochloridite (**8**) was prepared according to literature procedures.[143] The crude product was used in subsequent reactions without purification.

^{1}H-NMR (300 MHz, C_6D_6): δ (ppm) = 7.04 (s, 6H, Ar$\underline{H}$), 3.72 (septd, ^3J(H;H) = 6.8 Hz, ^5J(P,H) = 1.5 Hz, 4H, $CH_3C\underline{H}CH_3$), 1.21 (t, ^3J(H,H) = 6.8 Hz, 24H, $C\underline{H}_3CHCH_3$).
^{31}P{^{1}H}-NMR (121 MHz, C_6D_6): δ (ppm) = 174.3 (s).

8.2.1.8 Synthesis of (dma)P$_1$P-(Odipp)$_2$ (9)

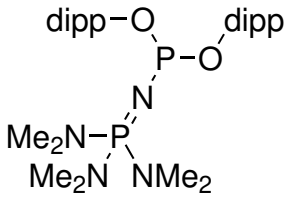

Tris(dimethylamino)phosphazene (**2a**) (1.50 mmol, 0.27 g, 1.0 eq.) was dissolved in THF (20 mL) and cooled to −78 °C. *n*-BuLi (0.6 mL of 2.5 M solution, 1.50 mmol, 1.0 eq.) was added dropwise over 10 min. The mixture was stirred at −78 °C for 1 h. Bis(2,6-diisopropylphenyl) phosphorochloridite (**8**) (0.64 g, 1.50 mmol, 1.0 eq.) was dissolved in THF (20 mL) and added dropwise to the reaction mixture over 10 min. The mixture was stirred at −78 °C for 1 h before it was allowed to warm up to RT overnight. The solvent was removed *in vacuo*, the residue was redissolved in pentane (20 mL) and filtered over Celite®. The filter cake was washed with pentane (3x 10 mL) and the solvent was removed *in vacuo*. Bis(2,6-diisopropylphenyl) (tris(dimethylamino)-λ^5-phosphineylidene)phosphoramidite (**9**) (0.56 g, 1.0 mmol, 67%) was obtained as a colorless solid.

^{1}H-NMR (300 MHz, C_6D_6): δ (ppm) = 7.18 (s, 2H, Ar$\underline{H}$), 7.18–7.04 (m, 3H, Ar$\underline{H}$), 4.09 (dsept, ^3J(H,H) = 6.5 Hz, ^5J(P,H) = 2.2 Hz, 4H, $CH_3C\underline{H}CH_3$), 2.27 (d, ^3J(P,H) = 10.0 Hz, 18H, $NC\underline{H}_3$), 1.33 (dd, ^3J(H,H) = 16.8 Hz, ^6J(P,H) = 2.9 Hz, 24H, $C\underline{H}_3CHCH_3$).
^{13}C{^{1}H}-NMR (75 MHz, C_6D_6): δ (ppm) = 148.5 (d, ^2J(P,C) = 1.5 Hz), 140.9 (d, ^2J(P,C) = 2.4 Hz), 122.6 (s), 122.4 (s), 38.8 (dd, J(P,C) = 2.9 Hz, J(P,C) = 4.0 Hz), 26.5 (d, ^2J(P,C) = 6.6 Hz), 23.4 (s), 22.8 (s).

^{31}P{^{1}H}-NMR (121 MHz, C_6D_6): δ (ppm) = 150.3 (d, ^{2}J(P,P) = 62.8 Hz, P(III)), 24.5 (d, ^{2}J(P,P) = 62.8 Hz
LIFDI(+)-HRMS = 562.356 55 [M-H]$^{+}$ calc., 562.354 91 [M-H]$^{+}$ found.

8.2.1.9 Synthesis of (dma)P_2P-*t*Bu (6a)

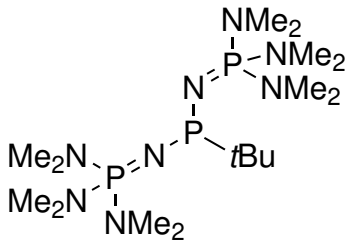

A solution of *n*-BuLi (1.12 mL of 2.5 M solution, 2.80 mmol, 2.0 eq.) was added dropwise to a solution of tris(dimethylamino)phosphazene (**2a**) (499.0 mg, 2.00 eq., 2.80 mmol) in Et_2O (50 mL) at −78 °C over a period of 30 min. This mixture was stirred for 1 h at −78 °C. Afterwards a solution of *t*-BuPCl_2 (222.6 mg, 1.40 mmol, 1.00 eq.) in Et_2O (50 mL) was added dropwise. The mixture was stirred at −78 °C for 1 h and was allowed to reach RT overnight. The solvent was removed *in vacuo* and the residue was redissolved in pentane (50 mL). The resulting solution was filtered over Celite®, the filter cake was washed with pentane (3 x 10 mL) and the solvent was removed *in vacuo*. [Bis(tris(dimethylamino)phosphazenyl]-(*tert*-butyl) phosphine (**6a**) was obtained as a colorless oil (434 mg, 0.98 mmol, 70%).

^{1}H-NMR (300 MHz, C_6D_6): δ (ppm) = 2.60 (d, ^{3}J(P,H) = 9.8 Hz, NC$\underline{H}_3$), 1.44 (d, ^{3}J(P,H) = 11.4 Hz, C$\underline{H}_3$).
^{13}C{^{1}H}-NMR (75 MHz, C_6D_6): δ (ppm) = 37.6 (d, ^{2}J(P,C) = 3.2 Hz, N$\underline{C}H_3$), 37.1 (dd, ^{1}J(P,C) = 22.0 Hz, ^{3}J(P,C) = 3.8 Hz, $\underline{C}CH_3$), 25.6 (d, ^{2}J(P,C) = 18.3 Hz, (C$\underline{C}H_3$).
^{31}P{^{1}H}-NMR (121 MHz, C_6D_6): δ (ppm) = 87.3 (t, ^{2}J(P,P) = 59.3 Hz, P(III)), 20.4 (d, ^{2}J(P,P) = 59.3 Hz, P(V)).
LIFDI(+)-HRMS = 443.305 83 [M-H]$^{+}$ calc., 443.305 59 [M-H]$^{+}$ found.

8.2.1.10 Synthesis of (pyrr)P_2P-*t*Bu (6b)

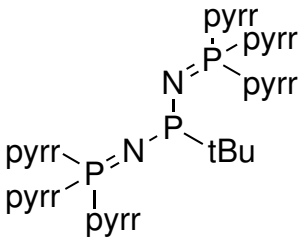

A solution of *n*-BuLi (1.54 mL (2.58 M solution), 1.99 mmol, 2.0 eq.) was added dropwise to a solution of tris(pyrrolidino)phosphazene (**2b**) (0.97 mg, 1.90 eq., 2.80 mmol) in Et_2O (50 mL) at −78 °C over a period of 30 min. Afterwards a solution of *t*-BuPCl_2 (316.9 mg, 1.99 mmol, 1.00 eq.) in Et_2O (50 mL) was added dropwise over 30 min. This mixture was stirred at −78 °C for 1 h before being allowed to reach RT overnight. Afterwards the solvent

was removed *in vacuo* and the residue was redissolved in pentane (50 mL). The mixture was filtered over Celite® and the filter cake was washed with pentane (3 x 10 mL). The solvent was removed *in vacuo* and the remaining phosphazene (**2b**) was removed by heating at 120 °C at $1*10^{-2}$ mbar. [Bis(tris(pyrrolidino)phosphazenyl]-(*tert*-butyl)phosphine (**6b**) was obtained as a colorless solid (0.90 g, 1.5 mmol, 75%).

^{1}H-NMR (300 MHz, C_6D_6): δ (ppm) = 3.37–3.19 (m, 24H, NC$\underline{H}_2$CH$_2$), 1.69–1.62 (m, 24H, NCH$_2$C$\underline{H}_2$), 1.52 (d, ^{3}J(P,H) = 11.2 Hz, 9H, CC$\underline{H}_3$).
^{13}C{^{1}H}-NMR (75 MHz, C_6D_6): δ (ppm) = 47.3 (t, J(P,C) = 3.2 Hz), 35.1 (dd, ^{1}J(P,C) = 38.9 Hz, ^{2}J(P,C) = 12.4 Hz, $\underline{C}$CH$_3$), 26.8 (d, ^{2}J(P,C) = 7.8 Hz), 26.2 (d, ^{2}J(P,C) = 18.3 Hz).
^{31}P{^{1}H}-NMR (121 MHz, C_6D_6): δ (ppm) = 84.0 (t, ^{2}J(P,P) = 59.6 Hz, P(III)), 6.8 (d, ^{2}J(P,P) = 59.6 Hz, P(V)).
LIFDI(+)-HRMS = 599.399 73 [M-H]$^{+}$ calc., 599.402 26 [M-H]$^{+}$ found.

8.2.1.11 Synthesis of Biaryl-P(NEt$_2$)$_2$ (11)

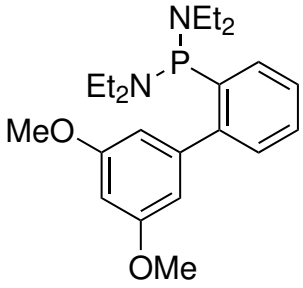

To a solution of 2-bromo-3',5'-dimethoxy-1,1'-biphenyl (**10**) (0.10 g, 0.34 mmol, 1.0 eq.) in Et$_2$O (10 mL) *n*-BuLi (0.14 mL of 2.5 M solution in hexane, 0.34 mmol, 1.0 eq.) was added dropwise at −78 °C. The reaction mixture was stirred for 1 h at this temperature before (NEt$_2$)$_2$PCl (71.9 mg, 0.34 mmol, 1.0 eq.) was added dropwise. The mixture was stirred again for 1 h at −78 °C before being allowed to reach RT and stir overnight. The solvent was removed *in vacuo* and the residue was dissolved in pentane (20 mL), filtered over Celite® and the solvent was removed *in vacuo* again. 1-(3',5'-dimethoxy-[1,1'-biphenyl]-2-yl)-*N*,*N*,*N*',*N*'-tetraethylphosphinediamine (**11**) (0.11 g, 0.28 mmol, 81%) was obtained as a viscous oil.

^{1}H-NMR (300 MHz, C_6D_6): δ (ppm) = 7.80–7.75 (m, 1H, AR$\underline{H}$), 7.38–7.24 (m, 2H, AR$\underline{H}$), 6.99 (d, ^{2}J(H,H) = 2.3 Hz, 2H, AR$\underline{H}$), 6.60 (t, ^{2}J(H,H) = 2.3 Hz, 2H, AR$\underline{H}$), 3.43 (s, 6H, OC$\underline{H}_3$), 2.96–2.82 (m, 8H, NC$\underline{H}_2$CH$_3$), 0.94 (t, 12H, ^{2}J(H,H) = 7.1 Hz, NCH$_2$C$\underline{H}_3$).
^{13}C{^{1}H}-NMR (75 MHz, C_6D_6): δ (ppm) = 160.6 (s), 131.4 (s), 131.2 (s), 126.8 (s), 107.4 (d, ^{2}J(P,C) = 5.9 Hz), 99.4 (s), 54.7 (s), 43.7 (d, ^{1}J(P,C) = 18.4 Hz), 14.7 (d, ^{2}J(P,C) = 3.4 Hz).
^{31}P{^{1}H}-NMR (121 MHz, C_6D_6): δ (ppm) = 96.3 (s).
LIFDI(+)-HRMS = 388.227 96 [M-H]$^{+}$ calc., 388.226 11 [M-H]$^{+}$ found.

8.2.1.12 Synthesis of Biaryl-PCl_2 (12)

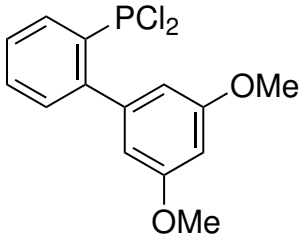

1-(3',5'-dimethoxy-[1,1'-biphenyl]-2-yl)-*N*,*N*,*N*',*N*'-tetraethylphosphinediamine (**11**)
(0.73 g, 1.86 mmol, 1.0 eq.) was dissolved in Et_2O (30 mL) and cooled to 0 °C. Afterwards HCl (4.0 M solution in dioxane, 1.86 mL, 7.44 mmol, 4.0 eq.) was added dropwise over 5 min. The mixture was allowed to reach RT and stirred for 1 h. The solution was filtered and washed with Et_2O (3 x 20 mL) and the solvent removed *in vacuo*. The resulting solid was recrystallized from Toluene / Et_2O. Dichloro(3',5'-dimethoxy-[1,1'-biphenyl]-2-yl)phosphine (**12**) (0.46 g, 1.46 mmol, 79%) was obtained as a colorless solid.

$^{31}P\{^1H\}$-NMR (121 MHz, C_6D_6): δ (ppm) = 159.5 (s).

8.2.1.13 Synthesis of (dma)P_2P-Biaryl (13)

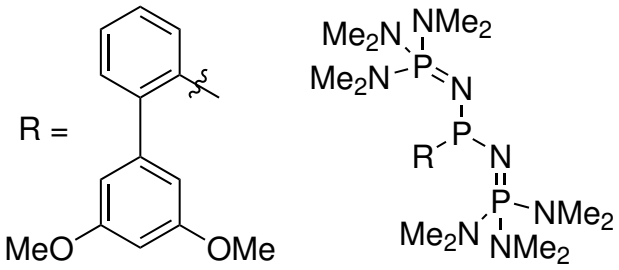

To a solution of Dichloro(3',5'-dimethoxy-[1,1'-biphenyl]-2-yl)phosphine (**12**)
(50.0 mg, 0.16 mmol, 1.0 eq.) in Et_2O (10 mL) was added a solution of $(NMe_2)_3PNLi$ (**2a-Li**) (58.4 mg, 0.32 mmol, 2.0 eq.) in Et_2O (10 mL) dropwise at −78 °C over 5 min. The mixture was stirred at −78 °C for 1 h before being allowed to reach RT and stir overnight. Afterwards the solvent was removed *in vacuo*, dissolved in pentane (20 mL), filtered over Celite® and washed with pentane (3 x 10 mL). The solvent was removed *in vacuo* to receive (dma)P_2P-Biaryl (**13**) (51 mg, 0.09 mmol, 54%) as a viscous oil. Notably, it was not possible to isolate this compound without impurities from $(Me_2N)_3PNH$ (**2a**) or traces of mono substituted BiarylP_1PCl. Additionally the reaction proceeded better when the lithium organyl was isolated prior to the reaction instead of generating it *in situ*.

^{1}H-NMR (300 MHz, C_6D_6): δ (ppm) = 8.94 (d, J(H,H) = 6.5 Hz, 1H, Ar<u>H</u>), 7.54–7.46 (m, 2H, Ar<u>H</u>), 7.28–7.17 (m, 4, Ar<u>H</u>), 6.60 (t, J(H,H) = 2.2 Hz, 1H, Ar<u>H</u>), 3.52 (s, 6H, OC<u>H</u>$_3$), 2.49 (d, 36H ^3J(P,H) = 9.8 Hz, NC<u>H</u>$_3$).
$^{13}C\{^1H\}$-NMR (75 MHz, C_6D_6): δ (ppm) = 160.0 (s), 130.9 (s), 128.5 (s), 109.8 (d, J(P,C) = 7.5 Hz), 98.5 (s), 54.6 (s), 37.3 (m), 37.0 (d, J(P,C) = 2.9 Hz).
$^{31}P\{^1H\}$-NMR (121 MHz, C_6D_6): δ (ppm) = 61.1 (t, ^2J(P,P) = 68.4 Hz, P(III)), 20.2 (d, ^2J(P,P) = 68.4 Hz, P(V)).

LIFDI(+)-HRMS = 599.326 96 $[M\text{-}H]^+$ calc., 599.327 91 $[M\text{-}H]^+$ found.

8.2.1.14 Attempted synthesis of Pincer phosphazene 18

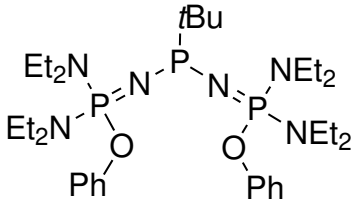

18

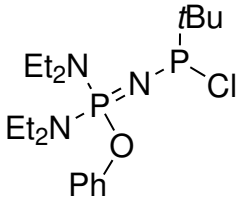

19

$(NEt_2)_2OPhPNH$ (**17**) (40.0 mg, 0.14 mmol, 1-0 eq.) was dissolved in Et_2O (5 mL) and cooled to −78 °C. *n*-BuLi (0.05 mL of 2.5 M solution in hexane, 0.14 mmol, 1.0 eq.) was added dropwise at −78 °C and the mixture was stirred for 1 h. Afterwards *t*-$BuPCl_2$ (11.2 mg, 0.07 mmol, 0.50 eq.) in Et_2O (5 mL) was added dropwise and the mixture was again stirred for 1 h. Afterwards the mixture was allowed to warm up to RT overnight. The mixture was filtered over Celite® and washed with Et_2O (3 x 10 mL) and the solvent was removed *in vacuo*. ^{31}P-NMR shows, that only monosubstitution has taken place leading to compound **19**.

$^{31}P\{^1H\}$-NMR (121 MHz, C_6D_6): δ (ppm) = 177.4 (d, ^2J(P,P) = 63.2 Hz, P(III)-Cl), 23.4 (d, ^2J(P,P) = 63.2 Hz, P(V)).

8.2.1.15 Synthesis of 20

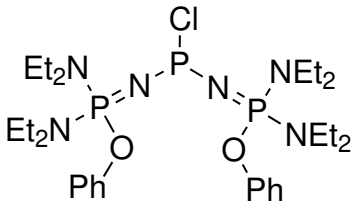

20

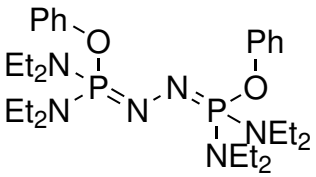

21

$(NEt_2)_2OPhPNH$ (**17**) (0.35 g, 1.22 mmol, 1.0 eq.) was dissolved in Et_2O (20 mL) and *n*-BuLi (0.47 mL of 2.5 M solution in hexane, 1.22 mmol, 1.0 eq.) was added dropwise at −78 °C. The mixture was stirred for 1 h at this temperature before PCl_3 (83.8 mg, 0.61 mmol, 0.5 eq.) was added dropwise. The mixture was again stirred at −78 °C for 1 h. Afterwards the mixture was allowed to reach RT and was stirred overnight. Afterwards it was filtered over Celite® and washed with Et_2O (3 x 10 mL) and the solvent was removed *in vacuo*. ^{31}P-NMR shows a mixture of **20** and **21**.

$^{31}P\{^1H\}$-NMR (121 MHz, C_6D_6): δ (ppm) = 155.5 (br. s, NP-P(III)Cl-NP), 26.8 (d, ^2J(P,P) = 91.7 Hz, P(V)-N-P(V)), 20.9 (d, ^2J(P,P) = 91.7 Hz, P(V)-N-P(V)), 12.3 (d, ^2J(P,P) = 76.9 Hz, P(V)-NPCl).

8.2.1.16 Attempted synthesis of pincer phosphazene 18 via 20

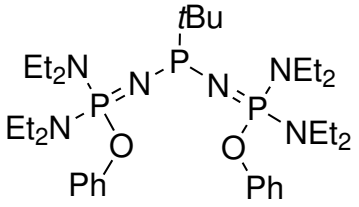

18

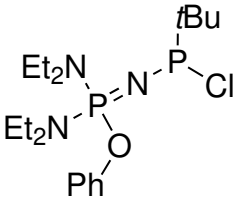

19

20 from the previous reaction was reacted with one equivalent of *t*-BuLi at −78 °C in Et_2O. After stirring for 1 h at this temperature the reaction mixture was allowed to reach RT and was stirred overnight. The mixture was filtered over Celite® and the solvent was removed *in vacuo*. ^{31}P-NMR shows full conversion to **19**.

^{31}P{^{1}H}-NMR (121 MHz, C_6D_6): δ (ppm) = 177.4 (d, ^{2}J(P,P) = 63.2 Hz, P(III)-Cl), 23.4 (d, ^{2}J(P,P) = 63.2 Hz, P(V)).

8.2.2 Synthesis of phosphazenyl phosphine selenides

8.2.2.1 General procedure for the generation of phosphazenyl phosphine selenides

To a solution of phosphine (0.20 mmol, 1.0 eq) in toluene (5 mL) gray selenium (0.25 mmol, 1.20 eq.) was added and the mixture was stirred at 90 °C for 1 h. After cooling to room temperature the mixture was filtered through a syringe filter and all volatile components were removed *in vacuo*. Afterwards the residue was dissolved in pentane (10 mL) and filtered through a syringe filter. The solvent was removed *in vacuo* and the selenides were obtained as colorless to yellow solids.

8.2.2.2 Synthesis of (dma)P$_1$P-(*t*Bu)$_2$-Se (22a)

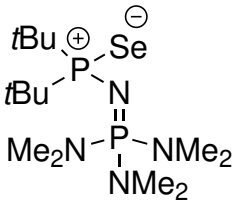

^{1}H-NMR (300 MHz, C_6D_6): δ (ppm) = 2.43 (d, ^{3}J(P,H) = 10.1 Hz, 18H, NC$\underline{H}_3$), 1.52 (d, ^{2}J(P,H) = 15.3 Hz, 18H, CC$\underline{H}_3$).
^{13}C{^{1}H}-NMR (75 MHz, C_6D_6): δ (ppm) = 39.5 (dd, ^{1}J(P,C) = 57.4 Hz, ^{3}J(P,C) = 4.4 Hz, $\underline{C}CH_3$), 36.9 (d, ^{2}J(P,C) = 3.8 Hz, N$\underline{C}H_3$), 27.6 (d, ^{2}J(P,C) = 2.4 Hz), C$\underline{C}H_3$).
^{31}P{^{1}H}-NMR (121 MHz, C_6D_6): δ (ppm) = 75.4 (dd, ^{2}J(P,P) = 3.7 Hz, ^{1}J(P,Se) = 756.1 Hz, P(III)), 24.5 (d, ^{2}J(P,P) = 3.7 Hz, P(V)).
^{77}Se-NMR (57.2 MHz, C_6D_6): δ (ppm) = −273.4 (d, ^{1}J(P,Se) = 756.1 Hz.
LIFDI(+)-HRMS = 402.158 04 $[M\text{-}H]^+$ calc., 402.158 97 $[M\text{-}H]^+$ found.

8.2.2.3 Synthesis of (pyrr)P_1P-(tBu)$_2$-Se (22b)

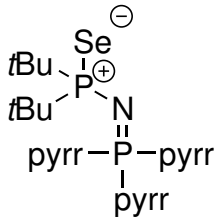

^{1}H-NMR (300 MHz, C_6D_6): δ (ppm) = 3.09 (td, ^3J(H,H) = 6.6 Hz, 12H, NC$\underline{H}_2$CH$_2$), 1.58 (d, ^3J(P,H) = 15.2 Hz, 18H, CC$\underline{H}_3$), 1.51 (tt, ^3J(H,H) = 6.6 Hz, 12H, NCH$_2$C$\underline{H}_2$).
^{13}C{^{1}H}-NMR (75 MHz, C_6D_6): δ (ppm) = 47.2 (d, ^2J(P,C) = 4.5 Hz, N$\underline{C}$H$_2$CH$_2$), 40.3 (dd, ^1J(P,C) = 57.2 Hz, ^3J(P,C) = 4.3 Hz, $\underline{C}$CH$_3$), 28.5 (d, J(P,C) = 2.2 Hz), 26.1 (d, J(P,C) = 8.2 Hz).
^{31}P{^{1}H}-NMR (121 MHz, C_6D_6): δ (ppm) = 73.0 (dd, ^1J(P,Se) = 693.0 Hz, ^2J(P,P) = 2.1 Hz, P(III)), 9.9 (d, ^2J(P,P) = 2.1 Hz, P(V)).
^{77}Se-NMR (57.2 MHz, C_6D_6): δ (ppm) = −257.4 (d, ^1J(P,Se) = 693.0 Hz
LIFDI(+)-HRMS = 480.204 99 [M-H]$^+$ calc., 480.207 01 [M-H]$^+$ found.

8.2.2.4 Synthesis of (cy)P_1P-(tBu)$_2$-Se (22c)

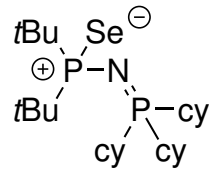

^{1}H-NMR (300 MHz, C_6D_6): δ (ppm) = 2.19–2.08 (m, 5H), 2.01–1.84 (m, 4H), 1.75–1.63 (m, 6H), 1.54 (d, ^3J(P,H) = 15.2 Hz, 18H; CC$\underline{H}_3$), 1.49–1.43 (m, 5H), 1.16–1.03 (m, 8H), 0.90–0.84 (m, 1H).
^{13}C{^{1}H}-NMR (75 MHz, C_6D_6): δ (ppm) = 40.7 (dd, ^1J(P,C) = 57.8 Hz, ^3J(P,C) = 2.8 Hz, $\underline{C}$CH$_3$), 37.3 (d, ^1J(P,C) = 61.5 Hz, $\underline{C}$HCH$_2$CH$_2$CH$_2$), 27.3 (d, ^2J(P,C) = 2.8 Hz), 27.0 (d, ^2J(P,C) = 12.0 Hz, C$\underline{C}$H$_3$), 26.1 (s).
^{31}P{^{1}H}-NMR (121 MHz, C_6D_6): δ (ppm) = 76.2 (dd, ^2J(P,P) = 26.4 Hz, ^1J(P,Se) = 692.4 Hz, P(III)), 28.2 (d, ^2J(P,P) = 26.4 Hz, P(V)).
^{77}Se-NMR (57.2 MHz, C_6D_6): δ (ppm) = −250.6 (d, ^1J(P,Se) = 692.4 Hz).
LIFDI(+)-HRMS = 519.266 19 [M-H]$^+$ calc., 519.267 48 [M-H]$^+$ found.

8.2.2.5 Synthesis of (*t*Bu)P$_1$P-(*t*Bu)$_2$-Se (22d)

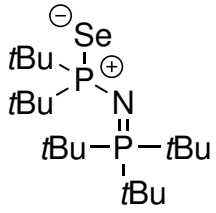

^{1}H-NMR (300 MHz, C_6D_6): δ (ppm) = 1.58 (d, ^3J(P,H) = 15.2 Hz, 12H, P(III)CC$\underline{H}_3$), 1.30 (d, ^3J(P,H) = 13.5 Hz, 18H, P(V)CC$\underline{H}_3$).
^{13}C{^{1}H}-NMR (75 MHz, C_6D_6): δ (ppm) = 42.3 (dd, ^1J(P,C) = 57.4 Hz, ^3J(P,C) = 2.0 Hz, $\underline{C}CH_3$), 40.6 (d, ^1J(P,C) = 50.8 Hz, $\underline{C}CH_3$), 29.8 (s), 29.2 (d, ^2J(P,C) = 2.7 Hz).
^{31}P{^{1}H}-NMR (121 MHz, C_6D_6): δ (ppm) = 74.2 (dd, ^2J(P,P) = 37.8 Hz, ^1J(P,Se) = 695.4 Hz, P(III)), 45.7 (d, ^2J(P,P) = 37.8 Hz, P(V)).
^{77}Se-NMR (57.2 MHz, C_6D_6): δ (ppm) = −222.5 (d, ^1J(P,Se) = 695.4 Hz.
LIFDI(+)-HRMS = 441.219 24 $[M\text{-}H]^+$ calc., 441.218 76 $[M\text{-}H]^+$ found.

8.2.2.6 Synthesis of (dma)P$_1$P-(Odipp)$_2$-Se (28)

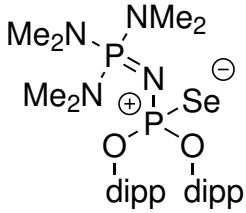

^{1}H-NMR (300 MHz, C_6D_6): δ (ppm) = 7.18 (d, ^2J(H,H) = 1.5 Hz, 2H, Ar$\underline{H}$), 7.11 (d, ^2J(H,H) = 1.3 Hz, 2H, Ar$\underline{H}$), 7.07 (m, 2H, Ar$\underline{H}$), 4.28 (sept, ^2J(H,H) = 6.8 Hz, 4H, $CH_3C\underline{H}CH_3$), 2.28 (d, ^3J(P,H) = 10.2 Hz, 18H, NC$\underline{H}_3$), 1.38 (d, ^2J(H,H) = 6.8 Hz, 12H, C$\underline{H}_3$CHCH_3), 1.35 (d, ^2J(H,H) = 6.8 Hz, $CH_3CHC\underline{H}_3$).
^{13}C{^{1}H}-NMR (75 MHz, C_6D_6): δ (ppm) = 148.2 (d, ^2J(P,C) = 11.8 Hz), 131.3 (d, ^3J(P,C) = 3.8 Hz), 123.9 (d, J(P,C) = 2.5 Hz), 123.2 (d, J(P,C) = 2.1 Hz), 36.1 (d, ^2J(P,C) = 4.1 Hz, N$\underline{C}H_3$), 26.8 (s), 23.7 (s), 22.8 (s).
^{31}P{^{1}H}-NMR (121 MHz, C_6D_6): δ (ppm) = 38.5 (dd, ^2J(P,P) = 68.8 Hz, ^1J(P,Se) = 902.2 Hz, P(III)), 21.5 (d, ^2J(P,P) = 68.8 Hz, P(V)).
^{77}Se-NMR (57.2 MHz, C_6D_6): δ (ppm) = −119.9 (d, ^1J(P,Se) = 902.2 Hz).
LIFDI(+)-HRMS = 642.273 07 $[M\text{-}H]^+$ calc., 642.273 26 $[M\text{-}H]^+$ found.

8.2.2.7 Synthesis of (dma)P_2P-*t*Bu-Se (23a)

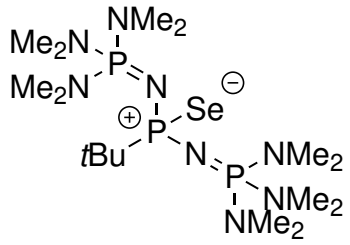

^{1}H-NMR (300 MHz, C_6D_6): δ (ppm) = 2.60 (d, ^2J(P,H) = 10.0 Hz, 36H, NC$\underline{H}_3$), 1.70 (d, ^2J(P,H) = 17.6 Hz, 9H, CC$\underline{H}_3$).
^{13}C{^{1}H}-NMR (75 MHz, C_6D_6): δ (ppm) = 39.4 (dt, ^1J(P,C) = 103.9 Hz, ^3J(P,C) = 7.8 Hz, $\underline{C}CH_3$), 37.5 (d, ^2J(P,C) = 4.2 Hz, N$\underline{C}H_3$), 26.4 (d, ^2J(P,C) = 2.0 Hz, C$\underline{C}H_3$).
^{31}P{^{1}H}-NMR (121 MHz, C_6D_6): δ (ppm) = 34.2 (td, ^2J(P,P) = 21.0 Hz, ^1J(P,Se) = 676.6 Hz, P(III)), 17.5 (d, ^2J(P,P) = 21.0 Hz, P(V)).
^{77}Se-NMR (57.2 MHz, C_6D_6): δ (ppm) = −97.5 (d, ^1J(P,Se) = 676.6 Hz).
LIFDI(+)-HRMS = 522.214 52 $[M\text{-}H]^+$ calc., 522.213 86 $[M\text{-}H]^+$ found.

8.2.2.8 Synthesis of (pyrr)P_2P-*t*Bu-Se (23b)

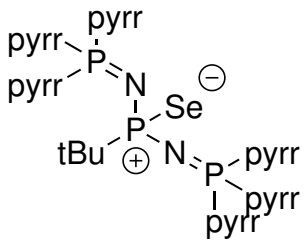

^{1}H-NMR (300 MHz, C_6D_6): δ (ppm) = 3.37 (m, 12H, NC$\underline{H}_2$CH$_2$), 3.23 (m, 12H, NC$\underline{H}_2$CH$_2$), 1.77 (d, ^2J(P,H) = 17.4 Hz, 9H, CC$\underline{H}_3$), 1.66 (m, 24H, NCH$_2$C$\underline{H}_2$).
^{13}C{^{1}H}-NMR (75 MHz, C_6D_6): δ (ppm) = 47.3 (d, ^2J(P,C) = 4.6 Hz), 39.7 (dt, ^1J(P,C) = 104.7 Hz, ^3J(P,C) = 9.0 Hz, $\underline{C}CH_3$), 27.0 (d, ^2J(P,C) = 2.0 Hz), 26.7 (d, ^2J(P,C) = 8.5 Hz, C$\underline{C}H_3$).
^{31}P{^{1}H}-NMR (121 MHz, C_6D_6): δ (ppm) = 31.0 (td, ^2J(P,P) = 16.3 Hz, ^1J(P,Se) = 665.5 Hz, P(III)), 2.9 (d, ^2J(P,P) = 16.3 Hz, P(V)).
^{77}Se-NMR (57.2 MHz, C_6D_6): δ (ppm) = −71.3 (d, ^1J(P,Se) = 665.5 Hz).
LIFDI(+)-HRMS = 678.308 42 $[M\text{-}H]^+$ calc., 678.307 83 $[M\text{-}H]^+$ found.

8.2.2.9 Synthesis of (dma)P_2P-Biaryl-Se (30)

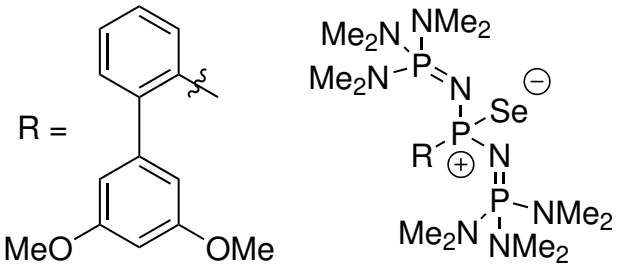

The compound could not be isolated free of impurities (ca. 10%).

^{1}H-NMR (300 MHz, C_6D_6): δ (ppm) = 7.82–7.76 (m, 1H, ArH), 7.54–7.50 (m, 1H, ArH), 7.35–7.29 (m, 1H, ArH), 7.28 (m, 2H, ArH), 7.23–7.18 (m, 1H, ArH), 7.07–6.99 (m, 1H, ArH), 6.97–6.91 (m, 2H, ArH), 6.83 (d, J(H,H) = 2.3 Hz, 1H), 6.55 (t, J(H,H) = 2.3 Hz, 1H), 3.52 (s, 6H, OCH$_3$), 2.47 (d, ^2J(P,H) = 9.9 Hz, 36H, NCH$_3$).
^{13}C{^{1}H}-NMR (75 MHz, DMSO): δ (ppm) = 159.6 (s), 132.6 (d, J(P,C) = 10.9 Hz), 129.3 (d, J(P,C) = 12.1 Hz), 128.0 (s), 127.3 (s), 55.3, 37.5 (dd, J(P,C) = 4.4 Hz, J(P,C) = 10.4 Hz).
^{31}P{^{1}H}-NMR (121 MHz, C_6D_6): δ (ppm) = 19.0 (d, ^2J(P,P) = 38.3 Hz, P(V)), 10.0 (t, ^2J(P,P) = 38.3 Hz, P(III)).
^{77}Se-NMR (57.2 MHz, C_6D_6): δ (ppm) = 26.7 (d, ^1J(P,Se) = 672.4 Hz).
LIFDI(+)-HRMS = 677.228 17 $[M\text{-}H]^+$ calc., 677.227 83 $[M\text{-}H]^+$ found.

8.2.3 Synthesis of phosphazenyl phosphine nickel carbonyl complexes

8.2.3.1 General procedure for the generation of phosphazene nickel tricarbonyl complexes

A solution of phosphine (1.00 eq, 0.20 mmol) in toluene (5 mL) was added dropwise to a solution of $[Ni(CO)_4]$ in toluene (5 mL). The mixture was stirred for 1 h. Afterwards the solvent was removed *in vacuo*, the residue dissolved in pentane and filtered through a syringe filter. The solvent was removed *in vacuo* to yield the corresponding phosphine nickeltricarbonyl complexes as orange to red solids.

8.2.3.2 Synthesis of [(dma)P_1P-(tBu)$_2$-Ni(CO)$_3$] (25a)

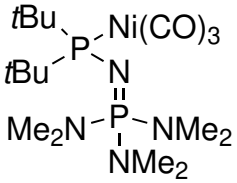

^{1}H-NMR (300 MHz, C_6D_6): δ (ppm) = 2.31 (d, ^2J(P,H) = 9.8 Hz, 18H, NCH$_3$), 1.30 (d, ^2J(P,H) = 13.0 Hz, 18H, CCH$_3$).
^{13}C{^{1}H}-NMR (75 MHz, C_6D_6): δ (ppm) = 200.0 (d, ^2J(P,C) = 2.3 Hz, NiCO), 38.4 (dd, ^1J(P,C) = 13.9 Hz, ^2J(P,C) = 4.5 Hz, CCH$_3$), 37.3 (d, ^2J(P,C) = 4.4 Hz, NCH$_3$), 28.4 (d, ^2J(P,C) = 8.1 Hz, CCH$_3$).

^{31}P{^{1}H}-NMR (121 MHz, C_6D_6): δ (ppm) = 101.4 (d, ^{2}J(P,P) = 16.4 Hz, P(III)), 13.4 (d, ^{2}J(P,P) = 16.4 Hz, P(V)).
LIFDI(+)-HRMS = 464.161 61 [M-H]$^{+}$ calc., 464.163 07 [M-H]$^{+}$ found.
IR (neat) = 2893 (w), 2803 (w), 2040 (s, CO), 1948 (vs, CO), 1480 (w), 1456 (m), 1386 (m), 1315 (m), 1261 (m), 1184 (m), 1100 (m), 1064 (m), 1017(m), 976 (s), 803 (m), 725 (m), 601 (w), 573 (w), 487 (m), 454 (s).

8.2.3.3 Synthesis of [(pyrr)P$_1$P-(*t*Bu)$_2$-Ni(CO)$_3$] (25b)

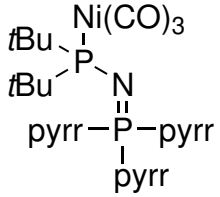

^{1}H-NMR (300 MHz, C_6D_6): δ (ppm) = 2.79 (m, 12H, NC$\underline{H}_2$CH$_2$), 1.28 (m, 12H, NCH$_2$C$\underline{H}_2$), 1.15 (d, ^{3}J(P,H) = 13.0 Hz, 18H, CC$\underline{H}_3$).
^{13}C{^{1}H}-NMR (75 MHz, C_6D_6): δ (ppm) = 200.5 (d, ^{2}J(P,C) = 2.6 Hz, Ni$\underline{C}$O), 47.1 (d, ^{2}J(P,C) = 4.6 Hz, N$\underline{C}$H$_2$CH$_2$), 38.5 (dd, ^{3}J(P,C) = 5.2 Hz, $\underline{C}$CH$_3$), 28.8 (d, ^{2}J(P,C) = 8.1 Hz, NCH$_2\underline{C}$H$_2$), 26.4 (d, ^{3}J(P,C) = 8.2 Hz, C$\underline{C}$H$_3$).
^{31}P{^{1}H}-NMR (121 MHz, C_6D_6): δ (ppm) = 100.0 (d, ^{2}J(P,P) = 24.0 Hz, P(III), 0.5 (d, ^{2}J(P,P) = 24.0 Hz, P(V)).
LIFDI(+)-HRMS = 542.208 [M-H]$^{+}$ calc., 542.210 02 [M-H]$^{+}$ found.
IR (neat) = 2960 (w), 2866 (w), 2042 (m, CO), 1974 (m), 1946 (s), 1259 (m), 1195 (m), 1070 (s), 1008 (s), 933 (w), 914 (w), 865 (w), 795 (s), 700 (w), 581 (m), 560 (m), 489 (w), 467 (w), 447 (m).

8.2.3.4 Synthesis of [(cy)P$_1$P-(*t*Bu)$_2$-Ni(CO)$_3$] (25c)

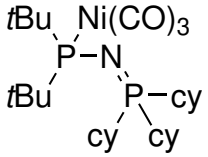

^{1}H-NMR (300 MHz, C_6D_6): δ (ppm) = 1.97 (d, J(H,H) = 12.5 Hz, 5H), 1.83 (m, 4H), 1.68 (m, 3H), 1.33 (d, ^{3}J(P,H) = 12.9 Hz, 18H, CC$\underline{H}_3$), 1.10 (m, 9H).
^{13}C{^{1}H}-NMR (75 MHz, C_6D_6): δ (ppm) = 200.0 (d, ^{2}J(P,C) = 1.9 Hz, Ni$\underline{C}$O), 39.1 (dd, ^{1}J(P,C) = 14.1 Hz, ^{3}J(P,C) = 2.9 Hz, $\underline{C}$CH$_3$), 37.7 (d, ^{1}J(P,C) = 63.0 Hz, $\underline{C}$HCH$_2$CH$_2$CH$_2$), 28.8 (d, ^{2}J(P,C) = 8.2 Hz, C$\underline{C}$H$_3$),
27.5 (d, ^{3}J(P,C) = 2.8 Hz, CHCH$_2\underline{C}$H$_2$CH$_2$), 26.9 (d, ^{2}J(P,C) = 12.4 Hz, CH$\underline{C}$H$_2$CH$_2$CH$_2$), 26.1 (s, CHCH$_2$CH$_2\underline{C}$H$_2$).
^{31}P{^{1}H}-NMR (121 MHz, C_6D_6): δ (ppm) = 104.5 (d, ^{2}J(P,P) = 4.0 Hz, P(III)), 20.4 (d, ^{2}J(P,P) = 4.0 Hz, P(V)).
LIFDI(+)-HRMS = 581.269 76 [M-H]$^{+}$ calc., 581.268 72 [M-H]$^{+}$ found.
IR (neat) = 2930.2 (m), 2851.8 (m), 2042.8 (m, CO), 1973.4 (s), 1957.2 (vs), 1927.1 (w), 1447.6 (vw), 1285.4 (m), 1255.3 (vs), 1174.2 (w), 1009.8 (w), 852.2 (vw), 801.3 (m), 650.7 (vw), 574.2 (w), 530.2 (m), 486.2 (m), 451.5 (vs).

8.2.3.5 Synthesis of [(*t*Bu)P$_1$P-(*t*Bu)$_2$-Ni(CO)$_3$] (25d)

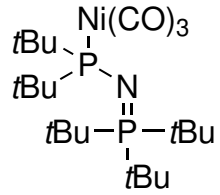

^{1}H-NMR (300 MHz, C_6D_6): δ (ppm) = 1.38 (d, ^3J(P,H) = 17.3 Hz, 12H, CC$\underline{H}_3$), 1.23 (d, ^3J(P,H) = 10.9 Hz, 18H, CC$\underline{H}_3$).
^{13}C{^{1}H}-NMR (75 MHz, C_6D_6): δ (ppm) = 200.1 (d, ^2J(P,C) = 2.2 Hz, Ni$\underline{C}$O), 42.1 (dd, ^1J(P,C) = 51.9 Hz, ^3J(P,C) = 2.0 Hz, $\underline{C}$CH$_3$), 41.8 (d, ^1J(P,C) = 10.7 Hz, ^3J(P,C) = 1.4 Hz, $\underline{C}$CH$_3$), 30.8 (s, C$\underline{C}$H$_3$), 30.5 (d, ^2J(P,C) = 7.9 Hz, C$\underline{C}$H$_3$).
^{31}P{^{1}H}-NMR (121 MHz, C_6D_6): δ (ppm) = 108.8 (d, ^2J(P,P) = 25.8 Hz, P(III)), 38.0 (d, ^2J(P,P) = 25.8 Hz, P(V)).
LIFDI(+)-HRMS = 503.222 81 [M-H]$^+$ calc., 503.225 10 [M-H]$^+$ found.
IR (neat) = 2908.1 (mb), 2039.4 (s, CO), 1951.6 (vs), 1472.9 (m), 1390.6 (m), 1248.6 (s), 1165.8 (s), 1011.2 (m), 933.8 (m), 805.4 (m), 618.9 (m), 491.6 (m), 448.3 (m).

8.2.3.6 Synthesis of [(dma)P$_1$P-(Odipp)$_2$-Ni(CO)$_3$] (29)

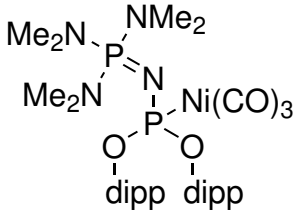

^{1}H-NMR (300 MHz, C_6D_6): δ (ppm) = 7.14 (m, 6H, Ar$\underline{H}$), 4.13 (sept, ^3J(H,H) = 6.7 Hz, 4H, CH$_3$C$\underline{H}$CH$_3$), 2.2 (d, ^3J(P,H) = 10.3 Hz, 18H, NC$\underline{H}_3$), 1.35 (d, ^3J(H,H) = 6.8 Hz, C$\underline{H}_3$), 1.30 (d, ^3J(H,H) = 6.8 Hz, CH$_3$CHC$\underline{H}_3$).
^{13}C{^{1}H}-NMR (75 MHz, C_6D_6): δ (ppm) = 195.8 (s, Ni$\underline{C}$O), 148.6 (d, ^2J(P,C) = 8.8 Hz), 141.2 (d, ^3J(P,C) = 3.4 Hz), 123.4 (s), 122.6 (s), 35.7 (d, ^4J(P,C) = 4.0 Hz, CH$_3\underline{C}$HCH$_3$), 27.2 (s), 22.7 (d, ^2J(P,C) = 10.0 Hz).
^{31}P{^{1}H}-NMR (121 MHz, C_6D_6): δ (ppm) = 132.3 (d, ^2J(P,P) = 46.0 Hz, P(III)), 15.2 (d, ^2J(P,P) = 46.0 Hz, P(V)).
LIFDI(+)-HRMS = 704.276 64 [M-H]$^+$ calc., 704.275 42 [M-H]$^+$ found.
IR (neat) = 3026.8 (w), 2104.5 (m, CO), 2019.4 (vs), 1492.4 (w), 1465.3 (m), 1318.0 (m), 1197.9 (s), 1114.6 (m), 1085.6 (m), 1066.2 (m), 1041.0 (m), 1000.3 (vs), 872.5 (s), 814.3 (m), 771.7 (m), 754.2 (m), 729.1 (m), 669.0 (w), 616.7 (w), 492.7 (w), 455.9 (m).

8.2.3.7 Synthesis of [(dma)P_2P-*t*Bu-Ni(CO)$_3$] (26a)

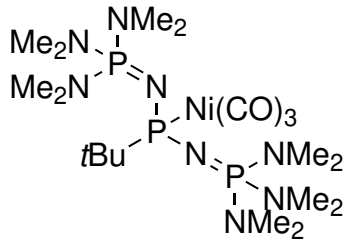

^{1}H-NMR (300 MHz, C_6D_6): δ (ppm) = 2.48 (d, ^3J(P,H) = 9.9 Hz, 36H, NC$\underline{H}_3$), 1.40 (d, ^3J(P,H) = 15.0 Hz, 9H, CC$\underline{H}_3$).
^{13}C{^{1}H}-NMR (75 MHz, C_6D_6): δ (ppm) = 202.0 (d, ^2J(P,C) = 4.6 Hz, Ni$\underline{C}$O), 39.8 (dt, ^1J(P,C) = 34.5 Hz, ^3J(P,C) = 6.9 Hz, $\underline{C}$CH$_3$), 25.8 (d, ^2J(P,C) = 9.6 Hz, N$\underline{C}$H$_3$).
^{31}P{^{1}H}-NMR (121 MHz, C_6D_6): δ (ppm) = 79.8 (t, ^2J(P,P) = 5.2 Hz, P(III)), 7.5 (d, ^2J(P,P) = 5.2 Hz, P(V)).
LIFDI(+)-HRMS = 584.218 09 [M-H]$^+$ calc., 584.219 51 [M-H]$^+$ found.
IR (neat) = 2960.1 (w), 2877.3 (m), 2796.5 (w), 2032.1 (s, NiCO), 1942.9 (vs), 1456.8 (w), 1375.9 (m), 1348.7 (m), 1309.5 (vs), 1256.2 (s), 1188.1 (m), 1092.3 (m), 1062.9 (m), 969.4 (vs), 865.0 (w), 798.7 (s), 749.7 (m), 641.8 (s), 641.8 (m), 597.4 (m), 574.0 (m), 484.8 (m), 460.7 (s), 433.7 (m).

8.2.3.8 Synthesis of [(pyrr)P_2P-*t*Bu-Ni(CO)$_3$] (26b)

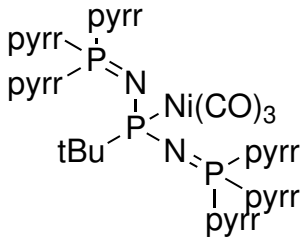

^{1}H-NMR (300 MHz, C_6D_6): δ (ppm) = 3.27–3.07 (m, 24H, NC$\underline{H}_2$CH$_2$), 1.71–1.54 (m, 24H, NCH$_2$C$\underline{H}_2$), 1.48 (d, ^3J(P,H) = 14.8 Hz, CC$\underline{H}_3$).
^{13}C{^{1}H}-NMR (75 MHz, C_6D_6): δ (ppm) = 201.9 (d, ^2J(P,C) = 5.0 Hz, Ni$\underline{C}$O), 46.9 (d, ^2J(P,C) = 4.9 Hz, N$\underline{C}$H$_2$CH$_2$), 39.5 (d, ^1J(P,C) = 35.2 Hz, $\underline{C}$CH$_3$), 26.7 (d, ^2J(P,C) = 8.7 Hz, NCH$_2\underline{C}$H$_2$), 26.0 (d, ^2J(P,C) = 9.6 Hz, C$\underline{C}$H$_3$).
^{31}P{^{1}H}-NMR (121 MHz, C_6D_6): δ (ppm) = 77.7 (s, P(III)), −5.6 (P(V)).
LIFDI(+)-HRMS = 740.311 99 [M-H]$^+$ calc., 740.310 98 [M-H]$^+$ found.
IR (neat) = 2961.2 (m), 2856.2 (m), 2030.4 (m, CO), 1937.8 (s) , 1258.2 (s), 1194.4 (m), 1124.4 (m), 1070.8 (s), 1004.9 (s), 912.3 (w), 869.0 (m), 805.2 (m), 759.9 (w), 683.7 (w), 597.2 (m), 558.0 (s).

8.2.3.9 Synthesis of [(dma)P_2P-Biaryl-Ni(CO)$_3$] (31)

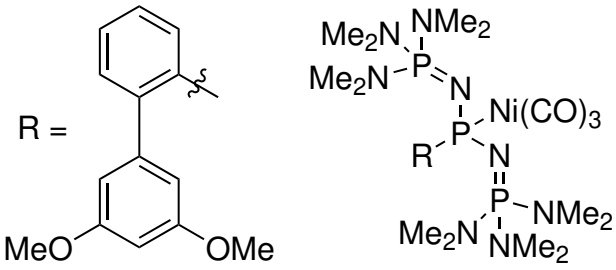

This compound could not be isolated without impurities.

^{1}H-NMR (300 MHz, C_6D_6): δ (ppm) = 9.09–8.89 (m, 1H, Ar$\underline{H}$), 7.55–7.30 (m, 4H, Ar$\underline{H}$), 6.62 (s, 2H, Ar$\underline{H}$), 3.58 (s, 6H, OC$\underline{H}_3$), 2.47 (s, ^2J(P,C) = 9.4 Hz, NC$\underline{H}_3$).
^{13}C{^{1}H}-NMR (75 MHz, C_6D_6): δ (ppm) = 159.9 (s), 109.6 (s), 54.7 (s), 37.0 (s).
^{31}P{^{1}H}-NMR (121 MHz, C_6D_6): δ (ppm) = 56.0 (t, ^2J(P,P) = 12.9 Hz, P(III)), 12.0 (d, ^2J(P,P) = 12.9 Hz, P(V)).
LIFDI(+)-HRMS = 740.239 22 $[M\text{-}H]^+$ calc., 740.240 99 $[M\text{-}H]^+$ found.
IR (neat) = 3000.3 (w), 2878.8 (m), 2798.5 (m), 2036.6 (m), 1939.8 (vs), 1799.8 (w), 1593.9 (s), 1455.9 (s), 1287.0 (vs), 1188.2 (vs), 1153.2 (vs), 1064.6 (vs), 974.0 (vs), 726.9 (vs), 576.6 (m), 533.4 (m), 475.7 (m), 453.0 (s).

8.2.4 Synthesis of phosphazenyl phosphine CO_2 adducts

8.2.4.1 Attempted Synthesis of (R)P_1P-(tBu)$_2$-CO_2 (39a to 39d)

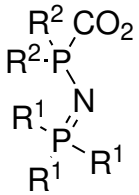

R1 = NMe_2, pyrr, cy, *t*Bu
R2 = *t*Bu

P_1P base (100 mg) was dissolved in pentane (10 mL) and cooled to −78 °C. Afterwards the argon atmosphere was removed and replaced by a CO_2 atmosphere for a total of three cycles. A white precipitate could be observed after stirring in this atmosphere for 5 min. The solution was decanted and the white precipitate was dissolved in Et_2O and a ^{31}P-NMR was taken. The resulting $P_1P{-}CO_2$ adducts turned out to be unstable at RT and in only one case it was possible to measure this adduct. Only pure P_1P base was detected in all other cases.

Data for (pyrr)P_1P-(tBu)$_2$-CO2 (**39b**):

^{31}P{^{1}H}-NMR (121 MHz, C_6D_6): δ (ppm) = 41.9 (s, P(III)), 11.9 (s, P(V)).

8.2.4.2 Synthesis of (dma)P_2P-*t*Bu-CO_2 (40a)

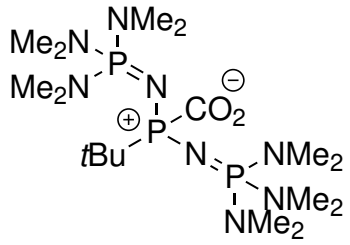

Synthetic route a)

(dma)P_2P-(*t*Bu) (**6a**) (100 mg, 0.23 mmol, 1.0 eq.) was dissolved in Et_2O (15 mL), cooled to −78 °C and freshly ground dry ice (excess) was dropped slowly into this solution. Afterwards the solution was stirred at −78 °C for 1 h and the solvent was removed *in vacuo*. (dma)P_2P-*t*Bu-CO_2 (**40a**) (109 mg, 0.23 mmol, quant.) was obtained as a white solid. This route does generate a small amount of protonated (dma)P_2P-*t*BuH^+ as a result of the dry ice being slightly wet.

Synthetic route b)

(dma)P_2P-(*t*Bu) (**6a**) (100 mg, 0.23 mmol, 1.0 eq.) was dissolved in Et_2O (15 mL) and cooled to −78 °C. The argon atmosphere was removed and replaced with a CO_2 atmosphere for a total of three cycles. Afterwards the solution was stirred at −78 °C for 1 h and the solvent was removed *in vacuo*. (dma)P_2P-*t*Bu-CO_2 (**40a**) (quant.) was obtained as a white solid.

^{1}H-NMR (300 MHz, C_6D_6): δ (ppm) = 2.50 (d, ^2J(P,H) = 10.1 Hz, 36H, NC$\underline{H}_3$), 1.63 (d, ^2J(P,H) = 15.2 Hz, 9H, CC$\underline{H}_3$).
^{13}C{^{1}H}-NMR (75 MHz, C_6D_6): δ (ppm) = 167.8 (d, ^1J(P,C) = 128.6 Hz, $\underline{C}O_2$), 37.2 (d, ^2J(P,C) = 3.7 Hz, N$\underline{C}H_3$), 25.5 (s, C$\underline{C}H_3$).
^{31}P{^{1}H}-NMR (121 MHz, C_6D_6): δ (ppm) = 19.2 (d, ^2J(P,P) = 19.4 Hz, P(V)), 4.3 (t, ^2J(P,P) = 19.4 Hz, P(III)).
MS-data is unavailable due to decomposition of the compound under MS conditions.
IR (neat) = 3002.4 (w), 2883.0 (m), 2800.6 (w), 1633.0 (s, CO_2), 1478.5 (m), 1455.9 (m), 1371.5 (m), 1282.9 (s), 1254.1 (s), 1177.9 (s), 1064.6 (m), 969.9 (vs), 801.1 (m), 729.0 (s), 628.1 (m), 586.9 (s), 514.8 (m), 465.4 (s).

8.2.4.3 Synthesis of (pyrr)P_2P-*t*Bu-CO_2 (40b)

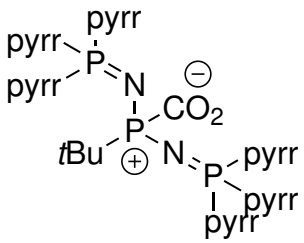

Synthetic route a)

(pyrr)P_2P-*t*Bu (**6b**) (100 mg, 0.17 mmol, 1.0 eq.) was dissolved in Et_2O (15 mL), cooled to −78 °C and freshly ground dry ice (excess) was dropped slowly into this solution. Afterwards the solution was stirred at −78 °C for 1h and the solvent was removed *in vacuo*. (pyrr)P_2P-*t*Bu-CO_2 (**40b**) (quant.) was obtained as a white solid. This route does generate a small amount of protonated (pyrr)P_2P-*t*Bu-H^+ as a result of the dry ice being slightly wet.

Synthetic route b)

(pyrr)P_2P-*t*Bu (**6b**) (100 mg, 0.17 mmol, 1.0 eq.) was dissolved in Et_2O (15 mL) and cooled to −78 °C. The argon atmosphere was removed and replaced with a CO_2 atmosphere for a total of three cycles. Afterwards the solution was stirred at −78 °C for 1h and the solvent was removed *in vacuo*. (pyrr)P_2P-*t*Bu-CO_2 (**40b**) (107 mg, 0.17 mmol, quant.) was obtained as a white solid.

^{1}H-NMR (300 MHz, C_6D_6): δ (ppm) = 3.27–3.11 (m, 32H, NC$\underline{H}_2$$CH_2$), 1.72 (d, ^2J(P,H) = 14.9 Hz, 9H, CC$\underline{H}_3$), 1.64–1.59 (m, 32H, $NCH_2C\underline{H}_2$).
^{13}C{^{1}H}-NMR (75 MHz, C_6D_6): δ (ppm) = 168.6 (d, ^1J(P,C) = 129.7 Hz, $\underline{C}O_2$), 46.8 (d, ^2J(P,C) = 4.7 Hz, N$\underline{C}H_2CH_2$), 26.3 (d, ^2J(P,C) = 8.6 Hz, N$\underline{C}H_3$), 25.8 (s, $NCH_2\underline{C}H_2$).
^{31}P{^{1}H}-NMR (121 MHz, C_6D_6): δ (ppm) = 4.12 (d, ^2J(P,P) = 18.1 Hz, P(V)), 2.9 (t, ^2J(P,P) = 17.8 Hz, P(III)).
MS-data is unavailable due to decomposition of the compound under MS conditions.
IR (neat) = 2948.9 (m), 2864.4 (m), 1630.9 (s, CO_2), 1451.8 (w), 1342.6 (m), 1258.2 (vs), 1196.4 (s), 1120.2 (s), 1072.9 (vs), 1009.0 (vs), 914.3 (m), 823.7 (m), 766.0 (m), 685.7 (m), 628.1 (s), 562.2 (vs), 531.3 (vs), 483.9 (s), 461.3 (vs).

8.2.4.4 Synthesis of (dma)P_3P-CO_2 (41a)

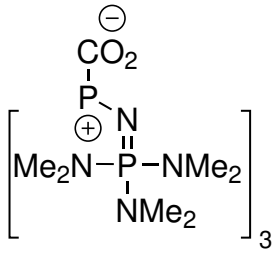

(dma)P_3P (**7a**) (100 mg, 0.18 mmol, 1.0 eq.) was dissolved in Et_2O (15 mL), cooled to −78 °C and freshly ground dry ice (excess) was dropped slowly into this solution. Afterwards the

solution was stirred at −78 °C for 1h and the solvent was removed *in vacuo*. (dma)$P_3P{-}CO_2$ (**41a**) (quant.) was obtained as a white solid. This route does generate a small amount of protonated (dma)$P_3P{-}H^+$ as a result of the dry ice being slightly wet.

Synthetic route b)

(dma)P_3P (**7a**) (100 mg, 0.18 mmol, 1.0 eq.) was dissolved in Et_2O (15 mL) and cooled to −78 °C. The argon atmosphere was removed and replaced with a CO_2 atmosphere for a total of three cycles. Afterwards the solution was stirred at −78 °C for 1h and the solvent was removed *in vacuo*. (dma)$P_3P{-}CO_2$ (**41a**) (107 mg, 0.18 mmol, quant.) was obtained as a white solid.

^{1}H-NMR (300 MHz, C_6D_6): δ (ppm) = 2.67 (d, ^2J(P,H) = 10.1 Hz, 54H, NC$\underline{H}_3$).
^{13}C{^{1}H}-NMR (75 MHz, C_6D_6): δ (ppm) = 172.3 (d, ^1J(P,C) = 191.9 Hz, $\underline{C}O_2$), 37.3 (d, ^2J(P,C) = 3.9 Hz, N$\underline{C}H_3$).
^{31}P{^{1}H}-NMR (121 MHz, C_6D_6): δ (ppm) = 16.6 (d, ^2J(P,P) = 29.2 Hz, P(V)), −17.9 (q, ^2J(P,P) = 29.2 Hz, P(III)).
MS-data is unavailable due to decomposition of the compound under MS conditions.
IR (neat) = 3000.3 (w), 2880.9 (m), 2841.8 (m), 2800.6 (m), 2149.9 (vw), 1612.4 (s, CO_2), 1458.0 (m), 1231.4 (vs), 1182.0 (vs), 1064.6 (m), 967.9 (vs), 836.1 (m), 729.0 (vs), 599.2 (vs), 529.2 (s), 500.4 (s), 471.6 (m), 420.1 (w).

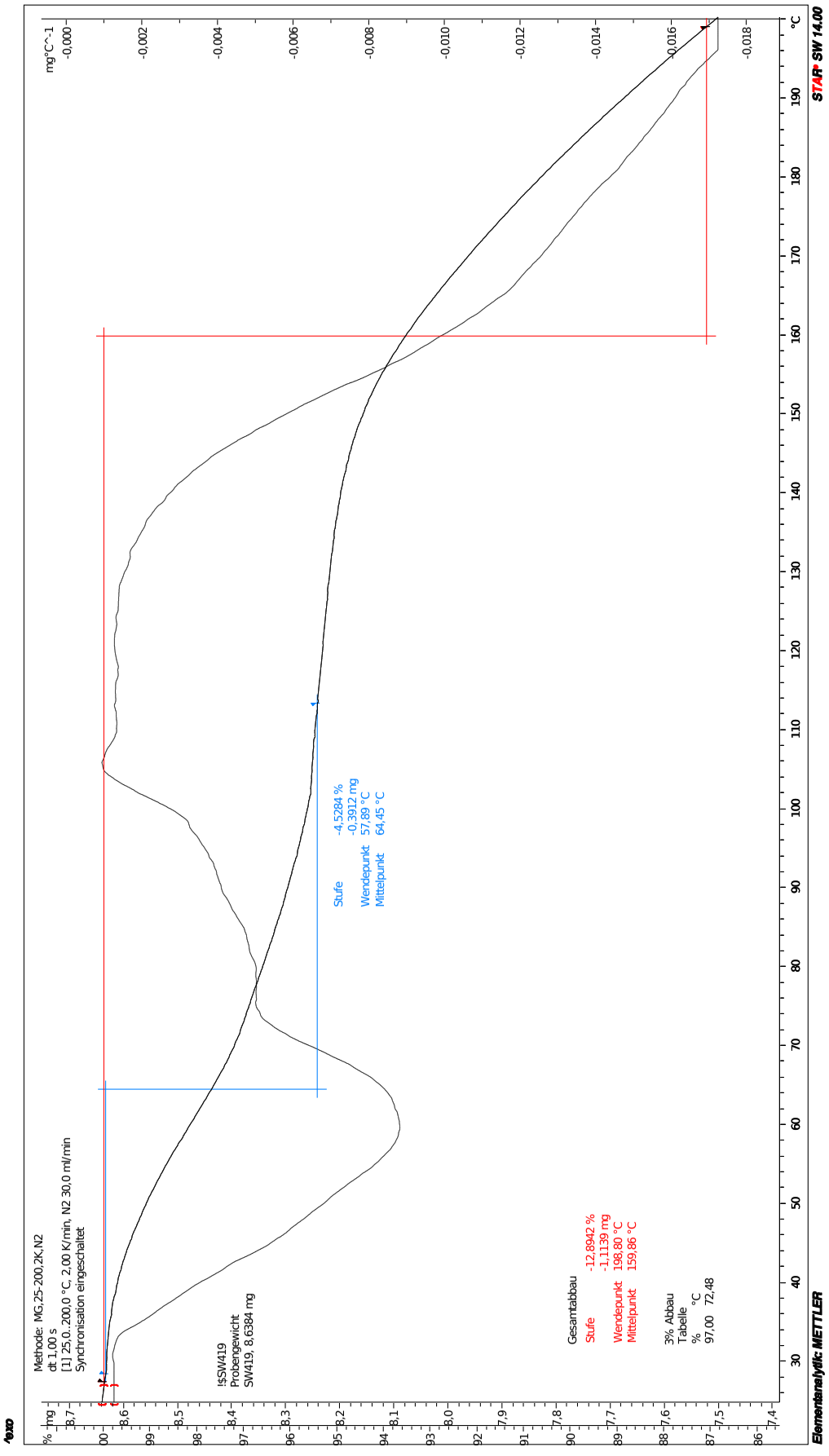
Methode: MG,25-200,2K,N2
dt 1,00 s
[1] 25,0..200,0 °C, 2,00 K/min, N2 30,0 ml/min
Synchronisation eingeschaltet
!$SW419
Probengewicht
SW419, 8,6384 mg
Stufe -4,5284 %
-0,3912 mg
Wendepunkt 57,89 °C
Mittelpunkt 64,45 °C
Gesamtabbau
Stufe -12,8942 %
-1,1139 mg
Wendepunkt 198,80 °C
Mittelpunkt 159,86 °C
3% Abbau
Tabelle
% °C
97,00 72,48
mg
mg°C^-1
°C
STAR° SW 14.00
Elementanalytik METTLER

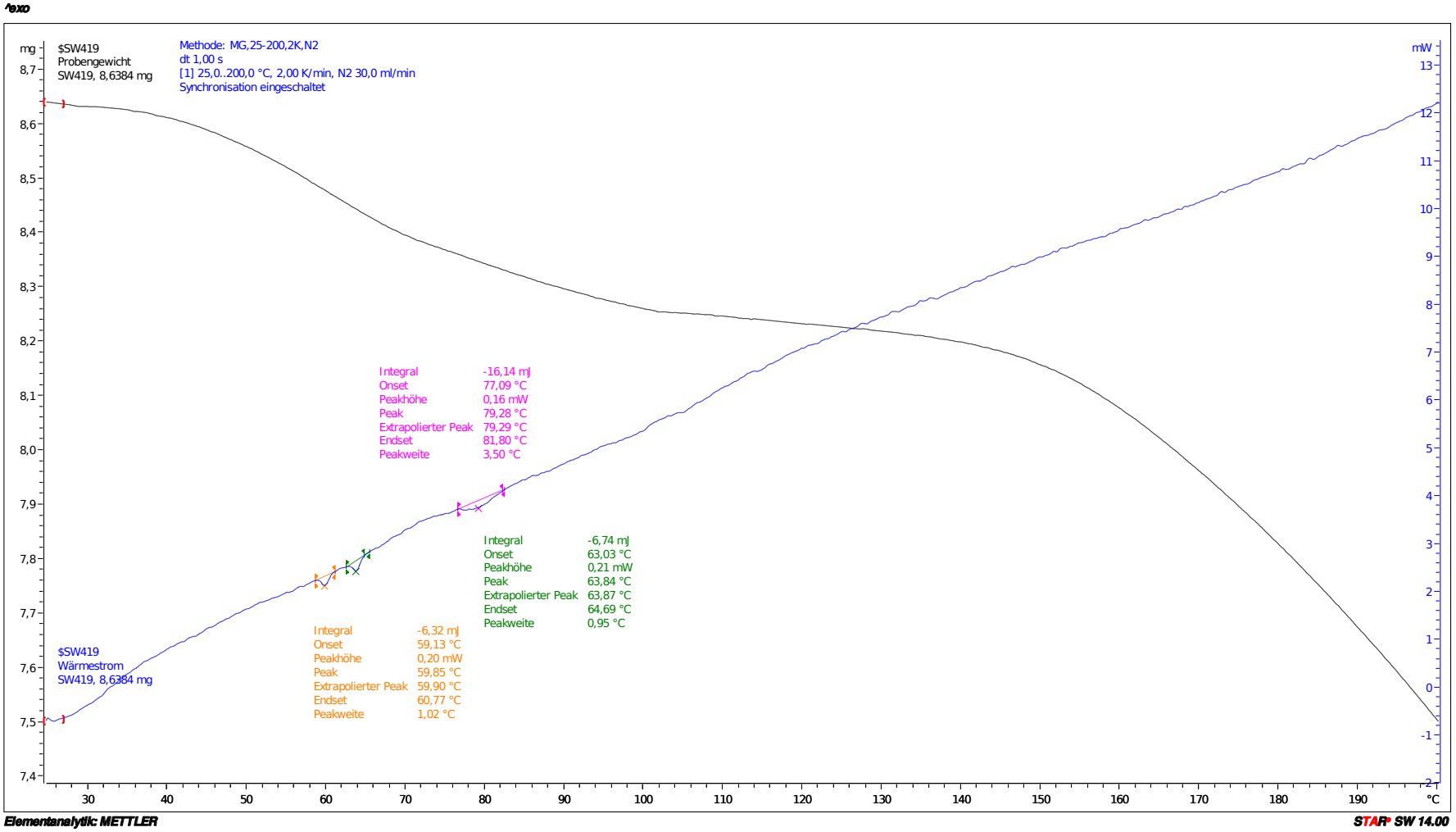
exo
mg
mW
$SW419
Probengewicht
SW419, 8,6384 mg
Methode: MG,25-200,2K,N2
dt 1,00 s
[1] 25,0..200,0 °C, 2,00 K/min, N2 30,0 ml/min
Synchronisation eingeschaltet
Integral -16,14 mJ
Onset 77,09 °C
Peakhöhe 0,16 mW
Peak 79,28 °C
Extrapolierter Peak 79,29 °C
Endset 81,80 °C
Peakweite 3,50 °C
Integral -6,74 mJ
Onset 63,03 °C
Peakhöhe 0,21 mW
Peak 63,84 °C
Extrapolierter Peak 63,87 °C
Endset 64,69 °C
Peakweite 0,95 °C
Integral -6,32 mJ
Onset 59,13 °C
Peakhöhe 0,20 mW
Peak 59,85 °C
Extrapolierter Peak 59,90 °C
Endset 60,77 °C
Peakweite 1,02 °C
$SW419
Wärmestrom
SW419, 8,6384 mg
°C
Elementanalytik: METTLER
STAR° SW 14.00

8.2.4.5 Synthesis of (pyrr)P_3P-CO_2 (41b)

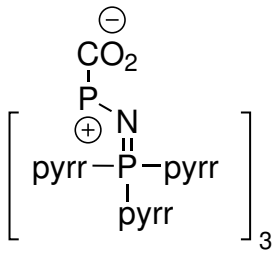

Synthetic route a)

(pyrr)P_3P (**7b**) (100 mg, 0.13 mmol, 1.0 eq.) was dissolved in Et_2O (15 mL), cooled to −78 °C and freshly ground dry ice (excess) was dropped slowly into this solution. Afterwards the solution was stirred at −78 °C for 1h and the solvent was removed *in vacuo*. dmaP_3P−CO_2 (**41b**) (quant.) was obtained as a white solid. This route does generate a small amount of protonated (pyrr)P_3P−H^+ as a result of the dry ice being slightly wet.

Synthetic route b)

(pyrr)P_3P (**7b**) (100 mg, 0.13 mmol, 1.0 eq.) was dissolved in Et_2O (15 mL) and cooled to −78 °C. The argon atmosphere was removed and replaced with a CO_2 atmosphere for a total of three cycles. Afterward, the solution was stirred at −78 °C for 1h and the solvent was removed *in vacuo*. (pyrr)P_3P−CO_2 (**41b**) (105 mg, 0.13 mmol, quant.) was obtained as a white solid.

^{1}H-NMR (300 MHz, C_6D_6): δ (ppm) = 3.42–3.35 (m, 36H, $NC\underline{H}_2CH_2$), 1.78–1.71 (m, 36H, $NCH_2C\underline{H}_2$).
^{13}C{^{1}H}-NMR (75 MHz, C_6D_6): δ (ppm) = 173.3 (d, ^1J(P,C) = 194.4 Hz, $\underline{C}O_2$), 46.8 (d, ^2J(P,C) = 4.6 Hz, $N\underline{C}H_2CH_2$), 26.5 (d, ^3J(P,C) = 8.6 Hz, $NCH_2\underline{C}H_2$).
^{31}P{^{1}H}-NMR (121 MHz, C_6D_6): δ (ppm) = 3.8 (d, ^2J(P,P) = 19.0 Hz, P(V)), −18.1 (q, ^2J(P,P) = 19.0 Hz, P(III)).
MS-data is unavailable due to decomposition of the compound under MS conditions.
IR (neat) = 2957.1 (m), 2860.3 (m), 1610.3 (m, CO_2), 1458.0 (w), 1233.5 (vs), 1200.5 (vs), 1124.3 (s), 1070.8 (vs), 1004.9 (vs), 871.0 (m), 811.3 (s), 764.0 (m), 683.7 (m), 574.5 (vs), 535.4 (m), 490.1 (s).

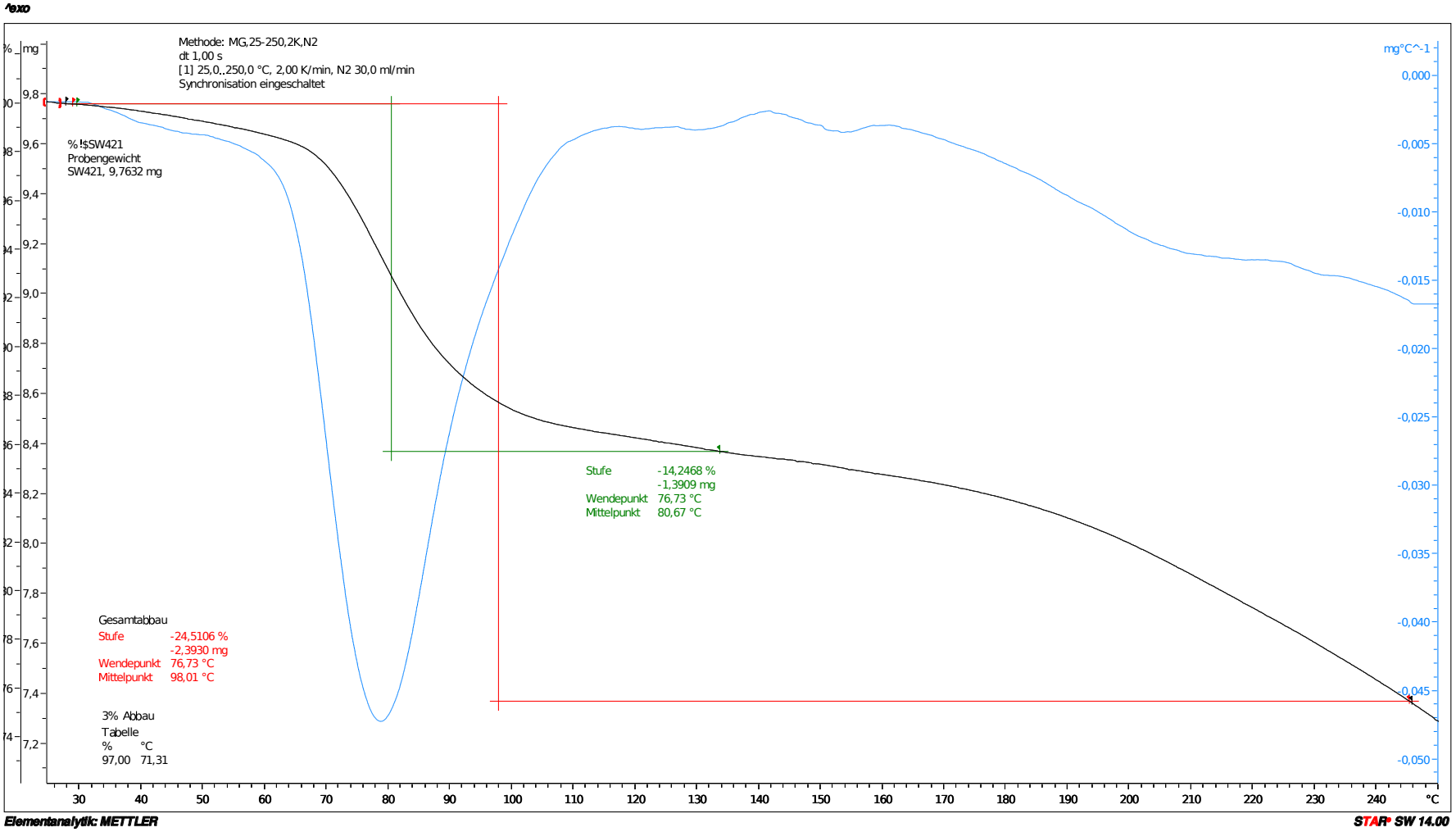
exo
Methode: MG,25-250,2K,N2
dt 1,00 s
[1] 25,0..250,0 °C, 2,00 K/min, N2 30,0 ml/min
Synchronisation eingeschaltet
%!sSW421
Probengewicht
SW421, 9,7632 mg
mg
%
mg°C^-1
Stufe -14,2468 %
-1,3909 mg
Wendepunkt 76,73 °C
Mittelpunkt 80,67 °C
Gesamtabbau
Stufe -24,5106 %
-2,3930 mg
Wendepunkt 76,73 °C
Mittelpunkt 98,01 °C
3% Abbau
Tabelle
% °C
97,00 71,31
°C
Elementaranalytik: METTLER
STAR° SW 14.00

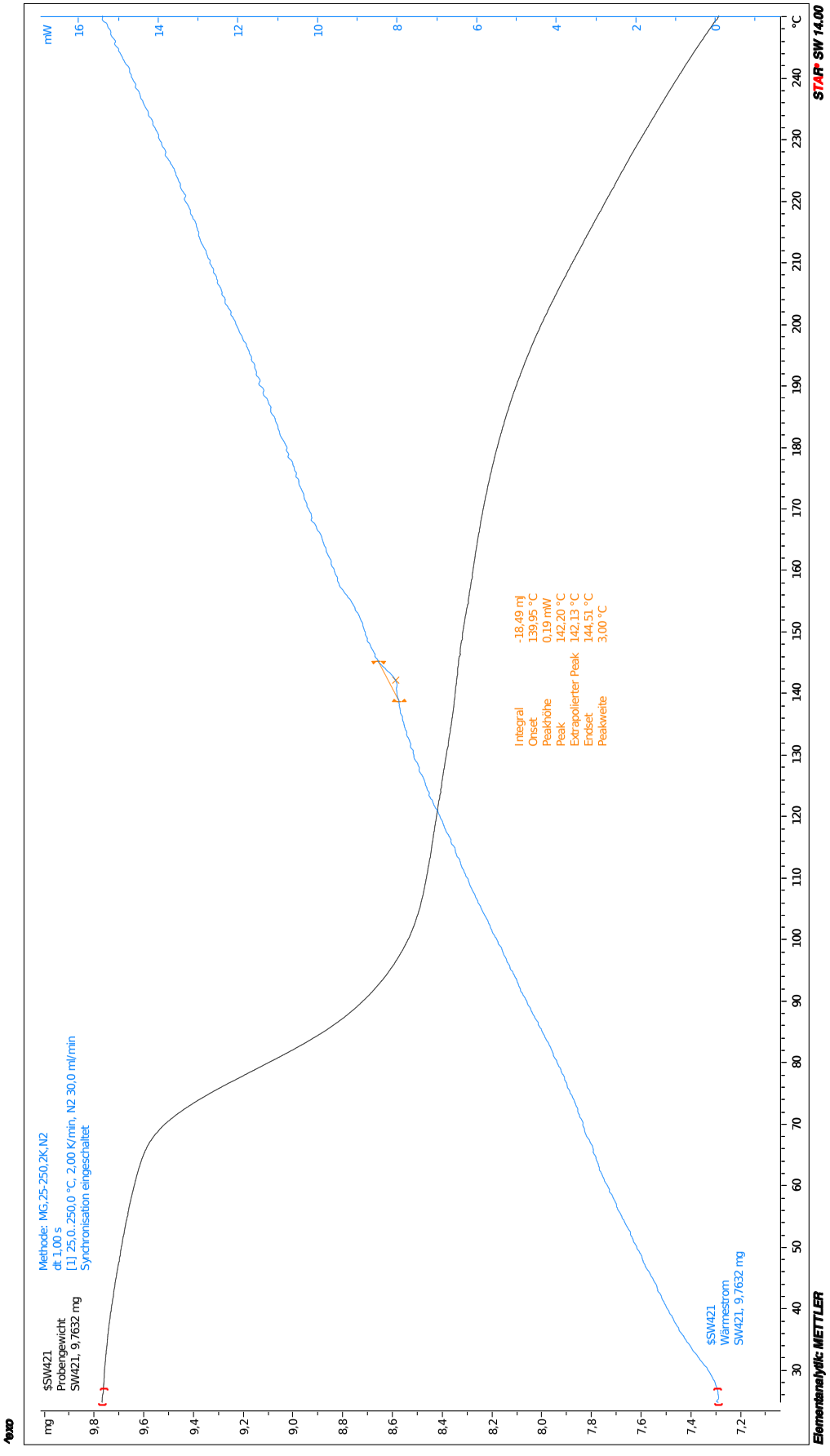
$SW421
Probengewicht
SW421, 9,7632 mg
Methode: MG,25-250,2K,N2
dt 1,00 s
[1] 25,0..250,0 °C, 2,00 K/min, N2 30,0 ml/min
Synchronisation eingeschaltet
Integral -18,49 mJ
Onset 139,95 °C
Peakhöhe 0,19 mW
Peak 142,20 °C
Extrapolierter Peak 142,13 °C
Endset 144,51 °C
Peakweite 3,00 °C
$SW421
Warmestrom
SW421, 9,7632 mg
mg
mW
°C
Elementanalytik METTLER
STAR SW 14.00

8.2.5 Palladium and gold complexes of phosphazene bases

8.2.5.1 Synthesis of [Pd(dma)P_1P-(tBu)$_2$-(η^3–cinn)Cl] (35a)

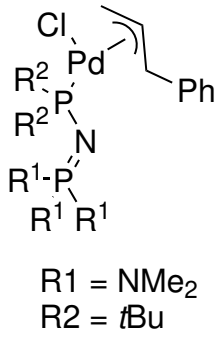

(dma)P_1P-(tBu)$_2$ (**5a**) (0.32 g, 1.00 mmol, 1.0 eq.) was dissolved in Et_2O (20 mL), [Pd(cinn)Cl]$_2$ (0.26 g, 0.50 mmol, 0.50 eq.) was added, and the mixture was stirred for 1 h at RT. Afterward, the solvent was removed *in vacuo* and the residue was washed with pentane and dried in high vacuum. [Pd(dma)P_1P-(tBu)$_2$-(η^3–cinn)Cl] (**35a**) (0.57 g, 0.98 mmol, 98%) was obtained as a yellow solid.

^{1}H-NMR (300 MHz, $CDCl_2$): δ (ppm) = 9.15–8.78 (m, 5H, ArH), 7.60–7.39 (m, 1H), 6.80–6.60 (m, 1H), 4.86–4.67 (m, 2H), 4.32 (d, ^2J(P,H) = 9.5 Hz, 18H, NCH$_3$), 2.96 (d, ^2J(P,H) = 14.0 Hz, 18H, CCH$_3$).
^{13}C{^{1}H}-NMR (75 MHz, $CDCl_2$): δ (ppm) = 139.8 (d, J(P,C) = 7.2 Hz), 130.2 (d, J(P,C) = 1.9 Hz), 129.2 (d, J(P,C) = 3.6 Hz), 128.7 (s), 112.4 (d, J(P,C) = 5.9 Hz), 102.5 (d, J(P,C) = 28.2 Hz), 50.7 (d, J(P,C) = 4.7 Hz), 42.1 (d, J(P,C) = 2.7 Hz), 41.8 (d, J(P,C) = 2.8 Hz), 39.6 (d, J(P,C) = 4.5 Hz), 30.8 (d, J(P,C) = 7.3 Hz).
^{31}P{^{1}H}-NMR (121 MHz, C_6D_6): δ (ppm) = 96.6 (d, ^2J(P,P) = 6.5 Hz, P(III)), 13.4 (s, P(V)).

8.2.5.2 Synthesis of [Pd(cy)P_1P-(tBu)$_2$-(η^3–cinn)Cl] (35c)

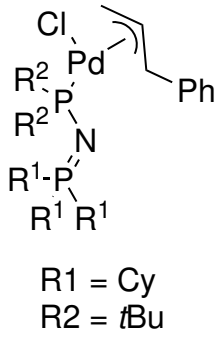

(cy)P_1P-(tBu)$_2$ (**5c**) (100 mg, 0.23 mmol, 1.0 eq.) was dissolved in Et_2O (20 mL), [Pd(cinn)Cl]$_2$ (58.9 mg, 0.11 mmol, 0.50 eq.) was added, and the mixture was stirred for 1 h at RT. Afterward, the solvent was removed *in vacuo* and the residue was washed with pentane and dried in high vacuum. [Pd(cy)P_1P-(tBu)$_2$-(η^3–cinn)Cl] (**35c**) (150 mg, 0.21 mmol, 94%) was obtained as a yellow solid.

^{1}H-NMR (300 MHz, C_6D_6): δ (ppm) = 7.51 (d, ^2J(H,H) = 7.7 Hz, 1H, ArH), 7.26–6.96 (m, 4H, ArH), 5.61–5.46 (m, 1H), 5.15–5.02 (m, 1H), 2.51 (q, ^2J(P,H) = 13.1 Hz, 2H), 2.26–2.06 (m, 4H), 1.72–1.51 (m, 8H), 1.40 (d, ^2J(P,H) = 12.1 Hz, 18H, CCH$_3$), 1.26–1.04 (m, 8H).
^{13}C{^{1}H}-NMR (75 MHz, C_6D_6): δ (ppm) = 137.7 (d, J(P,C) = 6.8 Hz), 128.9 (s), 128.2 (s), 126.8 (d, J(P,C) = 2.6 Hz), 125.3 (s), 107.4 (d, J(P,C) = 5.5 Hz), 100.9 (d, J(P,C) = 28.6 Hz), 44.6 (d, J(P,C) = 3.3 Hz), 39.9 (dd, J(P,C) = 2.6 Hz, J(P,C) = 20.9 Hz), 39.0 (s), 38.2 (s), 29.2 (d, J(P,C) = 7.5 Hz), 28.0 (d, J(P,C) = 2.4 Hz), 26.8 (d, J(P,C) = 12.4 Hz), 26.3 (s).
^{31}P{^{1}H}-NMR (121 MHz, C_6D_6): δ (ppm) = 102.2 (d, ^2J(P,P) = 7.9 Hz, P(III)), 27.1 (d, ^2J(P,P) = 8.2 Hz, P(V)).

8.2.5.3 Synthesis of [Pd(*t*Bu)P$_1$P-(*t*Bu)$_2$-(η^3–cinn)Cl] (35d)

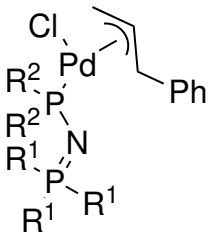

R1 = R2 = *t*Bu

(*t*Bu)P$_1$P-(*t*Bu)$_2$ (**5d**) (100 mg, 0.28 mmol, 1.0 eq.) was dissolved in Et_2O (20 mL), [Pd(cinn)Cl]$_2$ (71.7 mg, 0.14 mmol, 0.50 eq.) was added, and the mixture was stirred for 1 h at RT. Afterward, the solvent was removed *in vacuo* and the residue was washed with pentane and dried in high vacuum. [Pd(*t*Bu)P$_1$P-(*t*Bu)$_2$-(η^3–cinn)Cl] (**35d**) (160 mg, 0.26 mmol, 93%) was obtained as a yellow solid.

^{1}H-NMR (300 MHz, C_6D_6): δ (ppm) = 7.51 (d, ^2J(H,H) = 7.3 Hz, 1H, ArH), 7.26–7.10 (m, 5H, ArH), 5.59–5.45 (m, 1H), 5.14–5.02 (m, 1H, ArH), 3.11 (d, J(P,H) = 9.2 Hz, 2H), 1.50 (d, ^2J(P,H) = 13.6 Hz, 18H, CCH$_3$), 1.30 (d, ^2J(P,H) = 13.4 Hz, 27H, CCH$_3$).
^{13}C{^{1}H}-NMR (75 MHz, C_6D_6): δ (ppm) = 107.5 (d, J(P,C) = 5.8 Hz), 100.6 (s), 100.2 (s), 49.9 (s), 42.5 (d, J(P,C) = 15.7 Hz), 41.6 (dd, J(P,C) = 2.9 Hz, J(P,C) = 50.3 Hz), 31.4 (s), 31.0 (d, J(P,C) = 5.4 Hz), 30.9 (s), 30.7 (d, J(P,C) = 7.8 Hz), 29.8 (s).
Several signals overlap with the solvent Signal.
^{31}P{^{1}H}-NMR (121 MHz, C_6D_6): δ (ppm) = 105.1 (d, ^2J(P,P) = 27.8 Hz, P(III)), 44.9 (d, ^2J(P,P) = 27.8 Hz, P(V)).

8.2.5.4 Synthesis of [(dmaP$_1$P)$_2$Pd$_2$Cl$_4$] (36)

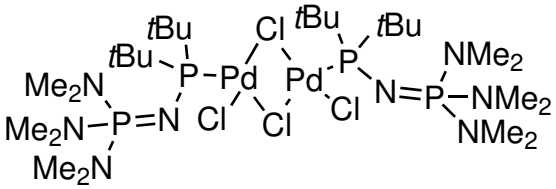

[Pd(dma)P_1P-(tBu)$_2$-(η^3−cinn)Cl] (**35a**) (200 mg, 0.34 mmol, 1.0 eq.) was dissolved in toluene (20 mL) and HCl in dioxane (excess), stirred for 1h and pentane was added to aid precipitation of an orange solid. Filtration and washing with pentane (3 x 20 mL) yielded (dmaP_1P)$_2$Pd$_2$Cl$_4$ (**36**) (0.340 mg, 0.34 mmol, 99%) as an orange solid.

^{1}H-NMR (300 MHz, CD_2Cl_2): δ (ppm) = 2.85 (d, ^2J(P,H) = 10.2 Hz, NC$\underline{H}_3$), 18H), 1.45 (d, ^2J(P,H) = 16.9 Hz, CC$\underline{H}_3$), 18H).
^{13}C{^{1}H}-NMR (75 MHz, CD_2Cl_2): δ (ppm) = 37.7 (d, ^2J(P,C) = 4.0 Hz), 26.0 (s).
^{31}P{^{1}H}-NMR (121 MHz, C_6D_6): δ (ppm) = 45.8 (d, ^2J(P,P) = 4.1 Hz, P(III)), 31.9 (s, P(V)).

8.2.5.5 Synthesis of [(dma)P_1P-(tBu)$_2$-AuCl] (32a)

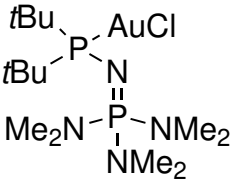

Synthetic route a)

(dma)P_1P-(tBu)$_2$ (**5a**) (200 mg, 0.62 mmol, 1.0 eq.) was dissolved in THF (10 mL) and PPh_3AuCl (307 mg, 0.62 mmol, 1.0 eq.) was added. The mixture was stirred overnight under exclusion of light for 1 h. Afterward, the solvent was removed *in vacuo*, pentane (10 mL) added and filtered hot. The solvent was removed *in vacuo* to yield [(dma)P_1P-(tBu)$_2$-AuCl] (**32a**) as a colorless solid. Impurities of PPh_3 are present in this route.

Synthetic route b)

(dma)P_1P-(tBu)$_2$ (**5a**) (100 mg, 0.31 mmol, 1.0 eq.) was dissolved in toluene (10 mL) and SMe_2AuCl (91.4 mg, 0.31 mmol, 1.0 eq.) was added. The mixture was stirred overnight under exclusion of light. Afterward, the solvent was removed *in vacuo*, pentane (10 mL) added and filtered hot. The solution was cooled to −30 °C and the resulting crystals were filtered off to yield [(dma)P_1P-(tBu)$_2$-AuCl] (**32a**) as a colorless solid.

^{1}H-NMR (300 MHz, $CDCl_3$): δ (ppm) = 2.78 (d, ^2J(P,H) = 9.9 Hz, 18H, NC$\underline{H}_3$), 1.28 (d, ^2J(P,H) = 15.5 Hz, 18H, CC$\underline{H}_3$).
^{13}C{^{1}H}-NMR (75 MHz, $CDCl_3$): δ (ppm) = 38.5 (d, ^2J(P,C) = 3.4 Hz), 28.4 (d, ^2J(P,C) = 6.7 Hz).
^{31}P{^{1}H}-NMR (121 MHz, $CDCl_3$): δ (ppm) = 86.1 (d, ^2J(P,P) = 21.6 Hz, P(III)), 27.3 (d, ^2J(P,P) = 21.3 Hz, P(V)).

8.2.5.6 Synthesis of [(tBu)P_1P-(tBu)$_2$-AuCl] (32d)

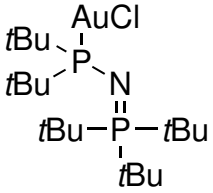

(*t*Bu)P_1P-(*t*Bu)$_2$ (**5d**) (110 mg, 0.30 mmol, 1.0 eq.) was dissolved in THF (10 mL) and SMe_2AuCl (89.6 mg, 0.30 mmol, 1.0 eq.) was added. The mixture was stirred overnight under exclusion of light. Afterward, the solvent was removed *in vacuo*, pentane (10 mL) added and filtered hot. The solution was cooled to −30 °C and the resulting crystals were filtered off to yield [(*t*Bu)P_1P-(*t*Bu)$_2$-AuCl] (**32d**) as a colorless solid. Significant amounts of side products were formed in this synthesis, only trace amount of product could be detected.

^{31}P{^{1}H}-NMR (121 MHz, C_6D_6): δ (ppm) = 104.1 (s, P(III)), 47.6 (d, ^2J(P,P) = 8.2 Hz, P(V)).

8.2.5.7 Synthesis of [(dma)P_2P-*t*Bu-AuCl] (33a)

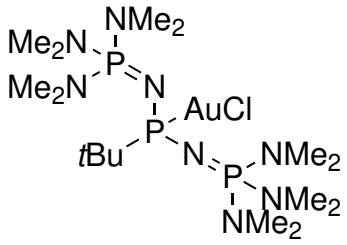

(dma)P_2P-(*t*Bu) (**6a**) (107 mg, 0.24 mmol, 1.0 eq.) was dissolved in toluene (10 mL) and PPh_3AuCl (120 mg, 0.24 mmol, 1.0 eq.) was added. The mixture was stirred overnight under exclusion of light. Afterward, the solvent was removed *in vacuo*, pentane (10 mL) added and filtered hot and transferred to a −30 °C freezer to crystallize. The resulting crystals were filtered off and dried *in vacuo* to yield [(dma)P_2P-*t*Bu-AuCl] (**33a**) as a colorless solid. Impurities of PPh_3 and other side products are present in this route.

^{1}H-NMR (300 MHz, C_6D_6): δ (ppm) = 2.60 (d, ^3J(P;H) = 9.9 Hz, 27H, NC$\underline{H}_3$), 1.56 (d, ^3J(P,H) = 14.9 Hz, 9H, CC$\underline{H}_3$).
^{13}C{^{1}H}-NMR (75 MHz, C_6D_6): δ (ppm) = 37.2 (d, J(P,C) = 3.8 Hz), 37.1 (dd, J(P,C) = 4.0 Hz, J(P,C) = 33.3 Hz), 26.7 (s).
^{31}P{^{1}H}-NMR (121 MHz, C_6D_6): δ (ppm) = 54.8 (t, ^2J(P,P) = 34.2 Hz, P(III)), 19.6 (d, ^2J(P,P) = 34.1 Hz, P(V)).

8.2.6 Cross coupling products

8.2.6.1 General procedure for the Suzuki Miyaura cross couplings with phosphazenyl phosphine ligands

Screening Procedure:

Phenylboronic acid (1.5 mmol, 1.5 eq), base (2.0 mmol, 2.0 eq), 1-chloro-4-methylbenzene (1.0 mmol, 1.0 eq.) and internal standard 1,3,5-trimethoxybenzene (10 mol%) were dissolved in toluene (16 mL). Ligand (4 mol%) and palladium cinnamylchloride dimer (0.5 to 2 mol%) were dissolved in toluene (4 mL) and stirred for 15 min at RT. The catalyst mixture was then added to the reaction mixture and the resulting suspension was stirred at 80 °C for 16 h. Aliquots were taken from the reaction mixture and transferred to mass vials. Water (0.2 mL) was added to quench the reaction. The organic phase was extracted with EtOAc (3x 1.0 mL)

and filtered through a cotton filled pipette. The solvent was removed *in vacuo* and dissolved in CD_2Cl_2. The conversion was measured through comparison of the integrals of the methyl group of the product and the -OCH_3 groups of the internal standard.

Isolation Procedure:

NaOMe (2.00 mmol, 108 mg, 2.0 eq.) was added to a SCHLENK flask in a glovebox. In a separate flask **5a** (12.9 mg, 4 mol%) and palladium cinnamyl chloride dimer (10.4 mg, 2 mol%) was added. The flasks were taken out of the glovebox and toluene was added (16 mL and 4 mL). To the base, boronic acid (1.50 mmol, 1.50 eq) and aryl chloride (1.0 mmol, 1.0 eq.) was added and stirred until dissolved. The catalyst mixture was added to the reaction mixture and heated to 80 °C for 16 h. Afterward, water (20 mL) was added, and the mixture extracted with EtOAc (3x 50 mL). In the case of insufficient phase separation, brine (20 mL) was added. The organic phases were combined, dried over $MgSO_4$ and the solvent was removed. The crude product was adsorbed onto silica and purified by flash chromatography (Hexane:EtOAc) to yield the final products.

8.2.6.2 Suzuki-Miyaura products

2,6-Dimethyl-1,1'-biphenyl (Entry 1)

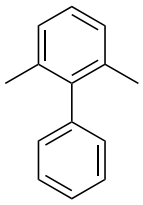

^{1}H-NMR (300 MHz, CD_2Cl_2): δ (ppm) = 7.52–7.45 (m, 2H, Ar<u>H</u>), 7.43–7.35 (m, 1H, Ar<u>H</u>), 7.24–7.13 (m, 5H, Ar<u>H</u>), 2.08 (s, 6H, C<u>H</u>$_3$).
^{13}C{^{1}H}-NMR (75 MHz, C_6D_6): δ (ppm) = 142.4 (s), 141.6 (s), 136.4 (s), 129.5 (s), 128.9 (s), 127.7 (s), 127.4 (s), 127.1 (s), 21.0 (s).
Eluent: 85:15 Hexane/EtOAc

The data matches the literature values.[266]

4'-Methoxy-2,6-dimethyl-1,1'-biphenyl (Entry 2)

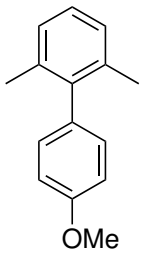

^{1}H-NMR (300 MHz, CD_2Cl_2): δ (ppm) = 7.16–7.02 (m, 5H, Ar<u>H</u>), 7.02–6.93 (m, 2H, Ar<u>H</u>), 3.85 (s, 3H, OCH3), 2.03 (s, 6H, CH3).

^{13}C{^{1}H}-NMR (75 MHz, CD_2Cl_2): δ (ppm) = 158.9 (s), 142.0 (s), 136.8 (s), 133.7 (s), 130.5 (s), 128.9 (s), 127.6 (s), 127.2 (s), 114.2 (s), 55.6 (s), 21.0 (s).
Eluent: 85:15 Hexane/EtOAc
The data matches the literature values.[267]

[1,1'-Biphenyl]-4-carbonitrile (Entry 3)

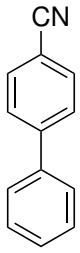

^{1}H-NMR (300 MHz, CD_2Cl_2): δ (ppm) = 7.77–7.69 (m, 4H, Ar<u>H</u>), 7.65–7.59 (m, 2H, Ar<u>H</u>), 7.53–7.41 (m, 3H, Ar<u>H</u>).
^{13}C{^{1}H}-NMR (75 MHz, CD_2Cl_2): δ (ppm) = 145.9 (s), 139.6 (s), 130.0 (s), 129.5 (s), 129.2 (s), 129.0 (s), 129.0 (s), 128.1 (s), 127.6 (s), 119.3 (s), 111.4 (s).
Eluent: 85:15 Hexane/EtOAc
The data matches the literature values.[268]

4'-Methoxy-[1,1'-biphenyl]-4-carbonitrile (Entry 4)

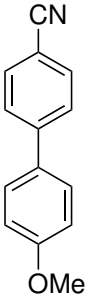

^{1}H-NMR (300 MHz, CD_2Cl_2): δ (ppm) = 7.75–7.62 (br m, 4H, Ar<u>H</u>), 7.57 (d, J(H,H) = 7.9 Hz, 2H, Ar<u>H</u>), 7.01 (d, J(H,H) = 7.9 Hz, 2H, Ar<u>H</u>), 3.85 (s, 3H, OC<u>H</u>$_3$).
^{13}C{^{1}H}-NMR (75 MHz, CD_2Cl_2): δ (ppm) = 160.7 (s), 145.5 (s), 133.0 (s), 131.8 (s), 128.7 (s), 127.4 (s), 119.4 (s), 114.9 (s), 110.5 (s), 55.8 (s).
Eluent: 85:15 Hexane/EtOAc
The data matches the literature values.[269]

4-Methoxy-4'-methyl-1,1'-biphenyl (Entry 5)

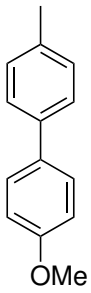

^{1}H-NMR (300 MHz, CD_2Cl_2): δ (ppm) = 7.54–7.49 (m, 2H, Ar<u>H</u>), 7.45 (d, J(H,H) = 8.1 Hz, 2H, Ar<u>H</u>), 7.23 (d, J(H,H) = 7.9 Hz, 2H, Ar<u>H</u>), 6.99–6.93 (m, 2H, Ar<u>H</u>), 3.83 (s, 3H, OC<u>H</u>$_3$), 2.37 (s, 3H, C<u>H</u>$_3$).
^{13}C{^{1}H}-NMR (75 MHz, CD_2Cl_2): δ (ppm) = 159.5 (s), 138.2 (s), 136.9 (s), 133.9 (s), 129.8 (s), 126.8 (s), 114.5 (s), 55.7 (s), 21.1 (s).
The data matches those from the literature.[270]

4-(Trifluoromethyl)-1,1'-biphenyl (Entry 6)

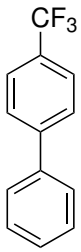

^{1}H-NMR (300 MHz, CD_2Cl_2): δ (ppm) = 7.77–7.68 (m, 4H, Ar<u>H</u>), 7.67–7.60 (m, 2H, Ar<u>H</u>), 7.53–7.40 (m, 2H, Ar<u>H</u>).
^{13}C{^{1}H}-NMR (75 MHz, CD_2Cl_2): δ (ppm) = 144.8 (d, ^{3}J(C,F) = 1.0 Hz), 139.6 (s), 128.9 (s), 128.2 (s), 127.4 (s), 127.4 (s), 127.2 (s), 126.6 (q, ^{1}J(C,F) = 3.8 Hz).
Eluent: 85:15 Hexane/EtOAc
The data matches those from the literature.[271]

4-Methoxy-4'-(trifluoromethyl)-1,1'-biphenyl (Entry 7)

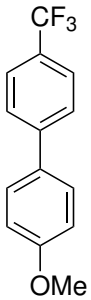

^{1}H-NMR (300 MHz, CD_2Cl_2): δ (ppm) = 7.72–7.64 (m, 4H, Ar<u>H</u>), 7.57 (d, ^{2}J(H,H) = 9.1 Hz, 2H, Ar<u>H</u>), 7.01 (d, ^{2}J(H,H) = 8.7 Hz, 2H, Ar<u>H</u>), 3.85 (s, 3H, OC<u>H</u>$_3$).

^{13}C{^{1}H}-NMR (75 MHz, CD_2Cl_2): δ (ppm) = 160.4 (s), 144.8 (d, ^{3}J(C,F) = 1.0 Hz), 132.3 (s), 128.7 (s), 127.2 (s), 126.0 (q, ^{1}J(C,F) = 3.8 Hz), 114.8 (s), 55.7 (s).
^{19}F-NMR (282 MHz, CD_2Cl_2): δ (ppm) = –62.6 (s).
Eluent: 85:15 Hexane/EtOAc
The data matches those from the literature.[272]

2,4'-Dimethoxy-1,1'-biphenyl (Entry 8)

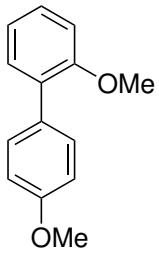

^{1}H-NMR (300 MHz, CD_2Cl_2): δ (ppm) = 7.44 (d, J(H,H) = 8.9 Hz, 2H, Ar<u>H</u>), 7.28 (d, J(H,H) = 7.4 Hz, 2H, Ar<u>H</u>), 7.03–6.90 (m, 4H, Ar<u>H</u>), 3.83 (s, 3H, OC<u>H</u>$_3$), 3.80 (s, 3H, OC<u>H</u>$_3$).
^{13}C{^{1}H}-NMR (75 MHz, CD_2Cl_2): δ (ppm) = 159.2 (s), 157.0 (s), 131.4 (s), 131.0 (s), 130.9 (s), 130.7, 128.6 (s), 121.2 (s), 113.8 (s), 111.6 (s), 55.8 (s), 55.7 (s).
Eluent: 85:15 Hexane/EtOAc
The data matches those from the literature.[273]

4-Methyl-1,1'-biphenyl (Entry 9)

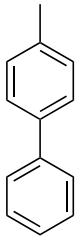

^{1}H-NMR (300 MHz, CD_2Cl_2): δ (ppm) = 7.72–7.66 (m, 2H, Ar<u>H</u>), 7.61 (d, J(H,H) = 8.6 Hz, 2H, Ar<u>H</u>), 7.56–7.49 (m, 2H, Ar<u>H</u>), 7.46–7.40 (m, 1H, Ar<u>H</u>), 7.36 (d, J(H,H) = 8.0 Hz, 2H, Ar<u>H</u>), 2.49 (s, 3H, C<u>H</u>$_3$).
^{13}C{^{1}H}-NMR (75 MHz, CD_2Cl_2): δ (ppm) = 141.0 (s), 138.1 (s), 137.2 (s), 129.4 (s), 128.7 (s), 127.0 (s), 126.8 (s), 20.8 (s).
Eluent: 100% Pentane
The data matches those from the literature.[274]

2-Methoxy-1,1'-biphenyl (Entry 10)

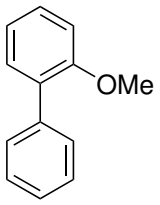

^{1}H-NMR (300 MHz, CD_2Cl_2): δ (ppm) = 7.53–7.47 (m, 2H, Ar$\underline{H}$), 7.43–7.28 (m, 5H, Ar$\underline{H}$), 7.06–6.98 (m, 2H, Ar$\underline{H}$), 3.81 (s, 3H, OC$\underline{H}_3$).
^{13}C{^{1}H}-NMR (75 MHz, CD_2Cl_2): δ (ppm) = 157.0 (s), 139.1 (s), 131.1 (s), 129.9 (s), 129.1 (s), 128.3 (s), 127.2 (s), 121.2 (s), 55.8 (s).
Eluent: 85:15 Hexane/EtOAc
The data matches those from the literature.[275]

4'-Methoxy-2,4,6-trimethyl-1,1'-biphenyl (Entry 11)

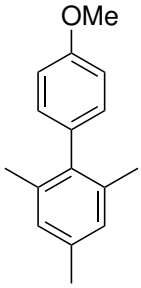

^{1}H-NMR (300 MHz, CD_2Cl_2): δ (ppm) = 7.06–7.00 (m, 2H, Ar$\underline{H}$), 6.98–6.89 (m, 4H, Ar$\underline{H}$), 3.84 (s, 3H, OC$\underline{H}_3$), 2.30 (s, 3H, p−C$\underline{H}_3$), 1.99 (s, 6H, C$\underline{H}_3$).
^{13}C{^{1}H}-NMR (75 MHz, CD_2Cl_2): δ (ppm) = 158.8 (s), 139.1 (s), 136.7 (s), 136.6 (s), 133.8 (s), 130.8 (s), 128.3 (s), 114.1 (s), 55.6 (s), 21.1 (s), 20.9 (s).
Eluent: 85:15 Hexane/EtOAc
The data matches those from the literature.[276]

1-(4'-Methoxy-[1,1'-biphenyl]-4-yl)ethan-1-one (Entry 12)

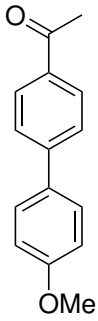

This compound was synthesized with the bromo substituted arene.

^{1}H-NMR (300 MHz, CD_2Cl_2): δ (ppm) = 8.04 (d, J(H,H) = 8.4 Hz, 2H, Ar$\underline{H}$), 7.72 (d, J(H,H) = 8.0 Hz, 2H, Ar$\underline{H}$), 7.66 (d, J(H,H) = 8.7 Hz, 2H, Ar$\underline{H}$), 7.05 (d, J(H,H) = 8.7 Hz, 2H,

Ar<u>H</u>), 3.90 (s, 3H, OC<u>H</u>$_3$), 2.65 (s, 3H, C<u>H</u>$_3$).
^{13}C{^{1}H}-NMR (75 MHz, CD_2Cl_2): δ (ppm) = 129.2 (s), 128.7 (s), 126.9 (s), 114.8 (s), 55.8 (s), 26.8 (s).
Eluent: 85:15 Hexane/EtOAc
The data matches those from the literature.[277]

2-Mesitylthiophene (Entry 13)

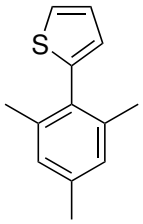

^{1}H-NMR (300 MHz, CD_2Cl_2): δ (ppm) = 7.44 (d, ^2J(H,H) = 6.1 Hz, 1H, Ar<u>H</u>), 7.17 (t, ^2J(H,H) = 4.2 Hz, 1H, Ar<u>H</u>), 6.99 (s, 2H, Ar<u>H</u>), 6.86 (d, ^2J(H,H) = 3.2 Hz, 1H, Ar<u>H</u>), 2.37 (s, 3H, p−C<u>H</u>$_3$), 2.16 (s, 6H, C<u>H</u>$_3$).
^{13}C{^{1}H}-NMR (75 MHz, CD_2Cl_2): δ (ppm) = 142.0 (s), 138.5 (s), 138.2 (s), 131.4 (s), 128.4 (s), 127.5 (s), 126.9 (s), 125.6 (s), 21.2 (s), 20.8 (s).
Eluent: 100% Hexane
The data matches those from the literature.[278]

2-Phenylthiophene (Entry 14)

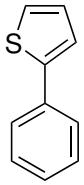

^{1}H-NMR (300 MHz, CD_2Cl_2): δ (ppm) = 7.72–7.65 (m, 2H, Ar<u>H</u>), 7.50–7.31 (m, 5H, Ar<u>H</u>), 7.18–7.12 (m, 1H, Ar<u>H</u>).
^{13}C{^{1}H}-NMR (75 MHz, CD_2Cl_2): δ (ppm) = 144.7 (s), 134.8 (s), 129.3 (s), 128.5 (s), 127.9 (s), 126.3 (s), 125.3 (s), 123.6 (s).
Eluent: 100% Hexane
The data matches those from the literature.[277]

2-(4-Methoxyphenyl)thiophene (Entry 15)

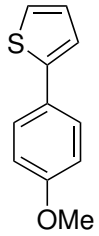

^{1}H-NMR (300 MHz, CD_2Cl_2): δ (ppm) = 7.58–7.52 (m, 2H, ArH), 7.25–7.20 (m, 2H, ArH), 7.08–7.04 (m, 1H, ArH), 6.95–6.90 (m, 2H, ArH), 3.82 (s, 3H, OCH_3).
^{13}C{^{1}H}-NMR (75 MHz, CD_2Cl_2): δ (ppm) = 159.8 (s), 144.6 (s), 128.4 (s), 127.6 (s), 127.5 (s), 124.2 (s), 122.5 (s), 114.7 (s), 55.7 (s).
Eluent: 100% Hexane in a gradient to 80:20 Hexane/EtOAc
The data matches those from the literature.[277]

2-Methoxy-6-(4-methoxyphenyl)pyridine (Entry 16)

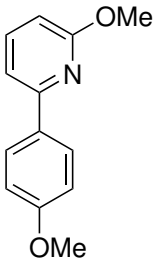

^{1}H-NMR (300 MHz, CD_2Cl_2): δ (ppm) = 8.01 (d, ^2J(H,H) = 9.0 Hz, 2H, ArH), 7.61 (dt, ^2J(H,H) = 7.9 Hz, 1H, ArH), 7.29 (d, ^2J(H,H) = 7.6 Hz, 1H, ArH), 6.98 (d, ^2J(H,H) = 8.8 Hz, 2H, ArH), 6.62 (d, ^2J(H,H) = 7.8 Hz, 1H, ArH), 4.00 (s, 3H, OCH_3), 3.85 (s, 3H, OCH_3).
^{13}C{^{1}H}-NMR (75 MHz, CD_2Cl_2): δ (ppm) = 164.2 (s), 160.9 (s), 154.8 (s), 139.6 (s), 132.1 (s), 128.3 (s), 114.3 (s), 112.2 (s), 108.7 (s), 55.8 (s), 53.4 (s).
Eluent: 85:15 Hexane/EtOAc
The data matches those from the literature.[279]

3-Methyl-5-phenylbenzo[b]thiophene (Entry 17)

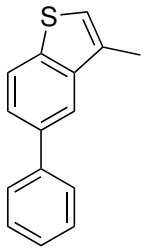

^{1}H-NMR (300 MHz, CD_2Cl_2): δ (ppm) = 7.98–7.89 (m, 2H, ArH), 7.74–7.67 (m, 2H, ArH), 7.61 (dd, J(H,H) = 8.4 Hz, J(H,H) = 1.8 Hz, 1H, ArH), 7.53–7.44 (m, 2H, ArH), 7.41–7.33 (m, 1H, ArH), 7.15 (d, J(H,H) = 1.0 Hz, 1H, ArH), 2.49 (d, J(H,H) = 1.1 Hz, 3H, CH_3).
^{13}C{^{1}H}-NMR (75 MHz, CD_2Cl_2): δ (ppm) = 141.9 (s), 140.7 (s), 139.8 (s), 137.8 (s), 132.9 (s), 129.2 (s), 127.8 (s), 127.6 (s), 124.0 (s), 123.4 (s), 122.7 (s), 120.5 (s), 14.1 (s).

Eluent: 100% Hexane with a gradient to 80:20 Hexane/EtOAc
The data matches those from the literature. (Literature only shows the spectra for S-oxide)[280]

5-(*Tert*-butyl)-[1,1'-biphenyl]-2-amine (Entry 18)

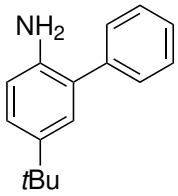

This compound was synthesized with the bromo substituted arene.

^{1}H-NMR (300 MHz, CD_2Cl_2): δ (ppm) = 7.50–7.41 (m, 4H, ArH), 7.39–7.30 (m, 1H, ArH), 7.20–7.10 (m, 2H, ArH), 3.68 (br. s, 2H, NH_2), 1.29 (s, 9H, CH_3).
^{13}C{^{1}H}-NMR (75 MHz, CD_2Cl_2): δ (ppm) = 141.7 (s), 141.6 (s), 140.6 (s), 129.5 (s), 129.1 (s), 127.7 (s), 127.4 (s), 125.8 (s), 115.7 (s), 34.2 (s), 31.7 (s).
Eluent: 85:15 Hexane/EtOAc in a gradient to 100% EtOAc.
The data matches those from the literature.[281]

8.2.6.3 General procedure for the Buchwald-Hartwig amination with phosphazenyl phosphine ligands

Screening procedure:

Base (2.0 eq, 2 mmol) was added to a Schlenk flask in a Glovebox. In a second flask, palladium precursor (0.25-2 mol%) and ligand (0.5-4 mol%) were added, and the flasks were removed from the Glovebox. Solvent (16 mL and 4 mL) was added and stirred. Haloarene (1.0 eq, 1.0 mmol), amine (1.5 eq. 1.5 mmol) and internal standard (10mol%) were added to the flask containing the base. The catalyst mixture was then added to the reaction mixture and stirred at 80 °C for the specified time. Aliquots were taken from the reaction mixture and transferred to mass vials. Water (0.2 mL) was added to quench the reaction. The organic phase was extracted with EtOAc (3x 1.0 mL) and filtered through a cotton filled pipette. The solvent was removed *in vacuo* and dissolved in CD_2Cl_2. The conversion was measured through comparison of the integrals of the methyl group of the product and the aromatic protons of the internal standard.

Isolation procedure:

KO*t*Bu (2.0 mmol, 108.1 mg, 2.0 eq.) was added to a Schlenk flask in a glovebox. In a second flask, ligand (50 μmol) and palladium cinnamyl chloride dimer (25 μmol, 13.0 mg) were added and dissolved in toluene (10 mL) in order to create a stock solution (5 µmol/mL). The flasks were taken out of the glovebox and toluene (19 mL) was added to the flask containing the base. To the base, amine (1.5 mmol, 1.5 eq) and aryl bromide (1.0 mmol, 1.0 eq.) was added and stirred until dissolved. To this mixture, 1 mL (5 μmol) of catalyst stock solution was added and heated to 80 °C for 1 h. Afterward, water (20 mL) was added, and the mixture extracted with EtOAc (3x 50 mL). In the case of insufficient phase separation, brine (20 mL) was added. The organic phases were combined, dried over $MgSO_4$ and the solvent was

removed. The crude product was adsorbed onto silica and purified by flash chromatography (Hexane:EtOAc) to yield the final products.

8.2.6.4 Buchwald-Hartwig amination products

4-Methyl-*N*-phenylaniline (Entry 1)

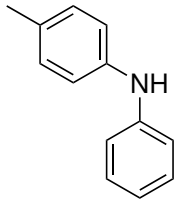

^{1}H-NMR (300 MHz, CD_2Cl_2): δ (ppm) = 7.24 (d, J(H,H) = 7.8 Hz, 2H, ArH), 7.10 (d, J(H,H) = 8.2 Hz, 2H, ArH), 7.06–6.96 (m, 4H, ArH), 6.87 (t, J(H,H) = 7.3 Hz, 1H, ArH), 5.70 (br. s, 1H, NH), 2.30 (s, 3H, CH_3).
^{13}C{^{1}H}-NMR (75 MHz, CD_2Cl_2): δ (ppm) = 144.5 (s), 140.8 (s), 131.3 (s), 130.2 (s), 129.7 (s), 120.6 (s), 119.0 (s), 117.1 (s), 20.8 (s).
Eluent: Hexane/EtOAc 9:1
The data matches those from the literature.[282]

4-Methoxy-*N*-phenylaniline (Entry 2)

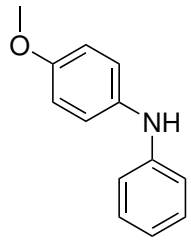

^{1}H-NMR (300 MHz, CD_2Cl_2): δ (ppm) = 7.24–7.16 (m, 2H, ArH), 7.11–7.04 (m, 2H, ArH), 6.94–6.78 (m, 5H, ArH), 5.59 (br. s, 1H, NH), 3.79 (s, 3H, OCH_3).
^{13}C{^{1}H}-NMR (75 MHz, CD_2Cl_2): δ (ppm) = 155.8 (s), 145.7 (s), 136.2 (s), 129.6 (s), 122.4 (s), 119.9 (s), 115.9 (s), 115.0 (s), 55.9 (s).
Eluent: Hexane/EtOAc 9:1
The data matches those from the literature.[282]

4-(Phenylamino)benzonitrile (Entry 3)

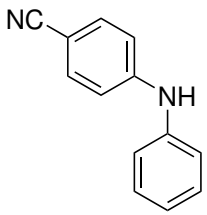

^{1}H-NMR (300 MHz, CD_2Cl_2): δ (ppm) = 7.52–7.45 (m, 2H, ArH), 7.40–7.31 (m, 2H, ArH), 7.22–7.15 (m, 2H, ArH), 7.15–7.07 (m, 1H, ArH), 7.03–6.97 (m, 2H, ArH), 6.22 (br. s, 1H, NH).

^{13}C{^{1}H}-NMR (75 MHz, CD_2Cl_2): δ (ppm) = 148.5 (s), 140.6 (s), 134.1 (s), 132.0 (s), 130.0 (s), 124.2 (s), 121.5 (s), 120.1 (s), 115.3 (s), 101.9 (s).
Eluent: Hexane/EtOAc 9:1 with a gradient to Hexane/EtOAc 1:1

The data matches those from the literature.[283]

2,4,6-Trimethyl-*N*-phenylaniline (Entry 4)

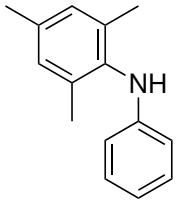

^{1}H-NMR (300 MHz, CD_2Cl_2): δ (ppm) = 7.13 (t, J(H,H) = 7.8 Hz, 2H, Ar$\underline{H}$), 6.96 (s, 2H, Ar$\underline{H}$), 6.92 (s, 2H, MesBr), 6.71 (t, J(H,H) = 7.3 Hz, 1H, Ar$\underline{H}$), 6.47 (d, J(H,H) = 7.7 Hz, 2H, Ar$\underline{H}$), 5.18 (br. s, 1H, N$\underline{H}$), 2.38 (s, 6H, MesBr), 2.31 (s, 3H, p–C$\underline{H}_3$), 2.25 (s, 3H, MesBr), 2.17 (s, 6H, C$\underline{H}_3$).
^{13}C{^{1}H}-NMR (75 MHz, CD_2Cl_2): δ (ppm) = 147.3 (s), 138.3 (s), 136.9 (s), 136.3 (s), 136.0 (s), 135.9 (s), 129.58 (s), 129.55 (s), 129.5 (s), 118.1 (s), 113.5 (s), 23.9 (s), 21.1 (s, MesBr), 20.8 (s, MesBr), 18.4 (s).
Eluent: Hexane/EtOAc 9:1
The sample contains some impurities from MesBr, these are mentioned in the data above.
The data matches those from the literature.[284]

2,4,6-Trimethyl-*N*-(*p*-tolyl)aniline (Entry 5)

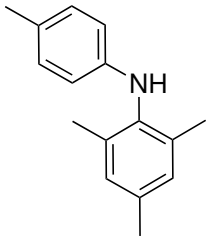

^{1}H-NMR (300 MHz, CD_2Cl_2): δ (ppm) = 6.96–6.90 (m, 4H, Ar$\underline{H}$), 6.38 (d, J(H,H) = 7.1 Hz, 2H, Ar$\underline{H}$), 5.08 (br. s, 1H, N$\underline{H}$), 2.28 (s, 3H, C$\underline{H}_3$), 2.21 (s, 3H, C$\underline{H}_3$), 2.14 (s, 6H, C$\underline{H}_3$).
^{13}C{^{1}H}-NMR (75 MHz, CD_2Cl_2): δ (ppm) = 144.8 (s), 136.5 (s), 136.0 (s), 135.5 (s), 130.0 (s), 129.5 (s), 127.4 (s), 113.7 (s), 21.0 (s), 20.5 (s), 18.3 (s).
Eluent: Hexane/EtOAc 8:2
The data matches those from the literature.[285]

4-Methoxy-*N*-(*p*-tolyl)aniline (Entry 6)

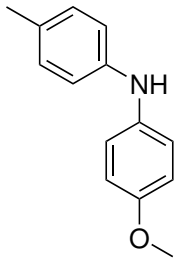

^{1}H-NMR (300 MHz, CD_2Cl_2): δ (ppm) = 7.08–6.98 (m, 4H, Ar<u>H</u>), 6.89–6.80 (m, 4H, Ar<u>H</u>), 5.48 (br. s, 1H, N<u>H</u>), 3.77 (s, 3H, OC<u>H</u>$_3$), 2.27 (s, 3H, C<u>H</u>$_3$).
^{13}C{^{1}H}-NMR (75 MHz, CD_2Cl_2): δ (ppm) = 155.2 (s), 142.9 (s), 137.2 (s), 130.1 (s), 129.7 (s), 121.2 (s), 116.8 (s), 115.0 (s), 55.9 (s), 20.6 (s).
Eluent: Hexane/EtOAc 8:2
The data matches those from the literature.[286]

Bis(4-methoxyphenyl)amine (Entry 7)

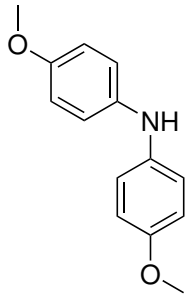

^{1}H-NMR (300 MHz, CD_2Cl_2): δ (ppm) = 6.96–6.89 (m, 4H, Ar<u>H</u>), 6.84–6.78 (m, 4H, Ar<u>H</u>), 5.36 (br. s, 1H, N<u>H</u>), 3.76 (s, 6H, OC<u>H</u>$_3$).
^{13}C{^{1}H}-NMR (75 MHz, CD_2Cl_2): δ (ppm) = 154.7 (s), 138.4 (s), 125.2 (s), 119.7 (s), 115.0 (s), 114.9 (s), 55.9 (s).
Eluent: Hexane/EtOAc 8:2
The data matches those from the literature.[287]

4-((4-Methoxyphenyl)amino)benzonitrile (Entry 8)

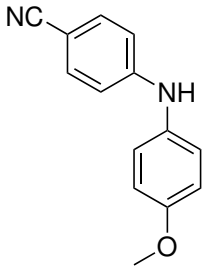

^{1}H-NMR (300 MHz, CD_2Cl_2): δ (ppm) = 7.47–7.40 (m, 2H, Ar<u>H</u>), 7.16–7.10 (m, 2H, Ar<u>H</u>), 6.95–6.89 (m, 2H, Ar<u>H</u>), 6.85–6.79 (m, 2H, Ar<u>H</u>), 6.03 (br. s, 1H, N<u>H</u>), 3.80 (s, 3H, OC<u>H</u>$_3$).

^{13}C{^{1}H}-NMR (75 MHz, CD_2Cl_2): δ (ppm) = 157.5 (s), 150.1 (s), 134.1 (s), 133.1 (s), 130.1 (s), 125.3 (s), 120.3 (s), 116.8 (s), 115.2 (s), 115.0 (s), 114.2 (s), 100.7 (s), 55.9 (s).
Eluent: Hexane/EtOAc 8:2
The data matches those from the literature.[288]

***N*-(4-Methoxyphenyl)-2,4,6-trimethylaniline (Entry 9)**

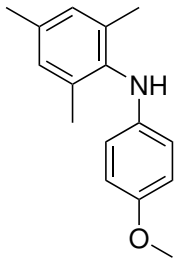

^{1}H-NMR (300 MHz, CD_2Cl_2): δ (ppm) = 6.93 (s, 2H, Ar<u>H</u>), 6.72 (d, J(H,H) = 8.9 Hz, 2H, Ar<u>H</u>), 6.44 (d, J(H,H) = 9.1 Hz, 2H, Ar<u>H</u>), 5.00 (br. s, 1H, N<u>H</u>), 3.71 (s, 3H, OC<u>H</u>$_3$), 2.29 (s, 3H, p–C<u>H</u>$_3$), 2.17 (s, 6H, C<u>H</u>$_3$).
^{13}C{^{1}H}-NMR (75 MHz, CD_2Cl_2): δ (ppm) = 153.0 (s), 141.1 (s), 137.0 (s), 135.5 (s), 135.2 (s), 129.6 (s), 115.1 (s), 56.0 (s), 21.0 (s), 18.3 (s).
Eluent: Hexane/EtOAc 1:1
The data matches those from the literature.[289]

4-Fluoro-*N*-(*p*-tolyl)aniline (Entry 10)

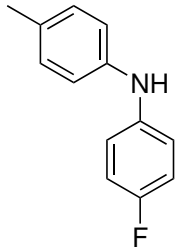

^{1}H-NMR (300 MHz, CD_2Cl_2): δ (ppm) = 7.13–6.84 (m, 8H, Ar<u>H</u>), 5.59 (br. s, 1H, N<u>H</u>), 2.29 (s, 3H, C<u>H</u>$_3$).
^{13}C{^{1}H}-NMR (75 MHz, CD_2Cl_2): δ (ppm) = 157.9 (d, ^{1}J(C,F) = 238.1 Hz), 141.5 (s), 140.5 (s), 131.0 (s), 130.2 (s), 119.5 (d, ^{3}J(C,F) = 7.7 Hz), 118.2 (s), 116.1 (d, ^{2}J(C,F) = 22.5 Hz), 20.7 (s).
Eluent: Hexane/EtOAc 9:1
The data matches those from the literature.[290]

4-Fluoro-*N*-(4-methoxyphenyl)aniline (Entry 11)

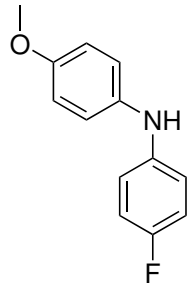

^{1}H-NMR (300 MHz, CD_2Cl_2): δ (ppm) = 7.10–6.76 (m, 8H, Ar<u>H</u>), 5.49 (br. s, 1H, N<u>H</u>), 3.78 (s, 3H, OC<u>H</u>$_3$).
^{13}C{^{1}H}-NMR (75 MHz, CD_2Cl_2): δ (ppm) = 157.5 (d, ^1J(C,F) = 237.1 Hz), 155.5 (s), 141.8 (s), 136.9 (s), 121.5 (s), 118.0 (d, ^3J(C,F) = 7.6 Hz), 116.0 (d, ^2J(C,F) = 22.5 Hz), 115.1 (s), 55.9 (s).
Eluent: Hexane/EtOAc 9:1
The data matches those from the literature.[191]

***N*-(4-Fluorophenyl)-2,4,6-trimethylaniline (Entry 12)**

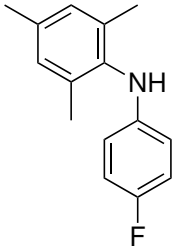

^{1}H-NMR (300 MHz, CD_2Cl_2): δ (ppm) = 6.94 (s, 2H, Ar<u>H</u>), 6.89–6.79 (m, 2H, Ar<u>H</u>), 6.48–6.35 (m, 2H, Ar<u>H</u>), 5.11 (br. s, 1H, N<u>H</u>), 2.29 (s, 3H, p–C<u>H</u>$_3$), 2.15 (s, 6H, C<u>H</u>$_3$).
^{13}C{^{1}H}-NMR (75 MHz, CD_2Cl_2): δ (ppm) = 156.4 (d, ^1J(C,F) = 235.1 Hz), 143.6 (s), 136.1 (t, ^2J(C,F) = 18.1 Hz), 129.6 (s), 115.9 (d, ^2J(C,F) = 22.4 Hz), 114.5 (d, ^3J(C,F) = 7.4 Hz), 21.0 (s), 18.3 (s).
Eluent: Hexane/EtOAc 9:1
The data matches those from the literature.[196]

4-Methyl-*N*-(4-nitrophenyl)aniline (Entry 13)

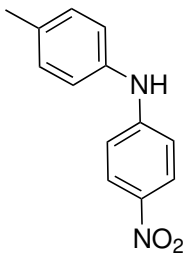

^{1}H-NMR (300 MHz, CD_2Cl_2): δ (ppm) = 8.07 (d, J(H,H) = 9.2 Hz, 2H, Ar<u>H</u>), 7.25–7.08 (m, 4H, Ar<u>H</u>), 6.90 (d, J(H,H) = 9.2 Hz, 2H, Ar<u>H</u>), 6.33 (br. s, 1H, N<u>H</u>), 2.35 (s, 3H, C<u>H</u>$_3$).

^{13}C{^{1}H}-NMR (75 MHz, CD_2Cl_2): δ (ppm) = 151.3 (s), 139.8 (s), 137.3 (s), 135.2 (s), 130.6 (s), 126.5 (s), 122.9 (s), 113.6 (s), 21.0 (s).
Eluent: Hexane/EtOAc 9:1
The data matches those from the literature.[185]

4-(*p*-Tolyl)morpholine (Entry 14)

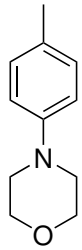

^{1}H-NMR (300 MHz, CD_2Cl_2): δ (ppm) = 7.07 (d, J(H,H) = 8.3 Hz, 2H, Ar$\underline{H}$), 6.81 (d, J(H,H) = 8.6 Hz, 2H, Ar$\underline{H}$), 3.84–3.78 (m, 4H, NC$\underline{H}_2$CH_2), 3.09–3.04 (m, 4H, NCH_2C$\underline{H}_2$), 2.26 (s, 3H, C$\underline{H}_3$).
^{13}C{^{1}H}-NMR (75 MHz, CD_2Cl_2): δ (ppm) = 149.8 (s), 139.7 (s), 130.0 (s), 116.2 (s), 67.3 (s), 50.3 (s), 20.5 (s).
Eluent: Hexane/EtOAc 9:1
The data matches those from the literature.[291]

1-(*p*-Tolyl)pyrrolidine (Entry 15)

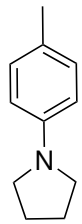

^{1}H-NMR (300 MHz, CD_2Cl_2): δ (ppm) = 7.02 (d, J(H,H) = 8.2 Hz, 2H, Ar$\underline{H}$), 6.52–6.46 (m, 2H, Ar$\underline{H}$), 3.29–3.20 (m, 4H, NC$\underline{H}_2$CH_2), 2.25 (s, 3H, C$\underline{H}_3$), 2.06–1.94 (m, 4H, NCH_2C$\underline{H}_2$).
^{13}C{^{1}H}-NMR (75 MHz, CD_2Cl_2): δ (ppm) = 146.7 (s), 129.9 (s), 124.6 (s), 121.1 (s), 48.2 (s), 25.8 (s), 20.4 (s).
Eluent: Hexane/EtOAc 9:1
The data matches those from the literature.[292]

***N*-butyl-4-methoxyaniline (Entry 16)**

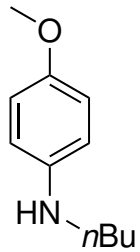

^{1}H-NMR (300 MHz, CD_2Cl_2): δ (ppm) = 6.79 (d, J(H,H) = 9.0 Hz, 2H, Ar$\underline{H}$), 6.60 (d,

J(H,H) = 8.9 Hz, 2H, ArH), 3.75 (s, 3H, OCH$_3$), 3.09 (t, J(H,H) = 7.0 Hz, 2H, NCH$_2$), 1.55–1.63 (m, 2H, CH$_2$), 1.39–1.50 (m, 2H, CH$_2$), 1.00 (t, J(H,H) = 7.3 Hz, 3H, CH$_3$).
^{13}C{^{1}H}-NMR (75 MHz, CD_2Cl_2): δ (ppm) = 154.3 (s), 151.9 (s), 143.2 (s), 122.0 (s), 114.7 (s), 114.5 (s), 113.8 (s), 55.6 (s), 55.5 (s), 44.6 (s), 31.8 (s), 20.3 (s), 13.7 (s).
Eluent: Hexane/EtOAc 9:1
The data matches those from the literature.[293]

8.2.7 Alkylation of Indols

8.2.7.1 General procedure for the alkylation of indols

Generation of KHMDS free (pyrr)P$_3$P (**7b**):

pyrrP$_3$P−HBF$_4$ (**7b**-HBF$_4$) (0.03 mmol, 22.1 mg, 2.5 mol%) and KHMDS (0.03 mmol, 4.99 mg, 2.5 mol%) were dissolved in toluene (5 mL) and stirred for 2 h at RT. Afterward, the suspension was centrifuged, the motherliquor removed and the solvent removed *in vacuo*. The residue was dissolved in pentane (10 mL), filtered over Celite® and washed (3 x 10 mL). The solvent was removed *in vacuo* to generate (pyrr)P$_3$P (**7b**) free of KHMDS.

Alkylation procedure:

Alkene (1.00 mmol, 1.0 eq.) was dissolved in THF (10 mL) and indole (1.50 mmol, 1.5 eq.) was added. Afterward, (pyrr)P$_3$P (**7b**) (0.03 mmol, 2.5 mol%) was added in THF and the mixture was stirred at a) RT or b) 60 °C for 1 to 16 h. Afterward, the solvent was removed, and the residue was purified by column chromatography on silica. Alternatively, 1,3,5-trimethoxybenzene (10 mol%) was added and a crude NMR was taken. The integrals of the product and the internal standard were compared, and a yield was measured.

8.2.7.2 Alkylation products

3-(*1H*-Indol-1-yl)butanenitrile (Entry 1)

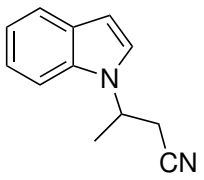

^{1}H-NMR (300 MHz, C_6D_6): δ (ppm) = 7.70–7.63 (m, 1H, ArH), 7.21–7.14 (m, 2H, ArH), 6.84–6.78 (m, 1H, ArH), 6.73 (d, J(H,H) = 3.30 Hz, 1H, ArH), 6.48 (d, J(H,H) = 3.0 Hz, 1H, ArH), 3.87 (sext., ^3J(H,H) = 6.5 Hz, 1H, CH$_3$CHCH$_2$), 1.61 (d, ^3J(H,H) = 6.1 Hz, 2H, CH$_2$CHCH$_3$), 0.97 (d, ^3J(H,H) = 6.9 Hz, 3H, CH$_2$CHCH$_3$).
^{13}C{^{1}H}-NMR (75 MHz, C_6D_6): δ (ppm) = 135.4 (s), 129.1 (s), 123.0 (s), 121.8 (s), 121.4 (s), 120.1 (s), 108.9 (s), 102.7 (s), 46.9 (s), 24.1 (s), 18.4 (s).
APCI-MS = 185.11 [M-H]$^+$ calc., 185.1070 [M-H]$^+$ found.
The data matches the literature values.[294]
Eluent: Hexane/EtOAc 85:15

3-(6-Methoxy-*1H*-indol-1-yl)butanenitrile (Entry 2)

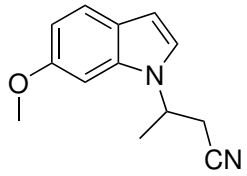

^{1}H-NMR (300 MHz, CD_2Cl_2): δ (ppm) = 7.36–7.14 (m, 5H, Ar$\underline{H}$), 6.99–6.86 (m, Ar$\underline{H}$, 1H), 6.53 (dd, J(H,H) = 12.6 Hz, J(H,H) = 3.1 Hz, 1H), 4.75 (sext., ^3J(H,H) = 6.5 Hz, 1H, $CH_3C\underline{H}CH_2$), 3.9 (s, 3H, $OC\underline{H}_3$), 2.74 (dd, J(H,H) = 1.6 Hz, ^3J(H,H) = 5.9 Hz, 2H, $C\underline{H}_2CHCH_3$), 1.69 (d, ^3J(H,H) = 6.9 Hz, 3H, $CH_2CHC\underline{H}_3$).
APCI-MS = 215.11 $[M\text{-}H]^+$ calc., 215.1178 $[M\text{-}H]^+$ found.

1-(1-Cyanopropan-2-yl)-*1H*-indole-6-carbonitrile (Entry 3)

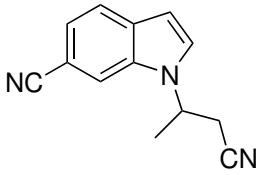

^{1}H-NMR (300 MHz, CD_2Cl_2): δ (ppm) = 7.98 (s, 1H, Ar$\underline{H}$), 7.56–7.36 (m, 3H, Ar$\underline{H}$), 6.69 (d, J(H,H) = 3.4 Hz, 1H, Ar$\underline{H}$), 4.92 (sext., ^3J(H,H) = 6.5 Hz, 1H, $CH_3C\underline{H}CH_2$), 2.87 (d, ^3J(H,H) = 6.2 Hz, 2H, $CH_3CHC\underline{H}_2$), 1.72 (d, ^3J(H,H) = 6.9 Hz, 3H, $C\underline{H}_3CHCH_2$).
APCI-MS = 210.10 $[M\text{-}H]^+$ calc., 210.1025 $[M\text{-}H]^+$ found.

Methyl 3-(*1H*-indol-1-yl)propanoate (Entry 4)

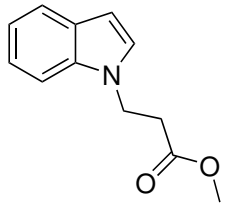

^{1}H-NMR (300 MHz, CD_2Cl_2): δ (ppm) = 7.78 (dd, J(H,H) = 2.6 Hz, J(H,H) = 8.4 Hz, 2H, Ar$\underline{H}$), 7.49 (d, J(H,H) = 8.0 Hz, 2H, Ar$\underline{H}$), 6.65 (dd, J(H,H) = 2.9 Hz, J(H,H) = 9.3 Hz, 2H, Ar$\underline{H}$), 4.53 (t, ^3J(H,H) = 6.8 Hz, 2H, $NC\underline{H}_2CH_2$), 3.76 (s, 3H, $CO_2C\underline{H}_3$), 2.91 (t, ^3J(H,H) = 6.8 Hz, 2H, $NCH_2C\underline{H}_2$).
APCI-MS = 204.10 $[M\text{-}H]^+$ calc., 204.1018 $[M\text{-}H]^+$ found.
The data matches the literature values.[295]

Methyl 3-(6-methoxy-*1H*-indol-1-yl)propanoate (Entry 5)

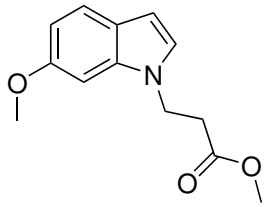

^{1}H-NMR (300 MHz, CD_2Cl_2): δ (ppm) = 7.29 (d, J(H,H) = 8.9 Hz, 1H, Ar$\underline{H}$), 7.15 (t, J(H,H) = 3.3 Hz, 2H, Ar$\underline{H}$), 6.93 (dd, J(H,H) = 2.5 Hz, J(H,H) = 8.9 Hz, 1H, Ar$\underline{H}$), 6.46 (d, J(H,H) = 6.8 Hz, 1H, Ar$\underline{H}$), 4.42 (t, ^3J(H,H) = 6.8 Hz, NC$\underline{H}_2$CH$_2$), 3.88 (s, 3H, OC$\underline{H}_3$), 3.68 (s, 3H, OC$\underline{H}_3$), 2.82 (t, ^3J(H,H) = 6.8 Hz, NCH$_2$C$\underline{H}_2$).
APCI-MS = 234.11 $[M\text{-}H]^+$ calc., 234.1122 $[M\text{-}H]^+$ found.
The data matches the literature values.[295]

Methyl 3-(6-cyano-*1H*-indol-1-yl)propanoate (Entry 6)

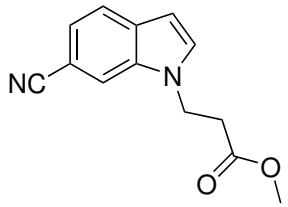

^{1}H-NMR (300 MHz, CD_2Cl_2): δ (ppm) = 7.94 (s, 1H, Ar$\underline{H}$), 7.44 (s, 2H, Ar$\underline{H}$), 7.31 (d, J(H,H) = 3.2 Hz, 1H, Ar$\underline{H}$), 6.58 (d, J(H,H) = 3.2 Hz, 1H, Ar$\underline{H}$), 4.46 (t, ^3J(H,H) = 6.6 Hz, 2H, NC$\underline{H}_2$CH$_2$), 3.63 (s, 3H, OC$\underline{H}_3$), 2.84 (t, ^3J(H,H) = 6.6 Hz, NCH$_2$C$\underline{H}_2$).
APCI-MS = 229.09 $[M\text{-}H]^+$ calc., 229.0971 $[M\text{-}H]^+$ found.

3-(*1H*-Indol-1-yl)propanamide (Entry 7)

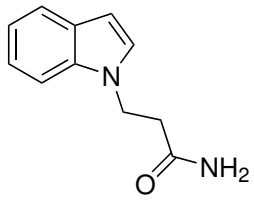

^{1}H-NMR (300 MHz, CD_2Cl_2): δ (ppm) = 7.74 (t, J(H,H) = 7.7 Hz, 1H, Ar$\underline{H}$), 7.42 (d, J(H;H) = 8.1 Hz, 1H, Ar$\underline{H}$), 7.33–7.27 (m, 1H, Ar$\underline{H}$), 7.25–7.17 (m, 3H, Ar$\underline{H}$), 6.56 (d, J(H,H) = 3.1 Hz, 1H, Ar$\underline{H}$), 6.08 (br. s, 2H, N$\underline{H}_2$), 4.40 (t, ^3J(H,H) = 6.7 Hz, 2H, NC$\underline{H}_2$CH$_2$), 2.56 (t, ^3J(H,H) = 6.7 Hz, 2H, NCH$_2$C$\underline{H}_2$).
APCI-MS = 189.10 $[M\text{-}H]^+$ calc., 189.1021 $[M\text{-}H]^+$ found.
The data matches the literature values.[296]

3-(6-Methoxy-*1H*-indol-1-yl)propanamide (Entry 8)

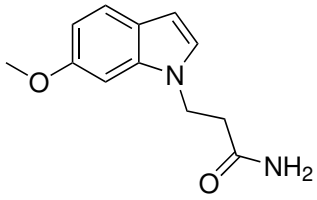

^{1}H-NMR (300 MHz, CD_2Cl_2): δ (ppm) = 7.26 (d, J(H,H) = 8.9 Hz, 1H, ArH), 7.16–7.09 (m, 2H, ArH), 6.91–6.85 (m, 1H, ArH), 6.41 (d, J(H,H) = 3.0 Hz, 1H, ArH), 4.36 (t, ^3J(H,H) = 6.7 Hz, 2H, NCH_2CH_2), 3.83 (s, 3H, OCH_3), 2.59 (t, ^3J(H,H) = 6.7 Hz, 2H, NCH_2CH_2).
APCI-MS = 219.11 $[M\text{-}H]^+$ calc., 219.1126 $[M\text{-}H]^+$ found.

3-(6-Cyano-*1H*-indol-1-yl)propanamide (Entry 9)

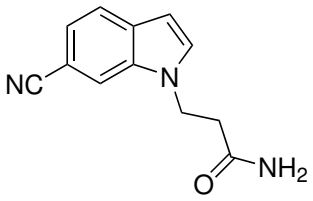

^{1}H-NMR (300 MHz, CD_2Cl_2): δ (ppm) = 7.92 (s, 1H, ArH), 7.53 (s, 1H, ArH), 6.61 (d, J(H,H) = 3.2 Hz, 1H, ArH), 6.26 (d, J(H,H) = 3.8 Hz, 1H, ArH), 5.70 (d, J(H,H) = 4.1 Hz, 1H, ArH), 4.47 (t, ^3J(H,H) = 6.6 Hz, 2H, NCH_2CH_2), 2.74 (t, ^3J(H,H) = 6.6 Hz, 2H, NCH_2CH_2).
APCI-MS = 214.09 $[M\text{-}H]^+$ calc., 214.0974 $[M\text{-}H]^+$ found.

8.3 Basicity measurements

The pK_{BH^+} values were determined as described in the literature.[85] A mixture of phosphazene base (5.00 mg, 1.00 eq.), reference base (5.00 mg, 1.00 eq.) and bistriflimidic acid (5.00 mg, 1.00 eq.) was dissolved in THF−d_8 (0.60 mL) transferred to an NMR tube and shaken. Quantitative ^{31}P-NMR spectra were recorded by inverse gated decoupling method with a relaxation delay of 40s. pK_{BH^+} values of the THF scale (measured) were correlated to the MeCN scale using correlation equation 8.3 reported by Leito *et al.*[23] The pK_{BH^+} (THF) values of reference bases MTBD and Ph_3PCH_2 are 18.6 and 26.6 respectively.[23]

8.3.1 Example calculation

(dma)P_1P-(tBu)$_2$ (8.57 mg, 26.6 µmol), MTBD (4.66 mg, 30.4 µmol) and triflimidic acid (5.78 mg, 26.6 µmol) were dissolved in THF−d_8 (0.60 mL) transferred to an NMR tube and shaken. The integrals of the resulting mixture of (dma)P_1P-(tBu)$_2$ and (dma)P_1P-(tBu)$_2$H$^+$ were 0.67 and 0.33. Therefore, we can calculate the molarity of (dma)P_1P-(tBu)$_2$ and MTBD as 17.74 µmol and 12.68 µmol. The molarities of (dma)P_1P-(tBu)$_2$H$^+$ and MTBDH$^+$ are the differences of starting molarity to calculated molarity.
We can now calculate the rate constant K by equation 8.1:

$$K = \frac{n((\text{dma})\text{P}_1\text{P} - (t\text{Bu})_2) * n(\text{MTBDH}^+)}{n(MTBD) * n((\text{dma})\text{P}_1\text{P} - (t\text{Bu})_2\text{H}^+)} \tag{8.1}$$

Now we we can calculate the pK_{BH^+} by subtracting the logarithm of K with the pK_{BH^+} of the reference base (MTBD = 18.6 in THF).

$$pK_{BH^+} = 18.6 - \log(K) = 18.6 - \log 2.80 = 18.15 \tag{8.2}$$

We can calculate the basicity in MeCN by equation 8.3:

$$pK_a(THF) = (0.92 \pm 0.02) * pK_a(MeCN) - (5.15 \pm 0.51) = 24.8 \pm 0.1 \tag{8.3}$$

8.3.2 Basicity of (dma)P_1P-(tBu)$_2$

Table 8.1: Data for basicity measurement of (dma)P_1P-(tBu)$_2$.

	Base	Reference Base		
	5a	MTBD	**5a**H$^+$	MTBDH$^+$
m [mg]	8.57	4.66		
n(start) [mmol]	26.58	30.41	0	0
n(end) [mmol]	17.74	12.68	8.84	17.74

$$pK_{BH^+} = 18.6 - \log(K) = 18.6 - \log 2.80 = 18.15 \tag{8.4}$$

$$pK_a(THF) = (0.92 \pm 0.02) * pK_a(MeCN) - (5.15 \pm 0.51) = 24.8 \pm 0.1 \tag{8.5}$$

8.3.3 Basicity of (pyrr)P_1P-(tBu)$_2$

Table 8.2: Data for basicity measurement of (pyrr)P_1P-(tBu)$_2$.

	Base	Reference Base		
	5b	MTBD	**5b**H$^+$	MTBDH$^+$
m [mg]	6.80	2.64		
n(start) [mmol]	16.99	17.20	0	0
n(end) [mmol]	6.95	10.30	10.0	6.94

$$pK_{BH^+} = 18.6 - \log(K) = 18.6 - \log 0.47 = 18.93 \tag{8.6}$$

$$pK_a(THF) = (0.92 \pm 0.02) * pK_a(MeCN) - (5.15 \pm 0.51) = 25.7 \pm 0.1 \tag{8.7}$$

8.3.4 Basicity of (cy)P_1P-(tBu)$_2$

Table 8.3: Data for basicity measurement of (cy)P_1P-(tBu)$_2$.

	Base	Reference Base		
	5c	MTBD	**5c**H$^+$	MTBDH$^+$
m [mg]	9.20	3.20		
n(start) [mmol]	20.93	20.90	0	0
n(end) [mmol]	12.0	8.920	8.96	11.98

$$pK_{BH^+} = 18.6 - \log(K) = 18.6 - \log 1.79 = 18.35 \tag{8.8}$$

$$pK_a(THF) = (0.92 \pm 0.02) * pK_a(MeCN) - (5.15 \pm 0.51) = 25.0 \pm 0.1 \tag{8.9}$$

8.3.5 Basicity of (tBu)P_1P-(tBu)$_2$

Table 8.4: Data for basicity measurement of (tBu)P_1P-(tBu)$_2$.

	Base	Reference Base		
	5d	MTBD	**5d**H$^+$	MTBDH$^+$
m [mg]	5.92	2.82		
n(start) [mmol]	16.37	18.40	0	0
n(end) [mmol]	11.15	7.26	5.22	11.15

$$pK_{BH^+} = 18.6 - \log(K) = 18.6 - \log 3.28 = 18.1 \tag{8.10}$$

$$pK_a(THF) = (0.92 \pm 0.02) * pK_a(MeCN) - (5.15 \pm 0.51) = 24.8 \pm 0.1 \tag{8.11}$$

8.3.6 Basicity of (dma)P_2P-tBu

Table 8.5: Data for basicity measurement of (dma)P_2P-tBu.

	Base	Reference Base		
	6a	Ph_3PCH_2	**6a**H$^+$	$Ph_3PCH_2H^+$
m [mg]	6.70	4.23		
n(start) [mmol]	15.14	15.32	0	0
n(end) [mmol]	8.91	6.31	6.23	8.91

$$pK_{BH^+} = 26.6 - \log(K) = 26.6 - \log 1.99 = 26.3 \tag{8.12}$$

$$pK_a(THF) = (0.92 \pm 0.02) * pK_a(MeCN) - (5.15 \pm 0.51) = 33.7 \pm 0.1 \tag{8.13}$$

8.3.7 Basicity of (pyrr)P_2P-*t*Bu

Table 8.6: Data for basicity measurement of (pyrr)P_2P-*t*Bu.

	Base	Reference Base		
	6b	Ph_3PCH_2	**6a**H^+	$Ph_3PCH_2H^+$
m [mg]	8.14	3.75		
n(start) [mmol]	13.60	13.58	0	0
n(end) [mmol]	3.44	10.14	10.15	3.44

$$pK_{BH^+} = 26.6 - \log(K) = 26.6 - \log 0.12 = 27.5 \tag{8.14}$$

$$pK_a(THF) = (0.92 \pm 0.02) * pK_a(MeCN) - (5.15 \pm 0.51) = 35.0 \pm 0.1 \tag{8.15}$$

8.4 General procedure for the determination of hydrolysis products

Phosphazene base (50 mg), was dissolved in dioxane (2 mL) and 3 mL of either (a) 1 M aqueous HCl, (b) 1 M aqueous NaOH or (c) H_2O were added. The mixture was stirred for 16 h at 100 °C. Afterward, the solvent was removed, and the residue dissolved in $CDCl_3$.^{31}P-NMR spectra as well as ESI-MS were measured to determine the stability of the respective phosphazenes.

8.4.1 Experimental data of hydrolysis reactions

8.4.1.1 (dma)P_1P-(*t*Bu)$_2$

^{31}P{^{1}H}-NMR (121 MHz, $CDCl_3$): δ (ppm) = 69.2 (s, P(III)=O), 45.8 (s, P(V)=O), 45.5 (d, ^2J(P,P) = 3.3 Hz, P(III)-H), 32.3 (d, ^2J(P,P) = 3.3 Hz, P(III)-H).
ESI-MS = 323.25 [M-H]$^+$ calc., 323.4 [M-H]$^+$ found;
339.24 [M=O]H$^+$ calc., 339.2433 [M=O]H$^+$ found.

8.4.1.2 (pyrr)P_1P-(*t*Bu)$_2$

^{31}P{^{1}H}-NMR (121 MHz, $CDCl_3$): δ (ppm) = 53.9 (s, P(III)-O), 37.5 (d, ^2J(P,P) = 34.8 Hz, P(V)=O), 43.7 (d, ^2J(P,P) = 23.3 Hz, P(III)-H), 26.9 (d, ^2J(P,P) = 23.3 Hz, P(V)-H).
ESI-MS = 401.54 [M-H]$^+$ calc., 401.2962 [M-H]$^+$ found;
417.29 [M=O]H$^+$ calc., 417.4 [M=O]H$^+$ found.

8.4.1.3 (cy)P_1P-(*t*Bu)$_2$

^{31}P{^{1}H}-NMR (121 MHz, $CDCl_3$): δ (ppm) = 41.0 (s, P(III)-H), 14.6 (s, P(V)-H), 43.0 (s, P(III)=O), 8.6 (s, P(V)=O).
ESI-MS = 440.36 [M-H]$^+$ calc., 440.3591 [M-H]$^+$ found;
456.35 [M=O]H$^+$ calc., 456.3527 [M=O]H$^+$ found.

8.4.1.4 (*t*Bu)P$_1$P-(*t*Bu)$_2$

^{31}P{^{1}H}-NMR (121 MHz, $CDCl_3$): δ (ppm) = 58.0 (d, ^2J(P,P) = 31.2 Hz, P(III)-H), 44.87 (d, ^2J(P,P) = 31.2 Hz, P(V)-H), 65.1 (s, P(III)=O), 40.9 (s, P(V)=O).
ESI-MS = 362.31 $[M\text{-}H]^+$ calc., 362.7 $[M\text{-}H]^+$ found;
378.30 $[M{=}O]H^+$ calc., 378.3052 $[M{=}O]H^+$ found.

8.4.1.5 (dma)P$_2$P-*t*Bu

^{31}P{^{1}H}-NMR (121 MHz, $CDCl_3$): δ (ppm) = 23.0 (d, ^2J(P,P) = 21.7 Hz, P(III)-H), 4.0 (t, ^2J(P,P) = 21.7 Hz, P(V)-H).
ESI-MS = 362.31 $[M\text{-}H]^+$ calc., 443.31 $[M\text{-}H]^+$ found;
459.30 $[M{=}O]H^+$ calc., 459.2995 $[M{=}O]H^+$ found.

8.4.1.6 (pyrr)P$_2$P-*t*Bu

^{31}P{^{1}H}-NMR (121 MHz, $CDCl_3$): δ (ppm) = 9.1 (d, ^2J(P,P) = 17.7 Hz, P(III)-H), 2.3 (t, ^2J(P,P) = 17.2 Hz, P(V)-H).
ESI-MS = 499.40 $[M\text{-}H]^+$ calc., 599.3999 $[M\text{-}H]^+$ found;
615.39 $[M{=}O]H^+$ calc., 615.3931 $[M{=}O]H^+$ found.

8.4.1.7 (dma)P$_3$P

^{31}P{^{1}H}-NMR (121 MHz, $CDCl_3$): δ (ppm) = 21.1 (d, ^2J(P,P) = 29.5 Hz, P(III)-H), −29.7 (q, ^2J(P,P) = 29.5 Hz, P(V)-H).
ESI-MS = 563.36 $[M\text{-}H]^+$ calc., 563.3623 $[M\text{-}H]^+$ found;
579.36 $[M{=}O]H^+$ calc., 579.3599 $[M{=}O]H^+$ found.

8.4.1.8 (pyrr)P$_3$P

^{31}P{^{1}H}-NMR (121 MHz, $CDCl_3$): δ (ppm) = 8.8 (d, ^2J(P,P) = 23.1 Hz, P(III)-H), −29.0 (q, ^2J(P,P) = 23.1 Hz, P(V)-H).
ESI-MS = 797.50 $[M\text{-}H]^+$ calc., 797.4999 $[M\text{-}H]^+$ found.

8.5 Reaction of PAP's with Iodoethane

PAP was dissolved in THF (5 mL) and iodoethane (excess) was added. The mixture was stirred for 1 h before the solvent was removed *in vacuo*. The residue was redissolved in MeCN−d_3 and analyzed by NMR and MS spectrometry. A quantitative ^{31}P-NMR spectrum was taken by inverse gated decoupling method with a relaxation delay of 40 s as described in the literature.[86] The alkylation/protonation ratio was analyzed by integrating the central phosphorus atoms intensities of the ^{31}P-NMR spectra.

8.5.1 Experimental data of ethylation reactions

8.5.1.1 (dma)P$_3$P-Et and (pyrr)P$_3$P-Et (7a-Et and 7b-Et)

(dma)P_3P and (pyrr)P_3P data is given in the literature.[86]

8.5.1.2 (dma)P_1P-(tBu)$_2$-Et (5a-Et)

(dma)P_1P-(tBu)$_2$ (9.99 mg, 31.0 µmol, 1.00 eq.) and EtI (9.67 mg, 62 µmol, 2.00 eq) gave a ratio of [dmaP_1PEt]/[dmaP_1H] of 60.9/39.1.

^{1}H-NMR (300 MHz, MeCN−d_3): δ (ppm) = 3.34 (dt, ^1J(P,H) = 936.2 Hz, ^3J(P,H) = 7.1 Hz, 1H, P-H), 2.66 (d, ^3J(P,H) = 10.8 Hz, 18H,CH_3N−P=NP≡−Et), 2.67 (d, ^3J(P,H) = 10.2 Hz, 18H, CH$_3$N−P=NP−H$^+$), 2.05 (q, ^2J(H;H) = 7.8 Hz, PCH2CH3), 1.30 (d, ^3J(P,H) = 14.9 Hz, 18H, P=NP≡CCH$_3$−H), 1.23 (td, ^2J(H,H) = 7.8 Hz, ^2J(P,H) = 15.9 Hz, 3H, PCH$_2$CH$_3$), 1.16 (d, ^3J(P,H) = 13.3 Hz, 18H, P=NP≡CCH$_3$−Et).
^{31}P{^{1}H}-NMR (121 MHz, MeCN−d_3): δ (ppm) = 46.0 (d, ^2J(P,P) = 29.4 Hz, P(III)-H+), 45.5 (d, ^2J(P,P) = 3.7 Hz, P(III)-Et+), 23.0 (s, P(V)-Et+), 21.0 (d, ^2J(P,P) = 29.4 Hz, P(V)-H+).
ESI-MS = 351.2806 [M-H]$^+$ calc., 351.2804 [M-H]$^+$ found.

8.5.1.3 (pyrr)P_1P-(tBu)$_2$-Et (5b-Et)

(pyrr)P_1P-(tBu)$_2$ (12.42 mg, 31.0 µmol, 1.00 eq.) and EtI (9.67 mg, 62 µmol, 2.00 eq.) gave a ratio of [pyrrP_1PEt]/[pyrrP_1H] of 51.7/48.3.

^{1}H-NMR (300 MHz, MeCN−d_3): δ (ppm) = 3.34 (dt, ^1J(P,H) = 936.5 Hz, ^3J(P,H) = 7.3 Hz, 1H, P-H), 3.2 (m, 12H, NCH$_2$CH$_2$), 2.15 (dq, ^2J(P;H) = 76.2 Hz, ^2J(H;H) = 7.4 Hz, 2H, PCH$_2$CH$_3$), 1.87 (m, 12H, NCH$_2$CH$_2$), 1.81 (m, 12H, NCH$_2$CH$_2$), 1.32 (d, ^2J(P,H) = 14.8 Hz, CCH$_3$), 1.25 (m, 3H, PCH$_2$CH$_3$), 1.19 (d, ^2J(P,H) = 13.3 Hz, CCH$_3$).
^{31}P{^{1}H}-NMR (121 MHz, MeCN−d_3): δ (ppm) = 44.5 (d, ^2J(P,P) = 26.5 Hz, P(III)H$^+$), 40.8 (s, P(III)Et$^+$), 8.3 (s, P(V)Et$^+$), 5.4 (d, ^2J(P,P) = 26.5 Hz, P(V)H$^+$).
ESI-MS = 429.3276 [M-H]$^+$ calc., 429.3270 [M-H]$^+$ found.

8.5.1.4 (cy)P_1P-(tBu)$_2$-Et (5c-Et)

(cy)P_1P-(tBu)$_2$ (13.63 mg, 31.0 µmol, 1.00 eq.) and EtI (9.67 mg, 62 µmol, 2.00 eq.) gave a ratio of [cyP_1PEt]/[cyP_1H] of 10.8/89.2.

^{1}H-NMR (300 MHz, MeCN−d_3): δ (ppm) = 3.34 (dt, ^1J(P,H) = 936.2 Hz, ^3J(P,H) = 7.0 Hz, 1H, P-H), 3.36 (m, 3H, PCHCH2CH2CH2), 2.22–2.17 (m, 7H), 2.05–1.98 (m, 6H), 1.83–1.76 (m, 11H), 1.72–1.68 (m, 4H), 1.62–1.51 (m, 6H), 1.31–1.19 (m, 12H), 1.14 (d, ^3J(P,H) = 13.5 Hz, 18H, CCH$_3$).
^{31}P{^{1}H}-NMR (121 MHz, MeCN−d_3): δ (ppm) = 56.1 (s, P(III)-Et$^+$), 50.5 (s, P(V)-Et$^+$), 42.3 (d, ^2J(P,P) = 22.4 Hz, P(III)-H$^+$), 27.6 (d, ^2J(P,P) = 22.4 Hz, P(V)-H$^+$).
ESI-MS = 468.3888 [M-H]$^+$ calc., 468.3900 [M-H]$^+$ found.

8.5.1.5 (tBu)P_1P-(tBu)$_2$-Et (5d-Et)

(tBu)P_1P-(tBu)$_2$ (11.21 mg, 31.0 µmol, 1.00 eq.) and EtI (9.67 mg, 62 µmol, 2.00 eq.) gave a ratio of [tBuP_1PEt]/[tBuP_1H] of 15.4/84.6.

^{1}H-NMR (300 MHz, MeCN−d_3): δ (ppm) = 3.34 (dt, ^1J(P,H) = 936.1 Hz, ^3J(P,H) = 7.0 Hz, P-H), 2.19 (q, ^2J(H;H) = 7.8 Hz, 2H, PCH$_2$CH$_3$), 1.52 (d, ^2J(P,H) = 14.2 Hz, 27H, CCH$_3$−Et), 1.50 (d, ^2J(P;H) = 13.4 Hz, 27H, CCH$_3$−H), 1.44 (dt, ^2J(P,H) = 14.8 Hz, ^2J(H,H) = 7.8 Hz, 3H, PCH$_2$CH$_3$), 1.26 (d, ^2J(P,H) = 13.4 Hz, CCH$_3$).

$^{31}P\{^{1}H\}$-NMR (121 MHz, MeCN−d_3): δ (ppm) = 55.0 (d, ^{2}J(P,P) = 22.4 Hz, P(III)-H^+), 46.3 (d, ^{2}J(P,P) = 31.9 Hz, P(III)-Et^+), 45.5 (d, ^{2}J(P,P) = 22.4 Hz, P(V)-H^+), 40.5 (d, ^{2}J(P,P) = 31.9 Hz, P(V)-Et^+).
ESI-MS = 390.3418 $[M\text{-}H]^+$ calc., 390.3432 $[M\text{-}H]^+$ found.

8.5.1.6 (dma)P_1P-(Odipp)$_2$-Et (9-Et)

(dma)P_1P-(Odipp)$_2$ (17.44 mg, 31.0 µmol, 1.00 eq.) and EtI (9.67 mg, 62 µmol, 2.00 eq.) gave a ratio of [PhosphiteP_1PEt]/[PhosphiteP_1H] of 7.0/93.0.

^{1}H-NMR (300 MHz, MeCN−d_3): δ (ppm) = 7.14 (d, ^{3}J(H,H) = 7.6 Hz, 2H, Ar$\underline{H}$), 7.09 (d, ^{3}J(H,H) = 7.6 Hz, 2H, Ar$\underline{H}$), 6.99 (t, ^{3}J(H,H) = 7.6 Hz, 2H, Ar$\underline{H}$), 3.37 (dt, ^{1}J(P,H) = 936.0 Hz, ^{3}J(P,H) = 7.2 Hz, P-$\underline{H}$), 3.83 (sept, ^{3}J(H,H) = 6.9 Hz, 4H, PEt−$CH_3C\underline{H}CH_3$), 3.73 (septd, ^{3}J(H,H) = 6.9 Hz, ^{5}J(P,H) = 2.5 Hz, 4H, PH−$CH_3C\underline{H}CH_3$), 3.37 (m, 2H, $PC\underline{H}_2CH_3$), 2.72 (d, ^{3}J(P,H) = 9.9 Hz, 18H, PEt−$NC\underline{H}_3$), 2.54 (d, ^{3}J(P,H) = 10.0 Hz, 18H, $PHNC\underline{H}_3$), 1.18 (d, ^{3}J(H,H) = 6.9 Hz, 6H, $PEtCH_3CHC\underline{H}_3$), 1.16 (d, ^{3}J(H;H) = 6.9 Hz, 6H, $PEtC\underline{H}_3CHCH_3$), 1.14 (d, ^{3}J(H;H) = 6.9 Hz, 6H, $PHC\underline{H}_3CHCH_3$), 1.12 (d, ^{3}J(H,H) = 6.9 Hz, 6H, $PHCH_3CHC\underline{H}_3$).
$^{31}P\{^{1}H\}$-NMR (121 MHz, MeCN−d_3): δ (ppm) = 24.3 (s, P(III)-Et^+), 22.3 (d, ^{2}J(P,P) = 69.6 Hz, P(III)-H^+), −12.0 (d, ^{2}J(P,P) = 69.6 Hz, P(V)-H^+), −16.7 (s, P(V)-Et^+).
ESI-MS = 591.3957 $[M\text{-}H]^+$ calc., 591.3955 $[M\text{-}H]^+$ found.

8.5.1.7 (dma)P_2P-(*t*Bu)-Et (6a-Et)

(dma)P_2P-(*t*Bu) (13.72 mg, 31.0 µmol, 1.00 eq.) and EtI (9.67 mg, 62 µmol, 2.00 eq.) gave a ratio of [dmaP_2PEt]/[dmaP_2H] of 45.4/54.6.

^{1}H-NMR (300 MHz, MeCN−d_3): δ (ppm) = 3.34 (dt, ^{1}J(P,H) = 936.2 Hz, ^{3}J(P,H) = 7.1 Hz, 1H, P-$\underline{H}$), 2.64 (d, ^{3}J(P,H) = 10.2 Hz, 18H, $NC\underline{H}_3$), 2.62 (d, ^{3}J(P,H) = 10.0 Hz, 18H, $NC\underline{H}_3$), 2.22–2.15 (m, 2H, PC$\underline{H}$2CH3), 1.22 (dt, ^{3}J(P,H) = 56.9 Hz, ^{3}J(H;H) = 7.2 Hz, 3H, $PCH_2C\underline{H}_3$), 1.15 (d, ^{3}J(P,H) = 17.6 Hz, 9H, $CC\underline{H}_3$), 1.06 (d, ^{3}J(P,H) = 15.0 Hz, 9H, $CC\underline{H}_3$).
$^{31}P\{^{1}H\}$-NMR (121 MHz, MeCN−d_3): δ (ppm) = 19.7 (d, ^{2}J(P,P) = 27.7 Hz, P(V)-Et^+), 17.0 (t, ^{2}J(P,P) = 27.7 Hz, P(III-Et^+), 14.9 (d, ^{2}J(P,P) = 21.1 Hz, P(V)-H^+), 12.9 (t, ^{2}J(P,P) = 21.1 Hz, P(III)-H^+).
ESI-MS = 471.3371 $[M\text{-}H]^+$ calc., 471.3396 $[M\text{-}H]^+$ found.

8.5.1.8 (pyrr)P_2P-*t*Bu-Et (6b-Et)

(pyrr)P_2P-*t*Bu (40.0 mg, 66.8 µmol, 1.00 eq.) and EtI (20.8 mg, 133.6 µmol, 2.00 eq.) gave a ratio of [PyrrP_2PEt]/[PyrrP_2H] of 1.4/98.6.

^{1}H-NMR (300 MHz, MeCN−d_3): δ (ppm) = 3.35 (dt, ^{1}J(P,H) = 562.3 Hz, ^{3}J(P,H) = 7.0 Hz, 1H, P-$\underline{H}$), 3.21–3.12 (m, $NC\underline{H}_2CH_2$, 24H), 2.26–2.18 (m, PC$\underline{H}$2CH3, 2H), 1.89–1.76 (m, $NCH_2C\underline{H}_2$, 24H), 1.30–1.19 (m, 5H, PCH_2CH_3), 1.13 (d, ^{3}J(P,H) = 16.2 Hz, 9H, $CC\underline{H}_3$).
$^{31}P\{^{1}H\}$-NMR (121 MHz, MeCN−d_3): δ (ppm) = 16.3 (t, ^{2}J(P,P) = 23.9 Hz, P(III)-H^+), 14.1 (d, ^{2}J(P,P) = 26.4 Hz, P(III)-Et^+), 3.7 (d, ^{2}J(P,P) = 25.9 Hz, P(V)-Et^+), 1.3 (d, ^{2}J(P,P) = 23.9 Hz, P(V)-H^+).
ESI-MS = 627.43 $[M\text{-}H]^+$ calc., 627.4308 $[M\text{-}H]^+$ found.

8.6 Computational section

All gas phase calculations were performed at the PBE[153]-def2tvp[154] or B3LYP[297–300]/6-31G*[301] level of theory. Solvent calculations were performed at the PBE-def2tzvp level of theory with the Conductor-like Polarizable Continuum Model (CPCM).[167] All structures were optimized without geometrical constraints and their vibrational frequencies were computed in order to confirm the energy surface of the optimized geometries as a global minimum. All calculations have been carried out using the ORCA program package.[302,303] Atom pairwise dispersion correction by Grimme *et al.* as well as auxiliary basis sets by Weigend *et al.*[304,305] were utilized. The vibrational entropy was computed according to Grimme.[306] Rotational entropy computed according to Herzberg.[307]

8.6.1 Donor capabilities

For the determination of the donor capabilities, the optimized structures of phosphazene base and the corresponding [L-Ni(CO)$_3$] complexes were calculated. After optimization, the molecules were aligned so that the Z-axis was aligned with the L-Ni bond. A single point frequency calculation was then carried out and the Mulliken Orbital charges were extracted. The values given were calculated as follows:[172]

$$\Delta s = s(L) - s(L - NiCO) \tag{8.16}$$

$$\Delta p_\sigma = p_z(L) - p_z(L - NiCO) \tag{8.17}$$

$$\Delta p_\pi = [p_x(L) + p_y(L)] - [p_x(L - NiCO) + p_y(L - NiCO)] \tag{8.18}$$

The sum of the donation ability of the ligand can now be calculated with with equation 8.19:[172]

$$\sum \Delta = \Delta s + \Delta P_\sigma - \Delta P_\pi \tag{8.19}$$

The ratio of σ- to π-donor ability is described by equation 8.20:[172]

$$\frac{\pi}{\sigma} = \frac{\Delta P_\pi}{(\Delta s + \Delta P_\sigma)} \tag{8.20}$$

s refers to the sum of all Mulliken s-type orbital charges.
$p_{x,y,z}$ refers to the sum of all Mulliken $p_{x,y,z}$-type orbital charges.

8.6.2 Bond energies

To calculate the bond and the fragmentation energies, phosphazene bases and their respective [L-Ni(CO)$_3$] complexes were calculated. The fragmentation energy was calculated using unrelaxed fragments of the complexes. The bond energy was calculated using relaxed fragments.[172]

$$E_{frag,bond} = E_{el}(L - Ni(CO)_3) - [E_{el}(L) + E_{el}(Ni(CO)_3] \tag{8.21}$$

8.6.3 Proton Affinities and Gas phase basicity

Gas phase basicities were calculated as the Gibbs free energy of the reaction:

$$L + H^+ \rightarrow LH^+$$

so that:

$$\Delta G = G_{(LH)} - [G_{(L)} + G_{(H^+)}] \tag{8.22}$$

Proton affinities have been calculated as the enthalpy of the aforementioned reaction.[85]

$$PA = H_{(LH^+)} - [H_{(L)} + H_{(H^+)}] \tag{8.23}$$

The values for the gas phase enthalpy and entropy of protons are:
$H_{(H^+)} = 1.48\ kcal/mol$
$S_{(H^+)} = 26.02\ kcal/(mol * K)$
$G_{(H^+)} = -6.28\ kcal/mol$.[166]

8.6.4 Cone Angles

Cone angles were calculated according to a mathematically rigorous method developed by Bilbrey *et al.*[109,110] This method is based on solving for the most acute right circular cone that contains the entire ligand. A Mathematica package FindSolidAngle developed by the authors was used to compute the cone angles.[168,308] The inputs for cone angle calculations were optimized geometries of [L-Ni] complexes.

8.6.5 Buried Volumes

Buried volumes were calculated according to a method developed by Cavallo et al.[309] Bond radii were scaled by 1.17, sphere radius of 3.5 Å, mesh spacing for numerical integration was 0.1 and H atoms were included in the calculations. The inputs were optimized geometries of [L-AuCl] complexes.

8.6.6 Basicity

All structures used for the determination of pK_A values have been calculated using the PBE functional[153] and def2tzvp[154] basis set. The values have been estimated according to the following thermodynamic cycle, as shown by Shields *et al.*[153]

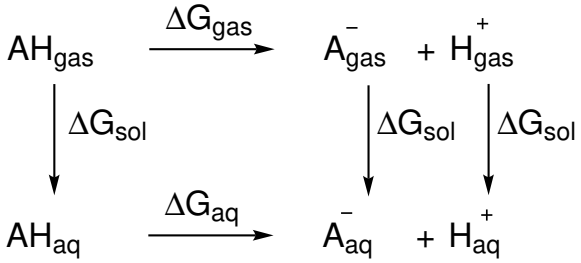

Abbildung 8.1: Thermodynamic cycle for estimating basicity in solution by SHIELDS *et. al.*

The basicity can therefore be described by the following equation:

$$\begin{aligned} pK_{(A)} = pK_{(AH^+)} + [&G_{gas}(B) - G_{gas}(A) - G_{gas}(BH^+) + G_{gas}(AH^+) + \\ &\Delta G_{sol}(B) - \Delta G_{sol}(A) - \Delta G_{sol}(BH^+) + \Delta G_{sol}(AH^+)] \ / \ 2.303\ RT \end{aligned} \tag{8.24}$$

As reference trimethylphosphine (PMe_3) was selected for MeCN. It has been chosen because of its similar geometry, electronic structure and known pK_A of 15.5.[310]

8.7 Crystallographic appendix

XRD Data were collected with a Bruker D8 Quest area detector diffractometer equipped with MoKα radiation, a graded multilayer mirror monochromator (λ = 0.71073 Å) and a Photon-100 CMOS detector or with a Stoe Stadivari diffractometer equipped with CuKα radiation, a graded multilayer mirror monochromator (λ = 1.54178 Å) and a Dectris Pilatus 300 K detector both using an oil-coated shock-cooled crystal at 100(2) K. Data collection, reduction, cell refinement and semi-empirical absorption correction (multi-scan) were performed within Bruker Apex3/Apex4[311–314] or Stoe X-Area.[315–318] Structures were solved with dual-space methods using ShelXT[319] and refined against F2 with ShelXL,[320] all within the user interface of WinGX[321] and ShelXLe.[322] Carbon bonded hydrogen atoms were calculated in their idealized positions and refined with fixed isotropic thermal parameters. Hydrogen atoms connected to heteroatoms were located on the Fourier map and refined isotropically. All molecular structures were illustrated with Diamond 4[323,324] using thermal ellipsoids at the 50% probability level. Peripheral protons as well as non-coordinating solvent molecules are omitted for clarity. In case of disorder, only the major component is displayed. Atom colors are assigned as shown below with reference to Jmol.[325] All Crystal structures were solved and refined by Eugen Sharikow.

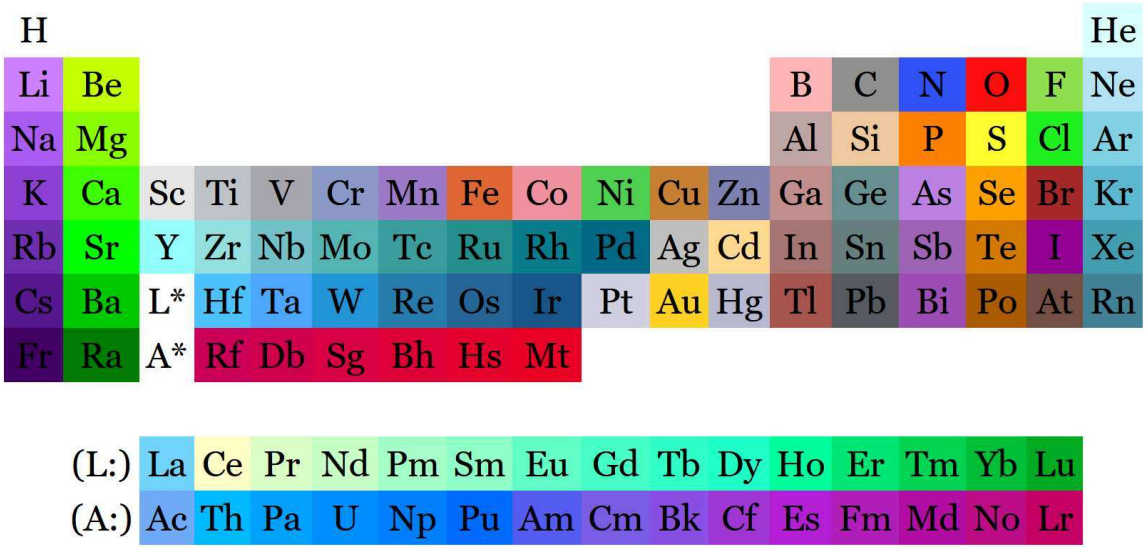

8.7.1 Crystal structure of dmaP$_1$P(tBu)$_2$-HBF$_4$ (SW71HBF4)

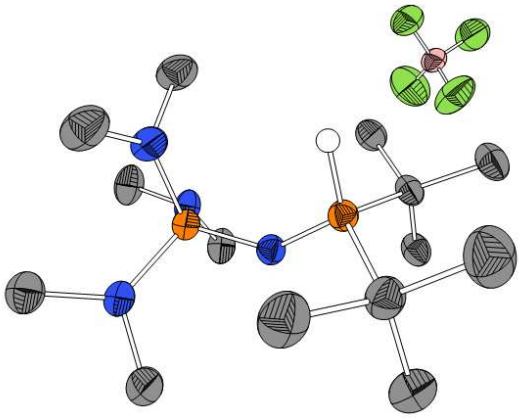

Crystal data

$C_{14}H_{37}BF_4N_4P_2$	M = 410.22 g mol^{-1}	monoclinic, $P\,21/a$
a = 8.9020(2) Å	b = 10.8893(2) Å	c = 22.6237(5) Å
α = 90°	β = 96.648(2)°	γ = 90°
V = 2178.32(8) Å^{-3}	Z = 4	
D_{calc} = 1.251 g cm^3	μ =2.161 mm^{-1}	$F(000)$ = 880
habit: colorless plate	0.395 x 0.279 x 0.158 mm^3	

Data collection

Diffraktometer: StadiVari	T = 100(2) K	λ = 1.54178 Å
$-5 \leq h \leq 11$	$-13 \leq k \leq 13$	$-28 \leq k \leq 25$
22945 Refl. collected	4486 independent refl.	3826 refl. [$I > 2\sigma(I)$]
R_{int} = 0.0367	$C_{67.679°}$ = 99.6%	θ = 3.934 to 76.046°
Absorption corr.: Multiscan	Tr_{min} = 0.2557	Tr_{max} = 0.9908

Refinement

4486 reflections	48 restraints	280 parameters
Solution: SHELXT	Ref.: SHELXL 2018/3	
R_1 ($I > 2\sigma(I)$) = 0.0632	R_1 (all) = 0.0704	$GooF$ (F^2) = 1.118
wR_2 ($I > 2\sigma(I)$) = 0.178	wR_2 (all) =0.1854	
$\Delta\rho_{min}$ = −0.505 e Å^{-3}	$\Delta\rho_{max}$ = 0.872 e Å^{-3}	

Refinement special details:
The dataset was refined with ISOR, SIMU and DELU. Parts of the structure were disordered with PART.

8.7.2 Crystal structure of [(dma)P_1P-(tBu)$_2$-Pd(cinn)Cl] (SW71PdCinn)

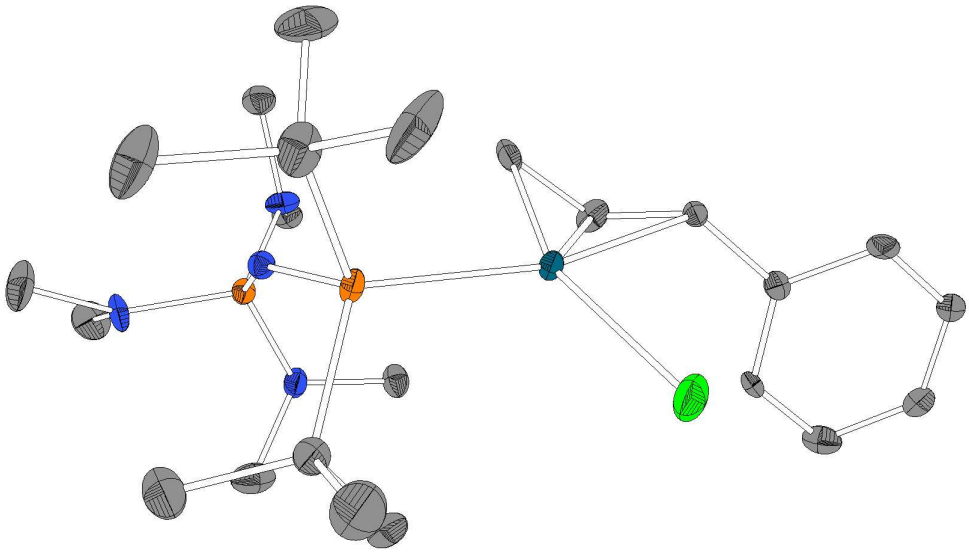

Crystal data

$C_{23}H_{45}ClN_4P_2Pd$	M = 581.42 g mol^{-1}	triclinic, P-1
a = 11.0253(7) Å	b = 15.3149(9) Å	c = 17.9705(11) Å
α = 107.041(2)°	β = 91.531(2)°	γ = 106.131(2)°
V = 2767.5(3) Å^{-3}	Z = 4	
D_{calc} = 1.395 g cm^3	μ =0.9 mm^{-1}	$F(000)$ = 1216
habit: colorless block	0.119 x 0.083 x 0.078 mm^3	

Data collection

Diffraktometer: D8 Quest	T = 100(2) K	λ = 0.71073 Å
$-13 \leq h \leq 13$	$-18 \leq k \leq 17$	$0 \leq k \leq 21$
10503 Refl. collected	10503 independent refl.	8796 refl. [$I > 2\sigma(I)$]
R_{int} = 0.0887	$C_{25.052°}$ = 92.2%	θ = 1.936 to 25.052°
Absorption corr.: Multiscan	Tr_{min} = 0.652333	Tr_{max} = 0.74516

Refinement

10503 reflections	36 restraints	585 parameters
Solution: SHELXT	Ref.: SHELXL 2018/3	
R_1 ($I > 2\sigma(I)$) = 0.0527	R_1 (all) = 0.0731	$GooF$ (F^2) = 1.06
wR_2 ($I > 2\sigma(I)$) = 0.0889	wR_2 (all) =0.0964	
$\Delta\rho_{min}$ = −1.366 e Å^{-3}	$\Delta\rho_{max}$ = 0.948 e Å^{-3}	E = 0.00057(10)

Refinement special details:
The dataset was refined with ISOR, SIMU and DELU and parts of the structure were disordered with PART.

8.7.3 Crystal structure of $(PPh_3)_2Pd(O_2)$ (SW77THF)

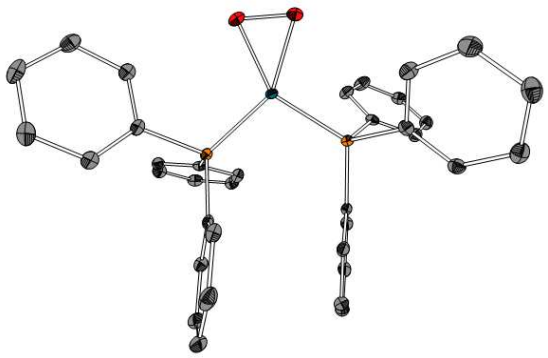

Crystal data

$C_{40}H_{38}O_3P_2Pd$	M = 735.04 g mol^{-1}	monoclinic, P21/c
a = 16.0159(7) Å	b = 11.2806(5) Å	c = 18.4150(8) Å
α = 90°	β = 90.982(2)°	γ = 90°
V = 3326.5(3) Å^{-3}	Z = 4	
D_{calc} = 1.468 g cm^3	μ =0.693 mm^{-1}	*F(000)* = 1512
habit: colorless block	0.472 x 0.320 x 0.206 mm^3	

Data collection

Diffraktometer: D8 Quest	T = 100(2) K	λ = 0.71073 Å
$-19 \leq h \leq 19$	$-13 \leq k \leq 13$	$-21 \leq k \leq 21$
63510 Refl. collected	5922 independent refl.	5712 refl. [$I > 2\sigma(I)$]
R_{int} = 0.023	$C_{25.116°}$ = 99.8%	θ = 2.117 to 25.116°
Absorption corr.: Multiscan	Tr_{min} = 0.6721	Tr_{max} = 0.7452

Refinement

5922 reflections	6 restraints	416 parameters
Solution: SHELXT	Ref.: SHELXL 2018/3	
R_1 ($I > 2\sigma(I)$) = 0.018	R_1 (all) = 0.0189	*GooF* (F^2) = 1.055
wR_2 ($I > 2\sigma(I)$) = 0.0458	wR_2 (all) =0.0463	
$\Delta\rho_{min}$ = −0.37 e Å^{-3}	$\Delta\rho_{max}$ = 0.403 e Å^{-3}	E = 0.00123(9)

Refinement special details:
The dataset was refined with ISOR.

8.7.4 Crystal structure of (dma)P_1P-(tBu)$_2$-AuCl (SW80)

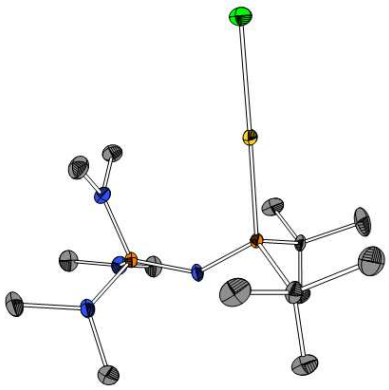

Crystal data

$C_{14}H_{36}AuClN_4P_2$	M = 554.82 g mol^{-1}	orthorhombic, P212121
a = 9.5324(4) Å	b = 13.6200(6) Å	c = 16.3089(8) Å
α = 90°	β = 90°	γ = 90°
V = 2117.41(17) Å^{-3}	Z = 4	
D_{calc} = 1.74 g cm^3	μ =7.228 mm^{-1}	$F(000)$ = 1096
habit: colorless block	0.300 x 0.287 x 0.168 mm^3	

Data collection

Diffraktometer: D8 Quest	T = 100(2) K	λ = 0.71073 Å
$-11 \leq h \leq 11$	$-16 \leq k \leq 16$	$-19 \leq k \leq 19$
20572 Refl. collected	3651 independent refl.	3613 refl. [$I > 2\sigma(I)$]
R_{int} = 0.0278	$C_{25\text{-}084^\circ}$ = 99.7%	θ = 2.475 to 25.084°
Absorption corr.: Multiscan	Tr_{min} = 0.4593	Tr_{max} = 0.7452

Refinement

3651 reflections	12 restraints	223 parameters
Solution: SHELXT	Ref.: SHELXL 2018/3	
R_1 ($I > 2\sigma(I)$) = 0.0125	R_1 (all) = 0.0127	$GooF$ (F^2) = 1.094
wR_2 ($I > 2\sigma(I)$) = 0.0311	wR_2 (all) =0.0312	
$\Delta\rho_{min}$ = −0.779 e Å^{-3}	$\Delta\rho_{max}$ = 0.329 e Å^{-3}	

Refinement special details:
Some reflections near the beamstop were omitted from the least-squares refinement using OMIT. The dataset was refined as 2-component inversion twin (97:3) and parts of the structure were disordered with ISOR and PART.

8.7.5 Crystal structure of (dma)P_1P-(tBu)$_2$-Ni(CO)$_3$ (SW81)

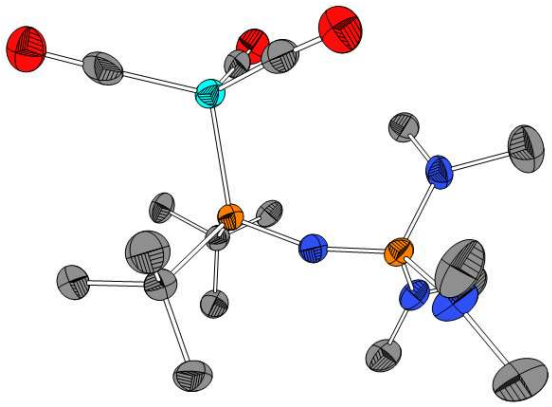

Crystal data

$C_{17}H_{36}N_4NiO_3P_2$	M = 465.15 g mol^{-1}	monoclinic, P21/c
a = 8.4273(4) Å	b = 13.0769(7) Å	c = 21.0193(10) Å
α = 90°	β = 90.469(4)	γ = 90°
V = 2316.3(2) Å^{-3}	Z = 4	
D_{calc} = 1.334 g cm^3	μ =2.707 mm^{-1}	*F(000)* = 992
habit: colorless block	0.050 x 0.037 x 0.021 mm^3	

Data collection

Diffraktometer: StadiVari	T = 100(2) K	λ = 1.54178 Å
$-10 \leq h \leq 10$	$-16 \leq k \leq 15$	$-16 \leq k \leq 25$
22270 Refl. collected	4787 independent refl.	3475 refl. [$I > 2\sigma(I)$]
R_{int} = 0.0832	$C_{67.679°}$ = 99.7%	θ = 3.981 to 75.929°
Absorption corr.: Multiscan	Tr_{min} = 1	Tr_{max} = 1

Refinement

4787 reflections	0 restraints	257 parameters
Solution: SHELXT	Ref.: SHELXL 2018/3	
R_1 ($I > 2\sigma(I)$) = 0.079	R_1 (all) = 0.1146	*GooF* (F^2) = 1.071
wR_2 ($I > 2\sigma(I)$) = 0.1855	wR_2 (all) =0.2133	
$\Delta\rho_{min}$ = −0.548 e Å^{-3}	$\Delta\rho_{max}$ = 0.535 e Å^{-3}	

Refinement special details:
Some reflections were omitted from the least-squares refinement using OMIT.

8.7.6 Crystal structure of (*t*Bu)P_1P-(*t*Bu)$_2$ (SW89)

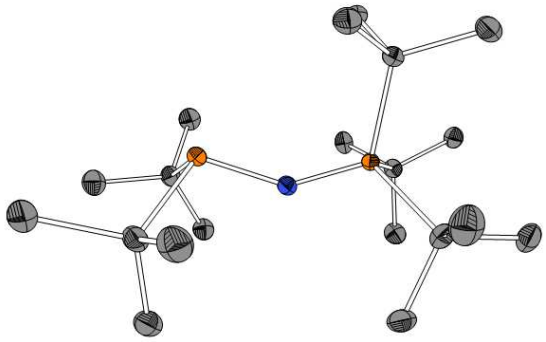

Crystal data

$C_{20}H_{45}N_1P_2$	M = 361.51 g mol^{-1}	monoclinic, P21/n
a = 8.5196(1) Å	b = 15.0254(16) Å	c = 17.1907(18) Å
α = 90°	β = 92.054(5)	γ = 90°
V = 2199.2(4) Å^{-3}	Z = 4	
D_{calc} = 1.092 g cm^3	μ =0.2 mm^{-1}	*F(000)* = 808
habit: colorless needle	0.428 x 0.220 x 0.152 mm^3	

Data collection

Diffraktometer: D8 Quest	T = 100(2) K	λ = 0.71073 Å
$-10 \leq h \leq 10$	$-17 \leq k \leq 17$	$-20 \leq k \leq 20$
42478 Refl. collected	3890 independent refl.	3504 refl. [$I > 2\sigma(I)$]
R_{int} = 0.0351	$C_{25.04°}$ = 99.9%	θ = 2.371 to 25.040°
Absorption corr.: Multiscan	Tr_{min} = 0.7159	Tr_{max} = 0.7452

Refinement

3890 reflections	0 restraints	223 parameters
Solution: SHELXT	Ref.: SHELXL 2018/3	
R_1 ($I > 2\sigma(I)$) = 0.0278	R_1 (all) = 0.031	*GooF* (F^2) = 1.068
wR_2 ($I > 2\sigma(I)$) = 0.0748	wR_2 (all) =0.0762	
$\Delta\rho_{min}$ = −0.188 e Å^{-3}	$\Delta\rho_{max}$ = 0.362 e Å^{-3}	

8.7.7 Crystal structure of (dma)P_1P-(tBu)$_2$-Se (SW90)

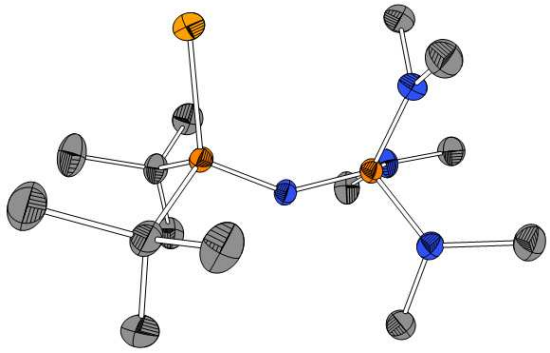

Crystal data

$C_{14}H_{36}N_4P_2Se$	M = 401.37 g mol^{-1}	monoclinic, P21/n
a = 15.0971(4) Å	b = 9.5672(2) Å	c = 15.9267(4) Å
α = 90°	β = 117.837(2)	γ = 90°
V = 2034.20(9) Å^{-3}	Z = 4	
D_{calc} = 1.311 g cm^3	μ =3.979 mm^{-1}	*F(000)* = 848
habit: yellow needle	0.266 x 0.195 x 0.100 mm^3	

Data collection

Diffraktometer: StadiVari	T = 100(2) K	λ = 1.54178 Å
$-13 \leq h \leq 18$	$-11 \leq k \leq 10$	$-19 \leq k \leq 16$
19499 Refl. collected	4165 independent refl.	3616 refl. [$I > 2\sigma(I)$]
R_{int} = 0.0417	$C_{67.679°}$ = 99.8%	θ = 3.332 to 75.504°
Absorption corr.: Multiscan	Tr_{min} = 0.4043	Tr_{max} = 0.9908

Refinement

4165 reflections	0 restraints	202 parameters
Solution: SHELXT	Ref.: SHELXL 2018/3	
R_1 ($I > 2\sigma(I)$) = 0.0346	R_1 (all) = 0.04	*GooF* (F^2) = 1.052
wR_2 ($I > 2\sigma(I)$) = 0.0951	wR_2 (all) =0.0974	
$\Delta\rho_{min}$ = −0.613 e Å^{-3}	$\Delta\rho_{max}$ = 0.46 e Å^{-3}	

8.7.8 Crystal structure of (*t*Bu)P_1P-(*t*Bu)$_2$-Ni(CO)$_3$ (SW92)

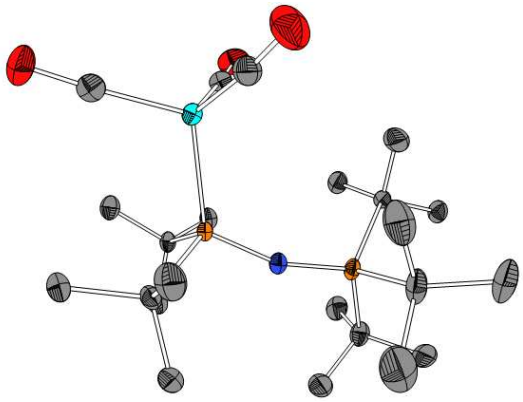

Crystal data

$C_{23}H_{45}NNiO_3P_2$	M = 504.25 g mol^{-1}	triclinic, P-1
a = 8.8282(5) Å	b = 10.0943(6) Å	c = 16.2338(10) Å
α = 105.948(2)	β = 91.650(2)	γ = 106.128(2)
V = 1327.56(14) Å^{-3}	Z = 2	
D_{calc} = 1.261 g cm^3	μ =0.874 mm^{-1}	*F(000)* = 544
habit: colorless plate	0.389 x 0.300 x 0.177 mm^3	

Data collection

Diffraktometer: D8 Quest	T = 100(2) K	λ = 0.71073 Å
$-10 \leq h \leq 10$	$-12 \leq k \leq 11$	$0 \leq k \leq 19$
35784 Refl. collected	4684 independent refl.	4333 refl. [$I > 2\sigma(I)$]
R_{int} = 0.0414	$C_{25.031°}$ = 99.7%	θ = 2.198 to 25.031°
Absorption corr.: Multiscan	Tr_{min} = 0.633837	Tr_{max} = 0.74516

Refinement

4684 reflections	22 restraints	379 parameters
Solution: SHELXT	Ref.: SHELXL 2018/3	
R_1 ($I > 2\sigma(I)$) = 0.0285	R_1 (all) = 0.0344	*GooF* (F^2) = 1.088
wR_2 ($I > 2\sigma(I)$) = 0.0614	wR_2 (all) =0.0642	
$\Delta\rho_{min}$ = −0.245 e Å^{-3}	$\Delta\rho_{max}$ = 0.314 e Å^{-3}	

Refinement special details:
The dataset was refined as 2-component inversion twin (80:20) and parts of the structure were disordered with ISOR, SAME and PART.

8.7.9 Crystal structure of $(dmaP_1P)_2Pd_2Cl_4$ (SW129)

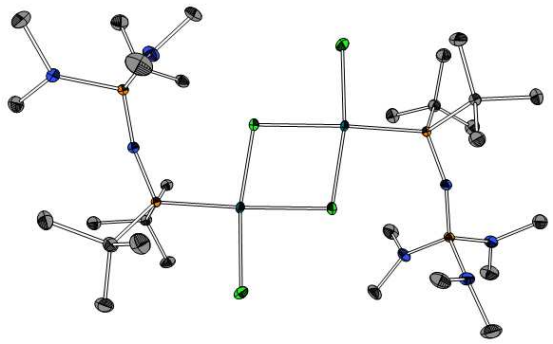

Crystal data

$C_{28}H_{72}Cl_4N_8P_4Pd_2$	M = 999.41 g mol^{-1}	monoclinic, P21/c
a = 15.0869(7) Å	b = 10.8816(5) Å	c = 14.4529(6) Å
α = 90	β = 116.5350(10)	γ = 90
V = 2122.79(17) Å^{-3}	Z = 2	
D_{calc} = 1.564 g cm^3	μ =1.281 mm^{-1}	*F(000)* = 1032
habit: yellow block	0.393 x 0.388 x 0.190 mm^3	

Data collection

Diffraktometer: D8 Quest	T = 100(2) K	λ = 0.71073 Å
$-19 \leq h \leq 19$	$-13 \leq k \leq 13$	$-18 \leq k \leq 18$
51567 Refl. collected	4715 independent refl.	4546 refl. [$I > 2\sigma(I)$]
R_{int} = 0.0227	$C_{25.242°}$ = 99.9%	θ = 2.404 to 27.181°
Absorption corr.: Multiscan	Tr_{min} = 0.6593	Tr_{max} = 0.7455

Refinement

4715 reflections	0 restraints	220 parameters
Solution: SHELXT	Ref.: SHELXL 2018/3	
R_1 ($I > 2\sigma(I)$) = 0.0151	R_1 (all) = 0.0159	*GooF* (F^2) = 1.127
wR_2 ($I > 2\sigma(I)$) = 0.0388	wR_2 (all) =0.091	
$\Delta\rho_{min}$ = −0.511 e Å^{-3}	$\Delta\rho_{max}$ = 0.393 e Å^{-3}	

Refinement special details:
Some reflections near the beamstop were omitted from the least-squares refinement using OMIT.

8.7.10 Crystal structure of (pyrr)P_1P-(tBu)$_2$ (SW135)

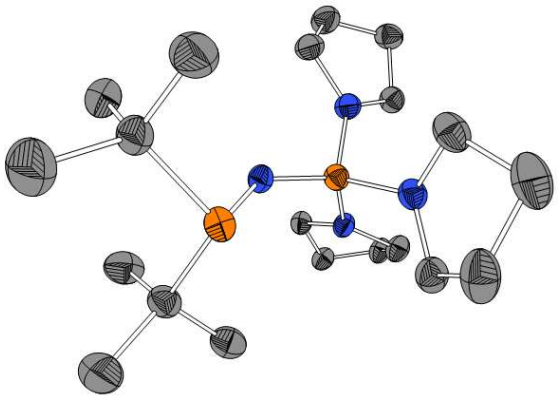

Crystal data

$C_{20}H_{42}N_4P_2$	M = 400.51 g mol^{-1}	monoclinic, P21/c
a = 11.5930(7) Å	b = 9.1066(4) Å	c = 22.1809(14) Å
α = 90	β = 100.754(5)	γ = 90
V = 2300.6(2) Å^{-3}	Z = 4	
D_{calc} = 1.156 g cm^3	μ =1.787 mm^{-1}	*F(000)* = 880
habit: colorless plate	0.350 x 0.130 x 0.101 mm^3	

Data collection

Diffraktometer: StadiVari	T = 100(2) K	λ = 1.54178 Å
$-11 \leq h \leq 14$	$-11 \leq k \leq 11$	$-24 \leq k \leq 27$
29409 Refl. collected	4731 independent refl.	3146 refl. $[I > 2\sigma(I)]$
R_{int} = 0.0862	$C_{67.679°}$ = 99.5%	θ = 3.881 to 75.940°
Absorption corr.: Multiscan	Tr_{min} = 0.197	Tr_{max} = 1

Refinement

4731 reflections	0 restraints	242 parameters
Solution: SHELXT	Ref.: SHELXL 2018/3	
R_1 ($I > 2\sigma(I)$) = 0.0527	R_1 (all) = 0.0782	*GooF* (F^2) = 0.912
wR_2 ($I > 2\sigma(I)$) = 0.1292	wR_2 (all) =0.1379	
$\Delta\rho_{min}$ = −0.351 e Å^{-3}	$\Delta\rho_{max}$ = 0.301 e Å^{-3}	E = 0.0026(3)

Refinement special details:
The dataset was refined as non-merohedral 2-component twin (80:20) and parts of the structure were disordered with ISOR, SAME and PART.

8.7.11 Crystal structure of (pyrr)P_1P-(tBu)$_2$-HPF_6 (SW135HPF6)

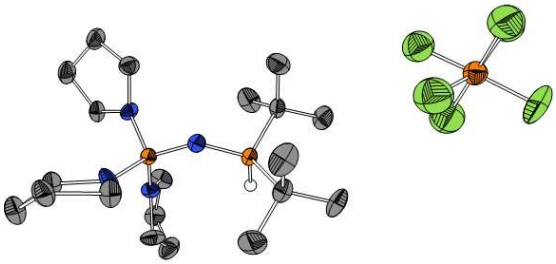

Crystal data

$C_{20}H_{43}F_6N_4P_3$	M = 546.49 g mol^{-1}	monoclinic, P21/n
a = 15.583(2) Å	b = 8.6366(12) Å	c = 20.321(3) Å
α = 90	β = 104.534(4)	γ = 90
V = 2647.4(6) Å^{-3}	Z = 4	
D_{calc} = 1.371 g cm^3	μ =0.283 mm^{-1}	*F(000)* = 1160
habit: colorless block	0.320 x 0.285 x 0.116 mm^3	

Data collection

Diffraktometer: D8 Quest	T = 100(2) K	λ = 0.71073 Å
$-18 \leq h \leq 18$	$-10 \leq k \leq 10$	$-23 \leq k \leq 24$
33463 Refl. collected	4676 independent refl.	3338 refl. [$I > 2\sigma(I)$]
R_{int} = 0.0937	$C_{25.021°}$ = 99.9%	θ = 2.071 to 25.021°
Absorption corr.: Multiscan	Tr_{min} = 0.6199	Tr_{max} = 0.7452

Refinement

4676 reflections	67 restraints	400 parameters
Solution: SHELXT	Ref.: SHELXL 2018/3	
R_1 ($I > 2\sigma(I)$) = 0.8	R_1 (all) = 0.1145	*GooF* (F^2) = 1.07
wR_2 ($I > 2\sigma(I)$) = 0.1811	wR_2 (all) =0.2017	
$\Delta\rho_{min}$ = −0.766 e Å^{-3}	$\Delta\rho_{max}$ = 1.056 e Å^{-3}	

Refinement special details:
The dataset was refined with ISOR and SHEL and parts of the structure were disordered with PART.

8.7.12 Crystal structure of (dma)P_2P-*t*Bu-AuCl (SW138)

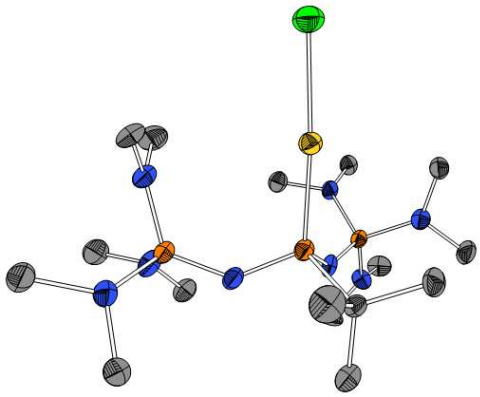

Crystal data

$C_{16}H_{45}AuClN_8P_3$	M = 674.92 g mol^{-1}	orthorhombic, P*bca*
a = 11.185(2) Å	b = 15.366(3) Å	c = 32.051(6) Å
α = 90	β = 90	γ = 90
V = 5508.7(19) Å^{-3}	Z = 8	
D_{calc} = 1.628 g cm^3	μ =5.631 mm^{-1}	*F(000)* = 2804
habit: colorless plate	0.406 x 0.296 x 0.114 mm^3	

Data collection

Diffraktometer: D8 Quest	T = 100(2) K	λ = 0.71073 Å
$-13 \leq h \leq 13$	$-18 \leq k \leq 18$	$-38 \leq k \leq 38$
93272 Refl. collected	4904 independent refl.	4011 refl. [$I > 2\sigma(I)$]
R_{int} = 0.084	$C_{25.093°}$ = 99.8%	θ = 2.220 to 25.093°
Absorption corr.: Multiscan	Tr_{min} = 0.5301	Tr_{max} = 0.7452

Refinement

4904 reflections	6 restraints	277 parameters
Solution: SHELXT	Ref.: SHELXL 2018/3	
R_1 ($I > 2\sigma(I)$) = 0.0492	R_1 (all) = 0.0699	*GooF* (F^2) = 1.314
wR_2 ($I > 2\sigma(I)$) = 0.0977	wR_2 (all) =0.0156	
$\Delta\rho_{min}$ = −2.766 e Å^{-3}	$\Delta\rho_{max}$ = 1.539 e Å^{-3}	

Refinement special details:
The dataset was refined with ISOR.

8.7.13 Crystal structure of $Pd(dmaP_1P)_2Cl_2$ (SW139)

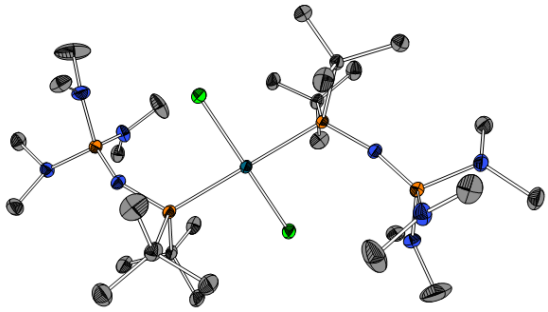

Crystal data

$C_{28}H_{72}Cl_2N_8P_4Pd$	M = 822.11 g mol^{-1}	orthorhombic, P*bca*
a = 15.1537(7) Å	b = 15.0034(6) Å	c = 17.8508(5) Å
α = 90	β = 90	γ = 90
V = 4058.5(3) Å^{-3}	Z = 4	
D_{calc} = 1.345 g cm^3	μ =6.618 mm^{-1}	*F(000)* = 1744
habit: yellow block	0.156 x 0.120 x 0.097 mm^3	

Data collection

Diffraktometer: StadiVari	T = 100(2) K	λ = 1.54178 Å
$-16 \leq h \leq 18$	$-17 \leq k \leq 14$	$-20 \leq k \leq 21$
45017 Refl. collected	3574 independent refl.	2719 refl. [$I > 2\sigma(I)$]
R_{int} = 0.0583	$C_{66.595°}$ = 99.9%	θ = 4.831 to 66.595°
Absorption corr.: Multiscan	Tr_{min} = 0.4262	Tr_{max} = 1

Refinement

3574 reflections	0 restraints	209 parameters
Solution: SHELXT	Ref.: SHELXL 2018/3	
R_1 ($I > 2\sigma(I)$) = 0.0237	R_1 (all) = 0.0349	*GooF* (F^2) = 0.908
wR_2 ($I > 2\sigma(I)$) = 0.0565	wR_2 (all) =0.0583	
$\Delta\rho_{min}$ = −0.327 e Å^{-3}	$\Delta\rho_{max}$ = 0.426 e Å^{-3}	E = 0.000088(17)

Refinement special details:
Some reflections were omitted from the least-squares refinement using OMIT and SHEL.

8.7.14 Crystal structure of $Pd(dmaP_1P)_2Cl_2$ (SW156)

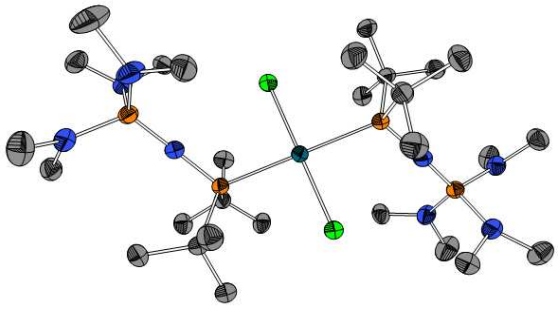

Crystal data

$C_{28}H_{72}Cl_2N_8P_4Pd$	M = 822.11 g mol^{-1}	triclinic, P -1
a = 8.6739(2) Å	b = 10.8336(2) Å	c = 11.8819(3) Å
α = 75.506(2)	β = 77.028(2)	γ = 70.012(2)
V = 1003.98(4) Å^{-3}	Z = 1	
D_{calc} = 1.36 g cm^3	μ =6.688 mm^{-1}	*F(000)* = 436
habit: yellow block	0.249 x 0.236 x 0.138 mm^3	

Data collection

Diffraktometer: StadiVari	T = 100(2) K	λ = 1.54178 Å
$-10 \leq h \leq 9$	$-13 \leq k \leq 12$	$-14 \leq k \leq 7$
24953 Refl. collected	4122 independent refl.	4063 refl. [$I > 2\sigma(I)$]
R_{int} = 0.0489	$C_{67.679°}$ = 99.4%	θ = 3.888 to 76.054°
Absorption corr.: Multiscan	Tr_{min} = 0.2865	Tr_{max} = 1

Refinement

4122 reflections	0 restraints	209 parameters
Solution: SHELXT	Ref.: SHELXL 2018/3	
R_1 ($I > 2\sigma(I)$) = 0.0471	R_1 (all) = 0.0475	*GooF* (F^2) = 1.131
wR_2 ($I > 2\sigma(I)$) = 0.1285	wR_2 (all) =0.1301	
$\Delta\rho_{min}$ = −0.928 e Å^{-3}	$\Delta\rho_{max}$ = 0.734 e Å^{-3}	E = 0.0089(7)

Refinement special details:
Some reflections were omitted from the least-squares refinement using OMIT.

8.7.15 Crystal structure of (dma)P_1P-(Odipp)$_2$ (SW185)

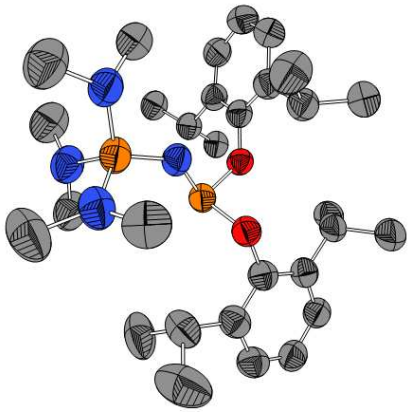

Crystal data

$C_{30}H_{52}N_4O_2P_2$	M = 562.69 g mol^{-1}	orthorhombic, P*bca*
a = 17.7533(3) Å	b = 16.6975(3) Å	c = 22.3427(5) Å
α = 90	β = 90	γ = 90
V = 6623.2(2) Å^{-3}	Z = 8	
D_{calc} = 1.129 g cm^3	μ =1.424 mm^{-1}	*F(000)* = 2448
habit: colorless needle	0.149 x 0.060 x 0.054 mm^3	

Data collection

Diffraktometer: StadiVari	T = 100(2) K	λ = 1.54178 Å
$-11 \leq h \leq 22$	$-20 \leq k \leq 19$	$-28 \leq k \leq 27$
80658 Refl. collected	6885 independent refl.	4173 refl. [$I > 2\sigma(I)$]
R_{int} = 0.1381	$C_{67.679°}$ = 99.9%	θ = 3.957 to 76.161°
Absorption corr.: Multiscan	Tr_{min} = 0.2047	Tr_{max} = 1

Refinement

6885 reflections	0 restraints	358 parameters
Solution: SHELXT	Ref.: SHELXL 2018/3	
R_1 ($I > 2\sigma(I)$) = 0.0986	R_1 (all) = 0.1365	*GooF* (F^2) = 0.993
wR_2 ($I > 2\sigma(I)$) = 0.2435	wR_2 (all) =0.292	
$\Delta\rho_{min}$ = −0.417 e Å^{-3}	$\Delta\rho_{max}$ = 0.509 e Å^{-3}	E = 0.0043(5)

Refinement special details:
Some reflections were omitted from the least-squares refinement using OMIT.

8.7.16 Crystal structure of SW196

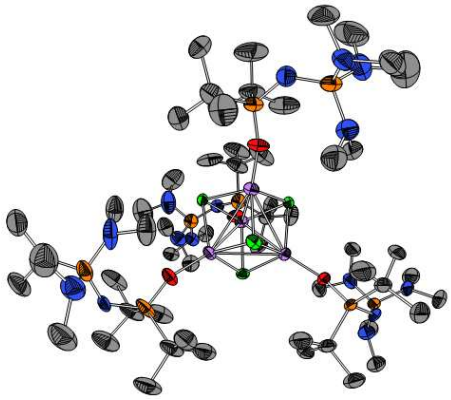

Crystal data

$C_{62}H_{158}Cl_4Li_4N_{16}O_4P_8$	M = 1609.35 g mol^{-1}	monoclinic, C2/c
a = 26.2404(14) Å	b = 13.5481(7) Å	c = 26.4904(15) Å
α = 90	β = 91.618(2)	γ = 90
V = 9413.8(9) Å^{-3}	Z = 4	
D_{calc} = 1.136 g cm^3	μ =0.308 mm^{-1}	*F(000)* = 3496
habit: colorless needle	0.410 x 0.172 x 0.148 mm^3	

Data collection

Diffraktometer: D8 Quest	T = 100(2) K	λ = 0.71073 Å
$-31 \leq h \leq 31$	$-16 \leq k \leq 16$	$-31 \leq k \leq 31$
81285 Refl. collected	8318 independent refl.	6089 refl. [$I > 2\sigma(I)$]
R_{int} = 0.0708	$C_{25.027°}$ = 100%	θ = 1.849 to 25.027°
Absorption corr.: Multiscan	Tr_{min} = 0.7102	Tr_{max} = 0.7452

Refinement

8318 reflections	257 restraints	645 parameters
Solution: SHELXT	Ref.: SHELXL 2018/3	
R_1 ($I > 2\sigma(I)$) = 0.0784	R_1 (all) = 0.1093	*GooF* (F^2) = 1.056
wR_2 ($I > 2\sigma(I)$) = 0.1781	wR_2 (all) =0.1974	
$\Delta\rho_{min}$ = −0.631 e Å^{-3}	$\Delta\rho_{max}$ = 1.128 e Å^{-3}	

Refinement special details:
Some reflections were omitted from the least-squares refinement using SHEL. The dataset was refined with ISOR and parts of the structure were disordered with PART and SAME.

8.7.17 Crystal structure of (cy)P_1P-(tBu)$_2$ (SW236)

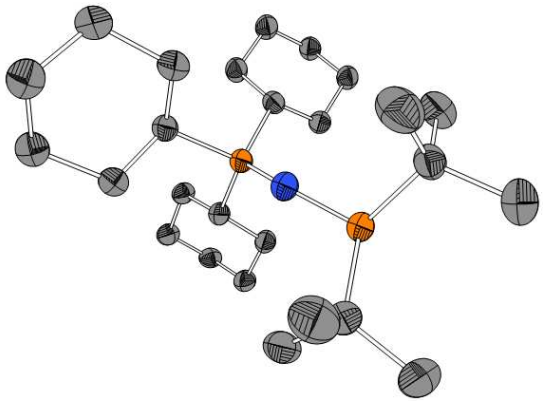

Crystal data

$C_{26}H_{51}NP_2$	M = 439.61 g mol^{-1}	triclinic, P-1
a = 9.7058(6) Å	b = 10.4638(6) Å	c = 13.7516(9) Å
α = 85.022(5)	β = 85.238(5)	γ = 78.102(5)
V = 1358.41(15) Å^{-3}	Z = 2	
D_{calc} = 1.075 g cm^3	μ =1.517 mm^{-1}	$F(000)$ = 488
habit: colorless needle	0.351 x 0.110 x 0.074 mm^3	

Data collection

Diffraktometer: StadiVari	T = 100(2) K	λ = 1.54178 Å
$-11 \leq h \leq 12$	$-13 \leq k \leq 12$	$-17 \leq k \leq 11$
33472 Refl. collected	5541 independent refl.	4331 refl. [$I > 2\sigma(I)$]
R_{int} = 0.0589	$C_{67.679°}$ = 99%	θ = 3.233 to 75.979°
Absorption corr.: Multiscan	Tr_{min} = 0.2843	Tr_{max} = 1

Refinement

5541 reflections	0 restraints	268 parameters
Solution: SHELXT	Ref.: SHELXL 2018/3	
R_1 ($I > 2\sigma(I)$) = 0.0594	R_1 (all) = 0.0713	$GooF$ (F^2) = 1.03
wR_2 ($I > 2\sigma(I)$) = 0.1594	wR_2 (all) =0.1673	
$\Delta\rho_{min}$ = −0.492 e Å^{-3}	$\Delta\rho_{max}$ = 0.839 e Å^{-3}	

Refinement special details:
Some reflections were omitted from the least-squares refinement using OMIT.

8.7.18 Crystal structure of (cy)P_1P-(tBu)$_2$·H_2O (SW236b)

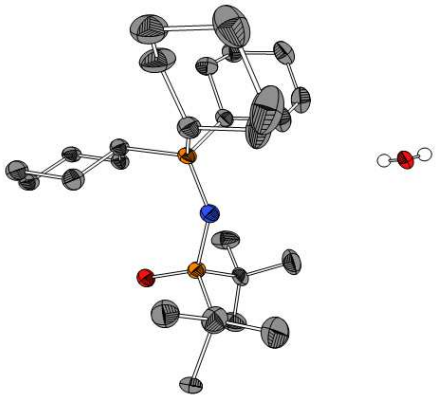

Crystal data

$C_{26}H_{53}NO_2P_2$	M = 473.63 g mol^{-1}	triclinic, P-1
a = 10.2581(3) Å	b = 10.9676(3) Å	c = 12.8716(3) Å
α = 87.674(2)	β = 82.154(2)	γ = 77.367(2)
V = 1399.77(7) Å^{-3}	Z = 2	
D_{calc} = 1.124 g cm^3	μ =1.559 mm^{-1}	*F(000)* = 524
habit: colorless plate	0.163 x 0.128 x 0.094 mm^3	

Data collection

Diffraktometer: StadiVari	T = 100(2) K	λ = 1.54178 Å
$-9 \leq h \leq 12$	$-11 \leq k \leq 13$	$-14 \leq k \leq 15$
30509 Refl. collected	4890 independent refl.	4068 refl. $[I > 2\sigma(I)]$
R_{int} = 0.0295	$C_{66.588°}$ = 98.9%	θ = 3.466 to 66.588°
Absorption corr.: Multiscan	Tr_{min} = 0.5176	Tr_{max} = 1

Refinement

4890 reflections	42 restraints	337 parameters
Solution: SHELXT	Ref.: SHELXL 2018/3	
R_1 ($I > 2\sigma(I)$) = 0.0478	R_1 (all) = 0.0566	*GooF* (F^2) = 1.096
wR_2 ($I > 2\sigma(I)$) = 0.1308	wR_2 (all) =0.1348	
$\Delta\rho_{min}$ = −0.355 e Å^{-3}	$\Delta\rho_{max}$ = 0.911 e Å^{-3}	

Refinement special details:
Some reflections were omitted from the least-squares refinement using OMIT. The dataset was refined with ISOR and EADP and parts of the structure were disordered with PART.

8.7.19 Crystal structure of (dma)P_1P-(tBu)$_2$ (SW244)

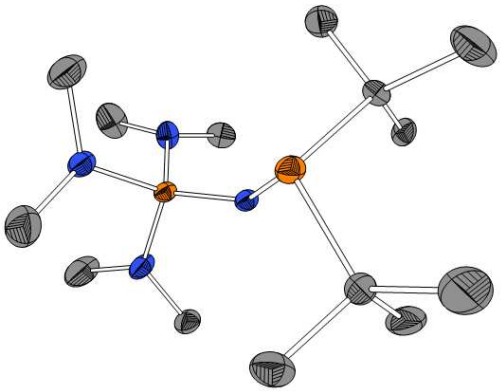

Crystal data

$C_{14}H_{36}N_4P_2$	M = 322.41 g mol^{-1}	monoclinic, P21/n
a = 8.3246(6) Å	b = 14.8514(10) Å	c = 15.8005(10) Å
α = 90	β = 93.081(2)	γ = 90
V = 1950.6(2) Å^{-3}	Z = 4	
D_{calc} = 1.098 g cm^3	μ =0.222 mm^{-1}	*F(000)* = 712
habit: colorless plate	0.430 x 0.341 x 0.240 mm^3	

Data collection

Diffraktometer: D8 Quest	T = 100(2) K	λ = 0.71073 Å
$-9 \leq h \leq 9$	$-17 \leq k \leq 17$	$-18 \leq k \leq 18$
18846 Refl. collected	3443 independent refl.	2429 refl. [$I > 2\sigma(I)$]
R_{int} = 0.0786	$C_{25.04°}$ = 99.9%	θ = 2.582 to 25.040°
Absorption corr.: Multiscan	Tr_{min} = 0.6594	Tr_{max} = 0.7452

Refinement

3443 reflections	30 restraints	233 parameters
Solution: SHELXT	Ref.: SHELXL 2018/3	
R_1 ($I > 2\sigma(I)$) = 0.0498	R_1 (all) = 0.0878	*GooF* (F^2) = 1.027
wR_2 ($I > 2\sigma(I)$) = 0.089	wR_2 (all) =0.1005	
$\Delta\rho_{min}$ = −0.256 e Å^{-3}	$\Delta\rho_{max}$ = 0.295 e Å^{-3}	

Refinement special details:
The dataset was refined with ISOR and parts of the structure were disordered with PART and SAME.

8.7.20 Crystal structure of $dma_3PNP(Ph)Cl$ (SW299)

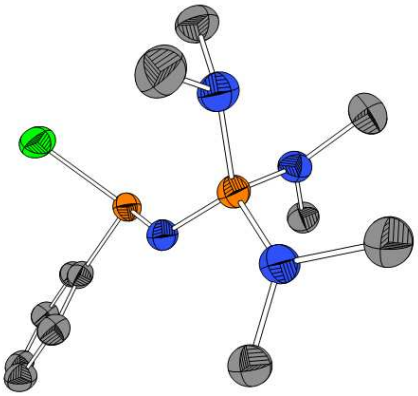

Crystal data

$C_{12}H_{23}ClN_4P_2$	M = 320.73 g mol^{-1}	monoclinic, P21/c
a = 14.2539(4) Å	b = 9.2439(2) Å	c = 12.3901(3) Å
α = 90	β = 97.511(2)	γ = 90
V = 1618.53(7) Å^{-3}	Z = 4	
D_{calc} = 1.316 g cm^3	μ =3.901 mm^{-1}	*F(000)* = 680
habit: colorless block	0.245 x 0.203 x 0.201 mm^3	

Data collection

Diffraktometer: StadiVari	T = 100(2) K	λ = 1.54178 Å
$-17 \leq h \leq 17$	$-8 \leq k \leq 11$	$-14 \leq k \leq 15$
18715 Refl. collected	3346 independent refl.	2973 refl. [$I > 2\sigma(I)$]
R_{int} = 0.0413	$C_{67.679°}$ = 99.7%	θ = 3.127 to 76.168°
Absorption corr.: Multiscan	Tr_{min} = 0.4208	Tr_{max} = 1

Refinement

3346 reflections	0 restraints	179 parameters
Solution: SHELXT	Ref.: SHELXL 2018/3	
R_1 ($I > 2\sigma(I)$) = 0.0596	R_1 (all) = 0.0634	*GooF* (F^2) = 1.137
wR_2 ($I > 2\sigma(I)$) = 0.1727	wR_2 (all) =0.1769	
$\Delta\rho_{min}$ = −0.548 e Å^{-3}	$\Delta\rho_{max}$ = 0.75 e Å^{-3}	E = 0.0045(8)

8.7.21 Crystal structure of $(NEt_2)_2P(Cl_3C)NH_2$-Cl (SW327)

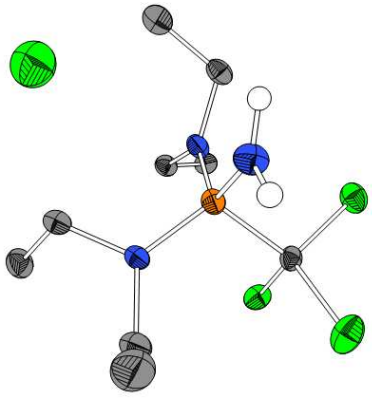

Crystal data

$C_9H_{22}Cl_4N_3P$	M = 345.06 g mol^{-1}	triclinic, P 1
a = 8.7687(3) Å	b = 8.7715(3) Å	c = 10.5572(3) Å
α = 86.983(2)	β = 77.473(2)	γ = 88.678(3)
V = 791.52(4) Å^{-3}	Z = 2	
D_{calc} = 1.448 g cm^3	μ =7.626 mm^{-1}	*F(000)* = 360
habit: colorless needle	0.250 x 0.100 x 0.095 mm^3	

Data collection

Diffraktometer: StadiVari	T = 100(2) K	λ = 1.54178 Å
$-10 \leq h \leq 10$	$-4 \leq k \leq 10$	$-12 \leq k \leq 12$
17223 Refl. collected	17223 independent refl.	14923 refl. [$I > 2\sigma(I)$]
R_{int} = 0.0489	$C_{66.592°}$ = 99.1%	θ = 4.295 to 66.592°
Absorption corr.: Multiscan	Tr_{min} = 0.3218	Tr_{max} = 1

Refinement

17223 reflections	3 restraints	316 parameters
Solution: SHELXT	Ref.: SHELXL 2018/3	
R_1 ($I > 2\sigma(I)$) = 0.0396	R_1 (all) = 0.0473	*GooF* (F^2) = 1.013
wR_2 ($I > 2\sigma(I)$) = 0.0926	wR_2 (all) =0.0951	
$\Delta\rho_{min}$ = −0.407 e Å^{-3}	$\Delta\rho_{max}$ = 0.314 e Å^{-3}	

Refinement special details:
The dataset was refined as non-merohedral 2-component twin (52:48). Some reflections were omitted from the least-squares refinement using OMIT and SHEL. The absolute configuration couldn't be determined, the Flack is x=0.003(14).

8.7.22 Crystal structure of $(NEt_2)_2P(OPh)NH_2$-Cl (SW329)

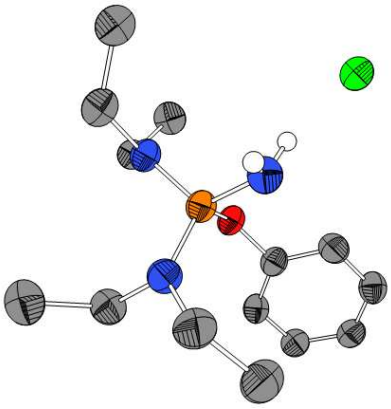

Crystal data

$C_{14}H_{27}ClN_3OP_4$	M = 319.8 g mol^{-1}	monoclinic, P21/n
a = 10.5454(2) Å	b = 13.7354(3) Å	c = 12.6809(2) Å
α = 90	β = 99.8230(10)	γ = 90
V = 1809.84(6) Å^{-3}	Z = 4	
D_{calc} = 1.174 g cm^3	μ =2.701 mm^{-1}	*F(000)* = 688
habit: colorless block	0.246 x 0.172 x 0.107 mm^3	

Data collection

Diffraktometer: StadiVari	T = 100(2) K	λ = 1.54178 Å
$-13 \leq h \leq 13$	$-17 \leq k \leq 15$	$-15 \leq k \leq 13$
42494 Refl. collected	3782 independent refl.	3164 refl. $[I > 2\sigma(I)]$
R_{int} = 0.0675	$C_{67.679°}$ = 100%	θ = 4.784 to 76.070°
Absorption corr.: Multiscan	Tr_{min} = 0.3691	Tr_{max} = 1

Refinement

3782 reflections	5 restraints	192 parameters
Solution: SHELXT	Ref.: SHELXL 2018/3	
R_1 ($I > 2\sigma(I)$) = 0.055	R_1 (all) = 0.0608	*GooF* (F^2) = 1.113
wR_2 ($I > 2\sigma(I)$) = 0.1551	wR_2 (all) =0.1602	
$\Delta\rho_{min}$ = −0.352 e Å^{-3}	$\Delta\rho_{max}$ = 0.269 e Å^{-3}	E = 0.0065(8)

Refinement special details:
The dataset was refined with DFIX and DANG.

8.7.23 Crystal structure of (pyrr)P_2P-*t*Bu (SW365)

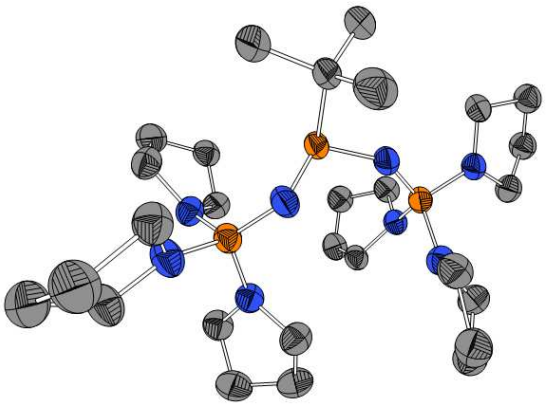

Crystal data

$C_{28}H_{57}N_8P_3$	M = 598.72 g mol^{-1}	monoclinic, P21/c
a = 17.5919(4) Å	b = 9.9547(3) Å	c = 18.8832(4) Å
α = 90	β = 99.091(2)	γ = 90
V = 3265.33(14) Å^{-3}	Z = 4	
D_{calc} = 1.218 g cm^3	μ =1.908 mm^{-1}	*F(000)* = 1304
habit: colorless plate	0.278 x 0.203 x 0.113 mm^3	

Data collection

Diffraktometer: StadiVari	T = 100(2) K	λ = 1.54178 Å
21 $\leq$ h $\leq$ 22	-12 $\leq$ k $\leq$ 11	-22 $\leq$ k $\leq$ 9
41037 Refl. collected	6660 independent refl.	5177 refl. [$I > 2\sigma(I)$]
R_{int} = 0.0946	$C_{67.679°}$ = 99.3%	θ = 4.743 to 75.649°
Absorption corr.: Multiscan	Tr_{min} = 0.0735	Tr_{max} = 1

Refinement

6660 reflections	0 restraints	365 parameters
Solution: SHELXT	Ref.: SHELXL 2018/3	
R_1 ($I > 2\sigma(I)$) = 0.0845	R_1 (all) = 0.0965	*GooF* (F^2) = 1.079
wR_2 ($I > 2\sigma(I)$) = 0.2385	wR_2 (all) =0.2506	
$\Delta\rho_{min}$ = −0.466 e Å^{-3}	$\Delta\rho_{max}$ = 0.584 e Å^{-3}	

Refinement special details:
Parts of the structure were disordered with PART.

8.7.24 Crystal structure of (pyrr)P_2P-*t*Bu-Se (SW372)

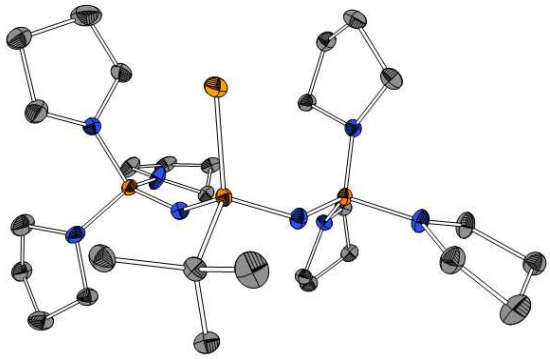

Crystal data

$C_{28}H_{57}N_8P_3Se$	M = 677.68 g mol^{-1}	monoclinic, P21/c
a = 18.445(3) Å	b = 10.2793(12) Å	c = 17.745(2) Å
α = 90	β = 101.588(6)	γ = 90
V = 3295.9(8) Å^{-3}	Z = 4	
D_{calc} = 1.366 g cm^3	μ =1.317 mm^{-1}	*F(000)* = 1440
habit: colorless block	0.286 x 0.178 x 0.130 mm^3	

Data collection

Diffraktometer: D8 Quest	T = 100(2) K	λ = 0.71073 Å
$-21 \leq h \leq 21$	$-12 \leq k \leq 12$	$-21 \leq k \leq 21$
654852 Refl. collected	5814 independent refl.	5257 refl. $[I > 2\sigma(I)]$
R_{int} = 0.0369	$C_{25.021°}$ = 99.9%	θ = 2.254 to 25.021°
Absorption corr.: Multiscan	Tr_{min} = 0.6844	Tr_{max} = 0.7452

Refinement

5814 reflections	6 restraints	403 parameters
Solution: SHELXT	Ref.: SHELXL 2018/3	
R_1 ($I > 2\sigma(I)$) = 0.0254	R_1 (all) = 0.0289	*GooF* (F^2) = 1.066
wR_2 ($I > 2\sigma(I)$) = 0.0688	wR_2 (all) =0.0703	
$\Delta\rho_{min}$ = −0.277 e Å^{-3}	$\Delta\rho_{max}$ = 0.436 e Å^{-3}	

Refinement special details:
The dataset was refined with ISOR and parts of the structure were disordered with PART.

8.7.25 Crystal structure of (dma)P_2P-Biaryl-Se (SW385)

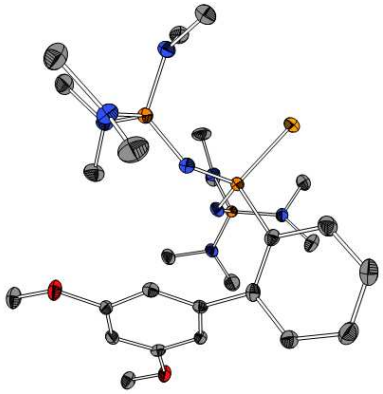

Crystal data

$C_{26}H_{49}N_8O_2P_3Se$	M = 677.6 g mol^{-1}	monoclinic, P21/n
a = 11.470(2) Å	b = 23.815(5) Å	c = 12.148(3) Å
α = 90	β = 94.221(5)	γ = 90
V = 3309.4(12) Å^{-3}	Z = 4	
D_{calc} = 1.36 g cm^3	μ =1.316 mm^{-1}	*F(000)* = 1424
habit: colorless block	0.308 x 0.194 x 0.107 mm^3	

Data collection

Diffraktometer: D8 Quest	T = 100(2) K	λ = 0.71073 Å
$-13 \leq h \leq 13$	$-28 \leq k \leq 28$	$-14 \leq k \leq 14$
59602 Refl. collected	5845 independent refl.	4753 refl. [$I > 2\sigma(I)$]
R_{int} = 0.0577	$C_{25.026°}$ = 99.9%	θ = 1.886 to 25.026°
Absorption corr.: Multiscan	Tr_{min} = 0.6746	Tr_{max} = 0.7452

Refinement

5845 reflections	0 restraints	3752 parameters
Solution: SHELXT	Ref.: SHELXL 2018/3	
R_1 ($I > 2\sigma(I)$) = 0.029	R_1 (all) = 0.041	*GooF* (F^2) = 1.046
wR_2 ($I > 2\sigma(I)$) = 0.0649	wR_2 (all) =0.0673	
$\Delta\rho_{min}$ = −0.296 e Å^{-3}	$\Delta\rho_{max}$ = 0.273 e Å^{-3}	

Refinement special details:
Some reflections near the beamstop were omitted from the least-squares refinement using OMIT.

8.7.26 Crystal structure of (dma)P_2P-*t*Bu-CO_2 (SW418)

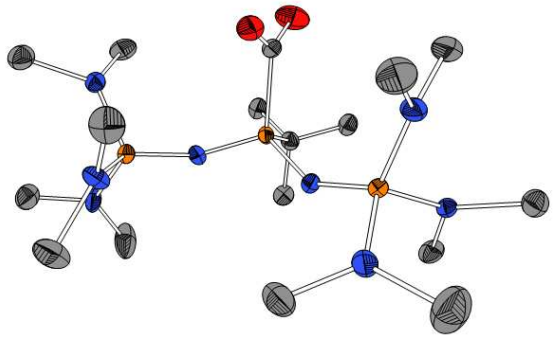

Crystal data

$C_{17}H_{45}N_8O_2P_3$	M = 486.52 g mol^{-1}	orthorombic, P $na21$
a = 12.054(3) Å	b = 13.239(3) Å	c = 16.547(4) Å
α = 90	β = 90	γ = 90
V = 2640.5(11) Å^{-3}	Z = 4	
D_{calc} = 1.224 g cm^3	μ =0.254 mm^{-1}	$F(000)$ = 1056
habit: colorless plate	0.138 x 0.074 x 0.059 mm^3	

Data collection

Diffraktometer: D8 Quest	T = 100(2) K	λ = 0.71073 Å
$-14 \leq h \leq 14$	$-15 \leq k \leq 15$	$-19 \leq k \leq 19$
24034 Refl. collected	4668 independent refl.	4053 refl. [$I > 2\sigma(I)$]
R_{int} = 0.0588	$C_{25.037°}$ = 100%	θ = 2.285 to 25.037°
Absorption corr.: Multiscan	Tr_{min} = 0.6984	Tr_{max} = 0.7452

Refinement

4668 reflections	1 restraints	286 parameters
Solution: SHELXT	Ref.: SHELXL 2018/3	
R_1 ($I > 2\sigma(I)$) = 0.0394	R_1 (all) = 0.0793	$GooF$ (F^2) = 1.051
wR_2 ($I > 2\sigma(I)$) = 0.0494	wR_2 (all) =0.0822	
$\Delta\rho_{min}$ = −0.265 e Å^{-3}	$\Delta\rho_{max}$ = 0.243 e Å^{-3}	

Refinement special details:
Some reflections near the beamstop were omitted from the least-squares refinement using OMIT.

8.7.27 Crystal structure of (dma)P_3P-CO_2 (SW419)

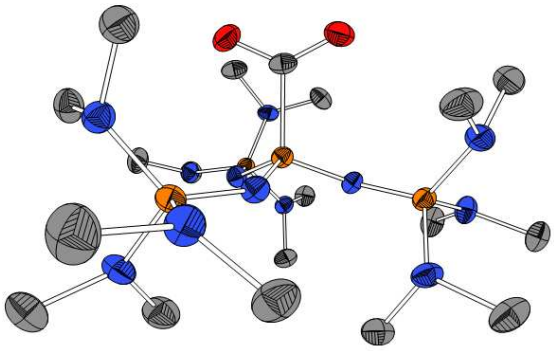

Crystal data

$C_{19}H_{54}N_{12}O_2P_4$	M = 606.62 g mol^{-1}	monoclinic, P21/n
a = 9.8516(2) Å	b = 19.6099(6) Å	c = 17.2329(5) Å
α = 90	β = 102.775(2)	γ = 90
V = 3246.79(15) Å^{-3}	Z = 4	
D_{calc} = 1.241 g cm^3	μ =2.457 mm^{-1}	*F(000)* = 1312
habit: colorless block	0.193 x 0.132 x 0.104 mm^3	

Data collection

Diffraktometer: StadiVari	T = 100(2) K	λ = 1.54178 Å
$-12 \leq h \leq 12$	$-27 \leq k \leq 20$	$-21 \leq k \leq 14$
38801 Refl. collected	6680 independent refl.	5034 refl. [$I > 2\sigma(I)$]
R_{int} = 0.0606	$C_{67.679°}$ = 99.9%	θ = 3.463 to 75.408°
Absorption corr.: Multiscan	Tr_{min} = 0.2895	Tr_{max} = 0.7915

Refinement

6680 reflections	0 restraints	352 parameters
Solution: SHELXT	Ref.: SHELXL 2018/3	
R_1 ($I > 2\sigma(I)$) = 0.052	R_1 (all) = 0.0711	*GooF* (F^2) = 1.042
wR_2 ($I > 2\sigma(I)$) = 0.1379	wR_2 (all) =0.1479	
$\Delta\rho_{min}$ = −0.415 e Å^{-3}	$\Delta\rho_{max}$ = 0.575 e Å^{-3}	

8.7.28 Crystal structure of (pyrr)P_3P-CO_2 (SW421)

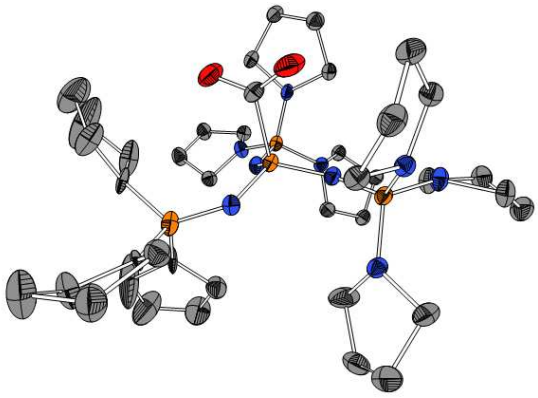

Crystal data

$C_{37}H_{72}N_{12}O_2P_4$	M = 840.94 g mol^{-1}	monoclinic, P21/c
a = 25.313(3) Å	b = 20.388(2) Å	c = 25.251(3) Å
α = 90	β = 99.456(4)	γ = 90
V = 12855(3) Å^{-3}	Z = 12	
D_{calc} = 1.304 g cm^3	μ =0.225 mm^{-1}	*F(000)* = 5448
habit: colorless block	0.372 x 0.248 x 0.176 mm^3	

Data collection

Diffraktometer: D8 Quest	T = 100(2) K	λ = 0.71073 Å
$-29 \leq h \leq 30$	$-24 \leq k \leq 24$	$-30 \leq k \leq 30$
223612 Refl. collected	22741 independent refl.	18655 refl. [$I > 2\sigma(I)$]
R_{int} = 0.0575	$C_{25.066°}$ = 99.7%	θ = 1.913 to 25.066°
Absorption corr.: Multiscan	Tr_{min} = 0.6542	Tr_{max} = 0.7452

Refinement

22741 reflections	66 restraints	1555 parameters
Solution: SHELXT	Ref.: SHELXL 2018/3	
R_1 ($I > 2\sigma(I)$) = 0.0404	R_1 (all) = 0.053	*GooF* (F^2) = 1.032
wR_2 ($I > 2\sigma(I)$) = 0.0967	wR_2 (all) =0.1019	
$\Delta\rho_{min}$ = −0.523 e Å^{-3}	$\Delta\rho_{max}$ = 0.535 e Å^{-3}	

Refinement special details:
Some reflections near the beamstop were omitted from the least-squares refinement using OMIT. The dataset was refined with ISOR and SIMU and parts of the structure were disordered with PART.

8.7.29 Crystal structure of SW429b

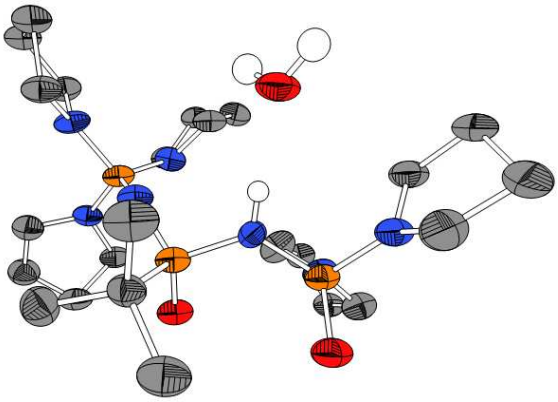

Crystal data

$C_{24}H_{51}N_7O_3P_3$	M = 578.62 g mol^{-1}	monoclinic, P21/c
a = 10.0783(6) Å	b = 13.9218(6) Å	c = 21.9199(16) Å
α = 90	β = 92.145(5)	γ = 90
V = 3073.4(3) Å^{-3}	Z = 4	
D_{calc} = 1.251 g cm^3	μ =2.076 mm^{-1}	*F(000)* = 1252
habit: colorless needle	0.227 x 0.054 x 0.045 mm^3	

Data collection

Diffraktometer: StadiVari	T = 100(2) K	λ = 1.54178 Å
$-10 \leq h \leq 12$	$-12 \leq k \leq 17$	$-27 \leq k \leq 27$
40075 Refl. collected	6333 independent refl.	2831 refl. [$I > 2\sigma(I)$]
R_{int} = 0.2619	$C_{67.679°}$ = 99.8%	θ = 3.762 to 75.824°
Absorption corr.: Multiscan	Tr_{min} = 0.0471	Tr_{max} = 1

Refinement

6333 reflections	0 restraints	345 parameters
Solution: SHELXT	Ref.: SHELXL 2018/3	
R_1 ($I > 2\sigma(I)$) = 0.0945	R_1 (all) = 0.1671	*GooF* (F^2) = 0.881
wR_2 ($I > 2\sigma(I)$) = 0.1855	wR_2 (all) =0.2133	
$\Delta\rho_{min}$ = −0.723 e Å^{-3}	$\Delta\rho_{max}$ = 0.573 e Å^{-3}	

Refinement special details:
Some reflections were omitted from the least-squares refinement using OMIT and SHEL. The dataset was refined as 2-component inversion twin (85:15).

8.7.30 Crystal structure of [Pd((dma)P_1P-(tBu)$_2$)$_2$] (SW498)

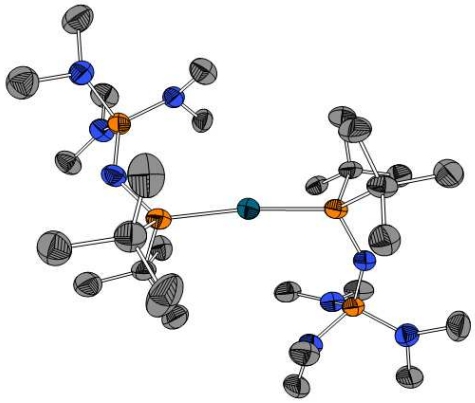

Crystal data

$C_{28}H_{72}N_8P_4Pd$	M = 751.21 g mol^{-1}	triclinic, P-1
a = 8.6730(2) Å	b = 13.3971(3) Å	c = 17.8384(5) Å
α = 100.680(2)	β = 90.638(2)	γ = 103.869(2)
V = 1974.06(9) Å^{-3}	Z = 2	
D_{calc} = 1.264 g cm^3	μ =5.539 mm^{-1}	*F(000)* = 804
habit: colorless block	0.134 x 0.054 x 0.043 mm^3	

Data collection

Diffraktometer: StadiVari	T = 100(2) K	λ = 1.54178 Å
$-9 \leq h \leq 10$	$-16 \leq k \leq 11$	$-22 \leq k \leq 22$
48493 Refl. collected	8051 independent refl.	5511 refl. $[I > 2\sigma(I)]$
R_{int} = 0.1446	$C_{67.679°}$ = 99.2%	θ = 3.464 to 76.027°
Absorption corr.: Multiscan	Tr_{min} = 0.1538	Tr_{max} = 1

Refinement

8050 reflections	0 restraints	394 parameters
Solution: SHELXT	Ref.: SHELXL 2018/3	
R_1 ($I > 2\sigma(I)$) = 0.083	R_1 (all) = 0.1049	*GooF* (F^2) = 0.966
wR_2 ($I > 2\sigma(I)$) = 0.2054	wR_2 (all) =0.2167	
$\Delta\rho_{min}$ = −2.029 e Å^{-3}	$\Delta\rho_{max}$ = 1.382 e Å^{-3}	

List of Figures

List of Tables

List of Schemes

Bibliography

[1] Lehrplan G8 Bayern 10. Klasse, Cited 20.12.22, https://www.lehrplanplus.bayern.de/fachlehrplan/gymnasium/10/chemie/ch.

[2] S. Arrhenius, *Z. Phys. Chem.* **1887**, *1U*, 631–648.

[3] The Nobel Prize in Chemistry 1903, Cited 20.12.22, https://www.nobelprize.org/prizes/chemistry/1903/summary/.

[4] G. L. Miessler, D. A. Tarr, *Inorganic chemistry*, Prentice Hall, Princeton, N.J., **2003**.

[5] J. N. Brönsted in *A Source Book in Chemistry, 1900-1950*, Harvard University Press, **2013**, pp. 204–207.

[6] T. M. Lowry, *J. Soc. Chem. Ind.* **1923**, *42*, 43–47.

[7] G. N. Lewis, *Valence and the Structure of Atoms and Molecules*, Chemical Catalog Company, Incorporated, **1923**.

[8] S.-H. Paik, *J. Chem. Educ.* **2015**, *92*, 1484–1489.

[9] R. G. Pearson, *J. Am. Chem. Soc.* **1963**, *85*, 3533–3539.

[10] M. Usanovich, *J. Gen. Chem. USSR* **1939**, *9*, 182.

[11] H. Lux, *Z. Elektrochem. angew. phys. Chem.* **1939**, *45*, 303–309.

[12] H. Flood, T. Förland, *Acta Chem. Scand.* **1947**, *1*, 592–606.

[13] Bordwell pKa Table, Cited 18.10.22, https://organicchemistrydata.org/hansreich/resources/pka/pka_data/evans_pKa_table.pdf.

[14] A. Bagno, G. Scorrano, *J. Am. Chem. Soc.* **1988**, *110*, 4577–4582.

[15] A. Trummal, L. Lipping, I. Kaljurand, I. A. Koppel, I. Leito, *J. Chem. Phys. A* **2016**, *120*, 3663–3669.

[16] J. F. Kögel, X. Xie, E. Baal, D. Gesevičius, B. Oelkers, B. Kovačević, J. Sundermeyer, *Chem. Eur. J.* **2014**, *20*, 7670–7685.

[17] R. Schwesinger, H. Schlemper, C. Hasenfratz, J. Willaredt, T. Dambacher, T. Breuer, C. Ottaway, M. Fletschinger, J. Boele, H. Fritz, D. Putzas, H. W. Rotter, F. G. Bordwell, A. V. Satish, G.-Z. Ji, E.-M. Peters, K. Peters, H. G. Schnering, L. Walz, *Liebigs Ann. Chem.* **1996**, *1996*, 1055–1081.

[18] X.-M. Zhang, A. J. Fry, F. G. Bordwell, *J. Org. Chem.* **1996**, *61*, 4101–4106.

[19] P. W. Atkins, T. Overton, J. Rourke, *Shriver and Atkins' Inorganic Chemistry*, 5th ed., Oxford University Press, Oxford ; New York, **2009**.

[20] F. G. Bordwell, *Acc. Chem. Res.* **1988**, *21*, 456–463.

[21] I. Kaljurand, T. Rodima, I. Leito, I. A. Koppel, R. Schwesinger, *J. Org. Chem.* **2000**, *65*, 6202–6208.

[22] T. Rodima, I. Kaljurand, A. Pihl, V. Mäemets, I. Leito, I. A. Koppel, *J. Org. Chem.* **2002**, *67*, 1873–1881.

[23] J. Saame, T. Rodima, S. Tshepelevitsh, A. Kütt, I. Kaljurand, T. Haljasorg, I. A. Koppel, I. Leito, *J. Org. Chem.* **2016**, *81*, 7349–7361.

[24] I. Kaljurand, T. Rodima, A. Pihl, V. Mäemets, I. Leito, I. A. Koppel, M. Mishima, *J. Org. Chem.* **2003**, *68*, 9988–9993.

[25] I. Kaljurand, J. Saame, T. Rodima, I. Koppel, I. A. Koppel, J. F. Kögel, J. Sundermeyer, U. Köhn, M. P. Coles, I. Leito, *J. Chem. Phys. A* **2016**, *120*, 2591–2604.

[26] R. Yamdagni, P. Kebarle, *J. Am. Chem. Soc.* **1976**, *98*, 1320–1324.
[27] F. Du, D. M. Warsinger, T. I. Urmi, G. P. Thiel, A. Kumar, J. H. Lienhard V, *Environ. Sci. Technol.* **2018**, *52*, 5949–5958.
[28] R. L. Trammell, L. H. Keith, D. B. Walters, Solubility of Organic and Inorganic Chemicals in Selected Solvents. Tech. rep. PB91119214, Radian Corp., Austin, TX.; National Toxicology Program, Research Triangle Park, NC., **1990**.
[29] J. Clayden, S. A. Yasin, *New J. Chem.* **2002**, *26*, 191–192.
[30] T. Ishikawa in *Superbases for Organic Synthesis*, John Wiley & Sons, Ltd, **2009**, pp. 1–7.
[31] S. Xu, I. Held, B. Kempf, H. Mayr, W. Steglich, H. Zipse, *Chem. Eur. J.* **2005**, *11*, 4751–4757.
[32] P. Caubere, *Chem. Rev.* **1993**, *93*, 2317–2334.
[33] M. Schlosser, *Modern Synthetic Methods* **1992**, *6*, 227–71.
[34] P. Muller, *Pure Appl. Chem.* **1994**, *66*, 1077–1184.
[35] K. Vazdar, D. Margetić, B. Kovačević, J. Sundermeyer, I. Leito, U. Jahn, *Acc. Chem. Res.* **2021**, *54*, 3108–3123.
[36] V. Raab, J. Kipke, R. M. Gschwind, J. Sundermeyer, *Chem. Eur. J.* **2002**, *8*, 1682–1693.
[37] D. A. Evans, D. Ripin, Evans pKa table.
[38] S. Tshepelevitsh, A. Kütt, M. Lõkov, I. Kaljurand, J. Saame, A. Heering, P. G. Plieger, R. Vianello, I. Leito, *Eur. J. Org. Chem.* **2019**, *2019*, 6735–6748.
[39] K. Issleib, M. Lischewski, *Synth. React. Inorg. Met.-Org. Chem.* **1973**, *3*, 255–266.
[40] L. M. Tolbert, M. E. Ogle, *J. Am. Chem. Soc.* **1990**, *112*, 9519–9527.
[41] R. F. Weitkamp, B. Neumann, H.-G. Stammler, B. Hoge, *Chem. Eur. J.* **2021**, *27*, 6465–6478.
[42] C. Palomo, M. Oiarbide, R. López, E. Gómez-Bengoa, *Tetrahedron Lett.* **2000**, *41*, 1283–1286.
[43] H. Kawai, Z. Yuan, E. Tokunaga, N. Shibata, *Org. Biomol. Chem.* **2013**, *11*, 1446–1450.
[44] A. G. Orpen, N. G. Connelly, *Organometallics* **1990**, *9*, 1206–1210.
[45] B. J. Dunne, R. B. Morris, A. G. Orpen, *J. Chem. Soc., Dalton Trans.* **1991**, 653–661.
[46] B. Kovačević, Z. B. Maksić, *Org. Lett.* **2001**, *3*, 1523–1526.
[47] M. Costa, G. P. Chiusoli, D. Taffurelli, G. Dalmonego, *J. Chem. Soc. Perkin Trans. 1* **1998**, 1541–1546.
[48] Y. Yamamoto, S. Kojima in *Amidines and Imidates (1991)*, John Wiley & Sons, Ltd, **1991**, pp. 485–526.
[49] R. Alder, P. Bowman, W. Steele, D. Winterman, *Chem. Commun.* **1968**, 723–724.
[50] R. W. Alder, R. E. Moss, R. B. Sessions, *J. Chem. Soc. Chem. Commun.* **1983**, 997–998.
[51] R. W. Alder, A. G. Orpen, R. B. Sessions, *J. Chem. Soc. Chem. Commun.* **1983**, 999–1000.
[52] R. Schwesinger, M. Mißfeldt, K. Peters, H. G. von Schnering, *Angew. Chem. Int. Ed.* **1987**, *26*, 1165–1167.
[53] J. G. Verkade, P. B. Kisanga, *Tetrahedron* **2003**, *59*, 7819–7858.
[54] J. F. Kögel, B. Oelkers, B. Kovačević, J. Sundermeyer, *J. Am. Chem. Soc.* **2013**, *135*, 17768–17774.
[55] D. Barić, B. Kovačević, *J. Phys. Org. Chem.* **2016**, *29*, 750–758.
[56] K. Vazdar, R. Kunetskiy, J. Saame, K. Kaupmees, I. Leito, U. Jahn, *Angew. Chem. Int. Ed.* **2014**, *53*, 1435–1438.

[57] Á. Kozma, J. Rust, M. Alcarazo, *Chem. Eur. J.* **2015**, *21*, 10829–10834.
[58] L. Belding, T. Dudding, *Chem. Eur. J.* **2014**, *20*, 1032–1037.
[59] S. Lapointe, A. Sarbajna, V. H. Gessner, *Acc. Chem. Res.* **2022**, *55*, 770–782.
[60] J. Handelmann, C. N. Babu, H. Steinert, C. Schwarz, T. Scherpf, A. Kroll, V. H. Gessner, *Chem. Sci.* **2021**, *12*, 4329–4337.
[61] C.-A. Wang, M. M. Rahman, E. Bisz, B. Dziuk, R. Szostak, M. Szostak, *ACS Catal.* **2022**, *12*, 2426–2433.
[62] S. Shi, S. P. Nolan, M. Szostak, *Acc. Chem. Res.* **2018**, *51*, 2589–2599.
[63] M. Klein, N. Demirel, A. Schinabeck, H. Yersin, J. Sundermeyer, *Molecules* **2020**, *25*.
[64] F. Ramirez, N. Desai, B. Hansen, N. McKelvie, *J. Am. Chem. Soc.* **1961**, *83*, 3539–3540.
[65] O. Gasser, H. Schmidbaur, *J. Am. Chem. Soc.* **1975**, *97*, 6281–6282.
[66] R. Appel, U. Baumeister, F. Knoch, *Ber.* **1983**, *116*, 2275–2284.
[67] R. Tonner, F. Öxler, B. Neumüller, W. Petz, G. Frenking, *Angew. Chem. Int. Ed.* **2006**, *45*, 8038–8042.
[68] I. Leito, I. A. Koppel, I. Koppel, K. Kaupmees, S. Tshepelevitsh, J. Saame, *Angew. Chem. Int. Ed.* **2015**, *54*, 9262–9265; *Angew. Chem.* **2015**, *127*, 9394–9397.
[69] S. Ullrich, B. Kovačević, B. Koch, K. Harms, J. Sundermeyer, *Chem. Sci.* **2019**, *10*, 9483–9492.
[70] J. F. Kögel, D. Margetić, X. Xie, L. H. Finger, J. Sundermeyer, *Angew. Chem. Int. Ed.* **2017**, *56*, 3090–3093; *Angew. Chem.* **2017**, *129*, 3136–3139.
[71] J. Tappen, I. Rodstein, K. McGuire, A. Großjohann, J. Löffler, T. Scherpf, V. H. Gessner, *Chem. Eur. J.* **2020**, *26*, 4281–4288.
[72] P. Weber, T. Scherpf, I. Rodstein, D. Lichte, L. T. Scharf, L. J. Gooßen, V. H. Gessner, *Angew. Chem. Int. Ed.* **2019**, *58*, 3203–3207; *Angew. Chem.* **2019**, *131*, 3235–3239.
[73] T. Scherpf, C. Schwarz, L. T. Scharf, J.-A. Zur, A. Helbig, V. H. Gessner, *Angew. Chem. Int. Ed.* **2018**, *57*, 12859–12864; *Angew. Chem.* **2018**, *130*, 13041–13046.
[74] C. Lensink, S. K. Xi, L. M. Daniels, J. G. Verkade, *J. Am. Chem. Soc.* **1989**, *111*, 3478–3479.
[75] J. G. Verkade, *Coord. Chem. Rev.* **1994**, *137*, 233–295.
[76] P. B. Kisanga, J. G. Verkade, R. Schwesinger, *J. Org. Chem.* **2000**, *65*, 5431–5432.
[77] B. Kovačević, D. Barić, Z. B. Maksić, *New J. Chem.* **2004**, *28*, 284–288.
[78] J. G. Verkade, *Acc. Chem. Res.* **1993**, *26*, 483–489.
[79] J. V. Kingston, J. G. Verkade, *J. Org. Chem.* **2007**, *72*, 2816–2822.
[80] C. V. Reddy, J. V. Kingston, J. G. Verkade, *J. Org. Chem.* **2008**, *73*, 3047–3062.
[81] P. Rotering, L. F. B. Wilm, J. A. Werra, F. Dielmann, *Chem. Eur. J.* **2020**, *26*, 406–411.
[82] F. Buß, M. B. Röthel, J. A. Werra, P. Rotering, L. F. B. Wilm, C. G. Daniliuc, P. Löwe, F. Dielmann, *Chem. Eur. J.* **2022**, *28*, e202104021.
[83] T. Witteler, H. Darmandeh, P. Mehlmann, F. Dielmann, *Organometallics* **2018**, *37*, 3064–3072.
[84] B. T. Ingoglia, C. C. Wagen, S. L. Buchwald, *Tetrahedron* **2019**, *75*, 4199–4211.
[85] S. Ullrich, B. Kovačević, X. Xie, J. Sundermeyer, *Angew. Chem. Int. Ed.* **2019**, *58*, 10335–10339; *Angew. Chem.* **2019**, *131*, 10443–10447.
[86] S. Ullrich, Design ungeladener Phosphor-, Kohlenstoff und Stickstoff-Superbasen, Dissertation, Phillips Universität Marburg, **2019**.
[87] B. Kovačević, Z. B. Maksić, *Chem. Commun.* **2006**, 1524–1526.
[88] P. B. Kisanga, J. G. Verkade, *Tetrahedron* **2001**, *57*, 467–475.
[89] C. A. Tolman, *J. Am. Chem. Soc.* **1970**, *92*, 2956–2965.

[90] C. A. Tolman, *Chem. Rev.* **1977**, *77*, 313–348.
[91] H. V. Huynh, *Chem. Rev.* **2018**, *118*, 9457–9492.
[92] M. Nonnenmacher, D. M. Buck, D. Kunz, *Beilstein J. Org. Chem.* **2016**, *12*, 1884–1896.
[93] Q. Teng, H. V. Huynh, *Dalton Trans.* **2017**, *46*, 614–627.
[94] H. V. Huynh, Y. Han, R. Jothibasu, J. A. Yang, *Organometallics* **2009**, *28*, 5395–5404.
[95] O. Back, M. Henry-Ellinger, C. D. Martin, D. Martin, G. Bertrand, *Angew. Chem. Int. Ed.* **2013**, *52*, 2939–2943.
[96] A. Liske, K. Verlinden, H. Buhl, K. Schaper, C. Ganter, *Organometallics* **2013**, *32*, 5269–5272.
[97] K. Verlinden, H. Buhl, W. Frank, C. Ganter, *Eur. J. Inorg. Chem.* **2015**, *2015*, 2416–2425.
[98] D. Setiawan, R. Kalescky, E. Kraka, D. Cremer, *Inorg. Chem* **2016**, *55*, 2332–2344.
[99] D. Cremer, E. Kraka, *Dalton Trans.* **2017**, *46*, 8323–8338.
[100] W. McFarlane, D. S. Rycroft, *J. Chem. Soc. Dalton Trans.* **1973**, 2162.
[101] H. A. Bent, *Chem. Rev.* **1961**, *61*, 275–311.
[102] D. W. Allen, B. F. Taylor, *J. Chem. Soc. Dalton Trans.* **1982**, 51–54.
[103] R. P. Pinnell, C. A. Megerle, S. L. Manatt, P. A. Kroon, *J. Am. Chem. Soc.* **1973**, *95*, 977–978.
[104] R. D. Kroshefsky, R. Weiss, J. G. Verkade, *Inorg. Chem* **1979**, *18*, 469–472.
[105] M. Marín, J. J. Moreno, M. M. Alcaide, E. Álvarez, J. López-Serrano, J. Campos, M. C. Nicasio, E. Carmona, *J. Organomet. Chem.* **2019**, *896*, 120–128.
[106] H. Duddeck, *Prog. Nucl. Magn. Reson. Spectrosc.* **1995**, *27*, 1–323.
[107] U. Beckmann, D. Süslüyan, P. C. Kunz, *Phosphorus Sulfur Silicon Relat. Elem.* **2011**, *186*, 2061–2070.
[108] D. White, B. C. Tavener, P. G. L. Leach, N. J. .Coville, *J. Organomet. Chem.* **1994**, *478*, 205–211.
[109] J. A. Bilbrey, A. H. Kazez, J. Locklin, W. D. Allen, *J. Chem. Theory Comput.* **2013**, *9*, 5734–5744.
[110] J. A. Bilbrey, A. H. Kazez, J. Locklin, W. D. Allen, *J. Comput. Chem.* **2013**, *34*, 1189–1197.
[111] A. Poater, B. Cosenza, A. Correa, S. Giudice, F. Ragone, V. Scarano, L. Cavallo, *Eur. J. Inorg. Chem.* **2009**, *2009*, 1759–1766.
[112] L. Falivene, R. Credendino, A. Poater, A. Petta, L. Serra, R. Oliva, V. Scarano, L. Cavallo, *Organometallics* **2016**, *35*, 2286–2293.
[113] T. Ishikawa in *Superbases for Organic Synthesis*, John Wiley & Sons, Ltd, **2009**.
[114] T. D. Lash, M. L. Thompson, T. M. Werner, J. D. Spence, *Synlett* **2000**, *2000*, 213–216.
[115] V. K. Aggarwal, A. Mereu, *J. Org. Chem.* **2000**, *65*, 7211–7212.
[116] D. A. Alonso, C. Nájera, M. Varea, *Tetrahedron Lett.* **2004**, *45*, 573–577.
[117] F. Buß, C. Mück-Lichtenfeld, P. Mehlmann, F. Dielmann, *Angew. Chem. Int. Ed.* **2018**, *57*, 4951–4955; *Angew. Chem.* **2018**, *130*, 5045–5049.
[118] A. Kondoh, K. Koda, M. Terada, *Org. Lett.* **2019**, *21*, 2277–2280.
[119] K. Suzawa, M. Ueno, A. E. H. Wheatley, Y. Kondo, *Chem. Commun.* **2006**, 4850–4852.
[120] S. B. Lee, J. H. Park, H. Y. Bae, *ChemSusChem* **2022**, *15*, e202200634.
[121] J. Grdadolnik, F. Merzel, F. Avbelj, *Proceedings of the National Academy of Sciences* **2017**, *114*, 322–327.
[122] S. Otto, J. B. Engberts, *Org. Biomol. Chem.* **2003**, *1*, 2809–2820.

[123] N. K. Pahadi, H. Ube, M. Terada, *Tetrahedron Lett.* **2007**, *48*, 8700–8703.
[124] D. Simoni, F. P. Invidiata, S. Manfredini, R. Ferroni, I. Lampronti, M. Roberti, G. P. Pollini, *Tetrahedron Lett.* **1997**, *38*, 2749–2752.
[125] D. Simoni, F. P. Invidiata, M. Manferdini, I. Lampronti, R. Rondanin, M. Roberti, G. P. Pollini, *Tetrahedron Lett.* **1998**, *39*, 7615–7618.
[126] Z. Wang, P. Kisanga, J. G. Verkade, *J. Org. Chem.* **1999**, *64*, 6459–6461.
[127] Z. Wang, B. Fetterly, J. G. Verkade, *J. Organomet. Chem.* **2002**, *646*, 161–166.
[128] T. Witteler, H. Darmandeh, P. Mehlmann, F. Dielmann, *Organometallics* **2018**, *37*, 3064–3072.
[129] M. A. Wünsche, P. Mehlmann, T. Witteler, F. Buß, P. Rathmann, F. Dielmann, *Angew. Chem. Int. Ed.* **2015**, *54*, 11857–11860; *Angew. Chem.* **2015**, *127*, 12024–12027.
[130] A. F. Littke, G. C. Fu, *Angew. Chem. Int. Ed.* **1998**, *37*, 3387–3388.
[131] S. Thiyagarajan, V. Krishnakumar, C. Gunanathan, *Chem. Asian J.* **2020**, *15*, 518–523.
[132] E. D. Nacsa, T. H. Lambert, *J. Am. Chem. Soc.* **2015**, *137*, 10246–10253.
[133] H. Sunaba, K. Kamata, N. Mizuno, *ChemCatChem* **2014**, *6*, 2333–2338.
[134] H. A. Duong, T. N. Tekavec, A. M. Arif, J. Louie, *Chem. Commun.* **2004**, 112–113.
[135] H. Zhou, W.-Z. Zhang, C.-H. Liu, J.-P. Qu, X.-B. Lu, *J. Org. Chem.* **2008**, *73*, 8039–8044.
[136] H. H. . P. u. H. S. W. Wolfsberger, *Z. Naturforsch. B* **1971**, *26b*, 979–981.
[137] E.-P. Flindt, *Z. Anorg. Allg. Chem.* **1982**, *487*, 119–129.
[138] J. F. Kögel, S. Ullrich, B. Kovačević, S. Wagner, J. Sundermeyer, *Z. anorg. allg. Chem.* **2020**, *646*, 923–932.
[139] Y. G. Gololobov, I. N. Zhmurova, L. F. Kasukhin, *Tetrahedron* **1981**, *37*, 437–472.
[140] R. D. Bertrand, F. B. Ogilvie, J. G. Verkade, *J. Am. Chem. Soc.* **1970**, *92*, 1908–1915.
[141] F. B. Ogilvie, J. M. Jenkins, J. G. Verkade, *J. Am. Chem. Soc.* **1970**, *92*, 1916–1923.
[142] K. Weber, K. Korn, M. Schulz, K. Korth, J. Sundermeyer, *Z. anorg. allg. Chem.* **1999**, *625*, 1315–1320.
[143] K. N. Gavrilov, V. N. Tsarev, M. G. Maksimova, O. G. Bondarev, E. A. Rastorguev, S. E. Lyubimov, P. V. Petrovskii, V. A. Davankov, *J. Mol. Catal. A: Chem.* **2006**, *259*, 267–274.
[144] G. N. K. A. P. Marchenko A. M. Pinchuk A. V. Kursanov, *Zh. Obshch. Khim.* **1984**, *54*, 1774–1782.
[145] M. Roberti, D. Pizzirani, M. Recanatini, D. Simoni, S. Grimaudo, D. Cristina, V. Abbadessa, N. Gebbia, M. Tolomeo, *J. Med. Chem.* **2006**, *49*, 3012–3018.
[146] K. C. Kennard, C. S. Hamilton, *Org. Synth.* **1957**, *37*, 82.
[147] A. P Marchenko, I. S. Zal'tsman, A. M. Pinchuk, *Zh. Obshch. Khim.* **1986**, *56*, 1910–1911.
[148] E. S. Kozlov, *Zh. Obshch. Khim.* **1980**, *50*, 2672–2675.
[149] E. S. Kozlov, *Zh. Obshch. Khim.* **1983**, *53*, 2348–2351.
[150] D. W. Stephan, J. C. Stewart, F. Guérin, S. Courtenay, J. Kickham, E. Hollink, C. Beddie, A. Hoskin, T. Graham, P. Wei, R. E. v. H. Spence, W. Xu, L. Koch, X. Gao, D. G. Harrison, *Organometallics* **2003**, *22*, 1937–1947.
[151] E. Hollink, P. Wei, D. W. Stephan, *Can. J. Chem.* **2004**, *82*, 1634–1639.
[152] G. J. Bullen, P. E. Dann, *Acta Crystallogr. B: Struct. Sci. Cryst. Eng. Mater.* **1973**, *29*, 331–337.
[153] A. M. Toth, M. D. Liptak, D. L. Phillips, G. C. Shields, *J. Chem. Phys.* **2001**, *114*, 4595–4606.
[154] F. Weigend, R. Ahlrichs, *PCCP* **2005**, *7*, 3297–3305.

[155] R. R. Dykstra in *Encyclopedia of Reagents for Organic Synthesis*, John Wiley & Sons, Ltd, **2001**.
[156] E. W. Vogel, A. T. Natarajan, *Mutat. Res. - Fundam. Mol. Mech. Mutagen.* **1995**, *330*, 183–208.
[157] H. R. Allcock, T. J. Fuller, K. Matsumura, *Inorg. Chem* **1982**, *21*, 515–521.
[158] D. G. Gusev, *Organometallics* **2009**, *28*, 6458–6461.
[159] F. Buß, P. Mehlmann, C. Mück-Lichtenfeld, K. Bergander, F. Dielmann, *J. Am. Chem. Soc.* **2016**, *138*, 1840–1843.
[160] D. G. Gusev, *Organometallics* **2009**, *28*, 763–770.
[161] P. Mehlmann, C. Mück-Lichtenfeld, T. T. Y. Tan, F. Dielmann, *Chem. Eur. J.* **2017**, *23*, 5929–5933.
[162] J. Löffler, R. M. Gauld, K.-S. Feichtner, I. Rodstein, J.-A. Zur, J. Handelmann, C. Schwarz, V. H. Gessner, *Organometallics* **2021**, *40*, 2888–2900.
[163] J.-A. Zur, M. Schmidt, K.-S. Feichtner, P. Duari, J. Löffler, T. Scherpf, V. H. Gessner, *Angew. Chem. Int. Ed.* **2022**, *61*, e202203950; *Angew. Chem.* **2022**, *134*, e202203950.
[164] R. R. Rodrigues, C. L. Dorsey, C. A. Arceneaux, T. W. Hudnall, *Chem. Commun.* **2014**, *50*, 162–164.
[165] P. Muller, *Pure Appl. Chem.* **1994**, *66*, 1077–1184.
[166] A. Moser, K. Range, D. M. York, *J. Chem. Phys. B* **2010**, *114*, 13911–13921.
[167] V. Barone, M. Cossi, *J. Phys. Chem. A* **1998**, *102*, 1995–2001.
[168] Cone Angle Package, Cited 24.12.22, `https://web.archive.org/web/20200807035834/https://www.ccqc.uga.edu/references/software.php`.
[169] H. Clavier, S. P. Nolan, *Chem. Comm.* **2010**, *46*, 841–861.
[170] L. Chen, P. Ren, B. P. Carrow, *J. Am. Chem. Soc.* **2016**, *138*, 6392–6395.
[171] A. O. Borissova, A. A. Korlyukov, M. Y. Antipin, K. A. Lyssenko, *J. Phys. Chem. A* **2008**, *112*, 11519–11522.
[172] F. Krämer, M. S. Luff, U. Radius, F. Weigend, F. Breher, *Eur. J. Inorg. Chem.* **2021**, *2021*, 3591–3600.
[173] C. C. C. Johansson Seechurn, A. DeAngelis, T. J. Colacot in *New Trends in Cross-Coupling: Theory and Applications*, The Royal Society of Chemistry, **2015**, pp. 1–19.
[174] P. Lloyd-Williams, E. Giralt, *Chem. Soc. Rev.* **2001**, *30*, 145–157.
[175] K. C. Nicolaou, C. N. C. Boddy, S. Bräse, N. Winssinger, *Angew. Chem. Int. Ed.* **1999**, *38*, 2096–2152.
[176] L. Pu, *Chem. Rev.* **1998**, *98*, 2405–2494.
[177] I. W. Ashworth, A. D. Campbell, J. H. Cherryman, J. Clark, A. Crampton, E. G. B. Eden-Rump, M. Evans, M. F. Jones, S. McKeever-Abbas, R. E. Meadows, K. Skilling, D. T. E. Whittaker, R. L. Woodward, P. A. Inglesby, *Org. Process Res. Dev.* **2018**, *22*, 1801–1808.
[178] A. Chartoire, C. Claver, M. Corpet, J. Krinsky, J. Mayen, D. Nelson, S. P. Nolan, I. Peñafiel, R. Woodward, R. E. Meadows, *Org. Process Res. Dev.* **2016**, *20*, 551–557.
[179] J. B. Sperry, K. E. Price Wiglesworth, I. Edmonds, P. Fiore, D. C. Boyles, D. B. Damon, R. L. Dorow, E. L. Piatnitski Chekler, J. Langille, J. W. Coe, *Org. Process Res. Dev.* **2014**, *18*, 1752–1758.
[180] C. Affouard, R. D. Crockett, K. Diker, R. P. Farrell, G. Gorins, J. R. Huckins, S. Caille, *Org. Process Res. Dev.* **2015**, *19*, 476–485.
[181] P. A. Forero-Cortés, A. M. Haydl, *Org. Process Res. Dev.* **2019**, *23*, 1478–1483.
[182] A. Suzuki, *J. Organomet. Chem.* **2002**, *653*, 83–90.
[183] C. C. C. Johansson Seechurn, T. Sperger, T. G. Scrase, F. Schoenebeck, T. J. Colacot, *J. Am. Chem. Soc.* **2017**, *139*, 5194–5200.

[184] M. R. Biscoe, B. P. Fors, S. L. Buchwald, *J. Am. Chem. Soc.* **2011**, *133*, 16707.
[185] B. P. Fors, N. R. Davis, S. L. Buchwald, *J. Am. Chem. Soc.* **2009**, *131*, 5766–5768.
[186] B. P. Fors, D. A. Watson, M. R. Biscoe, S. L. Buchwald, *J. Am. Chem. Soc.* **2008**, *130*, 13552–13554.
[187] A. J. Kendall, L. N. Zakharov, D. R. Tyler, *Inorg. Chem* **2016**, *55*, 3079–3090.
[188] M. C. D'Alterio, È. Casals-Cruañas, N. V. Tzouras, G. Talarico, S. P. Nolan, A. Poater, *Chem. Eur. J.* **2021**, *27*, 13481–13493.
[189] P. Ruiz-Castillo, S. L. Buchwald, *Chem. Rev.* **2016**, *116*, 12564–12649.
[190] N. C. Bruno, M. T. Tudge, S. L. Buchwald, *Chem. Sci.* **2013**, *4*, 916–920.
[191] N. Marion, O. Navarro, J. Mei, E. D. Stevens, N. M. Scott, S. P. Nolan, *J. Am. Chem. Soc.* **2006**, *128*, 4101–4111.
[192] M. S. Viciu, R. F. Germaneau, O. Navarro-Fernandez, E. D. Stevens, S. P. Nolan, *Organometallics* **2002**, *21*, 5470–5472.
[193] M. S. Viciu, R. F. Germaneau, S. P. Nolan, *Org. Lett.* **2002**, *4*, 4053–4056.
[194] T. Scherpf, H. Steinert, A. Großjohann, K. Dilchert, J. Tappen, I. Rodstein, V. H. Gessner, *Angew. Chem. Int. Ed.* **2020**, *59*, 20596–20603; *Angew. Chem.* **2020**, *132*, 20777–20784.
[195] I. Rodstein, D. S. Prendes, L. Wickert, M. Paaßen, V. H. Gessner, *J. Org. Chem.* **2020**, *85*, 14674–14683.
[196] P. Neigenfind, D. Knyszek, J. Handelmann, V. H. Gessner, *Catal. Sci. Technol.* **2022**, *12*, 3447–3453.
[197] D. R. Jensen, M. S. Sigman, *Org. Lett.* **2003**, *5*, 63–65.
[198] P. G. Gildner, T. J. Colacot, *Organometallics* **2015**, *34*, 5497–5508.
[199] H. Li, C. C. C. Johansson Seechurn, T. J. Colacot, *ACS Catal.* **2012**, *2*, 1147–1164.
[200] A. Leitgeb, M. Abbas, R. C. Fischer, A. Poater, L. Cavallo, C. Slugovc, *Catal. Sci. Technol.* **2012**, *2*, 1640–1643.
[201] U. Christmann, R. Vilar, *Angew. Chem. Int. Ed.* **2005**, *44*, 366–374.
[202] G. Li, S. Shi, P. Lei, M. Szostak, *Adv. Synth. Catal.* **2018**, *360*, 1538–1543.
[203] S. Díez-González, N. Marion, S. P. Nolan, *Chem. Rev.* **2009**, *109*, 3612–3676.
[204] D. P. Hruszkewycz, D. Balcells, L. M. Guard, N. Hazari, M. Tilset, *J. Am. Chem. Soc.* **2014**, *136*, 7300–7316.
[205] A. J. DeAngelis, P. G. Gildner, R. Chow, T. J. Colacot, *J. Org. Chem.* **2015**, *80*, 6794–6813.
[206] M. R. Espinosa, A. Doppiu, N. Hazari, *Adv. Synth. Catal.* **2020**, *362*, 5062–5078.
[207] N. C. Bruno, M. T. Tudge, S. L. Buchwald, *Chem. Sci.* **2013**, *4*, 916–920.
[208] N. Hadei, E. A. B. Kantchev, C. J. O'Brie, M. G. Organ, *Org. Lett.* **2005**, *7*, 3805–3807.
[209] G. M. Meconi, S. V. C. Vummaleti, J. A. Luque-Urrutia, P. Belanzoni, S. P. Nolan, H. Jacobsen, L. Cavallo, M. Solà, A. Poater, *Organometallics* **2017**, *36*, 2088–2095.
[210] P. R. Melvin, D. Balcells, N. Hazari, A. Nova, *ACS Catal.* **2015**, *5*, 5596–5606.
[211] A. A. C. Braga, N. H. Morgon, G. Ujaque, F. Maseras, *J. Am. Chem. Soc.* **2005**, *127*, 9298–9307.
[212] D. Ortiz, M. Blug, X.-F. Le Goff, P. Le Floch, N. Mézailles, P. Maître, *Organometallics* **2012**, *31*, 5975–5978.
[213] A. J. J. Lennox, G. C. Lloyd-Jones, *Chem. Soc. Rev.* **2014**, *43*, 412–443.
[214] A. T. Normand, A. Stasch, L.-L. Ooi, K. J. Cavell, *Organometallics* **2008**, *27*, 6507–6520.
[215] G. Ferguson, R. McCrindle, A. J. McAlees, M. Parvez, *Acta. Crystallogr. B. Struct. Sci. Cryst. Eng. Mater.* **1982**, *38*, 2679–2681.

[216] M. Tanaka, *Acta Crystallogr. C Struct. chem.* **1992**, *48*, 739–740.
[217] S. M. Raders, J. N. Moore, J. K. Parks, A. D. Miller, T. M. Leißing, S. P. Kelley, R. D. Rogers, K. H. Shaughnessy, *J. Org. Chem.* **2013**, *78*, 4649–4664.
[218] S. Lou, G. C. Fu, *Adv. Synth. & Catal.* **2010**, *352*, 2081–2084.
[219] C. M. Mömming, E. Otten, G. Kehr, R. Fröhlich, S. Grimme, D. W. Stephan, G. Erker, *Angew. Chem. Int. Ed.* **2009**, *48*, 6643–6646.
[220] J. L. Lamola, J. C. Shilubana, L. Ngodwana, B. Vatsha, A. S. Adeyinka, M. C. Maumela, C. W. Holzapfel, E. M. Mmutlane, *Eur. J. Inorg. Chem.* **2021**, *2021*, 2578–2582.
[221] O. Navarro, H. Kaur, P. Mahjoor, S. P. Nolan, *J. Org. Chem.* **2004**, *69*, 3173–3180.
[222] F. Schüth, M. D. Ward, J. M. Buriak, *Chem. Mater.* **2018**, *30*, 3599–3600.
[223] S. R. Stauffer, M. A. Steinbeiser, *Tetrahedron Lett.* **2005**, *46*, 2571–2575.
[224] M. Montgomery, H. M. O'Brien, C. Méndez-Gálvez, C. R. Bromfield, J. P. M. Roberts, A. M. Winnicka, A. Horner, D. Elorriaga, H. A. Sparkes, R. B. Bedford, *Dalton Trans.* **2019**, *48*, 3539–3542.
[225] M. J. Cawley, F. G. N. Cloke, R. J. Fitzmaurice, S. E. Pearson, J. S. Scott, S. Caddick, *Org. Biomol. Chem.* **2008**, *6*, 2820–2825.
[226] W. Zi, F. Dean Toste, *Chem. Soc. Rev.* **2016**, *45*, 4567–4589.
[227] B. Huang, M. Hu, F. D. Toste, *Trends Chem.* **2020**, *2*, 707–720.
[228] V. Lavallo, G. D. Frey, B. Donnadieu, M. Soleilhavoup, G. Bertrand, *Angew. Chem. Int. Ed.* **2008**, *47*, 5224–5228.
[229] C. Bartolomé, D. García-Cuadrado, Z. Ramiro, P. Espinet, *Organometallics* **2010**, *29*, 3589–3592.
[230] Y. Wang, Z. Wang, Y. Li, G. Wu, Z. Cao, L. Zhang, *Nature Comm.* **2014**, *5*, 3470.
[231] N. Chadha, O. Silakari, *Eur. J. Med. Chem.* **2017**, *134*, 159–184.
[232] S. Jiang, H. Lu, S. Liu, Q. Zhao, Y. He, A. K. Debnath, *Antimicrob. Agents Chemother.* **2004**, *48*, 4349–4359.
[233] B. Frydman, R. B. Frydman, A. Valasinas, E. S. Levy, G. Feinstein, *Philos. Trans. R. Soc. Lond. B Biol. Sci.* **1976**, *273*, 137–160.
[234] R. Chauhan, J. Dwivedi, A. A. Siddiqi Anees, D. Kishore, *Pharm. Chem. J.* **2011**, *44*, 542–550.
[235] S. D. Banister, S. M. Wilkinson, M. Longworth, J. Stuart, N. Apetz, K. English, L. Brooker, C. Goebel, D. E. Hibbs, M. Glass, M. Connor, I. S. McGregor, M. Kassiou, *ACS Chem. Neurosci.* **2013**, *4*, PMID: 23551277, 1081–1092.
[236] D. M. Fink, *Synlett* **2004**, *2004*, 2394–2396.
[237] B. E. Love, B. T. Nguyen, *Synlett* **1998**, *1998*, 1123–1125.
[238] A. Zicmanis, G. Vavilina, S. Drozdova, P. Mekss, M. Klavins, *Open Chem.* **2007**, *5*, 156–168.
[239] S. Thiyagarajan, V. Krishnakumar, C. Gunanathan, *Chem. Asian J.* **2020**, *15*, 518–523.
[240] H. Sunaba, K. Kamata, N. Mizuno, *ChemCatChem* **2014**, *6*, 2333–2338.
[241] E. D. Nacsa, T. H. Lambert, *J. Am. Chem. Soc.* **2015**, *137*, 10246–10253.
[242] A. Kütt, S. Tshepelevitsh, J. Saame, M. Lõkov, I. Kaljurand, S. Selberg, I. Leito, *Eur. J. Org. Chem.* **2021**, *2021*, 1407–1419.
[243] C. N. Matthews, J. S. Driscoll, G. H. Birum, *Chem. Commun. (London)* **1966**, 736–737.
[244] N. Kuhn, M. Steimann, G. Weyers, *Z. Naturforsch. B; J. Chem. Sci* **1999**, 427–433.
[245] C. Villiers, J.-P. Dognon, R. Pollet, P. Thuéry, M. Ephritikhine, *Angew. Chem. Int. Ed.* **2010**, *49*, 3465–3468.

[246] F. Buß, P. Mehlmann, C. Mück-Lichtenfeld, K. Bergander, F. Dielmann, *J. Am. Chem. Soc.* **2016**, *138*, 1840–1843.
[247] B. R. Van Ausdall, J. L. Glass, K. M. Wiggins, A. M. Aarif, J. Louie, *J. Org. Chem.* **2009**, *74*, 7935–7942.
[248] Z. Wang, F. Wang, X.-S. Xue, P. Ji, *Org. Lett.* **2018**, *20*, 6041–6045.
[249] L. F. B. Wilm, M. Das, D. Janssen-Müller, C. Mück-Lichtenfeld, F. Glorius, F. Dielmann, *Angew. Chem. Int. Ed.* **2022**, *61*, e202112344.
[250] H. Zhou, G.-X. Wang, W.-Z. Zhang, X.-B. Lu, *ACS Catal.* **2015**, *5*, 6773–6779.
[251] A.-D. Manick, J.-P. Dutasta, P. Nava, V. Dufaud, G. Gao, B. Chatelet, A. Martinez, *Chem. Asian J.* **2022**, *17*, e202200115.
[252] B. Chatelet, L. Joucla, J.-P. Dutasta, A. Martinez, V. Dufaud, *Chem. Eur. J.* **2014**, *20*, 8571–8574.
[253] M.-A. Courtemanche, M.-A. Légaré, É. Rochette, F.-G. Fontaine, *Chem. Commun.* **2015**, *51*, 6858–6861.
[254] M. Dittmar, I. Martin, Currently ongoing PhD work, Phillips Universität Marburg, **2023**.
[255] D. R. Burfield, R. H. Smithers, *J. Org. Chem.* **1978**, *43*, PMID: 22906067, 3966–3968.
[256] K. R. Roshan, R. A. Palissery, A. C. Kathalikkattil, R. Babu, G. Mathai, H.-S. Lee, D.-W. Park, *Catal. Sci. Technol.* **2016**, *6*, 3997–4004.
[257] M. J. Ajitha, C. H. Suresh, *Tetrahedron Lett.* **2011**, *52*, 5403–5406.
[258] J. P. Stambuli, S. R. Stauffer, K. H. Shaughnessy, J. F. Hartwig, *J. Am. Chem. Soc.* **2001**, *123*, 2677–2678.
[259] *Purification of Laboratory Chemicals (Eighth Edition)*, (Ed.: W. L. F. Armarego), Butterworth-Heinemann, **2017**.
[260] V. Mark, *Org. Synth.* **1966**, *46*, 42.
[261] S. Selberg, T. Rodima, M. Lõkov, S. Tshepelevitsh, T. Haljasorg, S. Chhabra, S. A. Kadam, L. Toom, S. Vahur, I. Leito, *Tetrahedron Lett.* **2017**, *58*, 2098–2102.
[262] T. Saget, N. Cramer, *Synth.* **2011**, *2011*, 2369–2371.
[263] R. Huang, Y. Fu, W. Zeng, L. Zhang, D. Wang, *J. Organomet. Chem.* **2017**, *851*, 46–51.
[264] L. Qin, X. Ren, Y. Lu, Y. Li, J. Zhou, *Angew. Chem. Int. Ed.* **2012**, *51*, 5915–5919.
[265] M. Murakoshi, T. Matsueda, EP839817, **1998**.
[266] H. Yang, G. Li, Z. Ma, J. Chao, Z. Guo, *J. Catal.* **2010**, *276*, 123–133.
[267] T. M. Razler, Y. Hsiao, F. Qian, R. Fu, R. K. Khan, W. Doubleday, *J. Org. Chem.* **2009**, *74*, 1381–1384.
[268] J. P. Wolfe, R. A. Singer, B. H. Yang, S. L. Buchwald, *J. Am. Chem. Soc.* **1999**, *121*, 9550–9561.
[269] C. Liu, Q. Ni, F. Bao, J. Qiu, *Green Chem.* **2011**, *13*, 1260–1266.
[270] A. H. Roy, J. F. Hartwig, *J. Am. Chem. Soc.* **2003**, *125*, 8704–8705.
[271] J.-H. Li, W.-J. Liu, *Org. Lett.* **2004**, *6*, 2809–2811.
[272] L. Zhang, J. Wu, *Adv. Synth. Catal.* **2008**, *350*, 2409–2413.
[273] S. E. Denmark, R. C. Smith, W.-T. T. Chang, J. M. Muhuhi, *J. Am. Chem. Soc.* **2009**, *131*, 3104–3118.
[274] F. McLachlan, C. J. Mathews, P. J. Smith, T. Welton, *Organometallics* **2003**, *22*, 5350–5357.
[275] S. Rostamnia, B. Zeynizadeh, E. Doustkhah, H. G. Hosseini, *J. Colloid Interface Sci.* **2015**, *451*, 46–52.
[276] S. E. Denmark, R. C. Smith, S. A. Tymonko, *Tetrahedron* **2007**, *63*, 5730–5738.
[277] L. Wu, X. Zhang, Z. Tao, *Catal. Sci. Technol.* **2012**, *2*, 707–710.

[278] S. Çalimsiz, M. Sayah, D. Mallik, M. G. Organ, *Angew. Chem. Int. Ed.* **2010**, *49*, 2014–2017; *Angew. Chem.* **2010**, *122*, 2058–2061.
[279] K. L. Billingsley, S. L. Buchwald, *Angew. Chem. Int. Ed.* **2008**, *47*, 4695–4698.
[280] R. Sang, A. Noble, V. K. Aggarwal, *Angew. Chem. Int. Ed.* **2021**, *60*, 25313–25317.
[281] Z. Zuo, J. Liu, J. Nan, L. Fan, W. Sun, Y. Wang, X. Luan, *Angew. Chem. Int. Ed.* **2015**, *54*, 15385–15389; *Angew. Chem.* **2015**, *127*, 15606–15609.
[282] H. Zhang, Q. Cai, D. Ma, *J. Org. Chem.* **2005**, *70*, 5164–5173.
[283] N. Kataoka, Q. Shelby, J. P. Stambuli, J. F. Hartwig, *J. Org. Chem.* **2002**, *67*, 5553–5566.
[284] L. Ackermann, R. Sandmann, W. Song, *Org. Lett.* **2011**, *13*, 1784–1786.
[285] L. Ackermann, J. H. Spatz, C. J. Gschrei, R. Born, A. Althammer, *Angew. Chem. Int. Ed.* **2006**, *45*, 7627–7630; *Angew. Chem.* **2006**, *118*, 7789–7792.
[286] G. C. H. Chiang, T. Olsson, *Org. Lett.* **2004**, *6*, 3079–3082.
[287] J. M. Chudomel, B. Yang, M. D. Barnes, M. Achermann, J. T. Mague, P. M. Lahti, *J. Chem. Phys. A* **2011**, *115*, 8361–8368.
[288] T. V. Nykaza, J. C. Cooper, G. Li, N. Mahieu, A. Ramirez, M. R. Luzung, A. T. Radosevich, *J. Am. Chem. Soc.* **2018**, *140*, 15200–15205.
[289] I. Sapountzis, P. Knochel, *Angew. Chem. Int. Ed.* **2004**, *43*, 897–900; *Angew. Chem.* **2004**, *116*, 915–918.
[290] A. Hajra, Y. Wei, N. Yoshikai, *Org. Lett.* **2012**, *14*, 5488–5491.
[291] J. P. Wolfe, H. Tomori, J. P. Sadighi, J. Yin, S. L. Buchwald, *J. Org. Chem.* **2000**, *65*, 1158–1174.
[292] J. P. Wolfe, S. L. Buchwald, *J. Am. Chem. Soc.* **1997**, *119*, 6054–6058.
[293] R. Nacario, S. Kotakonda, D. M. D. Fouchard, L. M. V. Tillekeratne, R. A. Hudson, *Org. Lett.* **2005**, *7*, 471–474.
[294] E. D. Nacsa, T. H. Lambert, *J. Am. Chem. Soc.* **2015**, *137*, 10246–10253.
[295] X. Hou, H. Hemit, J. Yong, L. Nie, H. A. Aisa, *Synth. Commun.* **2010**, *40*, 973–979.
[296] S. Roy, A. Eastman, G. W. Gribble, *Tetrahedron* **2006**, *62*, 7838–7845.
[297] A. D. Becke, *J. Chem. Phys.* **1993**, *98*, 5648–5652.
[298] C. Lee, W. Yang, R. G. Parr, *Phys. Rev. B* **1988**, *37*, 785–789.
[299] P. J. Stephens, F. J. Devlin, C. F. Chabalowski, M. J. Frisch, *J. Chem. Phys.* **1994**, *98*, 11623–11627.
[300] S. H. Vosko, L. Wilk, M. Nusair, *Can. J. Phys.* **1980**, *58*, 1200–1211.
[301] V. A. Rassolov, J. A. Pople, M. A. Ratner, T. L. Windus, *J. Chem. Phys.* **1998**, *109*, 1223–1229.
[302] F. Neese, *Wiley Interdiscip. Rev.-Comput. Mol. Sci.* **2018**, *8*, e1327.
[303] F. Neese, *Wiley Interdiscip. Rev.-Comput. Mol. Sci.* **2012**, *2*, 73–78.
[304] S. Grimme, J. Antony, S. Ehrlich, H. Krieg, *J. Chem. Phys.* **2010**, *132*, 154104.
[305] S. Grimme, S. Ehrlich, L. Goerigk, *J. Comput. Chem.* **2011**, *32*, 1456–1465.
[306] S. Grimme, *Chem. Eur. J.* **2012**, *18*, 9955–9964.
[307] G. Herzberg, *Infrared and Raman Spectra of Polyatomic Molecules*, Van Nostrand Reinhold, **1945**.
[308] I. Wolfram Research, Mathematica, Champaign, Illinois, **2021**.
[309] L. Falivene, Z. Cao, A. Petta, L. Serra, A. Poater, R. Oliva, V. Scarano, L. Cavallo, *Nat. Chem.* **2019**, *11*, 872–879.
[310] K. Haav, J. Saame, A. Kütt, I. Leito, *Eur. J. Org. Chem.* **2012**, 2167–2172.
[311] *SADABS*. Bruker AXS area detector scaling, Madison, Wisconsin, USA, **2016**.
[312] *SAINT*, Madison, Wisconsin, USA, **2015**.
[313] *Apex4*, Madison, Wisconsin, USA, **2022**.

[314] *Apex3*, Madison, Wisconsin, USA, **2016**.
[315] *X-Area LANA*, Darmstadt, Germany, **2016**.
[316] *X-Area Integrate*, Darmstadt, Germany, **2016**.
[317] *X-Area Recipe*, Darmstadt, Germany, **2015**.
[318] *X-Area Pilatus3_SV*, Darmstadt, Germany, **2016**.
[319] G. M. Sheldrick, *Acta Crystallogr. A* **2015**, *71*, 3–8.
[320] G. M. Sheldrick, *Acta Crystallogr. Sect. C: Cryst. Struct. Commun.* **2015**, *71*, 3–8.
[321] L. J. Farrugia, *J. Appl. Cryst.* **2012**, *45*, 849–854.
[322] C. B. Hübschle, G. M. Sheldrick, B. Dittrich, *J. Appl. Cryst.* **2011**, *44*, 1281–1284.
[323] *Diamond*, Bonn, Germany, **2012**.
[324] W. T. Pennington, *J. Appl. Cryst.* **1999**, *32*, 1028–1029.
[325] Jmol colours, 21.02.23, `https://jmol.sourceforge.net/jscolors/`.